Behavior of sulfur oxides in air and oxy-fuel combustion

Von der Fakultät Energie-, Verfahrens- und Biotechnik der Universität Stuttgart zur Erlangung der Würde eines Doktor-Ingenieurs (Dr.-Ing.) genehmigte Abhandlung

Vorgelegt von

Reinhold Spörl

aus Eichstätt

Hauptberichter:	Univ.-Prof. Dr. techn. Günter Scheffknecht
Mitberichter:	Emeritus Professor Dr. Terry F. Wall
Tag der mündlichen Prüfung:	17 / 07 / 2019

Institut für Feuerungs- und Kraftwerkstechnik (IFK)

2019

Acknowledgements

The work presented within this thesis has been conducted and evaluated between 2010 and 2018 while I was employed at the Institute of Combustion and Power Plant Technology (IFK). The main research activities included in this dissertation are related to the publicly funded research projects “ADECOS Komponenten” and “BiOxySorb” and to a bilateral cooperation with the research group of Prof. Terry Wall from the University of Newcastle in Australia with the title “Coal impurity impacts and gas quality control in oxy-fuel technology for CCS”. I gratefully acknowledge the financial support by the German Federal Ministry for Economic Affairs and Energy (BMWi) and the project partners ALSTOM Carbon Capture GmbH, Babcock Borsig Steinmüller GmbH, Clyde Bergemann GmbH, EnBW Energie Baden-Württemberg AG, E.ON Technologies GmbH, EVN AG, and Vattenfall Europe Generation AG that funded the “ADECOS Komponenten” reseach project (grant number: 03ET2026D), the financial support from the European Union’s Research Fund for Coal and Steel (RFCS), funding the “BiOxySorb” research project (grant number: RFCR-CT-2013-00010), and the financial support by Xstrata Coal Low Emissions R&D Corporation Pty Ltd that funded the project “Coal impurity impacts and gas quality control in oxy-fuel technology for CCS” (grant number: CC08-71). Their funding has enabled my employment as a research scientist at IFK and the completion of this dissertation project. I also acknowledge the support by advice and expertise of the project partners of “ADECOS Komponenten” (see above) and “BiOxySorb” (Fundación Ciudad de la Energía, Uniper Technologies Limited, Lhoist Recherche et Développement SA, and Gestamp Biomass Solutions).

I express my gratitude to Prof. Dr. techn. Günter Scheffknecht for providing me the opportunity to conduct research at the IFK, with its unique infrastructure for conduction of experiments in the field of energy process engineering. Moreover, I thank Prof. Scheffknecht for supervision of this dissertation project and his advice. My gratitude is extended to Emeritus Professor Dr. Terry Wall who invited me to visit his research group at the University of Newcastle (UoN) in Australia, offered to cover the costs of this visit, gave advice on my research, and agreed to be co-examiner of this thesis.

I thank the head of my former department “Firing Systems” (KWF) at IFK, Dipl.-Ing. Jörg Maier, for his guidance and for helping me to organize my work in a constructive manner. Furthermore, I am grateful to my colleagues from KWF for their help in a variety of aspects

related to my thesis. I thank Matthias Pagano, Simon Gratwohl, Timo Wagner, Marc Hein, Thomas Matthies, Mario Krautz, Björn Beeh, Eva Miller, Aaron Fuller, Collins Ndibe, Siqiang Qin, Manoj Paneru, Selahattin Babat, Marta Escoto de Tejada, Francisco Carrasco Maldonado, and Gosia Stein-Cichoszewska for their support in the performed experiments at "BTS-VR", "KSVA", and "OxyPP" and in SEM analyses af ash and deposit samples and my colleagues of Prof. Wall's research group at UoN, Lawrence Belo, Kalpit Shah, Rohan Stanger, Liza Elliot, and Jenny Martin for advice, guidance, and support in reseach and in organizing my research visit at UoN. I thank the students, who supported me as research assistants and in the framework of their student theses, Johannes Walker, Adriana Radu, Abbas Seifeddine, Andreas Scheyhing, Joel Däuwel, Stefan Pek, Benjamin Ebner, Markus Faulhaber, Mattias Djerv, Raphael Kober, Sabine Ott, Stefan Stade, Victor Gomez, Helmut Fischer, Roman Giniyatullin, and Reyhane Youssefi. Additional thanks go to Wolfgang Ross and his team of IFK's "Laboratory for Fuels, Ashes, and Slag" for supporting this work with lab analyses of fuels, liquid samples, ashes, and deposits and to IFK's work shop team led by Herbert Höll and Ralf Nollert for their help in modification of experimental systems and construction of equipment. Furthermore, special thanks go to Renate Klein, Ursula Docter, Beate Koch, Claus Nagel, Antje Radszuweit, and Marja Steinlechner for their help and support with regard to administrative and IT issues.
In addition, I thank my family: My father Reinhold, my mother Paula, my brother Hans, and my sister Johanna. Their moral support and faith have been determining factors for my successful studies and for this work to be realized. Finally, I express my warmest thanks to my wife Maren, who has been a constant source of inspiration and power as well as a caring and sympathetic supporter.

Contents

List of figures

List of tables

List of acronyms

Acronym	Meaning
A	Ash
APH	Air preheater
ASU	Air separation unit
BET	Brunauer–Emmett–Teller theory on physical gas adsorption, used to characterize the specific surface area of samples
BTS-VR	Staged fuel partitioning combustion reactor (German: Brennstoff-Trenn-Stufungs-Verbrennungsreaktor)
C_{fix}	Fixed carbon
CCS	Carbon capture and storage
CCU	Carbon capture and utilization
CDS	Circulating dry scrubber
CPU	CO_2 processing unit
daf	Dry, ash free (reference state for analyses of solids)
db	Dry basis (reference state for analyses of solids)
DeNOx	NO_x reduction system (e.g. SCR)
DSI	Dry sorbent injection
E1-E3	Samples from first (E1) to third (E3) ash separation compartment of the ESP
ECO	Economizer (steam boiler heat exchanger)
ESP	Electrostatic precipitator
EVAP	Evaporator (steam boiler heat exchanger)
FD	Forced draft (fan)
FGD	Flue gas desulfurization
FTIR	Fourier transform infrared spectroscopy
GH	Gas heater (synonymously used to GPH)

Acronym	Meaning
GPH	Gas preheater
IC	Ion chromatography
ICP-OES	Inductively coupled plasma optical emission spectrometry
ID	Induced draft (fan)
IFK	Institute of Combustion and Power Plant Technology (German: Institut für Feuerungs- und Kraftwerkstechnik)
IR	Infrared radiation
IT	Information technology
KSVA	Pulverized coal combustion rig (German: Kohlestaubfeuerungsanlage)
Lev	Akronym used to designate furnace levels
max.	Maximum
min.	Minimum
n.a.	Not available
n.d.	Not determinable
NCV	Net calorific value
NDIR	Non-dispersive infrared photometry
NO_x	Nitrogen oxides (in context of flue gas measurements, this refers to the sum of nitrogen monoxide NO and dioxide NO_2)
OFA	Over fire air (teriary air) used in air staging for NO_x reduction
OxyPP	Vattenfall's 30 MW_{th} oxy-fuel pilot plant "Schwarze Pumpe"
p.	Page
PF	Pulverized fuel
PSD	Particle size distribution
PTFE	Polytetrafluoroethylene, e.g. Teflon
RH	Reheater (steam generator heat exchanger)
SCR	Selective catalytic reduction reactor
SDA	Spray drier absorber
SEM-EDX	Scanning electron microscopy with wavelength dispersive X-ray spectrum scan
SEM-WDX	Scanning electron microscopy with energy dispersive X-ray spectrum scan
SH	Superheater (steam boiler heat exchanger)
SO_x	Sulfur oxides, i.e. SO_2 and SO_3

Acronym	Meaning
STP	Standard temperature and pressure (according to DIN 1343, i.e. 101325 Pa, 273.15 K)
UBC	Unburnt carbon
V	Volatiles
W	Water
WFGD	Wet flue gas desulfurization

List of symbols

Symbol	Meaning	Unit
a_{BET}	Specific surface area determined according to the BET method	$\frac{m^2}{g}$
$\alpha_{(Ca+Mg)/S}$	Molar ratio of the sum of calcium and magnesium versus sulfur in the fuel	-
$\alpha_{Ca/2Cl}$	Molar ratio of calcium (injected or in fuel) versus two times the amount of chlorine (in the fuel or in the flue gas in form of HCl)	-
$\alpha_{Ca/S}$	Molar ratio of calcium (injected or in fuel) versus sulfur (in the fuel or in the flue gas in form of SO_2)	-
$\alpha_{(Na+K)/2S}$	Molar ratio of the sum of sodium and potassium divided by two times the amount of sulfur in the fuel	-
Δ	Symbol indicating the difference between two values	-
D	Diameter	mm, m
D_{50}	Diameter for which 50 % of the particles (for analysis by laser diffraction on volume basis) of an analyzed sample have a smaller particle size, and 50 % have a larger particle size	µm
D_{90}	Diameter for which 90 % of the particles (for analysis by laser diffraction on volume basis) of an analyzed sample have a smaller particle size, and 10 % have a larger particle size	µm
$\overline{D_{por}}$	Mean pore diameter	nm
η_i	Capture efficiency for component i (SO_2, SO_3, or HCl)	%
η_{sorb}	Sorbent utilization efficiency (usually calculated in reference to the reaction products $CaSO_4$ and $CaCl_2$ or the reactants SO_2, SO_3, and HCl)	%

Symbol	Meaning	Unit
$\eta_{SO_x,lim}$	Minimum SO_x removal efficiency required by law for certain power plants	%
γ_i	Mass fraction of component i in the fuel	$\frac{kg}{kg}$
M_i	Mass of component i	g, kg, t
c_i	Mass concentration of component i in a gas stream	$\frac{\mu g}{m^3}$, *STP*
$c_{liq,i}$	Mass concentration of component i in a liquid stream	$\frac{mg}{l}$
$\dot{M}_i$	Mass flow of component i	$\frac{g}{h}$, $\frac{kg}{h}$, $\frac{t}{h}$
$M_{M,i}$	Molar mass of component i	$\frac{kg}{kmol}$
N_i	Molar amount of component i	mol, kmol
$\dot{N}_i$	Molar flow of component or stream i	$\frac{mol}{h}$, $\frac{kmol}{h}$
n_i	Fuel mass specific molar amount of component/stream i	$\frac{mol}{kg}$
n_{air}, $n_{O_2,rec}$, $n_{O_2,o-t}$	Stoichiometric air and oxy-fuel recycle and once-through O_2 ratio of combustion	-
$n_{Ca,Sorb}$	Mass specific partial amount of calcium in a sorbent, i.e. $n_{Ca,Sorb} = N_{Ca,Sorb}/m_{Sorb}$	$\frac{mol}{g}$, $\frac{kmol}{kg}$
P	Power of a combustor, boiler, etc.	kW, MW
p_i	Partial pressure of component i in a system	Pa, hPa, bar
p_0	Reference pressure used in the expression $log_{10}(p_{SO_2}/p_0)$ to render p_{SO_2} dimensionless: $p_0 = 1.013\,25 \cdot 10^5$ Pa	Pa
p_{tot}	Total pressure of a system	Pa, hPa, bar
κ_{23}	Molar SO_2 to SO_3 conversion ratio	-
ϑ	Temperature	°C
ϑ_{BTSi}	Temperature of heating zone i of the electrically heated BTS-VR furnace (i $\in \{1, 2, \ldots 5\}$)	°C
$\vartheta_{H_2SO_4,dew}$	H_2SO_4 dew point temperature	°C
$\vartheta_{ESP_{in}}$	Temperature measured at the inlet of KSVA's ESP	°C
$\vartheta_{ESP_{out}}$	Temperature measured at the outlet of KSVA's ESP	°C
$\vartheta_{i,exist,air/oxy}$	Maximum existence temperature of species i in an air or oxy-fuel fired environment	°C
ϑ_{Lev26}	Temperature measured in the KSVA furnace at level 26	°C
ϑ_{Lev4}	Temperature measured in the KSVA furnace at level 4	°C
$v^*_{CO_2,dos}$	Specific volumetric flow of clean CO_2/recycle gas used for fuel dosing	$\frac{m^3}{kg}$, *STP*

Symbol	Meaning	Unit
$\dot{V}_i$	Volumetric flow rate of component i	$\frac{m^3}{h}$, STP
V_{mol}	Molar volume = 22.414 $\frac{m^3}{kmol}$, STP	$\frac{m^3}{kmol}$, STP
$v_{por,meso}$	Porous volume of pores in the meso-porous size range between 10 and 30 nm	$\frac{cm^3}{g}$
$v_{por,tot}$	Total porous volume in the pore size range between 1.7 and 100 nm	$\frac{cm^3}{g}$
V_{sample}	Volume of sample gas at standard conditions	l, m^3, STP
$x_{i,j}$	Mass fraction of component i in material j	$\frac{kg}{kg}$
ξ_A	Fuel specific ash generation, i.e. ratio of generation of ash over the gravimetric fuel feed	$\frac{g}{g}$, $\frac{kg}{kg}$
$\xi_{byprod,i}$	Fuel specific by-product generation, i.e. ratio of generation of byproduct i over the gravimetric fuel feed (i: $Ca(OH)_2$, $CaCO_3$, $CaCl_2$)	$\frac{g}{g}$, $\frac{kg}{kg}$
$\xi^{SO_2}_{byprod,i}$	SO_2 specific by-product generation, i.e. ratio of generation of byproduct i over the gravimetric SO_2 production (i: $Ca(OH)_2$, $CaCO_3$, $CaCl_2$)	$\frac{g}{g}$, $\frac{kg}{kg}$
ξ_{sorb}	Ratio of gravimetric sorbent and fuel feeds	$\frac{g}{g}$, $\frac{kg}{kg}$
$\xi^{SO_2}_{sorb}$	Ratio of gravimetric sorbent feed and SO_2 production	$\frac{g}{g}$, $\frac{kg}{kg}$
$\xi_{oxy/air,dry}$	Ratio between $y_{SO_2,max,oxy,dry}$ and $y_{SO_2,max,air,dry}$	-
$\xi_{oxy/air,wet}$	Ratio between $y_{SO_2,max,oxy,wet}$ and $y_{SO_2,max,air,wet}$	-
ξ_{rec}	Volumetric/molar flue gas recirculation ratio in oxy-fuel combustion	$\frac{m^3}{m^3}$, $\frac{mol}{mol}$
$y_{i,j,k,l}$	Volume/molar fraction of component i (optional indices: j, k, l)	$\frac{m^3}{m^3}$, $\frac{mol}{mol}$
$y_{leak,dry}$	Volume fraction of ambient air ingressed to the process with respect to the volumetric flow of *dry* flue gas	$\frac{m^3}{m^3}$
$y_{i,lim}$	Legal emission limit concentration for component i (i.e. daily or half hourly average limits)	$\frac{m^3}{m^3}$, $\frac{mol}{mol}$

List of indices

Index	Meaning
A	Index referring to the component ash
air	Index referring to air conditions
$Alkali$	Index denoting the alkali elements Na and K
C	Index referring to the component carbon
$corr$	Index denoting a corrected/recalculated parameter (e.g. gas concentrations that are recalculated with respect to a certain reference O_2 level)
dry	Index referring to dry reference state (e.g. used to describe gas concentrations)
el	Index denoting electric (e.g. electric power)
exc	Index referring to excess properties (i.e. excess O_2)
FG	Index referring to flue gas
$furn$	Index denoting a parameter that is linked to the furnace (e.g. in- and outlet streams)
H	Index referring to the component hydrogen
HCl	Index referring to the component HCl
in	Index denoting a inlet flow
inj	Index denoting an injected component
max	Index denoting theoretical maximum concentrations
$^-$	Superscript bar indicating a mean/average value
N	Index referring to the component nitrogen
*	Index denoting a normalized parameter
O	Index referring to the component oxygen
$o-t$	Index denoting a once-through oxy-fuel parameter within the recycle system (in contrast to an oxy-fuel recycle parameter)
out	Index denoting an outlet flow

Index	Meaning
fil	Index denoting that a parameter refers to values measured at a filter
$a.f.$	Index denoting that a parameter refers to values measured after filter
$b.f.$	Index denoting that a parameter refers to values measured before filter
$blank$	Index denoting a blank value
liq	Index denoting a liquid
$oxid$	Index denoting oxidant gas streams/properties
oxy	Index referring to oxy-fuel conditions
$Probe$	Index referring to the surface of a sampling probe
RC	Index referring to raw coal (also more general raw fuel)
$reac$	Index denoting a reacted component
rec	Index denoting a recycle flow or an oxy-fuel recycle parameter (in contrast to an once-through oxy-fuel parameter; if no specification is given, parameters are generally oxy-fuel recycle ones
ref	Index denoting a reference concentration used as basis to calculate acid gas removal efficiencies in dry sorbent injection experiments
rem	Index denoting a removed flow
S	Index referring to the component sulfur
SO_2	Index referring to the component SO_2; Also used as superscript index of ξ_{sorb} and $\xi_{byprod,i}$ to indicate to which parameter those values are related
SO_3	Index referring to the component SO_3
$Sorb$	Index referring to the sorbent
$byprod$	Index referring to the byproducts (in DSI)
SO_x	Index referring to the component SO_x
$stoic$	Index denoting a parameter referring to stoichiometric combustion conditions (i.e. $n_{air}/n_{O_2} = 1$)
$\dot{}$	Superscript dot indicating a flow/stream
th	Index denoting thermal (e.g. thermal power)
tot	Index denoting a total sum of various parameters
W	Index referring to the component water
$fuel$	Index referring to the fuel
wet	Index referring to wet reference state (e.g. used to describe gas concentrations)

Abstract

This thesis evaluates the behavior of sulfur oxides in pulverized fuel (PF) fired air and oxy-fuel systems. Sulfur oxides are responsible for certain operational problems and considerable gas cleaning requirements in air as well as oxy-fuel firing. A better understanding of the related issues will allow for a technical and economical optimization of the oxy-fuel combustion technology. A range of experimental investigations studying the stability and retention of sulfur oxides in ashes and deposits, acid gas (SO_2, SO_3, and HCl) control in air and oxy-fuel combustion by dry sorbent injection, and SO_3 formation were conducted. The experimental work is in parts supported by theoretical considerations and thermodynamic equilibrium simulation.

Studies for different coals and lignites showed that in practically relevant oxy-fuel configurations the exclusion of airborne N_2 from combustion leads to an increase of the SO_2 concentrations in oxy-fuel, compared to air firing, by a factor of about 3.4 to 4.2, referring to dry, and of about 2.9 to 3.5, when referring to wet flue gas conditions. The increased SO_2 levels in oxy-fuel combustion are responsible for an increased stability of sulfates in oxy-fuel power boiler systems so that for example the decomposition temperature $CaSO_4$ rises by about 50 to 80 °C, depending on flue gas atmospheres. The enhanced stability of sulfates in deposits at high temperatures when operating with increased SO_2 levels was experimentally demonstrated. Compared to air firing, a considerable increase of the sulfur retention in the ash by 10 to 12 percentage points has been observed for oxy-fuel recycle combustion of Lusatian lignites. This leads to lower SO_2 emissions and higher SO_3 levels in process ashes and deposits. The results indicate that for fuels, such as the used lignites, the temperature level at which fouling by sulfatic deposits is problematic may be shifted to higher temperatures in oxy-fuel combustion and that the sintering of deposits by sulfation may be more pronounced. In contrast, in air and oxy-fuel combustion experiments with a hard coal with a low sulfur retention potential differences in the SO_3 contents and degrees of sulfation of ashes and deposits were small. Besides higher SO_3 contents and sulfation degrees, no other significant changes between the deposit samples from air and oxy-fuel combustion were identified. Experiments on dry sorbent injection in air and oxy-fuel mode showed that an increase of the average flue gas residence time in the furnace by flue gas recirculation and, to a lesser extent, the higher sulfate stability enhance the desulfurization efficiency in oxy-fuel recycle combustion considerably. SO_2 capture efficiencies

in oxy-fuel recycle combustion of 50 % to more than 80 % at moderate molar sulfur to calcium ratios between 1.7 and 2.9 were reached, when injecting $CaCO_3$ and $Ca(OH)_2$ together with the fuel or directly to the furnace. Under comparable injection conditions, the oxy-fuel performance was by as much as 29 percentage points higher than in air firing. Also an efficient SO_3 and HCl control by DSI could be demonstrated. Experiments on formation of SO_3 show that higher SO_2 levels in oxy-fuel firing are the most important parameter responsible for the observed increase of the SO_3 concentrations.

Kurzfassung

Diese Arbeit untersucht das Verhalten von Schwefeloxiden in Luft- und Oxy-Fuel-Staubfeuerungen. Bei der Luft- wie auch der Oxy-Fuel-Verbrennung sind Schwefeloxide für bestimmte Betriebsprobleme sowie einen erheblichen Rauchgasreinigungsbedarf verantwortlich. Ein besseres Verständnis von deren Verhalten ermöglicht eine weitergehende technische und wirtschaftliche Optimierung des Oxy-Fuel-Verbrennungsverfahrens. Im Rahmen der Arbeit wurden eine Reihe von experimentellen Untersuchungen zur Stabilität und zur Einbindung von Schwefeloxiden in Aschen und Belägen, zur Bildung von SO_3 und zur Abscheidung der sauren Gase (SO_2, SO_3 und HCl) im Luft- und Oxy-Fuel-Betrieb durchgeführt. Die experimentellen Arbeiten werden teilweise auch durch theoretische Überlegungen und thermodynamische Gleichgewichtssimulationen ergänzt.
Die durchgeführten Untersuchungen mit unterschiedlichen Stein- und Braunkohlen ergaben, dass die SO_2-Konzentrationen in praktisch relevanten Oxy-Fuel-Systemen, aufgrund des bei der Verbrennung fehlenden Luftstickstoffs, um einen Faktor von ca. 3,4 bis 4,2, bezogen auf trockenes und von ca. 2,9 bis 3,5, bezogen auf feuchtes Rauchgas, ansteigen. Die erhöhten SO_2-Gehalte bei der Oxy-Fuel-Verbrennung bewirken je nach Gasatmosphäre eine erhöhte Stabilität von Sulfaten, sodass beispielsweise die Zersetzungstemperatur von $CaSO_4$ um ca. 50 bis 80 °C ansteigt. Die Erhöhung der Sulfatstabilität in Belägen bei hohen Temperaturen, durch erhöhte SO_2-Konzentrationen, wurde experimentell demonstriert. Im Vergleich zur Luftfeuerung, wurde bei der Oxy-Fuel-Verbrennung mit Rauchgasrezirkulation von Lausitzer Braunkohle, eine Erhöhung der Schwefeleinbindung in die Asche um 10 bis 12 Prozentpunkte beobachtet. Die bessere Schwefeleinbindung ist für niedrigere SO_2-Emissionen und höhere SO_3-Gehalte in Aschen und Belägen verantwortlich. Die Ergebnisse deuten darauf hin, dass im Oxy-Fuel-Betrieb bei Brennstoffen wie den verwendeten Braunkohlen das Temperaturniveau, bei welchem die Verschmutzung durch sulfatische Beläge problematisch ist, hin zu höheren Temperaturen verschoben und, dass das Versintern von Belägen durch Sulfatisierung verstärkt ist. Im Gegensatz dazu, waren die Unterschiede, in Bezug auf SO_3-Gehalte und den Grad der Sulfatisierung von Aschen und Belägen aus Luft- und Oxy-Fuel-Verbrennungsversuchen mit einer Steinkohle mit niedrigem Potential zur Schwefeleinbindung, klein. Neben den erhöhten SO_3-Gehalten und Sulfatisierungsgraden, wurden keine weiteren signifikanten Änderungen zwischen den Belagsproben aus Luft- und Oxy-Fuel-Verbrennung beobachtet. Versuche zur

Eindüsung trockener Sorbentien im Luft- und Oxy-Fuel-Betrieb zeigten, dass die Erhöhung der mittleren Rauchgasverweilzeit in der Brennkammer durch die Rauchgasrezirkulation und, zu einem geringeren Anteil, die erhöhte Sulfatstabilität, die Entschwefelungseffizienz im Oxy-Fuel-Betrieb mit Rauchgasrückführung deutlich verbessern. Bei der Eindüsung von $CaCO_3$ und $Ca(OH)_2$ zusammen mit dem Brennstoff oder direkt in die Brennkammer konnten im Oxy-Fuel-Betrieb mit Rauchgasrezirkulation und moderaten molaren Schwefel-zu-Kalzium-Verhältnissen zwischen 1,7 und 2,9, SO_2-Abscheideeffizienzen von 50 % bis zu mehr als 80 % erzielt werden. Dabei war die Abscheideleistung bei vergleichbarer Sorbenseindüsung im Oxy-Fuel-Betrieb um bis zu 29 Prozentpunkte besser als bei konventioneller Luftverbrennung. Auch eine effiziente SO_3- und HCl-Abscheidung mittels Trockensorbenseindüsung konnte demonstriert werden. Versuche zur Bildung von SO_3 zeigen, dass die im Oxy-Fuel-Betrieb erhöhte SO_2-Konzentration der wichtigste Parameter hinsichtlich der Erhöhung der SO_3-Konzentrationen ist.

1 Introduction

1.1 CO_2 capture by oxy-fuel combustion

To reduce the impact of anthropogenic greenhouse gas emissions on the earth's climate, CO_2 capture technologies for thermal power generation have been developed that concentrate the generated CO_2 for processing and subsequent storage or utilization. Oxy-fuel combustion is one of these CO_2 capture technologies. To obtain a concentrated CO_2 rich gas stream, in oxy-fuel operation, the fuel is burned with a mixture of oxygen and recirculated flue gas, instead of air. The mixing of O_2 with recirculated flue gas is, among other issues, necessary to lower the temperature in the furnace, which otherwise would exceed the limits of construction materials of boilers [1].

Oxy-fuel combustion technologies for power plant application have been investigated for approximately two decades. This ultimately led to the construction of several oxy-fuel pilot and demonstration plants [2] (e.g. in Schwarze Pumpe, Germany [3] and in Callide, Australia [4]). These activities can be seen as the result of a first wave of carbon capture and storage (CCS) projects that were initiated several years ago. Unfortunately, in recent years a significant reduction of new projects in the field of CO_2 capture in general and in oxy-fuel combustion in particular could be observed. This is an effect of the reduced availability of funding in many countries, due to the global financial crisis that started in 2007, and in certain countries also a decline in the ambitions of CCS policies. Globally, and particularly in Europe, this has led to the cancellation of a number of CCS demonstration projects that had already reached advanced development stages. It seems that this situation has in addition deteriorated the perception of policy makers in respect to the viability of CCS technologies. This may have further reduced the political drive to foster the application of such technologies [5].

The current status of the implementation of CCS technologies can be related to the targets introduced in the IEA's "2 degree (2DS)" scenario[1] [6]. This is also the maximum tolerable level of increase, according to the international Paris Agreement [7]. To date (December 2019), this agreement has been ratified by 187 parties, including all member states of the EU [8]. According to the 2DS scenario, the total mass of CO_2 that would need to be captured and stored in 2025

[1] This is an energy system pathway with a probability of minimum 50 % of keeping the global temperature increase until 2100 below 2 °C compared to preindustrial temperature levels.

and 2060 is estimated to 400 $\frac{\mathrm{Mt}}{\mathrm{a}}$ and 6.8 $\frac{\mathrm{Gt}}{\mathrm{a}}$, respectively. When this is contrasted versus the mass of CO_2 that was captured and stored in 2017, of somewhat over 30 $\frac{\mathrm{Mt}}{\mathrm{a}}$, the urgency of a rapid deployment of CCS in the power sector and other energy intensive industries becomes evident [6]. It is obvious that an enormous acceleration in the global efforts in respect to the implementation of CCS is necessary to reduce anthropogenic CO_2 emissions and keep the goal of limiting the global warming below 2 °C. The oxy-fuel technology could contribute to a rapid deployment of CCS in the power industry, since the process has been successfully demonstrated. In pilot and demonstration scale, all major challenges of the technology could be controlled. Issues that require further research are mainly related to optimization of the process in respect to component lifetime, operability, availability, flexibility, efficiency, and cost. This thesis focuses on certain aspects of these issues that are related to the behavior of sulfur oxides in the pulverized fuel (PF) fired oxy-fuel process.

1.2 Motivation and objectives of this thesis

Due to a lack of dilution of the flue gas by airborne N_2 in oxy-fuel operation, the concentrations of CO_2, but also of other flue gas components, such as SO_2 and H_2O, increase considerably. From experimental investigations, increases by a factor of around 4, referring to the contents of CO_2 and SO_2 in dry flue gas, have been reported [1, 2, 9, 10]. The increased partial pressure of SO_2 stabilizes sulfates thermodynamically, which leads to a better sulfur capture in ash and deposits and in turn to lower energy based SO_2 emissions [11–17].
A better understanding of the fate of the flue gas impurities SO_2 and SO_3 in oxy-fuel coal combustion is an important issue, since those components impact the power plant process design, construction, and operation in various aspects. Sulfur oxides in gaseous, solid, and liquid forms are known for their corrosivity at high and low temperatures in the boiler, downstream equipment, and in oxy-fuel flue gas recirculation lines, and they play a key role in furnace slagging and in fouling of convective heat exchangers, SCR catalysts, and regenerative gas preheaters. Moreover, sulfates in process ashes may impact the utilization of those byproduct streams. The liquefaction of CO_2 and the subsequent transport of supercritical CO_2 in pipelines require a high degree of removal of SO_2 and SO_3 in upstream unit operations of an oxy-fuel power plant [18]. A sound understanding of the formation and reduction of these flue gas impurities in the oxy-fuel combustion process is therefore crucial for a technically and economically optimal design of an oxy-fuel power plant and its impurity control equipment. The present thesis aims to contribute to this, covering the objectives listed below:

1. Assessment of the expected increase of the SO_2 levels in relevant oxy-fuel configurations, compared to air firing, for different coal qualities and analysis of the impact of this increase on the thermodynamic stability of sulfates in relevant ash systems.

2. Comparative experimental assessment of SO_x retention in deposits and ashes in air and oxy-fuel combustion.

3. Evaluation of the performance of dry sorbent injection (DSI) for SO_x and HCl control in air and oxy-fuel combustion.

4. Assessment of the impact of oxy-fuel combustion on the formation of SO_3.

5. Provision of a broad, comparative, air-versus-oxy-fuel data basis on sulfur retention in ash and deposits, SO_3 formation, and dry sorbent injection performance.

While part of these objectives have been previously studied by others, other aspects have not or only partially been covered. The increase in the SO_2 levels in oxy-fuel, compared to air combustion, has been discussed by others (e.g. [9]). However, such studies did not assess the sensitivity of this increase in respect to important process parameters, such as the oxygen excess, the air ingress, and the required partial cleaning of the primary recycle gas. Also, such studies generally focused on the dry flue gas composition that is relevant in respect to the produced CO_2 quality, but not for the thermodynamic stability of sulfates in oxy-fuel systems. This dissertation covers these aspects. The study on the increase of SO_2 levels in oxy-fuel combustion is linked to a comparative assessment on the impact of the different combustion modes on the thermodynamic stability of sulfates in the ash. Similar investigations have been conducted by others [19, 20], but they only considered one oxidizing combustion atmosphere. In the present thesis, this is extended to wider ranges of oxidizing and reducing flue gas atmospheres that have been assessed, applying a newly developed thermodynamic phase mapping technique. The conducted studies focus in particular on ash systems that were identified to be relevant to the deposit formation when combusting Lusatian lignite. The comparative, experimental, air and oxy-fuel studies of this thesis on the retention of SO_x in furnace and boiler deposits go beyond what has been previously reported by others. Only very few studies managed to obtain comparable samples from both combustion environments (e.g. [21–23]). In this thesis, a significant number of ash and deposit samples from both combustion modes with various fuels is assessed comparatively to identify relevant differences.
Studies on dry sorbent injection for acid gas control in air and oxy-fuel operation were so far either very limited and not comprehensively documented [24], or did only rely on modeling and experiments conducted in small scale, with simulated O_2/CO_2 atmospheres but without flue gas recirculation [11]. In a very recent publication by Liu et al. [25] summarizing the current understanding of SO_2 control by DSI in oxy-fuel combustion, the authors highlight that experimental investigations "concerning desulfurization in O_2/CO_2 combustion have been limited, and many unknowns about in-furnace desulfurization in O_2/CO_2 pulverized coal combustion need to be studied" . Theoretical considerations on the effects of recycle combustion on DSI performance and a comprehensive experimental study in this context that includes

pilot scale DSI experiments in oxy-fuel recycle combustion are part of this thesis. These DSI studies also cover low temperature sorbent injection and control of SO_3 and HCl.
The comparative experimental studies of this dissertation in respect to the formation of SO_3 in air and simulated oxy-fuel combustion, in which the oxidant gas composition and fuels have been purposely altered in order to better understand the impact of these parameters on the SO_3 formation in oxy-fuel combustion, are extending the work by others. Those studied the same issue only in simulations, in small scale laboratory experiments without actual fuel combustion, or without a systematic alteration of the oxy-fuel combustion atmospheres and fuels [26–29].

1.3 Previously published results included in this thesis

During the course of this dissertation project, a number of publications and conference presentations have been prepared that the author of this thesis has authored as the lead or as a co-author. To some extent, these publications have been used as a basis of this thesis. Only text passages thereof that were originally written by the author of this dissertation have been incorporated here. Nonetheless, such text passages have been updated and modified but correspond in parts to the original publications. All experimental data and results that have been previously published have been carefully assessed to ensure that the data evaluation (e.g. reference O_2 levels or the settings to evaluate FTIR spectra) is consistent throughout this thesis. For that reason, the results presented here may slightly deviate from the ones that were published previously. The following paragraph lists those own publications that were incorporated in this thesis.
Parts of the background chapter 2 are based on the respective sections of a comprehensive review paper on oxy-fuel combustion in power production [2], on a book chapter on SO_x mitigation technologies for combustion systems [30], and on a report on the state of the art in science and technology in respect to dry sorbent injection technologies [31]. Moreover, also previously published text passages and results by the author of this thesis from other own publications on impurities and especially on the SO_x emission behavior and control by DSI [32–39], and the behavior of ashes and deposits [40–43] in air and oxy-fuel combustion are included in the background, methodology, and results chapters and the annex of this thesis. Part of the descriptions in the methodology chapter are based on the respective sections of papers on mercury emissions and removal in oxy-fuel combustion [35, 44]. The experiments described in these papers were the same as the ones on SO_3 formation included in this thesis. All publications mentioned above, with the exception of [2, 30, 43], were produced and submitted by the author of this thesis as lead author that conducted the bulk of the work of these publications with support mainly in the execution of experiments and the analysis of samples. Publications [2, 30, 43] were led by other authors with significant contribution and full responsibility for certain parts or sections of the work by the author of this thesis. Only these sections were used

as a basis for this dissertation.
Besides the publications mentioned above, students have supported the conduction of experiments and evaluation of results included in this dissertation in the framework of their student theses [45–52]. These theses were conducted under the supervision of, and in close cooperation with the author of this dissertation and part of the results and data that was reported therein are also used within this thesis. All results previously included in such student theses were carefully assessed and the corresponding data has been re-evaluated for this dissertation so that the results evaluation is done in a consistent manner throughout the thesis.

2 Background

This chapter aims to introduce fundamentals of key processes of relevance to this thesis with a focus on the fuel and flue gas side (i.e. PF, dry bottom, air and oxy-fuel combustion). In addition, a comprehensive overview on the formation and retention of sulfur oxides (SO_x) in ashes and their control, with a special focus on oxy-fuel operation, is given. Also, information on the sulfur oxide and hydrochloric acid (HCl) control by dry sorbent injection (DSI) is included. More detailed information on topics that are only briefly covered can be found in text books on power plant technology and combustion, such as the one by Spliethoff [53], and in review papers (e.g. oxy-fuel: [2, 54]; ashes/deposits: [55, 56]; DSI: [57, 58]).

2.1 Pulverized fuel (PF) combustion

2.1.1 Introduction to PF combustion in power plants

In steam power plants, electric power and in certain cases steam is produced. Combined heat and power plants produce heat in addition. In steam power plants fired with coal and other fuels the fuel is combusted with oxygen from the combustion air to release its latent heat generating hot flue gases. This heat is then transfered convectively and by radiation to steam that is the working fluid of the power plant's steam cycle process. The generated steam drives a steam turbine that converts its thermal energy into mechanical energy that is transferred to a generator, which finally produces electrical energy. Each of these energy conversion steps is subject to energy losses, the majority of which are related to the steam cycle that requires condensation of steam. The released heat needs to be rejected by a cooling system if it cannot be used otherwise. In addition to that, significant losses occur in the steam generator, mainly, due to the non-recoverable heat of the flue gases leaving the steam boiler and, due to the power plant's consumption of auxiliary power [53].
Steam power plants can be driven by the combustion of pulverized coal and lignite, which is one of the most common, and in case of modern plant layouts, one of the most efficient forms of heat provision from solid fuels. Large hard coal fired plants built recently in Germany reach overall electrical efficiencies of up to about 46 % [59, 60]. Power plants operated with raw lignite are, due to the higher moisture content of the fuel, less efficient, with the best plant

in Germany reaching just above 43 % [61]. Such high efficiencies have been accomplished by continuous improvement of the power plant design over decades. While coal fired power plants in the late 1980s reached efficiencies somewhat below 40 %, the efficiency gain since then is to a large extent accomplished by increasing the power plant's steam conditions up to maximum pressures of about 270 bar and temperatures of the superheated and reheated steam of around 600 °C, or slightly above. The increase of the steam conditions went along with an increase of the size of individual power plant blocks that reach now up to about 1100 MW in Europe and up to about 1300 MW in the USA [53].

2.1.2 Fundamentals of fuel conversion in PF power plants

Solid fuels contain moisture, combustibles, and ash forming components. The combustion of fuels with air in PF fired systems involves the drying that generally starts already during the fuel milling. After the injection of the pulverized fuel to the furnace (particle sizes are typically below 100 to 200 µm), the particles heat up rapidly (with heating rates in the range of 10^4 to 10^6 $\frac{K}{s}$). In the furnace they undergo the completion of their drying and to some extent in parallel a pyrolysis, in which the volatile fraction of the fuel (i.e. hydrocarbons) is released in form of gaseous products. This is followed by the ignition of the released volatiles (at temperatures of 500 to 700 °C), their combustion, and finally the combustion of the residual char. In PF combustion, drying and pyrolysis take place in under 0.1 s and volatiles combustion essentially occurs instantaneously at the rate of their release. The heterogeneous char combustion requires another 1 to 2 s. This time requirement is governing the furnace dimensions that are necessary to provide a sufficient residence time for a complete combustion before flue gases reach convective heat exchangers. The main products that are formed when oxidizing the combustibles of the fuel are CO_2 and H_2O [53, 56].

During combustion of the fuel also a range of pollutants are formed, the most important of which are carbon monoxide (CO), nitrogen oxides (NO_x), SO_x, and particulate matter. The impurities can be categorized in products of incomplete combustion, such as CO, hydrocarbons and soot, and products formed from impurities contained in the fuel, such as SO_x, mercury, and chlorine compounds. The bulk of particulate matter formed in coal combustion originates from the ash minerals in the fuel. NO_x formed in combustion processes can originate from nitrogen, contained in the fuel and in the combustion air, via different formation pathways (i.e. thermal, fuel, and prompt NO_x formation) [53].

2.1.3 Typical process configuration of conventional PF power plants

Figure 2.1 shows schematically the typical layout of a conventional, dry ash removal, pulverized hard coal power plant with the steam generator and systems for flue cleaning as they are found in plants in Western Europe. The coal is milled and in parallel dried by preheated air (300 to

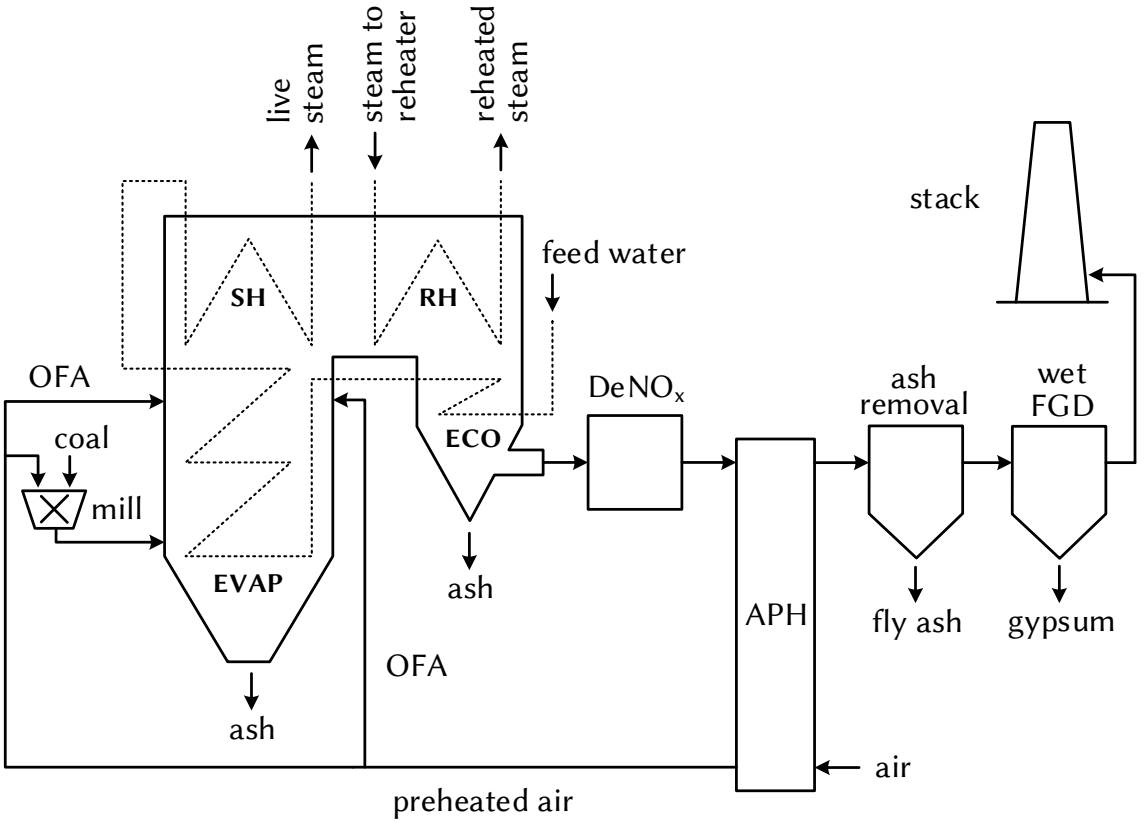

Figure 2.1: Schematic of a conventional pulverized coal power plant (APH: Air preheater; OFA: Over fire air; ECO: Economizer; $DeNO_x$: Selective catalytic NO_x reduction unit; FGD: Flue gas desulfurization; EVAP: Evaporator; RH: Reheater; SH: Superheater).

400 °C), or in case of raw lignite boilers, by recirculated flue gas (approx. 1100 °C) that is fed to the mill and is also used to pneumatically transport the coal dust to the burners. Multiple burners are arranged at furnace walls or corners in various arrangements. In the furnace, the coal is burned with preheated combustion air, producing ash and hot flue gases at peak temperatures in the range of 1400 to 1600 °C in hard coal fired plants and somewhat lower for raw lignite fired systems. For complete combustion of the fuel, preheated secondary air, and in case of air-staging for primary NO_x reduction, tertiary over-fire air is added. The hot flue gases and particles heat the furnace walls that represent the evaporator of a steam cycle, mainly by radiation. In the evaporator, liquid demineralized boiler feed water is evaporated. In that way, flue gases are cooled down to reach furnace outlet temperatures of around 1100 to 1300 °C in hard coal fired systems. For lignites, they range from about 950 to 1100 °C. The furnace is designed to achieve stable ignition, complete burnout, and, as far as possible, to prevent slagging and corrosion of the furnace walls, and slagging, fouling, and corrosion of convective heat exchangers. After the furnace, flue gases enter the convective heat transfer section of a boiler. These heat exchangers are arranged so that flue gases with the highest temperature, directly after the furnace, are used for superheating of high pressure steam which is then directed to the high pressure turbine. Colder flue gases after the superheater are used for

reheating of medium pressure steam that is fed to the reheater from the high pressure turbine outlet. The reheater is followed by the economizer which is used for preheating the boiler feed water before it enters the evaporator. The economizer cools the flue gases from about 450 °C to about 350 °C. The feed water fed to the economizer is preheated to a temperature of 200 to 300 °C with steam extracted from the turbine, to maintain the economizer outer wall temperature at a level that securely prevents condensation of acids and moisture. The high pressure superheated steam pipework is, beside the turbine, one of the most stressed systems of a power plant. In conventional power plants, it is usually designed for a service life of 200 000 h. The heat exchangers in power plants can be arranged in a one- or two-pass construction, with certain advantages of both designs depending on fuel and site specific conditions [53]. Exemplary, a two-pass boiler construction is shown in figure 2.1.
The power plant's boiler is followed by units that control impurities in the flue gas, such as dust, NO_x, and SO_x, to tolerable levels, according to the emission regulations. A typical flue gas cleaning system in a Western European PF power plant involves a secondary NO_x control system (i.e. a selective catalytic NO_x reduction - SCR - unit) in hard coal fired plants. Lignite fired systems were so far able to maintain their legal NO_x emission limits by primary measures, such as flue gas recirculation, and air staging (also applied in form of low NO_x burners). The SCR process requires temperatures in the range of 300 to 350 °C, which is the reason for its common placement in a high dust arrangement, directly after the economizer, but before the air preheater and the fly ash separation system. The air preheater recovers part of the heat contained in the hot flue gases leaving the SCR reactor to preheat the combustion air. In that way, flue gases are cooled to about 130 °C. For ash separation, fabric filters and electrostatic precipitators (ESP) are available, with ESP systems being the most common system in large European PF boilers, due to the favorable ash resistivities of the used fuels. Besides the fly ash (approx. 80-90 % of the ash) that is produced at the ash removal unit, in addition, bottom ash (approx. 10-20 % of the ash) is generated at the boiler. The final flue gas cleaning stage is a wet scrubber that removes SO_2 and other acid gases, using a limestone slurry as absorption liquid. In this wet system, flue gases cool to about 45 to 50 °C and gypsum is produced as a by-product. After the FGD, flue gases are fed to the stack. In modern plants that use evaporative cooling towers, often, no dedicated stack is used, but flue gases are fed to the cooling tower and are released together with evaporated water [53].

2.1.4 Ashes and deposits in PF power plants

Ash formation: Ash that is formed in combustion of coal, originates from minerals and inorganic elements contained in the fuel. Minerals may be present in the fuel in form of distinct mineral particles, separate to the coal particles (i.e. excluded minerals, such as sand), in form of salts, dissolved in the fuel moisture, and in form of minerals that are finely dispersed in the coal (i.e. included minerals, such as pyrite) [56]. In addition, inorganic elements may be organically

bound in the coal matrix (e.g. alkalis and earth alkalis: potassium, sodium, magnesium, calcium) [53, 55]. Typical elements that make up for the bulk of coal ashes from PF fired systems are aluminum, calcium, iron, potassium, magnesium, manganese, phosphorous, silicon, sulfur, and titanium.
During combustion, minerals and inorganic matter undergo transformations, such as fragmentation, melting, coalescence, evaporation, condensation, and agglomeration that ultimately form the ash particles. The formation of individual ash particles is linked to the composition and hence, to the properties of the different inorganic matter compounds contained in the fuel (e.g. their melting and evaporation temperatures). In addition, it is governed by the local conditions in the furnace (oxidizing/reducing conditions, temperatures). The different mechanisms involved in ash formation influence the size of the formed ashes, with ash formed by fragmentation, melting, fusion, and agglomeration, typically reaching sizes of 1 to 20 µm and such formed by evaporation and condensation, yielding very fine ashes in the range of 0.02 to 0.2 µm. Usually, the ash forming elements in a fuel are not homogeneously distributed, and hence, also the ash that is formed consists of various classes of ash particles [53, 56].

Ash deposits in the boiler: Fly ash that is formed in the furnace, is entrained by the flue gases and transported together with vaporized inorganic compounds through the boiler and its radiative and convective heat exchangers. As highlighted before, one challenge in furnace design is to ensure sufficient residence times and temperatures for a complete fuel burnout. Another limitation is, to avoid considerable melting/softening of the ash, which would cause excessive formation of deposits on the heat exchangers. Usually deposition phenomena in boilers can be categorized in slagging, which occurs in the furnace or close to the furnace exit by formation of liquid deposits, and fouling, which relates to deposition of solid ash particles that can be loosely attached or partially sintered. The formation of deposits on heat exchangers is problematic, due to their detrimental effect on the heat transfer from flue gas to steam. The reason for this is their low thermal conductivity. Moreover, they can block the flue gas path, which reduces convection at certain parts of the heat exchangers, and also increases the pressure drop of a boiler. Other problematic issues involve damages by large dropping deposit pieces and corrosion phenomena that are caused by interactions between heat exchanger materials, deposits, and the flue gas atmosphere. Most relevant to high temperature corrosion in the boiler are mechanisms that involve reactions with chlorine (HCl and alkali salts) and sulfur (alkali iron and alkali aluminum sulfates). It is possible to clean a boiler to certain extents from deposits by soot blowing (i.e. cleaning with an air or steam blast) and other techniques. Generally, deposits formed by fouling can be easier removed by such measures, compared to more heavily fused slagging deposits. However, over time also those can become more sintered and hence, more difficult to remove. Combustion engineering measures to reduce slagging and fouling in boilers involve lowering and homogenizing furnace temperatures to reduce ash

melting and vaporization. In addition, the boiler design can be adapted to consider problematic properties of the fuel, e.g. by a reduction of the furnace outlet temperature or an adaption of the spacing and arrangement of convective heat exchanger tubes [53, 55, 56, 62].
The formation of deposits on heat exchanger tubes is governed by the composition and the particle size of fly ash and the local temperature and velocity of the flue gas as well as the flue gas composition. It requires the transport of a particle to a tube, the penetration of the particle through the boundary layer around the tube, and its final deposition on the tube surface by forces that keep the particle attached to the tube (e.g. Van der Waals forces, surface tension or friction). Transportation of ash to boiler tubes can occur by a range of mechanisms: Inertial impaction happens to large ash particles (> 10 µm) that, due to their inertia, cannot follow the flow of flue gases around a heat exchanger pipe and hence, impact the pipe. It is often reported to be the dominant deposition mechanism in terms of weight gain if the tube surface is sticky enough so that particles hitting the tube are not re-entrained. Another deposition mechanism is governed by thermophoresis. This term describes the diffusional transport of fine particles (i.e. in the range of about 0.1 to 10 µm) from hot to colder temperatures, due to the temperature gradient in the surrounding environment. A third important mechanism is due to diffusion of inorganic compounds in vapor phase towards a heat exchanger pipe along a concentration gradient followed by condensation or chemical reaction of the vapor on the tube surface. The condensation and reactions reduce the gas phase concentration of the compound at the tube surface and therefore, maintains the concentration gradient. Due to their low condensation temperatures, this mechanism is most important to alkali compounds (e.g. KCl, NaCl, K_2SO_4, Na_2SO_4). An important chemical reaction to bind gas phase compounds on the surface is sulfation. Chemical reactions between deposited material and vapor phase compounds can lead to transformations in the deposits to form melts (e.g. low temperature eutectics of sodium, iron, calcium, etc.) that increase the stickiness of the surface for other particles or induce the sintering of deposited ashes, e.g. by formation of sulfates. Other deposition mechanisms that have been reported are “eddy impaction”, caused by eddy currents in the vicinity of pipes that accelerate small particles, so that they can impact through the boundary layer around a tube, or electrophoresis that happens due to an electric field affecting ash particles [53, 55, 56, 62].
The buildup of a deposit on a superheater tube is assumed to proceed in different stages. Firstly, a relatively clean tube develops an initial deposit layer. For the buildup of this initial deposit layer, condensation and thermophoresis play an important role, since the pipe is originally clean, relatively cold, and not sticky. Molten or partly molten particles approaching such a clean tube by their inertia cool rapidly and often solidify before their impact. Since the surface of a clean tube is not sticky, the particles have a low probability to adhere to it and may instead bounce back. When the initial deposit layer grows, its outer surface temperature rises and becomes eventually more and more sticky, once it exceeds melting temperatures of certain ash compounds. Once a tube has developed such a sticky outer surface, the contribution

of ash deposition by inertial impaction becomes more important compared to condensation and thermophoresis. This can be explained by a significantly higher probability of larger ash particles to adhere to a sticky tube compared to a clean one. With rising surface temperature of the outer deposit surface, it can become more and more molten and more sticky. In that way fully liquid deposits can form, e.g. on superheater tubes [53, 55, 56, 62].

Ash utilization: Ashes from PF combustion can be utilized as long as their composition and properties fulfill requirements, defined in standards for certain applications. One of the most common (i.e. about 75 % of the ashes from hard coal firing are utilized in that way) and economically most attractive fly ash utilization routes, is the utilization in concrete production. For this application, the fly ash needs to comply with standard EN 450 [63]. Ashes need to have a siliceous character (sum of the contents of SiO_2, Al_2O_3 and Fe_2O_3 > $70 \cdot 10^{-2}$ $\frac{kg}{kg}$), with pozzolanic properties[2], and a suitable hardening behavior and strength of the produced concrete material. Certain chemical[3] and physical properties are set as prerequisites for fly ash utilization according to EN 450. Suitable ash qualities can replace cement in the production of concrete, which explains their relatively high value. Lignite ashes do in most instances not conform to standard EN 450, due to their calcareous character (high CaO and SO_3 contents). Most of the lignite ashes are used in open pit lignite mines for backfilling or landscaping activities. Ashes that do not fulfill EN 450 (application in concrete production) may be used in production of cement if they comply with standard EN 197 [64]. This standard allows for blending of fly ashes with siliceous and calcareous character together with cement clinker in ratios of 6 to $35 \cdot 10^{-2}$ $\frac{kg}{kg}$, to produce different cement qualities. The requirements of EN 197 are somewhat less stringent than those of EN 450. For example, depending on the cement class to be produced, the sulfate content (expressed as SO_3) can be up to $4 \cdot 10^{-2}$ $\frac{kg}{kg}$. Other lower value fly ash utilization routes include application as hydraulic road binders, fillers, base materials for mortar and brick production, additives for soil improvement, and others [53, 63, 64].

2.1.5 Introduction to the oxy-fuel combustion technology

Oxy-fuel combustion is a process in which a fuel is combusted in a mixture of oxygen and recirculated flue gas, instead of air. One characteristic of the oxy-fuel technology is that, due to the exclusion of airborne nitrogen from combustion, in its flue gas the concentrations of CO_2, but also of other flue gas components, such as SO_2 and H_2O, are increased. The NO_x formation is also altered being affected by O_2 injection conditions, burner configuration, and airborne N_2 exclusion from the combustion [2, 65].

The changes in the flue gas composition in oxy-fuel combustion have certain impacts on the

[2]The ability to from calcium silicate hydrates at room temperature, similarly to cement.

[3]E.g. loss on ignition for category A fly ash below $5 \cdot 10^{-2}$ $\frac{kg}{kg}$, content of SO_3 below $3 \cdot 10^{-2}$ $\frac{kg}{kg}$, content of Cl below $0.1 \cdot 10^{-2}$ $\frac{kg}{kg}$, content of reactive CaO below $10 \cdot 10^{-2}$ $\frac{kg}{kg}$)

fuel conversion and heat transfer in the boiler. Fuel pyrolysis and char burnout reactions are affected by higher CO_2 and H_2O levels. In addition, higher oxidant O_2 levels that are often used in oxy-fuel, compared to air combustion, affect the fuel conversion [2]. A significant difference between air and oxy-fuel combustion is due to the different thermodynamic properties of the CO_2 and H_2O rich oxy-fuel flue gas and the N_2 rich flue gas in air firing, with considerably higher heat capacities and emissivities of the oxy-fuel flue gas [66]. On basis of these changed properties, also the adiabatic flame temperature and the radiative and convective heat transfer change. However, the oxy-fuel technology allows to tune the heat transfer by adjusting the flue gas recirculation ratio and thereby the O_2 level in the oxidant gas and the flue gas flow rate through the boiler. On that basis, oxy-fuel process parameters can be selected that allow for similar heat transfer characteristics in the boiler as in air firing. Depending on the fuel and the recycle configuration (dry/wet), an oxidant O_2 level in the range of about 27 to $28 \cdot 10^{-2} \frac{m^3}{m^3}$, wet reaches such conditions [2, 10]. Since, due to the increased oxidant O_2 level, the flue gas production is reduced in oxy-fuel, compared to air firing, the residence time of the flue gases in a furnace and boiler of the same size is higher in oxy-fuel combustion.
The PF oxy-fuel combustion technology has been developed rapidly in the past years with a number of industrial pilot and demonstration projects that were conducted successfully. These include Vattenfall's 30 MW (thermal) [3], CIUDEN's 20 MW (thermal) [67], and HUST's 35 MW (thermal) [68] pilot plants in Germany, Spain, and China, and CS Energy's 30 MW (electric) [4] demonstration project. These projects have demonstrated the oxy-fuel technology's feasibility with thousands of operational hours and provided a comprehensive understanding of its performance. For example, at Vattenfall's pilot plant, CO_2 purities over $95 \cdot 10^{-2} \frac{m^3}{m^3}$, dry and an CO_2 overall removal ratio of 92 % were reached [69].

2.1.6 Detailed discussion of the oxy-fuel PF process

PF oxy-fuel power plant process configurations: In oxy-fuel combustion usually between about 60 and $80 \cdot 10^{-2} \frac{m^3}{m^3}$, wet of the flue gas is recirculated to the boiler together with the fuel and oxygen from an air separation unit (ASU) [70–76]. Compared to an air fired system, an oxy-fuel power plant has a considerably lower electrical efficiency, which is mainly due to the high energy consumption of the ASU for O_2 provision and the CO_2 processing unit (CPU). A recent study by Babcock & Wilcox [77] states that with not fully optimized integration of the oxy-fuel power plant system that is expected in retrofit applications, an efficiency penalty of around 10-11 percentage points (on GCV basis) can be expected. With optimal integration, this could be reduced to about 6-7 percentage points (on GCV basis). Other studies focusing on newly built oxy-fuel power plants report energy penalties of about 10 % (on NCV basis) for non-optimized systems and around 7.5 % (on NCV basis) for an optimized system [66].
There are a number of different configurations possible to include gas cleaning units in the oxy-fuel system with three basic design concepts that have received greater attention by industries

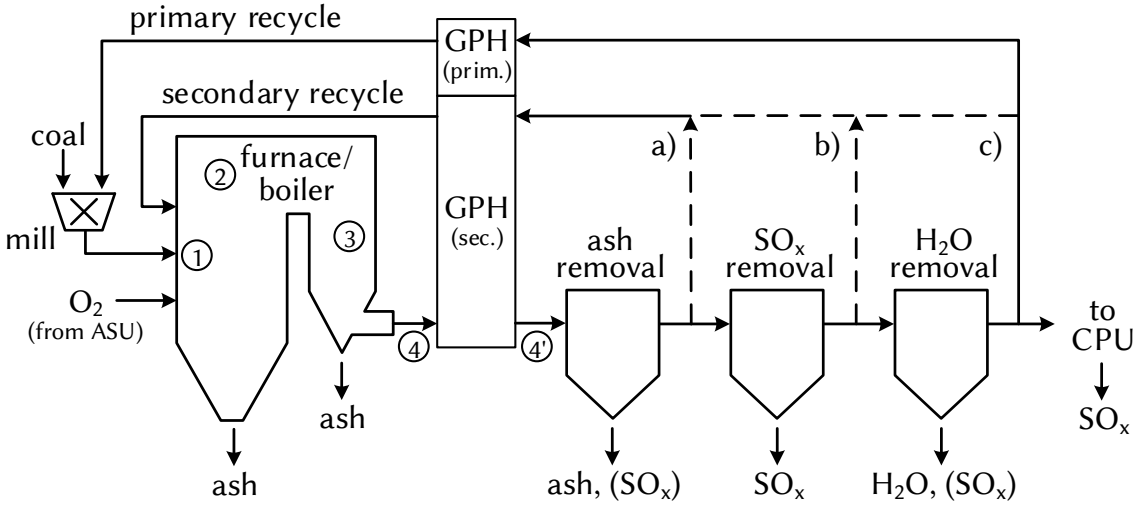

Figure 2.2: Schematic of an oxy-fuel PF power plant: a), b), and c) show various recycle options; numbers 1, 2, 3, 4, and 4´ show possible locations for dry sorbent injection (DSI).

and researchers [44, 75, 78–81]. Those are included in figure 2.2 that shows the oxy-fuel process schematically with (a) flue gas recirculation after ash removal, (b) flue gas recirculation after SO_x removal, and (c) flue gas recirculation after moisture removal.

Removal of ash before recirculation of flue gases can be considered essential in order to avoid extremely high ash concentrations in the process that would lead to problems, due to erosion and fouling. Therefore, the recirculation after the removal of particulates in a fabric filter or ESP (a) can be considered as the "dirtiest" of the practically relevant flue gas recirculation configurations. Even though filters and ESPs can remove impurities other than ash (e.g. SO_3 [38, 44, 82]), a large part of the sulfur in the flue gas as well as the moisture is recirculated to the boiler in this configuration. This leads to relatively high levels of SO_2 and H_2O in the furnace. Depending on the sulfur retention potential of the ash (i.e. the calcium, magnesium, potassium, and sodium content), high SO_x levels in the oxy-fuel recycle system without SO_x removal can also lead to a more efficient sulfur retention in the ash and therefore, higher sulfur levels in the ash which may have negative implications on ash utilization [41, 42]. In configuration a), $DeSO_x$ and H_2O removal units can be designed much smaller than in the other configurations, since they handle only the flue gas stream exiting the oxy-fuel recycle loop. This stream is considerably smaller than the gas stream within the recycle loop and, due to the absence of airborne N_2, corresponds to only about one fifth of the flue gas flow of a comparable air fired combustor. This is fundamentally different in process configurations b) and c), where SO_x (b) and SO_x and moisture (c) are removed from the recirculated flue gas. The larger gas stream that is to be handled in the respective gas cleaning equipment requires larger unit sizes and therefore, higher investment costs. On the other hand, the separation of SO_x within the recycle leads to much lower SO_x levels in the boiler which is desirable in respect to boiler fouling and corrosion and can also minimize problems associated with low temperature acid corrosion in

the recycle lines. In addition, it may be beneficial for an oxy-fuel power plant to be capable to keep the legal emission limits during conventional air fired operation periods. This may, for example, be required during start-up and shut-down. Due to the much smaller design of a gas cleaning system in process configuration a) the system may not be capable to keep the legal emission limits (e.g. for SO_x). Configuration b) may provide additional flexibility in that context. If H_2O is removed from the recycled gas, also water concentrations in the boiler are decreased. Water makes up for a large part of the flue gas in an uncleaned recycle configuration (i.e. system a), with reported oxy-fuel H_2O concentrations of up to $28 \cdot 10^{-2}$ $\frac{m^3}{m^3}$, wet in pre-dried lignite combustion [36]. A removal of H_2O within the recycle can reduce the water concentration in the boiler by a factor of approx. 4-5. However, the removal of H_2O from the flue gas that is done by cooling and condensation, leads to much lower temperatures of the recirculated gas. Due to flue gas cooling, low temperature heat is generated that is difficult to utilize and hence, often is lost. A similar effect is observed with the application of a wet FGD system that is also related to excessive flue gas cooling and therefore, an energy penalty.

The selection of a recycle configuration for an oxy-fuel power plant depends to a large extent on the sulfur content of the combusted coal [66]. McDonald [80] and Lockwood [66] discussed different process configurations that are suitable for low, medium, and high sulfur coals. They concluded that for low sulfur coals, recirculation after particulates removal (system a), for medium sulfur coals recirculation after a desulfurization step (system b), and for high sulfur coals, recirculation after desulfurization and moisture removal (system c), would be most suitable. For the final design of the Futuregen 2.0[4] 90 MW (electric, net) oxy-fuel fired power plant that was planned to use a medium sulfur coal blend, configuration b) with a circulating dry scrubber (CDS) for desulfurization was foreseen [77]. A partial desulfurization by DSI may also allow the application of higher sulfur fuels in configuration a).

Stakeholders from research and industry generally agree that, in all relevant oxy-fuel recycle configurations, the recirculated flue gas that is fed to the mills for coal drying and conveying (i.e. the primary recycle gas) needs to be desulfurized, dried, and reheated [73, 74, 80, 81, 83]. Drying and reheating of the recirculated gas is necessary, so that the gas is capable to dry the coal. The desulfurization of the gas should be done in order to avoid SO_3 or SO_2 induced low temperature corrosion in the recycle lines and mills that would occur if temperatures drop below the sulfuric acid or water dew point, respectively [80].

Since recycled NO_x is reburned efficiently when passing the flame zone [17, 65], the recirculation of NO_x poses no critical operational problems to the oxy-fuel combustion process and hence, NO_x reduction units (i.e. SNCR, SCR) are not strictly needed in an oxy-fuel recycle loop. However, in industrial practice, an oxy-fuel power plant would possibly be operating with conventional air firing during certain periods, such as start-up and shut-down. Depending on

[4]The FutureGen 2.0 oxy-fuel project has been stopped just before starting construction in 2015, due to a lack in public co-funding.

the local emission regulations, it may be necessary for an oxy-fuel power plant to have flue gas cleaning equipment, such as SCR, SNCR, and wet FGD, available in order to keep emission limits during air fired operation. Different regulatory situations in various countries are to some degree reflected in the actual or planned designs of oxy-fuel pilot and demonstration plants. For example, in Australian (CS Energy's 'Callide' project [81]) or US oxy-fuel projects (FutureGen 2.0 designs [77, 80]) no SCR system was included, while in European projects, SCR systems were foreseen as an option (e.g. Vattenfall's oxy-fuel pilot plant "Schwarze Pumpe" [84]; Design of Vattenfall's oxy-fuel demonstration project [85]) or plants have been built with a fully operational SCR system, such as CIUDEN's 20 MW (thermal) oxy-fuel system [86].
An important part of the design of an oxy-fuel recycle system is the addition of oxygen to the process. Even though, explosion hazards in $21/79 \cdot 10^{-2}\ \frac{m^3}{m^3}$, dry mixtures of O_2 and N_2 (i.e. air) and O_2 and CO_2 (i.e. oxy-fuel) are comparable, the addition of O_2 to the primary gas poses a general risk of increased O_2 concentrations in this gas stream in events, such as mill start-up and shut-down, and failures of equipment, such as the recycle gas fan [87]. Therefore, in practical systems no O_2 is added to the primary gas, supplied to the mills. It should however be noted that the primary recycle gas does contain few percent of O_2 that originate from the O_2 excess of combustion. Instead, O_2 can either be added to the secondary recycle gas or it can be directly injected to the furnace via pure O_2 annuli or lances of the burner. Moreover, a hybrid operation with partial O_2 premixing to the secondary recycle and additional direct O_2 injection via the burner is possible [2, 88–90]. The direct O_2 injection and the hybrid injection showed positive effects on the combustion behavior in pilot tests by Vattenfall [88].

Factors affecting the purity of the generated CO_2: The product of the oxy-fuel combustion process is a CO_2 rich flue gas stream that is subsequently cleaned and liquefied for transport and storage. To reduce the energy requirement for CO_2 compression and liquefaction, high CO_2 purities of the oxy-fuel flue gas are desirable [91]. This purity depends on the extent of air ingress, the oxygen excess in combustion, and the purity of the used oxygen. Depending on these factors, the recirculated flue gas after drying may contain around 5-30 % of the ballast gases O_2, N_2, and Ar [69, 85, 88, 89, 92–94]. In addition, impurities, such as CO, NO_x, SO_x, and mercury that origin from the fuel or its combustion are present in the oxy-fuel flue gas, but their concentrations are usually much lower. Nonetheless, these components are problematic, due to their corrosivity, so that they need to be removed.
One measure to obtain high CO_2 purities in the oxy-fuel combustion process is the application of highly pure O_2 (i.e. $99.5 \cdot 10^{-2}\ \frac{m^3}{m^3}$, dry). However, in future commercial oxy-fuel projects an economic optimum for oxygen purity from the ASU is around $95 \cdot 10^{-2}\ \frac{m^3}{m^3}$, dry [85, 88]. The approx. $5 \cdot 10^{-2}\ \frac{m^3}{m^3}$,dry of N_2 and Ar that are supplied with the O_2 feed will lead to an increase on the ballast gas in the flue gas in a similar order of magnitude. The ingress of air to an oxy-fuel combustion process is another source of ballast gas that can lead to a considerable

contamination of the CO_2 purity and therefore, an increased energy requirement for CO_2 purification [91]. Since N_2 from air leakage accumulates in the recycle loop, even small leaks with only little air ingress can lead to a considerable flue gas contamination [88, 92, 95]. Another source of dilution of the CO_2 purity is O_2 that originates from the operation of the combustion process with excess oxygen. To achieve a high burnout and low CO concentrations in the flue gas, O_2 needs to be supplied in excess to balance imperfect mixing in the furnace. This implies that CO_2 contamination by few percentage points of excess oxygen cannot be avoided in oxy-fuel combustion processes. In Vattenfall's oxy-fuel pilot plant "Schwarze Pumpe" stoichiometric ratios of combustion between approx. 1.1 and 1.2 were necessary to avoid excessive CO generation [89]. A difference between air and oxy-fuel combustion is that different oxidant O_2 concentrations imply different excess O_2 concentrations to reach the same combustion stoichiometry (see also section 4.2.1.4). Higher oxidant O_2 concentrations that are equivalent to low flue gas recirculation ratios are desirable to reduce gas streams in the process and therefore, plant dimensions and auxiliary fan power. On the other hand, at high oxidant O_2 concentrations, a complete combustion of the fuel without generation of high CO concentrations requires considerably higher excess O_2 concentration levels [88] and therefore, leads to increased contamination of the CO_2 rich flue gas by O_2. This problem can be counterbalanced by an enhancement of the oxy-fuel firing system so that it can be reliably operated at a stoichiometry lower than the ones applied in conventional air fired systems. For example, after optimization, Vattenfall's oxy-fuel pilot plant "Schwarze Pumpe" could be successfully operated with $2.5 \cdot 10^{-2}\ \frac{m^3}{m^3}$, wet excess O_2 at an oxidant O_2 concentration of $31 \cdot 10^{-2}\ \frac{m^3}{m^3}$, wet (i.e. $n_{O_2,loc} \approx 1.1$) [88].
The flue gas that leaves the oxy-fuel recycle loop is fed to a CO_2 processing unit. In this system, it is compressed and impurities, such as H_2O, NO_x, SO_x, and mercury, are removed according to the requirements of the CPU system and the downstream handling (i.e. pipeline transport, geological storage, or CO_2 utilization). A removal of part of the impurities before compression (i.e. in the low pressure oxy-fuel system) may be mandatory or economic (e.g. the bulk of SO_x and H_2O). The cleaned and compressed CO_2 rich stream is finally liquefied in the CPU. Ballast gases that cannot be liquefied in the CO_2 liquefaction system need to be vented.

2.2 Formation and impacts of sulfur oxides in PF boilers

2.2.1 Sulfur, alkalis, and earth alkalis in fuels

Sulfur in coal and lignite: Fossil fuels contain sulfur in various forms, such as sulfides (especially pyrite: FeS_2), sulfates (e.g. $CaSO_4$), as organically bound sulfur, and to a small portion as elemental sulfur. The sulfur content of coals varies significantly [53, 96]. Central

European lignites contain between 0.2 up to about $5 \cdot 10^{-2}\ \frac{kg}{kg}$ of sulfur[5] [96]. In hard coals, sulfur levels up to $11 \cdot 10^{-2}\ \frac{kg}{kg}$[6] have been reported [97], even though contents in coals used in Western European power plants are often much lower. Coals can be categorized in low sulfur ($\gamma_S < 1 \cdot 10^{-2}\ \frac{kg}{kg}$), medium sulfur ($1 \cdot 10^{-2}\ \frac{kg}{kg} < \gamma_S < 3 \cdot 10^{-2}\ \frac{kg}{kg}$), and high sulfur coals ($\gamma_S > 3 \cdot 10^{-2}\ \frac{kg}{kg}$)[7] [97]. Due to the costs for gas cleaning and other issues related to the sulfur contained in coals, the prices for higher sulfur coals are lower than those for low sulfur coals. Coals imported to Europe usually are from the low and medium sulfur category. The form in which sulfur is present in coals is influenced by the coalification degree, with younger coals and lignites showing higher contents of sulfur in organic form or in form of sulfates. Generally, the bulk of the sulfur in fuels is present as pyrite and organically bound sulfur [53, 97].

Alkalis and earth alkalis in coal and lignite ash: Besides other elements, coals contain alkalis and earth alkalis (most importantly potassium, sodium, calcium, magnesium) that can react with sulfur in the furnace and downstream equipment. These elements can be present in coal in dissolved form within the moisture (dissolved salts, such as NaCl or KCl), as organically bound compounds (i.e. bound in the coal matrix), as included (e.g. calcium oxalate), and as excluded minerals (e.g. limestone; clays and alumino-silicates rich in potassium, sodium, and calcium). The form in which those elements occur in coals depends also on the coalification degree, with younger fuels, such as lignites, containing more organically bound alkalis and earth alkalis, and in general, more elements that are water soluble and can therefore be depleted during coal aging. This explains the often lower contents of alkalis and earth alkalis in older hard coals. Sodium, potassium, magnesium, and calcium can represent more than $60 \cdot 10^{-2}\ \frac{mol}{mol}$ of the inorganic matter contained in lignites, while in hard coals this number is often considerably below $20 \cdot 10^{-2}\ \frac{mol}{mol}$. The organically bound alkali and earth alkali elements in lignites are usually more reactive than alkalis and earth alkalis in hard coals. An exception to this are alkali salts found in hard coals that have been exposed to salt water [53, 56, 62, 98].

2.2.2 Sulfur oxides in flue gases, ashes, and deposits

2.2.2.1 SO_2 and SO_3 formation and retention in ash

Formation of SO_2: During combustion, sulfur contained in the fuel is oxidized almost completely, forming mainly sulfur dioxide, following reaction 2.1 [53, 99]:

$$S + O_2 \longrightarrow SO_2 \tag{2.1}$$

[5] Adolphi [96] does not give the fuel reference state related to this concentration.
[6] Chou [97] does not give the fuel reference state related to this concentration.
[7] Chou [97] does not give the fuel reference state related to these concentrations. Since these ranges are indicative and the dry and ash free reference state allows to compare different fuels, this reference state is considered in the following.

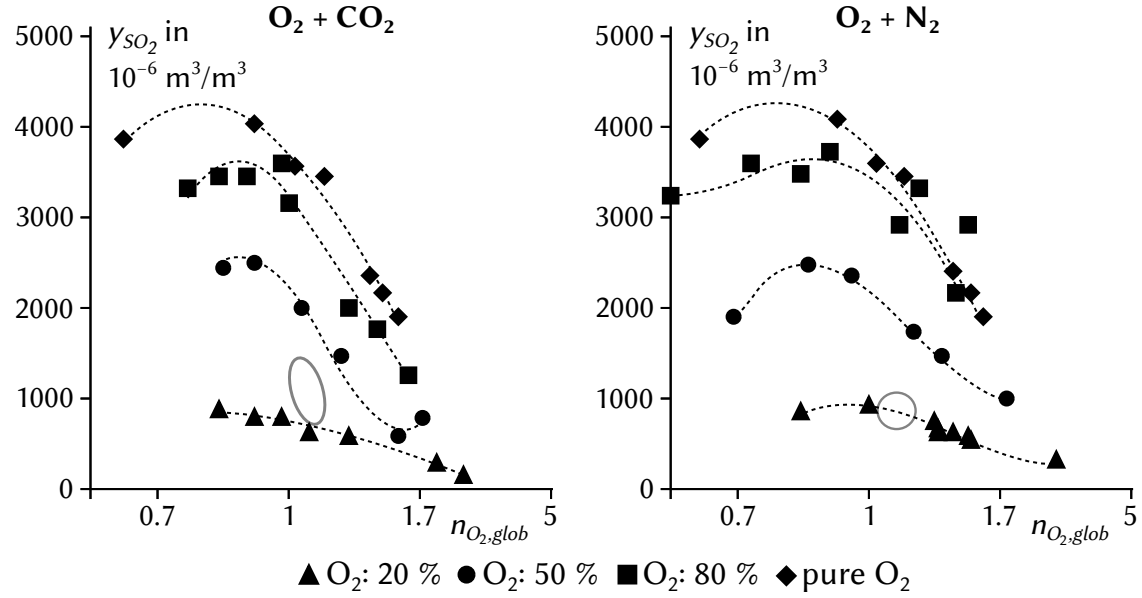

Figure 2.3: Influence of $n_{O_2,glob}$ on SO_2 concentrations y_{SO_2} (not corrected to the same O_2 level) in coal combustion, for various O_2 contents in CO_2 (left) and N_2 based (right) oxidants at 1000 °C. Gray circles indicate typical operation regimes for air and oxy-fuel PF combustion (graphic plotted on basis of [100]; equivalence ratio replaced by stoichiometric ratio).

In air and oxy-fuel firing, the most important parameters influencing the extent of SO_2 formation are the sulfur content of the fuel, the availability of oxygen (i.e. stoichiometric ratio of combustion - $n_{O_2,glob}$, n_{air}), the alkaline and earth alkaline content of the fuel's ash, and the temperature-residence-time-profile of the combustion process. Since SO_2 is formed by combustion of the fuel's sulfur, it is obvious that the SO_2 concentration increases with a rising sulfur content of the coal. In combustion tests using coal under N_2/O_2 and CO_2/O_2 atmospheres, Hu et al. [100] found a significant influence of $n_{O_2,glob}$ on the SO_2 concentrations in the flue gas (see section 4.2.1.4 for the definition of $n_{O_2,glob}$). The effect can be seen in figure 2.3 that shows experimentally measured flue gas SO_2 concentrations versus $n_{O_2,glob}$. The SO_2 concentrations in figure 2.3 are not corrected to the same O_2 level and hence, are subject to a variable dilution of flue gases with excess oxidant gas at different $n_{O_2,glob}$ values[8].

Starting from fuel-lean mixtures, the SO_2 concentration rises with decreasing $n_{O_2,glob}$ until it reaches a maximum at $n_{O_2,glob}$ values of around 0.85. This is caused to large extent by a decreasing dilution of the flue gas by excess oxidant gas but also by a reduced sulfur retention in the ash when decreasing $n_{O_2,glob}$. The reduction of the sulfur retention in the ash can be explained by the fact that the capture reactions of sulfur require O_2 (see reaction 2.3), which is less available at lower combustion stoichiometries. The increase of the SO_2 concentration with decreasing $n_{O_2,glob}$ is more pronounced at high O_2 contents in the oxidant gas than at O_2

[8]The article by Hu et al. [100] also provides plots on fuel mass specific SO_2 emissions that are not subject to variable flue gas dilution.

concentrations of $20 \cdot 10^{-2}\ \frac{m^3}{m^3}$, dry and is found in N_2 as well as in CO_2 atmospheres. At the same level of $n_{O_2,glob}$ the dilution of the flue gas by excess oxidant gas is strongly influenced by the O_2 concentration in the oxidant gas (it is more pronounced at lower O_2 concentrations in the oxidant gas; see also section 4.2.1.4). When decreasing $n_{O_2,glob}$ further below values of around 0.85, the SO_2 concentration falls. The reason for this is that at such low stoichiometries, not enough oxygen is available for a complete oxidation of the sulfur to SO_2 and hence, other sulfur species, such as H_2S, are formed.

Retention of SO_2 in the ash: Alkaline and earth alkaline compounds can take up SO_x from the flue gas to form solid sulfates. Therefore, the content of those compounds in the coal ash influences the SO_2 flue gas concentration, in air as well as oxy-fuel fired systems, substantially. The most important desulfurization reaction chain includes firstly a calcination of $CaCO_3$ to CaO (reaction 2.2) and subsequently, a sulfation of CaO with SO_2 and O_2 (reaction 2.3). Both these (reversible) reactions are shown below [11]:

$$CaCO_3 \longrightarrow CaO + CO_2 \tag{2.2}$$

$$CaO + SO_2 + \frac{1}{2}O_2 \longrightarrow CaSO_4 \tag{2.3}$$

$$CaCO_3 + SO_2 + \frac{1}{2}O_2 \longrightarrow CaSO_4 + CO_2 \tag{2.4}$$

A similar reaction chain exists for $MgCO_3$. SO_2 can also be captured by reactions with potassium and sodium compounds, forming K_2SO_4 and Na_2SO_4. The direct desulfurization of $CaCO_3$, shown in equation 2.4, is generally assumed to be of minor importance in conventional PF combustion but, due to the greater stability of $CaCO_3$, may be of greater importance in CO_2 and SO_2 rich oxy-fuel atmospheres [101], even though the contribution of this reaction pathway might still be limited [25]. The SO_2 capture in the ash under air as well as under oxy-fuel conditions depends, besides the alkaline and earth alkaline content of the ash, on the level of the SO_2 in the flue gas (i.e. the SO_2 partial pressure) and therefore, on the sulfur content of the coal [102]. Higher SO_2 partial pressures influence the stability of sulfates and the diffusion of SO_2 towards and reactions with alkali and earth alkali compounds positively [103]. In addition to the SO_2 level, also the temperature (see figure 2.4a) and the residence time of flue gases in the temperature range relevant for desulfurization (see figure 2.4b) is determining the desulfurization efficiency $\eta_{SO_2,glob}$ in a PF combustion system.
It can be seen from figure 2.4 that there is an increase in the efficiency of desulfurization with increasing sulfur content of the coal and hence, increasing SO_2 levels in the flue gas. At certain temperatures, there is a desulfurization maximum (in air firing at approx. 1100 °C, in oxy-fuel combustion at approx. 1200 °C; temperature levels established by Liu et al. [11] for exemplary air and O_2/CO_2 systems without consideration of particle sintering). Such a maximum can be explained as follows: Initially, the desulfurization reactions run more and more efficiently with

rising temperatures. However, depending on the SO_2 partial pressure $CaSO_4$ decomposes at high temperatures, whereby SO_2 is released (reverse reaction 2.3). At high temperatures, the decomposition reaction reduces the efficiency of the flue gas desulfurization until the $CaSO_4$ decomposition outbalances its formation and no SO_2 is captured anymore. From figure 2.4 another effect can be seen: The flue gas desulfurization efficiency in O_2/CO_2 (i.e. oxy-fuel) atmosphere, compared to air firing, is increased by a factor of about 4 to 6 and obviously runs over a wider temperature range with higher maximum temperatures [11]. This rise in the desulfurization efficiency is explained by a (compared to air combustion) increased residence time of the flue gases at temperatures suitable for efficient desulfurization, due to flue gas recirculation in oxy-fuel operation. Section 4.1.3 of this thesis covers and illustrates the effect in greater detail. The positive effect of increased flue gas residence times on the desulfurization efficiency in oxy-fuel recycle combustion was not proven experimentally by Liu and coworkers [11, 104, 105] but was proposed based on simulation results, obtained from an air and oxy-fuel in-furnace desulfurization model. In addition to the increased residence time of SO_2 molecules in oxy-fuel recycle combustion, the substantial increase in SO_2 concentrations under oxy-fuel conditions suppresses the decomposition of $CaSO_4$ and shifts it to higher temperatures [11, 19, 54]. This extents the reaction volume inside a boiler in which desulfurization can occur and is

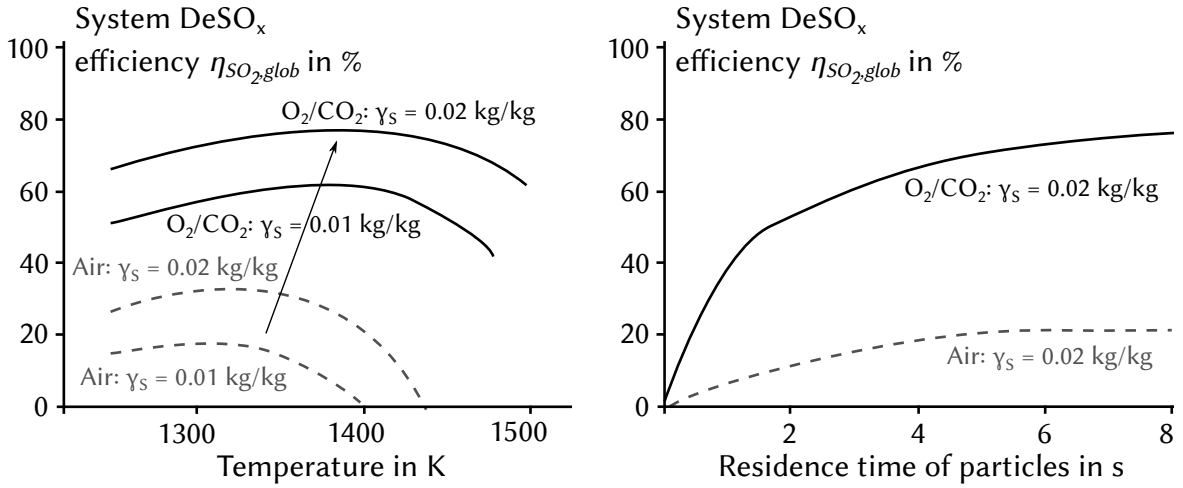

(a) $\eta_{SO_2,glob}$ vs. Temperature **(b)** $\eta_{SO_2,glob}$ versus residence time

Figure 2.4: (a) Calculated temperature dependency of the desulfurization efficiency $\eta_{SO_2,glob}$ at a combustion stoichiometry of $n_{O_2,glob}$ = 1.2, 8 s residence time (once-through), a molar Ca/S ratio $\alpha_{Ca/S}$ = 5, and a 10 µm $CaCO_3$ particle diameter for coal combustion in O_2/CO_2 atmosphere with a recirculation rate ξ_{rec} of 0.84 and for air combustion, and (b) calculated dependency of the desulfurization efficiency $\eta_{SO_2,glob}$ on the residence time at 1400 K, a combustion stoichiometry $n_{O_2,glob}$ =1.2, a molar Ca/S ratio $\alpha_{Ca/S}$ = 5, and a 10 µm $CaCO_3$ particle diameter for coal combustion in O_2/CO_2 atmosphere with a recirculation rate ξ_{rec} of 0.84 and for air combustion.

(Adapted with permission from Energy Fuels, Vol. 15 (2), Liu, H.; Katagiri, S.; Okazaki, K., Drastic SO_x Removal and Influences of Various Factors in O_2/CO_2 Pulverized Coal Combustion System, pp 403–412., [11]; Copyright (2001) American Chemical Society.)

beneficial for SO_2 capture [11]. The higher SO_2 partial pressure in oxy-fuel firing, in addition, has a positive impact on the desulfurization reaction kinetics and on the diffusion of SO_2 from bulk flue gas to CaO rich particles [106]. Besides, in oxy-fuel combustion also the elevated CO_2 partial pressure may have a positive impact porosity of CaO rich particles and therefore, the desulfurization efficiency may be enhanced [25, 107, 108].
To sum up, the retention of sulfur in the ash in oxy-fuel systems is enhanced, compared to air firing, but this also depends on a variety of individual factors, which differ between fuels, plants, and combustion settings, and therefore, the predominance of the effect differs in different experiments [41, 42]. Fleig et al. [12] found in tests at a 100 kW (thermal) test rig with low sulfur lignite a 67 % conversion rate of sulfur from the fuel to SO_2 for air combustion and between 41-46 % in oxy-fuel firing. In a review of other published literature, Fleig et al. [109] showed that increased sulfur retention in the ash and hence, lower fuel sulfur to SO_2 conversion efficiencies were also found by several other researchers.

SO_2 levels in oxy-fuel combustion: As mentioned above, the exclusion of N_2 in oxy-fuel combustion leads to an increase of SO_2 concentrations by a factor of around 4. Thus, in oxy-combustion extremely high SO_2 levels can occur. SO_2 concentrations up to above $20\,000 \cdot 10^{-6}\ \frac{m^3}{m^3}$, dry were measured during oxy-fuel combustion of a sulfur rich coal [15]. In contrast to the SO_2 concentrations, due to the improved sulfur capture in the ash, the energy based SO_2 emissions (i.e. SO_2 mass flow related to energy supply by fuel, e.g. in mg SO_2/MJ) in oxy-fuel operation are lower than in air firing [1, 10, 54, 110]. However, high SO_3 levels in the ash, caused by an enhanced sulfur retention, may impact its utilization negatively.

SO_3 formation and retention in the ash: During combustion and along the flue gas path, SO_3 is formed from SO_2 in a homogeneous (bi- or trimolecular) gas phase reaction (equation 2.5) or in a heterogeneous, solids catalyzed reaction for example on iron oxides [99, 111].

$$SO_2 + \frac{1}{2}O_2 + M \longrightarrow SO_3 + M \tag{2.5}$$

Generally, the extent of SO_3 formation in air and oxy-fuel firing is significantly influenced by the sulfur content of the coal (i.e. SO_2 partial pressure in flue gas), the alkaline and earth alkaline content of its ash, the availability of oxygen, the content of catalytically active compounds in the ash, the temperature-residence-time-profile of the flue gas in the plant, and the application of SCR equipment [53, 99]. The sulfur content of the coal affects directly the SO_2 partial pressure and therefore, indirectly the SO_3 levels and is one of the most important parameters influencing the concentrations of SO_3 in the flue gas (see also figure 4.37 in the results chapter with results on SO_3 formation in air and oxy-fuel combustion from this thesis and from others). Hochbruck highlights a directly proportional correlation between the SO_2 and the SO_3 levels [112]. It is obvious that higher SO_2 levels in oxy-fuel firing are related to higher SO_3 concentrations [26,

38]. The O_2 concentration in the flue gas has also a direct effect on the SO_3 formation rate, which increases with increasing oxygen content [20, 26, 29, 112–114].
The SO_3 formation in the boiler and down to temperatures of approx. 500 °C is influenced by the presence and amount of catalytically active compounds (e.g. Fe_2O_3), with higher contents leading to higher SO_3 formation [29, 111–113]. Catalytic SO_3 formation is highly dependent on temperature, with a maximum of the SO_2 to SO_3 conversion at about 700 °C [29, 115]. The catalytic SO_3 formation takes place on entrained fly ash particles as well as on ash deposits in the boiler [116]. Laboratory studies on the SO_2 to SO_3 conversion on fly ashes[9] in simulated air and oxy-fuel atmospheres did not show significant differences in the conversion efficiencies [29, 113]. The homogeneous just as the catalytic SO_3 formation, clearly shows a temperature-dependent behavior [26, 29]. Both are relatively slow [29, 111–113], which is the reason why in practical firing systems no equilibrium concentrations of SO_3 can be observed. Therefore, the temperature-residence-time-profile of the flue gas in a plant is another key parameter influencing the formation of SO_3 [26, 29, 99]. In addition to the mentioned points, the installation of an SCR unit can significantly increase SO_3 concentrations. SO_2 to SO_3 conversion ratios of 0.5-2 % have been observed at SCR systems [111, 117]. Also the presence of nitrogen oxides may have a positive impact on SO_3 formation [112, 114].
Another important parameter determining the SO_3 formation during combustion is the content of alkaline and earth alkaline compounds in the ash. Similarly to the reactions with SO_2, those can capture SO_3 in form of sulfates directly (see reaction 2.10) but also reduce the SO_3 formation indirectly by capturing SO_2, the precursor of SO_3. Since under oxy-fuel fired conditions, the capture of SO_2 in the ash is enhanced, this also affects indirectly the generation of SO_3.

SO_3 levels in air and oxy-fuel combustion: In practice, SO_2 to SO_3 conversion rates between 1 and 5 % [16], with SO_3 concentrations up to about $40 \cdot 10^{-6}$ $\frac{m^3}{m^3}$, dry in coal fired air and over $180 \cdot 10^{-6}$ $\frac{m^3}{m^3}$, dry in oxy-fuel facilities were reported [15, 118]. This considerable increase might be mainly a result of the increased SO_2 concentration under oxy-fuel fired conditions. In an experimental combustion study by Fleig et al. [26], no clear trends were observed in respect to changes in the SO_2 to SO_3 conversion rates between air and oxy-fuel firing.

H_2SO_4 formation and condensation: At temperatures below about 400 °C, gaseous sulfuric acid (H_2SO_4) starts to form from the reaction of SO_3 and water vapor and reaches complete transformation of the SO_3 at approximately 200 °C [119, 120]. The dew point of the formed H_2SO_4 depends on the concentrations of H_2O and SO_3/H_2SO_4 in the flue gas. It can be calculated based on those species' partial pressures, according to Verhoff and Banchero [121], Okkes [122], or by a more recent correlation by ZareNezhad [123]. In power plants, H_2SO_4 dew points

[9] Fly ashes used by Belo [29, 113] have been obtained in experiments of this thesis, introduced in sections 3.3.4 and 4.2.3.

typically range between 95 and 160 °C. With increased H_2O and SO_3/H_2SO_4 concentrations in oxy-fuel operation, considerably higher dew point temperatures than in air firing are reached (i.e. 20 to 30 °C higher [109]). When temperatures fall below the H_2SO_4 dew point gaseous H_2SO_4 starts to condense. In power plants, relevant temperatures are found in the region of fly ash filters and precipitators and air preheaters, where substantial problems due to low temperature corrosion[10] and fouling, can occur [53, 123]. Fouling is caused by the condensation of sulfuric acid on cold surfaces. The liquid that is formed acts then as a sticky surface at which fly ash can deposit. It is known that ashes rich in CaO and MgO reduce temperatures at which low temperature fouling becomes problematic. The removal efficiency of H_2SO_4 by condensation on cold air preheater surfaces can be significant [53]. To control sulfuric acid induced fouling and corrosion problems, air preheater outlet temperatures are selected high enough to minimize problems cause by acid condensation. Depending on the sulfur and CaO and MgO content of the fuel, these temperatures are in a range of 120 to 140 °C for hard coal and somewhat higher (140 to 170 °C) for lignite fired systems [53]. The heat that remains in the flue gases after the air preheater cannot be recuperated and hence, lowers a power plant's efficiency. In oxy-fuel plants the recycle lines are also critical in respect to low temperature H_2SO_4 corrosion [66]. At temperatures below the H_2SO_4 dew point, SO_3/H_2SO_4 can also be separated from gas phase effectively by condensation on fly ash particles [117]. Such temperatures can for example be found at ESPs and filters.

2.2.2.2 Sulfur oxides in deposits

The role of sulfur oxides in slagging, fouling, and corrosion: Sulfur oxides can react with components of the ash, most importantly alkali and earth alkali species to form sulfates. This may happen with the entrained ash but also with ash that has been deposited on heat exchanger surfaces. In this context, SO_x plays an important role in slagging and fouling. For example, from lignite fired systems, slagging by low temperature $CaS/CaSO_4$ eutectics is a known phenomenon. Another problematic deposit system is characterized by an eutectic mixture of $NaSO_4$ and NaCl with melting temperatures as low as 625 °C. Via reactions between alkali sulfates (e.g. K_2SO_4), iron oxide, aluminum oxides (i.e. Fe_2O_3, Al_2O_3), and sulfur trioxide, complex alkali iron and alkali aluminum tri-sulfates can form. Those are liquid and stable at temperatures between about 550 and 700 °C and are known to attack even highly alloyed heat exchanger materials. The corrosion by such sulfatic melts is known to be inhibited by earth alkalis in the ash. High temperature corrosion problems by alkali metal tri-sulfates may be counteracted by lowering the heat exchanger (i.e. steam) temperature or if this option is not available, by the application of more corrosion resistant materials or coatings, and by fuel additives. The sulfation of alkali chlorides contained in deposited ash (i.e. NaCl, KCl) that

[10] H_2SO_4 is highly hygroscopic and takes up moisture from the flue gas, forming an electrolyte that is known for its high corrosivity to low alloyed steels used in the respective sections of power plants.

releases chlorine, is responsible for chlorine-induced high temperature corrosion [53].
As introduced in section 2.1.4, sulfatic deposits in liquid phase play also an important role in the mechanism of ash deposition on boiler tubes when they form a sticky layer that holds other solid ash particles that hit this layer. Moreover, the sulfation of ash deposited on heat exchanger tubes by gaseous SO_2 and SO_3 can be responsible for heavy sintering of deposits [62]. This occurs on convective heat exchangers if flue gas and outer deposit temperatures are below the sulfate decomposition temperature (for $CaSO_4$ this is between about 1100 and 1200 °C in air firing). An optimization of the cleaning intervals of soot-blowers can help to reduce sintering of deposits. SO_3 plays also an important role in fouling of SCR catalysts by ammonium sulfate and ammonium hydrogen sulfate [53] and is responsible for problems in respect to air preheater fouling.

Sulfur oxides in ashes and deposits in oxy-fuel combustion: It can be stated that, even though a considerable number of publications is available dealing with deposits in oxy-fuel combustion, only few of them include systematic experimental comparisons of air and oxy-fuel ashes and deposits. Generally, the altered flue gas composition and changes in the temperature profile of an oxy-fuel fired process can impact the formation and transformation of ashes and deposits. Previous studies indicated that the changes in firing mode may not necessarily change the ash transformation behavior [124, 125]. Available literature on transformation of carbonate minerals (e.g. $CaCO_3$) suggests that under oxy-fuel conditions carbonate decomposition temperatures are significantly increased [124], which means that they may be stable in deposits at somewhat higher temperatures. However, temperatures in the furnace and in parts of the boiler are still well above the carbonate decomposition temperatures, which limits the effect of their increased stability in oxy-fuel combustion. Moreover, in coal fired systems, usually a significant amount of sulfur is present which, due to their thermodynamic stability, causes the formation of sulfates preferentially to carbonates. However, for low sulfur and high alkali and earth alkali fuels carbonate formation in boilers cannot be ruled out [20]. In fact, higher degrees of ash and deposit sulfation and stable sulfates at higher temperatures than in air firing have been observed in oxy-fuel combustion by the author of this thesis [41, 42] (see also sections 4.2.1.1, 4.2.1.3 and 4.2.1.2) but were also mentioned by others [9, 126]. A thermodynamic equilibrium study on the differences in respect to ashes and deposits between air and oxy-fuel firing by Schnurrer et al. [19] showed that higher SO_2 levels in oxy-fuel operation shift the temperature regions in which SO_x containing species are stable to higher temperatures. The temperature shifts that were observed in this study are in a range of 30 to 60 °C.
Wigley et. al [124] also highlighted that mineral transformation can be altered considerably if combustion temperatures are changed in oxy-fuel firing. Thus, not only the altered flue gas atmosphere may play a decisive role in oxy-fuel ash/deposit formation and transformations but also changes in flue gas flow rates and thermal properties. Nonetheless, to date and with

the oxy-fuel process configurations that are currently favored (i.e. $\xi_{rec} \approx 0.7$), no significant changes are expected. Few researchers studied the deposition behavior in air and oxy-fuel combustion of coals comparatively and made partly opposing observations (i.e. increased as well as decreased deposition) [127–129]. The observations have been explained by all these researchers on basis of changes in the velocity, particle trajectories, particle sizes, and molten ash viscosities between air and oxy-fuel firing. In these studies, the crystallographic and chemical analyses of ashes did not show significant differences between the combustion modes. Comparative air and oxy-fuel investigations at Vattenfall's oxy-fuel pilot plant "Schwarze Pumpe" showed that chemical compositions and morphology of superheater deposits were similar [21, 22, 130]. Deposition rates in the same study were increased in oxy-fuel, compared to air fired combustion. Adams et al. observed slightly finer ash particle sizes in deposits from oxy-fuel combustion with one of three tested fuels [23].
To sum up the experiences in respect to differences of oxy-fuel deposits, compared to air firing, the statement given in 2010 by Toftegaard at al. [54] that "investigations reported till now indicate that the changes to depositions in an oxy-fuel plant, compared to an air fired unit, will not be of essential significance to the plant operation" seems to be still valid with an exception in respect to sulfates for coals that have a significant sulfur capture potential (i.e. high alkali and earth alkali contents). For such fuels, higher contents of sulfates in ashes and deposits need to be expected and such sulfates may occur at higher temperatures.

Corrosion by sulfur in oxy-fuel combustion: Sulfur oxides in deposits can also cause corrosion of heat exchanger materials. In corrosion studies with material samples that were firstly exposed to oxy-fuel combustion atmospheres and then further reacted in similar atmospheres in a laboratory oven, no indications of high temperature sulfur corrosion even in high SO_2 atmospheres have been detected, even though the deposits attached to the boiler materials were rich in sulfates [131, 132]. It was speculated that the sulfur-binding capacity of compounds in the deposits (e.g. earth alkalis) may capture SO_x diffusing towards the heat exchanger surface and hence, play a protective role in respect to sulfur corrosion [131]. Also others did not find evidence of increased corrosion rates at moderate levels of SO_2 (i.e. up to $3200 \cdot 10^{-6}\ \frac{m^3}{m^3}$, dry) in comparative air and oxy-fuel laboratory corrosion studies [133] and in experiments at Vattenfall's oxy-fuel pilot plant "Schwarze Pumpe" [21, 130]. However, in experiments burning a high sulfur coal, without recycle gas desulfurization, reaching very high SO_2 levels (i.e. $17\,642 \cdot 10^{-6}\ \frac{m^3}{m^3}$, dry) [23, 134], an extreme increase in the wastage rate[11] of an austenitic steel was observed. This was associated to the presence of molten alkali metal trisulfates. However, it was stated by the authors of that study that in an industrial oxy-fuel system one would not allow such high SO_2 levels.
In general, it can be stated that high temperature sulfur corrosion by sulfate melts is expected

[11] For this study, an electrochemical online corrosion probe was used.

to occur in oxy-fuel combustion similarly to air firing [66]. The temperature range in which this mechanism is active may be shifted to higher temperatures, due to increased SO_2 and SO_3 partial pressures in oxy-fuel combustion [19, 135, 136], and the effect may be more severe especially at very high levels of SO_x. This can be counterbalanced by burning lower sulfur fuels and/or desulfurization of the recirculated flue gas.

2.2.2.3 Legal and technical SO_x emission limits

Legal sulfur oxide emission limitations in conventional PF plants: European emission limits for power plants are regulated in directive 2010/75/EU on industrial emissions [137]. The regulations in this directive have to be transferred to national laws in the member states of the European Union keeping all emission limits set therein. National laws may however set stricter emission limits than the ones stated in directive 2010/75/EU. This is the case for Germany. In Germany, large pulverized coal fired power plants need to follow the emission limits set by the 13^{th} ordinance on the implementation of the federal immission control act (ordinance on large combustion plants and gas turbine plants: 13. BImSchV [138]). The compliance to the emission limits for SO_x[12] needs to be validated by continuous emission monitoring[13]. The German and the corresponding European Union emission regulations for new, large, pulverized coal and lignite fired power plants for SO_x and required minimum desulfurization efficiencies $\eta_{SO_x,lim}$ are given in table 2.1. Depending on the thermal power P_{th} of the facilities, different emission limits apply.

For older plants and plants operating for less than 1500 h per year, less strict regulations exist on European and also on German national level. For example, for the newest generation of German PF power plants with a thermal power above 300 MW that have been authorized between November 2002 and January 2013 and went in operation between November 2003 and January 2014, the daily average SO_x emission limit is 200 $\frac{\text{mg}}{\text{m}^3}$, (STP) and the half hourly average limit is 400 $\frac{\text{mg}}{\text{m}^3}$, (STP). In addition, the plants need to keep a minimum desulfurization efficiency $\eta_{SO_x,lim}$ of 85 %. The German and European emission limits for large, solid fuel fired plants[14] refer to a flue gas at an oxygen level of $6 \cdot 10^{-2}$ $\frac{\text{m}^3}{\text{m}^3}$, dry [137, 138].

In other countries, much less strict emission limits apply. For example, in New South Wales, Australia[15], four of five of the large coal fired power stations have so called reporting limits for SO_2, while one plant has no such limitation at all [139]. These reporting limit values require the power plants to operate a continuous SO_2 emission monitor and file non-compliance reports[16] if the reporting limit is exceeded. The SO_2 reporting limit for the respective power stations is

[12] In the context of the German emission regulations, SO_x refers to the sum of SO_2 and SO_3, expressed as SO_2.

[13] If a continuous emission monitor for SO_2 is operated, the concentration of SO_3 can be determined by calibration measurements and can be further considered in the emission data by calculation.

[14] Except for waste incinerators that fall under a different ordinance.

[15] In Australia no federal emission limitations for power plants exist and emissions are regulated on a state level.

[16] These have to give details on dates, times, durations, and reasons of the exceedance and any actions taken to address future exceedances [139].

Table 2.1: Current (as of December 2017) SO_x (i.e. sum of SO_2 and SO_3 expressed as SO_2: $y_{SO_x,lim}$) daily and half hourly average emission limits (referring to an oxygen level of $6 \cdot 10^{-2}\ \frac{m^3}{m^3}$, dry) and minimum desulfurization efficiencies $\eta_{SO_2,lim}$ for new, large, PF fired power plants in Germany and the corresponding European Union emission limits.

	Germany						EU
	domestic lignite†			other solid fuels			solid fuels
	$y_{SO_x,lim}$		$\eta_{SO_x,lim}$	$y_{SO_x,lim}$		$\eta_{SO_x,lim}$	$y_{SO_x,lim}$
P_{th}	daily	1/2 hourly		daily	1/2 hourly		daily
MW	$\frac{mg}{m^3}$, (STP)			$\frac{mg}{m^3}$, (STP)			$\frac{mg}{m^3}$, (STP)
50 - 100	-	-	93 %	400	800	-	400
100 - 300	300	600	93 %	200	400	85 %††	200
> 300	400	800	97 %	150	300	85 %††	150

† These limits apply to domestic lignites that, due to their sulfur content, cannot keep the emission limits for other solid fuels with a proportionate effort.

†† In case, the 85 % desulfurization requirement would lead to SO_x emissions below 50 $\frac{mg}{m^3}$, (STP), a minimum desulfurization efficiency $\eta_{SO_2,lim}$ that corresponds to a SO_x emission of 50 $\frac{mg}{m^3}$, (STP), needs to be maintained.

1760 $\frac{mg}{m^3}$, (STP). In addition, all coal fired power plants in New South Wales need to follow a concentration limit for sulfuric acid mist (i.e. H_2SO_4, expressed as SO_3) of 100 $\frac{mg}{m^3}$, (STP) [139].

Technical limitations in respect to sulfur oxides in conventional PF plants: Since in conventional PF power plants, the SO_x level in the boiler can usually only be controlled on basis of the fuel selection, boilers need to be designed in a way that allows them to withstand the respective SO_x levels and the negative impacts of SO_x in respect to slagging, fouling, and corrosion. A number of engineering measures, such as selecting more corrosion resistant steels or accepting a higher material wastage, the application of soot blowing and other heat exchanger cleaning techniques, and lowering furnace outlet and/or steam temperatures, are available to control such issues. However, these measures are associated to an increase of equipment and operational costs of a power plant and/or a reduction of the power plant's efficiency. Even with such measures in operation, a power plant's availability may be negatively impacted by a higher sulfur fuel, compared to a low sulfur one. In practice, the sulfur content of coals combusted in conventional power plants is in most cases not strictly limited for technical reasons but rather by balancing fuel cost and power plant equipment and operational costs as well as availability. The sulfur content of coal blends used in power generation generally is in a range of 0.5 to $2.5 \cdot 10^{-2}\ \frac{kg}{kg}$[17] [140] and hence, a sulfur content of maximum about $2.5 \cdot 10^{-2}\ \frac{kg}{kg}$ can be considered as a techno-economic optimum for application of coals in today's conventional power boilers. This is not a strict limit and, depending on fuel availability

[17] Nalbandian [140] does not give the fuel reference state related to this concentration range.

and other circumstances, also fuels with much higher sulfur levels may be combusted.
For power plants that import hard coals, the selection of coals with a certain sulfur content is rather flexible. Most of such power plants use different coal qualities that they blend on-site depending on the limitations of the power plant's design (especially of the $DeSO_x$ system). For example, when power plants operate in part load their $DeSO_x$ systems may not reach their SO_2 capture capacity limits. During such periods, power plants may use more of the cheaper, higher sulfur coals available on-site in their coal blend. Plants that use domestic locally sourced coal and lignite are less flexible in respect to adjusting their fuel's sulfur content [140].

Limitations in respect to sulfur oxides in oxy-fuel fired PF plants: Conventional air and oxy-fuel PF plants differ from each other considerably in respect to their gaseous emissions. In an oxy-fuel plant, the bulk of the CO_2 rich flue gas is cleaned and liquefied, while in an air fired system, a large flue gas stream is emitted to the atmosphere, after gas cleaning to keep legal emission limits. During normal oxy-fuel operation, an oxy-fuel plant's CPU will also emit a relatively small gaseous stream that is vented to the atmosphere. The bulk of this stream are gases that cannot be liquefied in the CO_2 liquefaction unit (i.e. Ar, O_2, N_2). Moreover, this stream contains SO_x and NO_x. Due to its different composition compared to combustion flue gas and the much smaller mass flow, compared to a conventional power plant's flue gas stream, current power plant emission regulations may not be applicable to this stream and modified regulations may be required in future. As mentioned previously, oxy-fuel power plants will also need to emit nitrogen rich flue gas via a conventional stack during start-up and shout-down. It is likely that during such times, SO_x emission limits similar to the ones mentioned in the emission regulations for conventional power plants would apply.
In addition to that, the SO_x content of the liquid CO_2 produced in the CPU will be limited. While in a report by IEAGHG from 2011 [141], SO_2 and SO_3 levels in the CO_2 produced by an oxy-fuel fired plant below $50 \cdot 10^{-6}$ $\frac{mol}{mol}$ and $20 \cdot 10^{-6}$ $\frac{mol}{mol}$, respectively, are anticipated for pipeline transport and geological storage, for Vattenfall's "Schwarze Pumpe" oxy-fuel pilot project considerably lower values are mentioned [142]. Roland Ritter [142], who was involved in Linde's activities at the CO_2 processing and liquefaction unit of this pilot plant, gave limits in respect to the SO_2 and SO_3 contents in the produced liquid CO_2 of $2.5 \cdot 10^{-6}$ $\frac{mol}{mol}$ and $0.5 \cdot 10^{-6}$ $\frac{mol}{mol}$, respectively[18]. At the CPU of Vattenfall's oxy-fuel pilot plant, concentrations of these two components below the detection limit of the used analyzer (i.e. close to nil) were reached. Similarly low values were reported for the Callide oxy-fuel project, using a CPU system by Air Liquide [66]. The low SO_2 and SO_3 limits highlight that practically all sulfur oxides present in the oxy-fuel flue gas need to be removed from the flue gas. Depending on the levels of SO_x in the flue gas and the available atmospheric pressure desulfurization equipment, a partial SO_x removal before flue gas compression may be obligatory or economically beneficial

[18]This corresponds to CO_2 quality 2.7 that can be used in enhanced oil and gas recovery and for sequestration.

for an oxy-fuel power plant.
In addition to the CO_2 quality, also the operation of the oxy-fuel boiler and recycle system and its auxiliaries may require a limitation of the SO_x level, to limit slagging, fouling, and corrosion. The research by Fry et al. [134] and Adams et al. [23] gave indications that very high SO_x levels in oxy-fuel combustion may not be tolerable. Due to the lack of extensive experimental data, it is difficult to define strict, technical SO_x limits for oxy-fuel boilers. Mancuso et al. estimated the limit to be around 2000 to $3000 \cdot 10^{-6} \frac{m^3}{m^3}$ of SO_2 and highlighted that without recycle desulfurization, this limit would require fuels with below $0.5 \cdot 10^{-2} \frac{kg}{kg}$[19] of sulfur [143]. A general assumption that can be made and is also supported by McDonald, who was involved in the US Futuregen 2.0 project, working for Babcock & Wilcox Inc. [144], is that SO_x levels that are currently acceptable in conventional coal boilers can also be tolerated in oxy-fuel systems. This means that oxy-fuel power plants would either be restricted to the utilization of low sulfur coals (i.e. below approx. $1 \cdot 10^{-2} \frac{kg}{kg}$, waf) or require a means of desulfurization within the recycle loop to control the SO_x level in the boiler and downstream equipment (see also section 2.1.6).

2.3 Control of gaseous sulfur oxides in PF combustion

The control of the flue gas impurities SO_2 and SO_3, and in case of chlorine rich fuels, also HCl is an important issue in air fired systems, due to legal emission limits, and in oxy-fuel combustion, since those components impact the power plant process design, construction, and operation in various aspects. Available technologies can be classified into five categories: Dry sorbent injection (DSI) systems, spray drier absorbers (SDA), circulating dry scrubbers (CDS), regenerative $DeSO_x$, and wet flue gas desulfurization (WFGD) processes. These technologies are incorporated in the combustion process at different locations between boiler and stack, as can be seen in figure 2.5 (regenerative $DeSO_x$ is not shown here). Details about other but less common flue gas desulfurization processes can be found in the literature [145].
WFGD systems are generally installed after filters, while CDS and SDA systems are placed after air preheater but before filters. DSI technologies can be employed either in the furnace, in the economizer region of the boiler, after the SCR system but before APH, after APH but before filters, or after the ash removal system but before a secondary by-product filter. The following pages focus on processes that allow for a control of gaseous SO_2, SO_3, and HCl levels. Section 2.3.1 briefly introduces wet and semi-dry desulfurization processes (e.g. WFGD, SDA, CDS, regenerable FDG) while section 2.3.2 presents dry desulfurization technologies for SO_x and HCl control in greater detail since experiments studying DSI are part of this thesis.

[19] Mancuso et al. [143] does not give the fuel reference state related to this concentration.

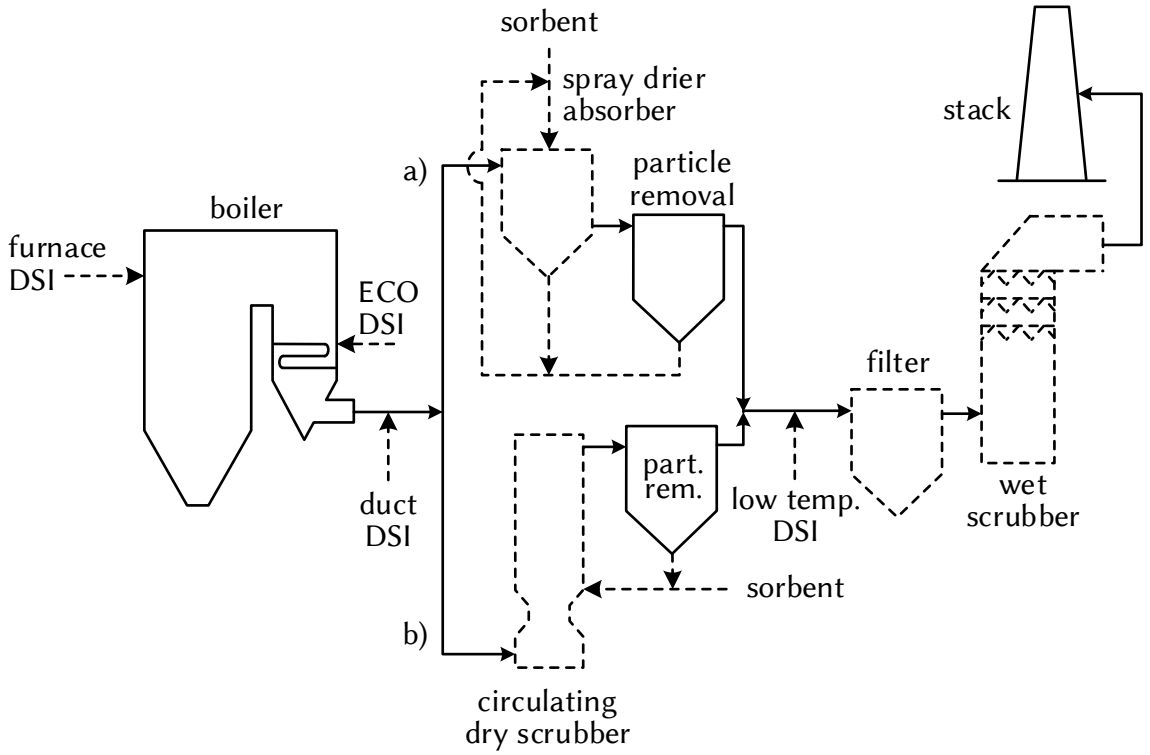

Figure 2.5: Schematic showing the placement of different desulfurization systems (dashed) in a conventional power plant system. Options a) and b) show the alternatives SDA and CDS that are both placed at the same location, upstream the particulates control device.

2.3.1 Wet and semi-dry DeSO$_x$ processes

2.3.1.1 Wet flue gas desulfurization

Wet desulfurization systems using widely available and inexpensive $CaCO_3$ as sorbent are the most common SO_x control systems applied in power plants around the world. WFGD units are generally placed after particulate removal and use a limestone slurry as sorbent in a complex process covering several reactions and phase transfers [146, 147]. In a scrubber, SO_2 from the flue gas is contacted with the alkaline limestone slurry in which it dissolves and reacts forming solid gypsum ($CaSO_4 \cdot 2\,H_2O$). The SO_2 absorption in the scrubber is controlled mainly by gas- and liquid-phase diffusion. Since it is placed downstream of ash removal systems, the WFGD process is not impacting the fly ash quality. In air fired processes, WFGD systems reach SO_2 removal efficiencies greater than 99 %. However, fine SO_3/H_2SO_4 droplets can slip through wet scrubbers. The desulfurization in most wet scrubbers uses the limestone-forced oxidation process [30, 148], with the net desulfurization reaction 2.6.

$$CaCO_3 + SO_2 + 2\,H_2O + \frac{1}{2}\,O_2 \longrightarrow CaSO_4 \cdot 2\,H_2O + CO_2 \tag{2.6}$$

2.3.1.2 Semi-dry desulfurization processes

CDS units are placed between the air/recycle gas preheater and the filter of a plant. In the CDS process, the flue gas reacts with a mixture of dry $Ca(OH)_2$, ash, and recirculated by-products in a circulating fluidized bed, before passing through a fabric filter for solids removal [79]. Solids collected in the filter are recirculated, to increase the utilization degree of the sorbent. Since the reaction products of the desulfurization process are removed together with fly ash, fly ash quality is impacted by this process. The CDS desulfurization efficiency is enhanced by water addition to the scrubber for humidification and to keep the reaction temperature closely (i.e. 10 to 15 °C) above the water dew point temperature [149]. CDS systems can achieve a high SO_2 removal efficiency (up to 98 %) and have been applied to power plants with sizes between approx. 50 and 350 MW (electric) [30, 79]. The CDS process can also capture acid gases other than SO_2 efficiently (i.e. HCl, HF, SO_3) [77, 79]. The desulfurization reactions taking place in a CDS system between the sorbent $Ca(OH)_2$ and SO_2 are shown in equations 2.7 and 2.8 [77]. As by-product calcium sulfite hemihydrate ($CaSO_3 \cdot \frac{1}{2} H_2O$) is formed.

$$Ca(OH)_2 + SO_2 \longrightarrow CaSO_3 + H_2O \tag{2.7}$$

$$CaSO_3 + \frac{1}{2} H_2O \longrightarrow CaSO_3 \cdot \frac{1}{2} H_2O \tag{2.8}$$

SDA systems are similar to the CDS process and are placed at the same location in the power plant process (i.e. between air/recycle preheater and filter). The desulfurization reactions are essentially the same as in the CDS system (equations 2.7 and 2.8). Similar to CDS, unreacted by-product is recycled to the SDA scrubber to enhance the sorbent utilization [53]. In conventional air firing, SDA systems are employed for small and medium sized plants (up to 400 MW, electric) burning low to medium sulfur coals (i.e. $\gamma_S \leq 2 \cdot 10^{-2} \frac{kg}{kg}$, waf) [150]. Different to CDS, in SDA systems, $Ca(OH)_2$ is injected to an absorber vessel in form of an aqueous slurry, resulting in SO_2 absorption and chemisorption in the slurry droplets that evaporate in the hot flue gas. The evaporation of the droplets is critical for an optimal SDA operation. Incomplete droplet evaporation can cause fouling problems, while a too rapid evaporation decreases the SO_2 removal efficiency, since SO_2 absorption benefits from the presence of a liquid phase. This is why the SDA process temperature is controlled to approach closely to the water saturation of the flue gas. In the absorber, a mixture of dry calcium sulfite and calcium sulfate is formed that is removed together with the ash in a fabric filter so that the fly ash composition is impacted by SDA. For air fired operation, SO_2 removal efficiencies of 70–98 % have been reported that are strongly dependent on parameters, such as the sorbent properties and the sulfur content of the coal [145]. SDA systems are also known for their efficient SO_3 removal.

2.3.1.3 Regenerable desulfurization processes

Regenerable desulfurization systems are installed after ash removal and are characterized by a regeneration of sorbents after absorption of SO_x so that the sorbents can be recycled back to the absorber. The obtained sulfur (e.g. in form of SO_2) is processed to obtain a product, such as elemental sulfur or H_2SO_4 that can be sold [149]. Due to the complexity of the process, the high operation and maintenance costs, and the limited value of the by-products only few regenerable FGD systems have been installed in commercial plants.

2.3.1.4 Wet and semi-dry DeSO$_x$ processes in oxy-fuel combustion

Flue gas desulfurization techniques that are used in conventional air fired combustion systems can in principle also be applied to the oxy-fuel process. Issues that may generally impact the performance of any FGD process in oxy-fuel combustion are the increased CO_2, SO_2, and SO_3 levels, as well as altered gas velocities, gas and particle travel times (including flue gas recycling), and temperature-profiles of the process. Due to these changes, modifications of conventional air fired FGD applications may be required for an optimal operation. FGD technologies for oxy-fuel fired processes that have been discussed include the DSI, CDS, SDA, and WFGD processes [80]. In addition, the SO_2 removal in a direct contact cooler upstream the CO_2 compression by addition of NaOH to the cooling water [81, 151, 152] and different desulfurization processes at elevated pressures during or after compression were considered and tested [94, 142, 153].

In oxy-fuel PF combustion, FGD units can be placed inside and/or outside the recirculation loop. The FGD location in the system ultimately impacts the size of the equipment and (together with the fuel sulfur content) the SO_x levels in the flue gas that needs to be treated. Moreover, it impacts other components of the combustion process by changing the composition and temperature of flue gases. In oxy-fuel combustion, also the combination of different FGD technologies may be a beneficial solution. For instance, in a process configuration with expectedly high SO_3 concentrations, a dedicated SO_3 cleaning step (e.g. by DSI) could be used to reduce SO_3 levels in the recycle loop, while SO_2 control is done via WFGD [80]. Also the combination of a partial desulfurization within and an additional flue gas cleaning step outside the recycle loop may be a good solution. Inside the recycle loop, $DeSO_x$ technologies without excessive flue gas cooling and its associated energy penalty (e.g. SDA, CDS, DSI) can be used. Outside the recycle loop, a cleaning unit can be operated before (e.g. direct contact cooler) or after (e.g. high pressure scrubber) the flue gas compressor as an additional flue gas polishing step.

Published results on the application of SDA and CDS systems in oxy-fuel firing are not available. Nonetheless, the design of the 90 MW (electric, net) FutureGen 2.0 oxy-fuel demonstration project in the USA was changed from the originally planned layout with a WFGD to a CDS system for $DeSO_x$. It was stated that a CDS system is optimally suited for this application since

it can achieve a high SO_2 removal efficiency at a lower cost, compared to a WFGD system [79]. Moreover, it is attractive for the oxy-fuel process, due to its efficient SO_3 removal. Also a SDA system has been proposed in one of the initial flow sheets for the FutureGen 2.0 project, but this approach was not followed further on [80]. For WFGD operation in oxy-fuel fired systems, comprehensive details are available since this process was extensively tested in Vattenfall's oxy-fuel pilot plant [82, 88, 154–156]. The plant's oxy-fuel WFGD used a wet scrubber that is (different to conventional absorbers in air firing) equipped with a separate sulfite oxidation and degassing tank. This is necessary to avoid contamination of the oxy-fuel flue gas by oxidation air that is in conventional systems directly added to the wet FGD sump. The process behavior of this system was similar to air fired conditions. A high SO_2 removal efficiency (> 99 %) was achieved, even when combusting high sulfur lignite (i.e. SO_2 up to 20 500 $\frac{mg}{m^3}$, STP) and the gypsum quality reached specifications required for construction applications.

2.3.2 Dry sorbent injection (DSI)

In DSI processes, dry sorbents are injected to the process at various possible locations (see figure 2.5) and are removed in dust collectors of combustion systems together with the fuel ash or in a separate filter. The correlations introduced in section 2.2.2.1 in respect to SO_x retention in the ash, generally apply also to SO_x retention with injected dry sorbents. For DSI processes, usually no dedicated reactor is required, but reactions take place directly in the existing boiler, flue gas duct, and downstream particulate removal equipment. This makes DSI processes for SO_2, SO_3, and HCl control very suitable for retrofit applications. The type of the installed particulate removal system (ESP, cyclone, or fabric filter) can have a strong impact on the performance of the DSI process [157]. Generally, the combination of a DSI process with a fabric filter can show an improved desulfurization performance, due to the better gas-solid contact compared to ESP or cyclone systems [57, 158]. In all injection locations, a homogeneous dispersion of the dry sorbent within the flue gas is crucial, to ensure that acid gases present in the gas get in contact to the injected sorbent [159, 160]. For DSI applications in PF combustion, the flue gas-sorbent contact times for adsorption and chemisorption are usually in a range of few seconds. This is why DSI desulfurization processes need to proceed rapidly, and improvements that can accelerate the SO_x and HCl capture reactions (e.g. increase of porosity and/or specific surface area) have a significant impact on the overall process performance. An approach that is often applied to improve the sorbent utilization is a separation and re-injection of unreacted sorbent with and without additional processing, which increases the gas-sorbent contact time [57, 58]. If a certain SO_2, SO_3, or HCl removal efficiency needs to be reached, a combination of different injection approaches (e.g. in-furnace $Ca(OH)_2$ injection and low temperature sodium based sorbent injection) can be a viable solution [57, 58]. Moreover, the combination of DSI with other flue gas cleaning techniques can be applied to solve particular operational problems, such as a SO_3 slip of a wet FGD scrubber that is controlled by a dedicated injection of $Ca(OH)_2$ to

the scrubber.
Acid gases react competitively with calcium and sodium based sorbents [161, 162]. The reactivity of the different acid gases and the stability of the reaction products at different temperatures governs their capture. Lime producers generally state that at lower temperatures, the reactivity of acid gases for the reactions with $Ca(OH)_2$ decrease in the order HF, SO_3, HCl, SO_2, with SO_2 being much less reactive compared to the other gases [162–164]. At higher temperatures, SO_2 seems to be most reactive followed by the other gases in the order HF, SO_3, HCl [162, 164].

2.3.2.1 Dry sorbents for flue gas cleaning

Sorbents for DSI applications to mitigate acid gas emissions are usually basic materials that form sulfates or chlorides, when reacting with SO_x and HCl, respectively. The required large amount of sorbent for industrial scale flue gas cleaning applications and associated sorbent costs as well as the sorbent reactivity and availability limit the selection of sorbent materials in practice to alkaline and earth alkaline compounds of sodium, magnesium, and, most importantly, calcium as well as mixtures thereof. Basic sorbents that react with SO_2, SO_3, and HCl, generally can also react with CO_2 to form carbonates. Since in flue gases, CO_2 concentrations are considerably higher than SO_2, SO_3, and HCl concentrations[20], it is important for the performance of a DSI sorbent that it reacts fast with SO_2, while reacting slowly with CO_2 in the temperature window in which it is applied [157].
Possible candidates for DSI processes are the naturally occurring minerals limestone, dolomite, nahcolite, and trona[21] and derivatives thereof [157, 165]. Generally, the performance of sorbents benefits from a large internal and external sorbent surface area and from the accessibility of the internal surface by pores big enough to allow diffusion of acid gas molecules [165, 166]. Therefore, sorbents are generally milled or produced with a small particle size. Hydrated lime/calcium hydrate ($Ca(OH)_2$) can be produced with much higher porosities and surface areas than limestone [157]. $Ca(OH)_2$ with its higher reactivity often offsets its higher price, compared to limestone, due to a better $DeSO_x$ efficiency. Sodium based sorbents have received increased attention for the dedicated removal of SO_3 from flue gas [167, 168]. This development is driven by the increased application of SCR systems in the USA that caused an increase of SO_3 emissions.

2.3.2.2 DSI for SO_2, SO_3, and HCl control

Figure 2.6 aims to summarize key information, presented in more detail in the following sections. It shows typical injection locations and temperatures for different sorbents, target acid gas components, and important physical, chemical, and thermodynamic fundamentals

[20] In air fired operation: Up to about $18 \cdot 10^{-2}$ $\frac{m^3}{m^3}$, dry CO_2 vs. maximum few $1000 \cdot 10^{-6}$ $\frac{m^3}{m^3}$, dry of acid gases; In oxy-fuel operation: CO_2 and SO_2 levels increased by a factor of 3-5.
[21] Nahcolite and trona are the naturally occuring ores from which $NaHCO_3$ and Na_2CO_3 are produced.

of the respective DSI processes. Three temperature ranges are commonly considered for the injection of dry sorbents in industrial combustion processes: Injection to the furnace at approx. 1100 to 1250 °C (also co-injection with fuel), injection near the economizer in the boiler at approx. 450 to 550 °C, and injection upstream of the general or an additional dust removal system at temperatures from approx. 200 to 250 °C to close to the water dew point temperature in the flue gas [57]. At the different injection locations, different sorbent types are usually used: Before filter hydrated lime or sodium based sorbents, such as trona, can be injected for acid gas control. Limestone and hydrated lime can be co-injected with the fuel or into the furnace at around 1100 °C. Each of the injection temperatures can, due to preferential reactivities, be associated with the primary abatement of a particular impurity (solid arrows in figure 2.6) but may also remove other impurities as a co-benefit (dashed arrows in figure 2.6), e.g. the injection at high temperatures to the furnace will primarily reduce SO_2 emissions but can also reduce SO_3 and HCl levels. In the bottom of figure 2.6, the most important physical, chemical,

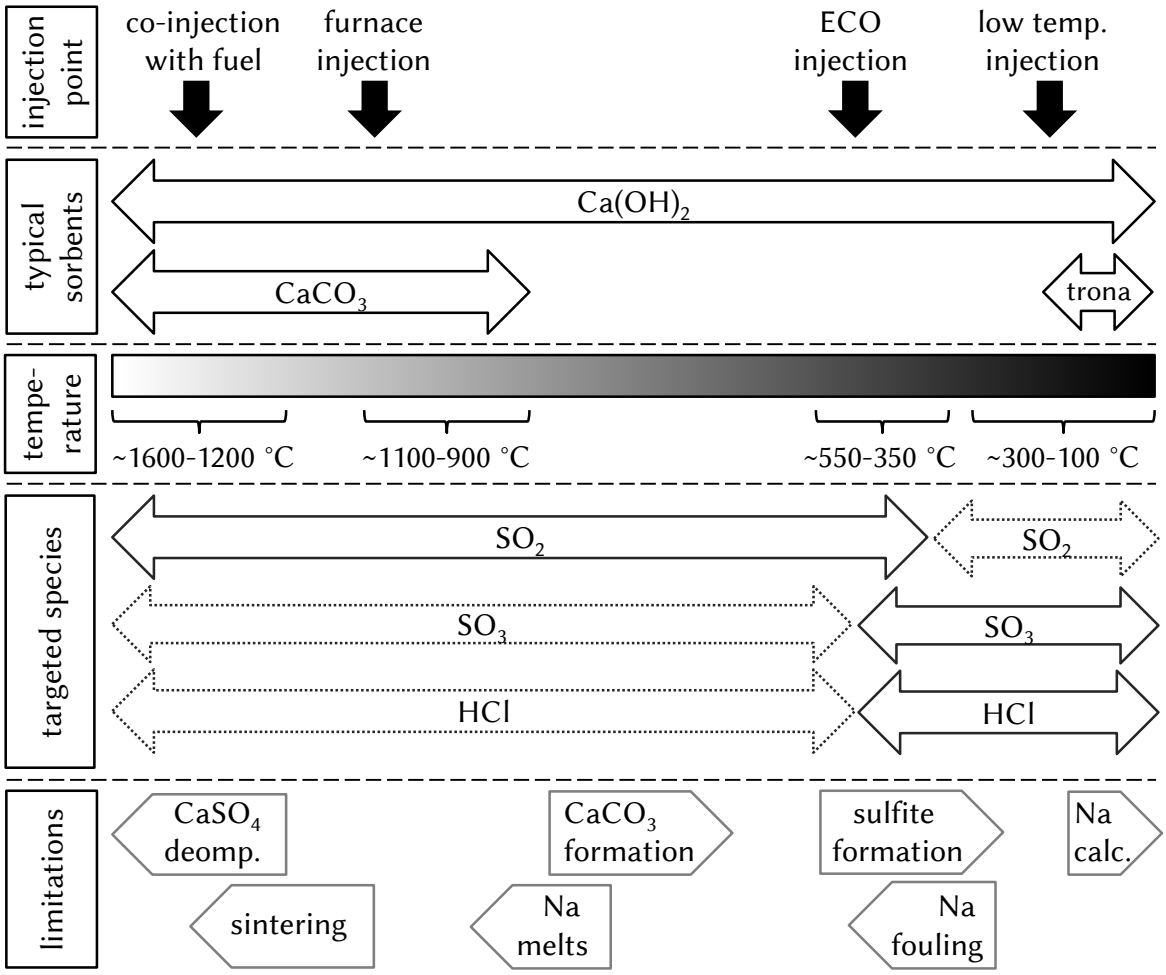

Figure 2.6: Schematic showing typical injection locations and temperatures for different sorbents, primary (solid arrows), and secondary (dashed arrows) target acid gas components and the most important physical, chemical, and thermodynamic basics of the respective DSI processes.

and thermodynamic limitations for the application of DSI at different temperatures are shown. These limitations are fundamentally responsible for the selection of injection locations and temperatures for different sorbents. For example, the injection of sodium based sorbents, due to their fouling behavior, is limited to lower temperatures. The performance of calcium based sorbents will be negatively impacted by sorbent particle sintering above approx. 1100 °C [53, 169] and $CaSO_4$ decomposition above approx. 1200 °C. Co-injection of sorbents with the fuel may suffer from these limitations, but also is a very cost efficient way to introduce sorbents homogeneously to a combustion system.
A more detailed discussion on DSI desulfurization reaction mechanisms when sorbents are injected to the furnace can be found in a review paper by Cheng et al. [169]. Fundamental studies on the reactions of CaO, $CaCO_3$, and $Ca(OH)_2$ with HCl and SO_2 are included in a dissertation by Balekdjian [166].
A comparison of data on DSI performances from different studies is often difficult since different authors generally work with different reactor systems, sorbents, fuels, and test conditions. These parameters can significantly impact the performance of DSI. Here, data on sorbent performance is only reported for experiments that seemed reasonably similar to the ones conducted in this thesis, even though, differences between the experimental conditions always occur.

SO_x control by in-furnace sorbent injection: For DSI into the furnace, mainly sorbents on basis of calcium, magnesium, or mixtures of both (e.g. dolomite) are used. When limestone is injected directly into the furnace or co-injected together with the fuel, it experiences high temperatures which cause its rapid calcination (see reaction 2.2). Similarly, hydrated lime rapidly dehydrates to CaO when injected into the furnace (reaction 2.9). It is assumed that the rapid decomposition of limestone and hydrated lime, with an instantaneous release of CO_2 and H_2O, is responsible for an increase of the porosity and a fragmentation of sorbent particles, which improves their sorption properties [53, 166]. The CaO formed from $CaCO_3$ or $Ca(OH)_2$ then reacts with SO_2 and SO_3 (reactions 2.3 and 2.10). Also a sulfation of Ca(OH)Cl and $CaCl_2$ that forms via reactions between the sorbent and HCl in the flue gas has been reported [170]. The calcination and dehydration reactions of magnesium compounds and dolomites are similar to the ones of calcium. However, the reactivity of magnesium for desulfurization is much lower, so that most of the magnesium leaves the furnace unreacted [57].

$$Ca(OH)_2 \longrightarrow CaO + H_2O \tag{2.9}$$

$$CaO + SO_3 \longrightarrow CaSO_4 \tag{2.10}$$

The efficiency of the two-step $DeSO_x$ process with calcium based sorbents is temperature dependent. At temperatures above approx. 1250 °C (depending on SO_2 partial pressure), $CaSO_4$ becomes unstable and decomposes [57], while at temperatures above 1100 °C the porous CaO

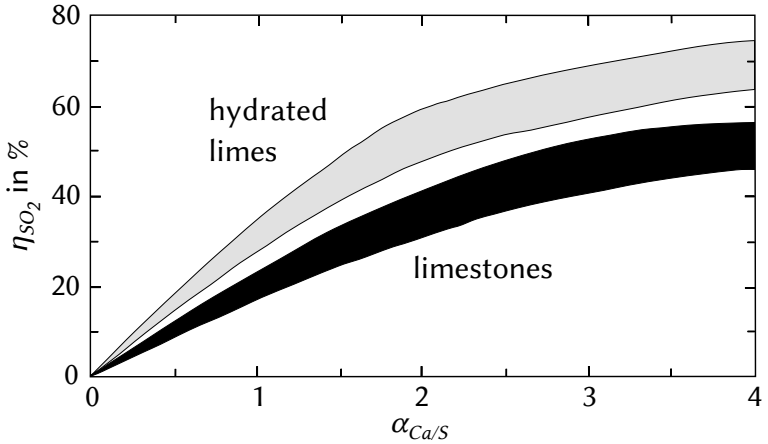

Figure 2.7: Effect of sorbent type (i.e. limestone and hydrated lime) and molar injection stoichiometry $\alpha_{Ca/S}$ on in-furnace desulfurization efficiency η_{SO_2} (adapted from [57]).

particles start to sinter, which reduces their porosity and therefore, reactivity [53, 169]. With dropping temperatures and proceeding sulfation, at temperatures between 870 and 900 °C efficient sulfation stops, which is associated to the reaction kinetics, increased diffusional resistances, and a reduced surface, due to the formed $CaSO_4$ product layer, crystal growth, and sintering [57]. The equilibrium of the sulfation reaction (i.e. with enough SO_x, a full sulfation of the sorbent would be accomplished) cannot be reached by in-furnace injection in industrial combustion processes. Therefore, injection of sorbents needs to be performed at an over-stoichiometric ratio (i.e. Ca/S molar ratio above 1). In practice, sorbent utilization of in-furnace DSI is often relatively low (10-25 %) and a large excess of sorbent needs to be injected [171]. The SO_x removal efficiency that can be achieved by DSI to the furnace depends on the sorbent type, the injection temperature, the temperature-time-history of the flue gas, the calcined sorbent's surface area and particle size, and the initial SO_2 level [57]. The dependency of the SO_2 removal of the Ca/S molar ratio is illustrated schematically in figure 2.7. The SO_2 removal performance of hydrated limes is higher than that of limestones. At a molar Ca/S ratio of 2, hydrated lime furnace injection can reach 40-60 % SO_2 removal in pilot and full scale tests, while with limestone only about 20-40 % can be accomplished [57, 58]. Experiments studying sorbent co-injection to PF fired lignite boilers yielded somewhat lower desulfurization efficiencies of 20-40 % for $Ca(OH)_2$ and 15-30 % for $CaCO_3$ [102]. In-furnace DSI can be optimized for a better sorbent utilization and SO_2 capture efficiency with a humidification and cooling of the flue gas by water injection before the particulate collector [57, 58]. This leads to an additional SO_x removal with unspent sorbent on the dust separation system.

The injection of dry sorbents to the furnace can also reduce SO_3 emissions considerably [58], via a reduction of SO_2 the precursor of SO_3, and, via the reaction of the injected sorbent with highly reactive SO_3. This may take place at high temperatures, but also at lower temperatures at which SO_2 capture is kinetically limited. SO_3 reduction efficiencies greater than 98 % were reported from in-furnace injection of hydrated lime [172].

SO_x control by economizer sorbent injection: At gas temperatures found near the economizer section of a boiler (around 450 to 550 °C) only $Ca(OH)_2$ can be applied as a sorbent since these temperatures are too low for the calcination of limestone. At these temperatures, the dehydration of $Ca(OH)_2$ (reaction 2.9) is relatively slow. This enables a direct reaction between hydrated lime and SO_2 in the flue gas, without a dehydration step (reaction 2.7) [57]. This reaction is competing with the reaction of abundant CO_2 with $Ca(OH)_2$ to form $CaCO_3$. At temperatures below 550 °C however, the very fast reaction 2.7, in which sulfite ($CaSO_3$) is formed dominates. At higher temperatures, the dehydration of $Ca(OH)_2$ is accelerated, enabling a more efficient carbonation of the formed CaO, at the expense of the sulfite reaction. The sulfite formation is only fast in a narrow temperature window of approx. 450 to 550 °C. The majority of the $CaSO_3$ that will be found in the fly ash if it is not further oxidized to $CaSO_4$, may require special treatment of the ash [58]. SO_2 removal efficiencies with hydrated lime injection to the economizer may be in a similar range to those of an injection into the furnace (e.g. about 50 % at a Ca/S molar ratio of 2.2) [157]. Also the removal of SO_3, whose formation is nearly finished at temperatures below 500 °C, can be expected to be efficient with DSI in the economizer region of boilers.

SO_x control by low temperature sorbent injection: $Ca(OH)_2$ and sodium based sorbents, such as trona, can be injected also at lower temperatures after the air preheater and before the dust collector of a power plant. To avoid contamination of the coal combustion fly ash with sorbent based material, an application is possible in which the sorbent is injected after the primary fly ash collector of a plant but before a secondary particulate removal system (i.e. a fabric filter) [58, 146]. Also in low temperature sorbent injection, over-stoichiometric amounts of sorbent need to be used. The necessary excess is lower for sodium based sorbents and particularly for SO_3 control with those sorbents, compared to calcium based materials. The basic desulfurization reactions between $Ca(OH)_2$ and SO_2 and SO_3 can be found in reaction equations 2.7 and 2.11. At temperatures below 400 °C the primary reaction products of the desulfurization reactions with SO_2 and SO_3 are $CaSO_3 \cdot \frac{1}{2}\ H_2O$ and $CaSO_4 \cdot 2\ H_2O$, respectively.

$$Ca(OH)_2 + SO_3 \longrightarrow CaSO_4 + H_2O \tag{2.11}$$

Details on reactions of sodium based sorbents, such as trona, with SO_2 and SO_3 can be found in [30]. An efficient reaction of trona and other sodium carbonates with acid gases involves a calcination reaction, which requires temperatures greater than approx. 135 °C. During this reaction, the sorbent is converted to Na_2CO_3, releasing H_2O or both, H_2O and CO_2. This reaction leads to particle fragmentation and a porosity increase, leading to an increased reactive surface area [57, 173]. The injection of sodium based sorbents at higher temperatures may suffer from the formation of sticky sodium rich melts causing fouling and corrosion problems. This generally limits the application of sodium based sorbents to temperatures below approx.

800 to 850 °C [174].

Low temperature DSI can be employed for SO_2 removal (which simultaneously removes SO_3) or primarily to control SO_3. When only SO_3 needs to be controlled, the amount of sorbent that is injected is considerably lower than in SO_2 control applications. For SO_2 control, humidification and cooling of the flue gases to temperatures closely (i.e. less than 10 °C) approaching the saturation temperature of water in the flue gas is generally carried out to improve the sorbent performance. At an approach to saturation of 30 °C, $Ca(OH)_2$ injection obtained a SO_2 reduction of 24 %, while at an approach temperature of 10 °C, 50-54 % of the SO_2 was captured (both with molar Ca/S ratios of 2) [57]. At low temperatures, sodium based sorbents such as trona or $NaHCO_3$, show considerably higher SO_2 removal efficiencies than calcium based sorbents. SO_2 removal efficiencies of 67 and 80 % were obtained at a stoichiometric ratio of 1 for the two sorbents, respectively [57]. The SO_2 removal efficiencies, reported above correspond to results obtained with fabric filters. ESP systems can yield considerably lower performances (by 10-30 %) [57].

For DSI control of SO_3, also sodium and magnesium based sorbents can be injected downstream of the economizer and SCR and upstream of the air preheater to remove SO_3 that is responsible for ammonia bisulfate formation and air preheater plugging [167, 168, 171]. With sodium based sorbents good SO_3 removal performances can be obtained reducing SO_3 concentrations to below $2 \cdot 10^{-6} \frac{m^3}{m^3}$, dry. The injection of powdered $Ca(OH)_2$ at low temperatures after the air preheater for SO_3 control can yield high SO_3 removal efficiencies (60-80 %) but requires a higher excess of sorbent (e.g. Ca/SO_3 of 8-17, depending on lime) [171].

Dry sorbent injection for HCl control: Sorbents used for SO_x control, generally also remove HCl efficiently. At temperatures above the $CaCO_3$ and $Ca(OH)_2$ calcination temperatures, these sorbents are calcined to CaO (reactions 2.2 and 2.9) which then reacts with HCl to form $CaCl_2$, according to reaction 2.12 [53, 175]. At temperatures at which $Ca(OH)_2$ is stable, also a direct reaction between $Ca(OH)_2$ and HCl, according to equation 2.13, may be possible. However, various authors [159, 175–178] highlighted that Ca(OH)Cl seems to be an important intermediate product in a reaction path, involving reactions 2.14 and 2.15. Dal Pozzo et al. [179] state that Ca(OH)Cl as final reaction product seems to dominate at lower temperatures, while at temperatures in the range of 500 °C and above, $CaCl_2$ is the main product. A further pathway to capture HCl involves the reaction of $CaSO_3 \cdot \frac{1}{2} H_2O$ and HCl that can release captured SO_2. In contrast to $CaSO_3 \cdot \frac{1}{2} H_2O$, $CaSO_4$ and $CaSO_4 \cdot 2 H_2O$ are stable in respect to reactions with HCl [176]. Partanen et al. [178, 180] showed in TGA studies that at higher temperatures (650 and 850 °C) in presence of SO_2 the sulfation of CaO and $CaCO_3$ suppresses the chlorination of the sorbents strongly. Similar observations were made by Lin and Chyang [181]. On the other hand, Partanen et al. [178, 180] found that the presence HCl in the gas atmosphere considerably improved the sulfur capture with limestone. This effect was explained by the formation of a

molten $CaCO_3$-$CaCl_2$-$CaSO_4$ and at higher temperatures a molten $CaCl_2$-$CaSO_4$ phase, which reduces diffusional resistances of the solid product layer and alters the particle morphology so that additional sorbent material becomes accessible to the acid gases. The positive effect of such melts is also active at temperatures below the calcination temperature of $CaCO_3$. When sodium carbonate based sorbents are used to control HCl, they should be injected at temperatures above 135 °C to allow for sorbent flash calcination, which increases the sorbent's surface area and therefore, its performance. The calcination product Na_2CO_3 then reacts with HCl [173].

$$CaO + 2\,HCl \longrightarrow CaCl_2 + H_2O \tag{2.12}$$

$$Ca(OH)_2 + 2\,HCl \longrightarrow CaCl_2 + 2\,H_2O \tag{2.13}$$

$$Ca(OH)_2 + HCl \longrightarrow Ca(OH)Cl + H_2O \tag{2.14}$$

$$Ca(OH)Cl + HCl \longrightarrow CaCl_2 + H_2O \tag{2.15}$$

In industrial practice, with calcium based as well as with sodium based sorbents, HCl removal ratios greater than 95 % can be achieved at relatively moderate injection stoichiometries [162, 164, 173, 182–184]. Unfortunately, the authors of such publications, who represent commercial sorbent manufacturers, do not give sorbent injection stoichiometries and only insufficient information to allow for a calculation of those. For one of these publications [164], injection ratios relating the sorbent and acid gas mass flows are given. Assuming that the only relevant acid gas species in this context was HCl, the molar calcium to Cl_2 ratios can be estimated. In these experiments ($y_{HCl} \approx 200 \cdot 10^{-6}\ \frac{m^3}{m^3}$) with injection of a highly porous $Ca(OH)_2$ sorbent upstream both, a fabric filter and an ESP system, a HCl removal efficiency of 90 % was reached at $\alpha_{Ca/2Cl}$ values of 1.35 and 1.2 for the two ash separator systems, respectively [164].

2.3.2.3 Process alterations and problems due to dry sorbent injection

DSI has undesired effects to power plants. The furnace and boiler injection of dry sorbents can result in convective tube fouling [57, 58, 169, 185], even though the formed deposits are often relatively soft so that they can be removed by soot blowing [58]. Fouling problems induced by DSI may also occur at air preheaters, flue gas ducts, and particulate removal systems [58, 171]. This can be particularly problematic with DSI upstream of ash separators when flue gas temperatures are closely approaching the water saturation temperature in the flue gas [57].
DSI increases the particulate loading in the flue gas and thus, it may happen that particulate removal systems cannot keep the respective emission limits anymore [160]. The extent of the increase of the ash loading depends on the application. If DSI technologies are used primarily to reduce SO_3 levels or if only low levels of HCl and SO_2 are present in the flue gas, the DSI sorbent feed rates are low and the impact on the flue gas particulate loading is limited. However, if significant SO_2 removal extents are desired and higher sulfur coals are combusted, a significant increase of the particulate loading is to be expected [186]. In addition to the increased ash

loading, DSI changes the particle size distribution (PSD) of the ash generally reducing the average particle size of the ash and by-product mixture and can also change the cohesivity of ashes. This can impact downstream particulate removal equipment leading to particulate (re-)entrainment in ESP systems and increased dust cake pressure losses in fabric filters [158, 186]. Sorbent injection can also change the particulate resistivity of the ash and by-product mix. The ash resistivity may be increased or decreased, depending on the particular application (e.g. in-furnace or low temperature sorbent injection, type of sorbent) [172, 186, 187]. This can impact the ESP ash collection efficiency.
Sodium based sorbents show a high solubility in water, which may have negative impacts on ash utilization and disposal limiting the ash saleability or increasing disposal costs [160, 167, 168], when limits in the respective standards (e.g. [63, 188]) are exceeded. The products of the desulfurization reaction with calcium based sorbents are not easily leachable and therefore, produced by-products are less problematic [157]. However, the ash saleability may still be impacted by the application of such sorbents if the content of CaO, free CaO, chlorine, and sulfur for the utilization of fly ashes in concrete or cement are exceeded [63, 188, 189] (see also section 2.1.4). To avoid contamination of fly ash, DSI downstream of a primary fly ash separator but upstream a secondary particulate removal system is possible [146].

2.3.2.4 Dry desulfurization processes in oxy-fuel combustion

Published information on the application of DSI in oxy-fuel firing is limited and especially experimental data from test facilities of significant scales, with actual flue gas recirculation instead of a simulation of the oxy-fuel combustion atmosphere, is missing. Liu and his coworkers [11, 104, 105, 190–192] have studied reactions relevant to desulfurization in O_2/CO_2 and in O_2/N_2 atmospheres experimentally and developed desulfurization models for oxy-fuel recycle combustion that predict a very efficient desulfurization in such systems (see also p. 21). As introduced in section 2.2.2.1, the desulfurization efficiency is positively impacted by longer residence times and higher SO_2 concentrations. Both these parameters are increased in practical oxy-fuel systems and hence, a better desulfurization performance is expected in oxy-fuel operation. The published experimental work by Liu and coworkers [11, 104, 105, 190–192] did not involve experiments testing DSI desulfurization in an actual oxy-fuel recycle combustion system. The predicted effect of a significantly enhanced desulfurization performance in oxy-fuel operation was first validated in oxy-fuel recycle experiments by the author of this dissertation [37, 39] and section 4.2.2 of this thesis summarizes the findings comprehensively.
Other work on DSI in oxy-fuel operation has been focusing on an application of the DSI technology for SO_3 control [24]. Public information from this study is very limited and the used sorbents are not specified, even though SO_3 removal efficiencies up to 95 % by DSI were reported with no significant difference of the performance in air and oxy-fuel firing. The observed SO_3 removal was better when the sorbent was injected not into the furnace but downstream at SCR

inlet temperatures. In oxy-fuel process designs for the Futuregen 2.0 demonstration project, DSI has been considered for control of excessive SO_3 levels that may trigger low temperature corrosion [80]. In a proposed layout for high sulfur coal oxy-fuel combustion, a dry trona injection is placed after the gas preheater and before the fabric filter.

3 Methods

Throughout this thesis SI units are used. In order to ease comprehension of reported values for a reader who is more familiar to units such as volumetric and mass percentages and parts-per-million, SI units are used with pre-factors keeping the same numeric dimensions, i.e. $10^{-2}\,\frac{\mathrm{m}^3}{\mathrm{m}^3}$, $10^{-2}\,\frac{\mathrm{kg}}{\mathrm{kg}}$, and $10^{-6}\,\frac{\mathrm{m}^3}{\mathrm{m}^3}$. As far as possible, for gas concentrations and volumetric flow rates reported in this thesis information on their wet or dry reference state is given. Also for fuel analyses, the analysis reference state (i.e. raw, dry, dry and ash free) is usually given. In few instances, reporting data from others, such indications are not possible due to a lack of the respective information.

3.1 Experimental combustion rigs

3.1.1 20 kW combustion rig (BTS-VR)

Certain experiments of this thesis were carried out at the electrically heated, once-through combustion rig BTS-VR that is shown schematically in figure 3.1. The system is designed for a maximum thermal power of approx. 20 kW and is fed with fuels by a gravimetrically controlled screw feeder. The fuel is transported to the furnace pneumatically with a small amount of carrier gas (approx. 1.5 $\frac{\mathrm{m}^3}{\mathrm{h}}$, *STP*, dry). It is introduced to the furnace via the core pipe of the top-mounted burner that is surrounded by two concentric ring annuli for primary and secondary oxidant gas introduction. Carrier, primary, and secondary gas streams can be controlled independently with help of mass flow controllers. They can be supplied with air or mixtures of CO_2 and O_2, to simulate oxy-fuel combustion atmospheres. In order to simulate recirculation of impurities, such as SO_2, NO, Hg, and moisture, those components can be added to the secondary gas line. When steam was injected, the line was trace heated to avoid condensation of water. Addition of SO_2 and NO was done with help of mass flow controllers that were supplied by gas bottles containing those components in pure form. Hg vapor was provided with a system that can saturate a small nitrogen gas stream in a temperature-controlled elemental Hg evaporation vessel. The addition of steam was realized with help of a flow-type water evaporator supplied with a defined mass flow of liquid water via a peristaltic pump. This mass flow was determined on basis of the weight loss of the water tank that was measured

by a balance. The accuracy and stability of this steam generation system was successfully crosschecked versus H_2O concentration measurements with help of an FTIR gas analyzer. The furnace has a length of 2.5 m and a diameter of 0.2 m. Its electrical heating is divided into five zones that can be operated individually up to temperatures of 1400 °C. The furnace of BTS-VR offers access for sampling of flue gases, deposits, and ashes and for sorbent injection via a lateral port in a distance of 1.5 m from the burner and via the furnace exit. A sorbent injection probe can be introduced from the furnace exit counter-currently to the gas flow (see also figure 3.6). The flue gas production in all experiments of this thesis was kept constant at about 11.5 $\frac{m^3}{h}$, *STP*, wet. At the exit of the furnace, the majority of the produced flue gas (about 9.5 to 10 $\frac{m^3}{h}$, *STP*, wet) was extracted into a main flue gas duct, with the remainder being directed to an exhaust system. Since the bottom part of the BTS-VR furnace, with its provisions for introduction of sampling and DSI probes, is difficult to seal gas tight, this overflow of gas

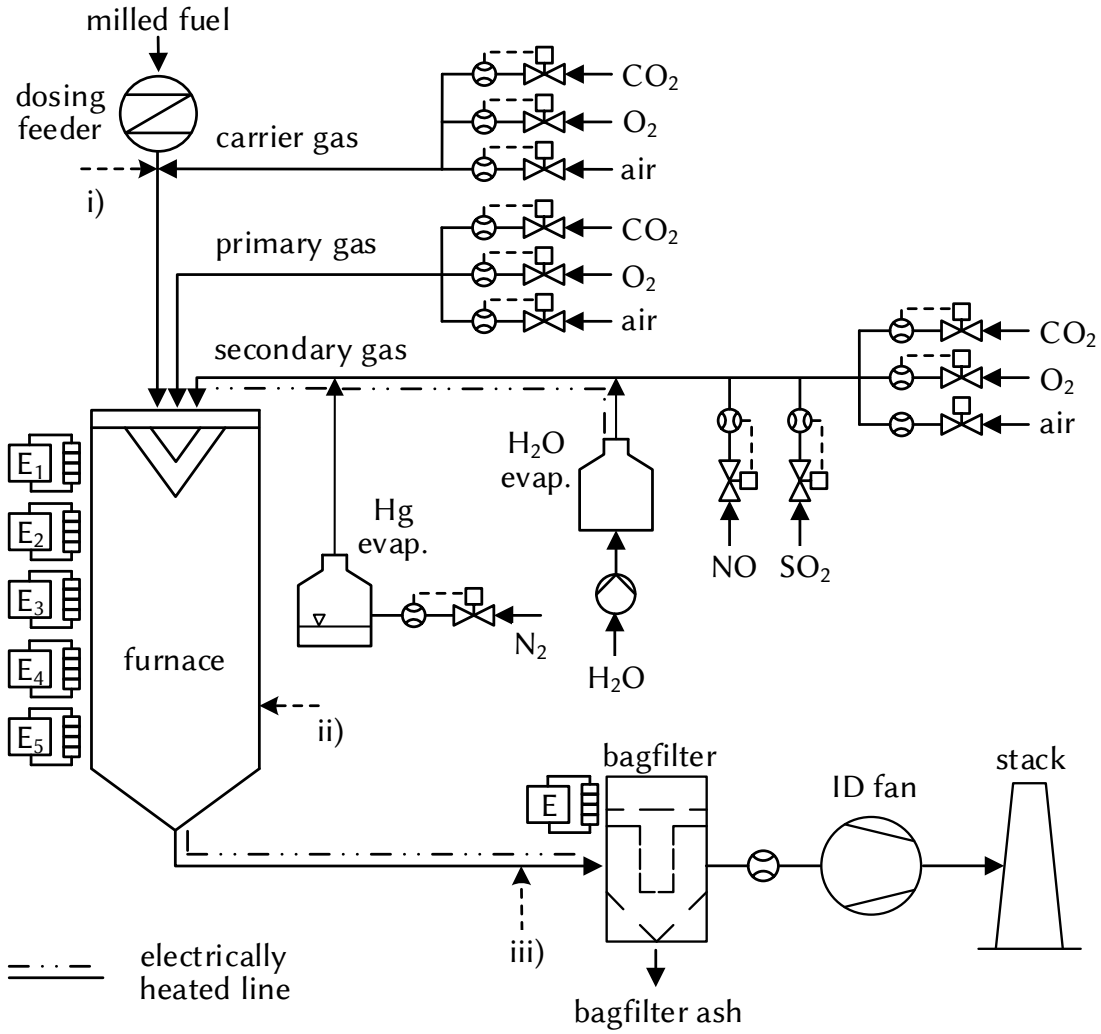

Figure 3.1: Schematic of the 20 kW combustion test facility BTS-VR. The locations at which dry sorbents have been injected in DSI experiments are highlighted by dashed arrows and marked with i), ii), and iii).

is required to avoid ambient air from being introduced into the main flue gas duct. This is of particular importance for experiments investigating SO_3 formation and DSI that are included in this thesis. Those experiments rely on reliable gas concentration measurements along the main flue gas duct. The flue gas duct of BTS-VR is electrically trace heated to reduce heat losses and maintain a temperature and residence time profile that is similar to the one of a power plant. Also the facility's fabric filter is electrically heated to maintain operating temperatures in a range of about 200 °C. In the experiments included in this thesis, a number of different experimental settings were tested that are introduced in detail in sections 3.3.1, 3.3.4, and 3.3.3.1.

3.1.2 500 kW combustion rig (KSVA)

The 500 kW (thermal) atmospheric, pulverized coal combustion test rig (KSVA, see figure 3.2) can be operated in air and in oxy-fuel combustion mode with flue gas recirculation. In the conducted

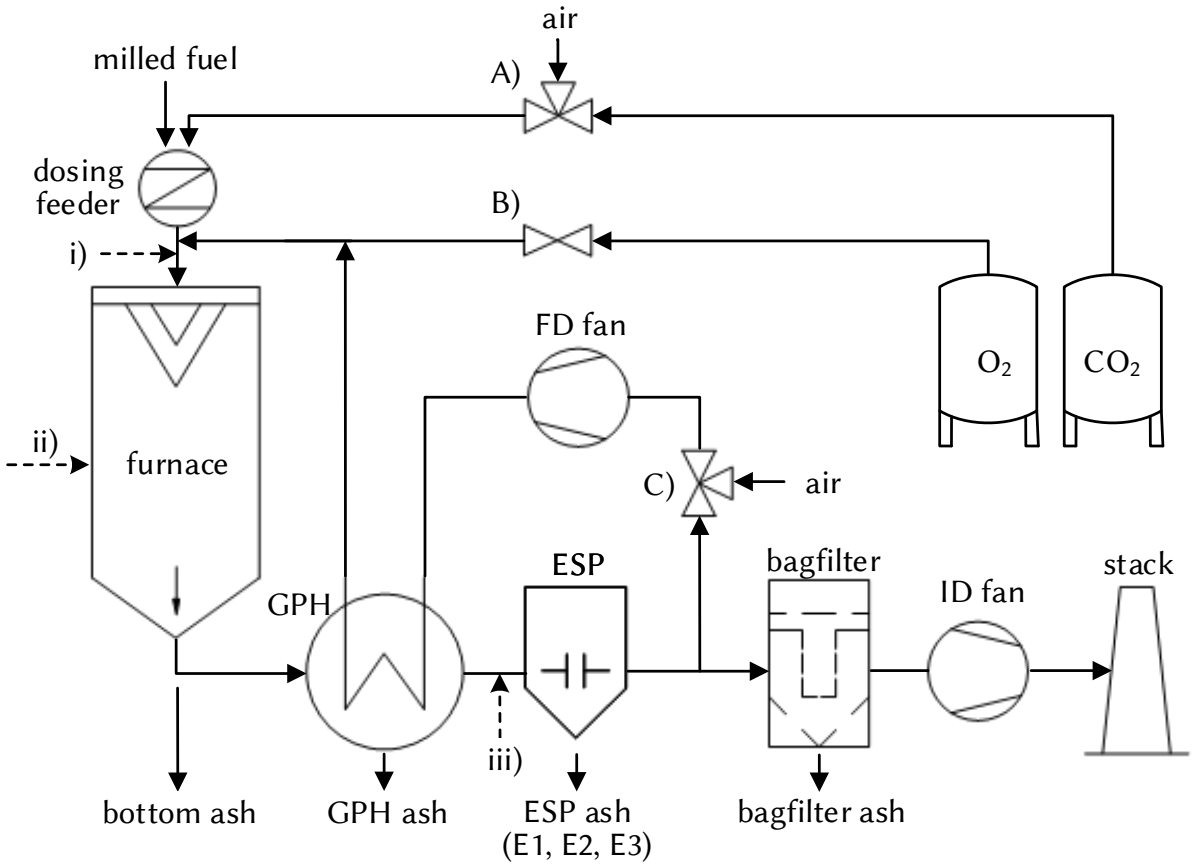

Figure 3.2: Schematic of the 500 kW (thermal) combustion test facility KSVA. The valves A), B), and C) allow to operate the plant in air as well as oxy-fuel mode. The locations at which dry sorbents have been injected in dedicated experiments are highlighted by dashed arrows and marked with i), ii), and iii).

experiments, KSVA was operated at a load of about 300 kW (thermal), which corresponds to fuel feed rates of about 40 $\frac{kg}{h}$ for hard coal and about 60 $\frac{kg}{h}$ for lignite. The KSVA plant is not electrically heated which implies a relatively long start-up and heating phase (approx. 10 to

20 h) to prepare for experiments. Therefore, for all experimental campaigns included in this thesis the facility has been continuously operated in a 24 h-3-shift mode for durations of around 100 h. The plant's furnace has a total length of approx. 7 m and an internal diameter of 0.8 m (see figure 3.6b). The milled fuel is fed to the top mounted burner pneumatically by air or, in oxy-fuel operation, by CO_2, using a gravimetric feeding system. At the burner, the fuel is mixed with oxidant gas (i.e. air or oxygen enriched recirculated flue gas). The KSVA facility is equipped with an air/oxidant gas pre-heater and an ESP. In oxy-fuel operation, flue gas is recirculated wet after the electrostatic precipitator (ESP), preheated in the oxidant preheater, mixed with O_2 from a tank, and supplied to the burner. Certain experiments reported in this thesis (oxy-fuel combustion of lignite L2) were conducted without premixing of O_2 and instead, with direct injection of pure O_2 via separate nozzles of the burner. There are measuring ports all along the furnace (see figure 3.6b) that can be used for gas composition, temperature, and other measurements and to sample fly ash and deposits from the furnace with dedicated sampling probes. A permanent flue gas sampling and analysis system is installed at the furnace exit for continuous measurement of the flue gas composition (O_2, CO, CO_2, SO_2, and NO_x). H_2O can be measured after the ESP.

3.1.3 30 MW oxy-fuel pilot plant "Schwarze Pumpe"

Several authors previously described Vattenfall's oxy-fuel pilot plant and its process configuration [3, 155, 193, 194]. The pilot plant was operated between 2008 and 2014 and was located in Lusatia (Eastern Germany), next to the 1600 MW (electric) lignite fired power plant "Schwarze Pumpe". The facility was fired by a single, 30 MW (thermal), top-mounted burner and was equipped with an ASU, flue gas cleaning equipment (i.e. ESP, WFGD), a flue gas condenser, and a CPU. The system could be operated in air and oxy-fuel mode. For oxy-fuel combustion it employed a flue gas recirculation downstream the ESP (as in the KSVA facility) and upstream WFGD (i.e. recycle option a in figure 2.2). This implies that wet sulfur rich flue gas is recirculated to the boiler leading to considerably increased SO_2 levels in oxy-fuel operation, compared to air firing. The gas for fuel feeding was cleaned and dried recirculated flue gas.
During the tests reported in this thesis the lignite L3 was combusted under oxy-fuel conditions in a mixture of recirculated flue gas and O_2. Fly ash and deposits were sampled from measuring ports in the first and second draft of the plant's boiler in a distance of approx. 0.5 m from the furnace wall. The boilers first draft has a quadratic cross-sectional area of approx. 16 m^2 and a height of approx. 9.5 m. Figure 3.3 displays the boiler's first and second draft schematically, with the locations of sampling ports used in the present study. Samples were taken from level 4 in the first draft and level 8 at the entry of the second draft just before the first convective heat exchanger (SH1). During the sampling campaign reported in this thesis flue gas was sampled just downstream of the ESP and its composition was continuously analyzed. In addition, SO_3 measurements have been conducted at two locations upstream the ESP: Directly before ESP

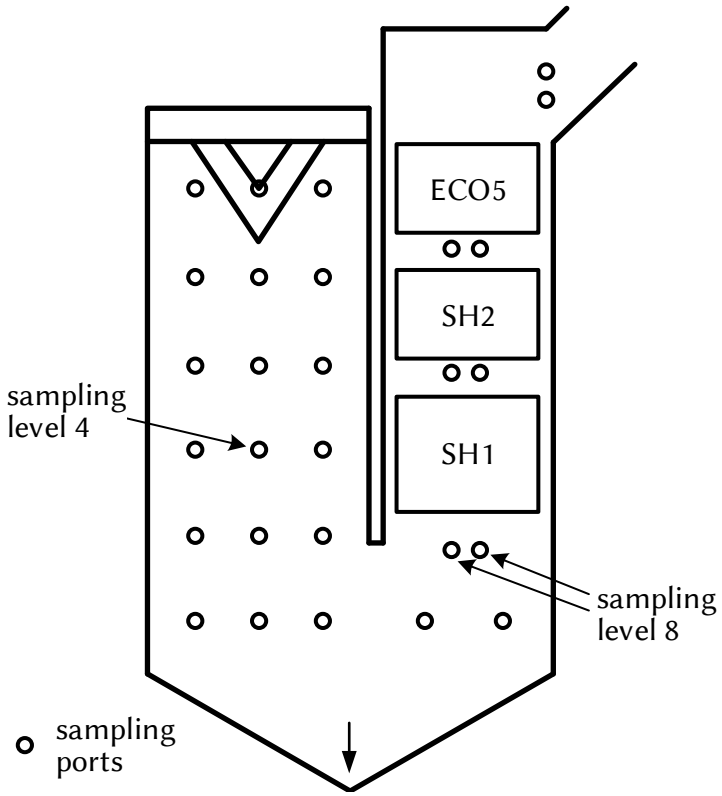

Figure 3.3: Schematic of the first and second draft of the boiler of the oxy-fuel pilot plant "Schwarze Pumpe" with the ash and deposit sampling ports used in this study. SH1, SH2, and ECO5 indicate different convective heat exchangers placed in the second draft.

at a flue gas temperature of about 180 °C and in the third draft between the economizer heat exchangers at a gas temperature of approx. 330 °C.

3.2 Used materials

3.2.1 Fuels

For this thesis, three different lignites (L1, L2, L3) and four different hard coals (high-volatile bituminous coals: C1, C2, C3, C4) have been used in experiments at different facilities. In table 3.1, NCV, proximate, and elemental analyses of these fuels are presented. The investigations on the stability of sulfates in ashes and deposits and on the self-retention of sulfur within the fuel's ash were conducted with 3 different batches of pulverized, pre-dried Lusatian lignite. Investigations at IFK's 20 kW (thermal) BTS-VR rig were conducted using the lignite L2. Experiments at the 500 kW (thermal) KSVA were using both lignite qualities L1 and L2. The test campaign at Vattenfall's 30 MW (thermal) oxy-fuel pilot plant was performed combusting the lignite L3. The L2 lignite is of a comparable quality to the L3 lignite. These two lignites are relatively low in ash and sulfur (approx. $6 \cdot 10^{-2}\,\frac{\mathrm{kg}}{\mathrm{kg}}$ and $0.7 \cdot 10^{-2}\,\frac{\mathrm{kg}}{\mathrm{kg}}$, respectively), compared to the L1 lignite quality ($18.8 \cdot 10^{-2}\,\frac{\mathrm{kg}}{\mathrm{kg}}$ and $1.98 \cdot 10^{-2}\,\frac{\mathrm{kg}}{\mathrm{kg}}$, respectively) that represents a more

Table 3.1: Net calorific value (NCV), proximate, and elemental analyses of the fuels used in this thesis.

	NCV	W	A	V	C_{fix}	C	H	N	S	O	Cl
	$\frac{J}{g}$	$10^{-2}\ \frac{kg}{kg}$									
fuel	raw		db	daf							
L1	18300	9.1	18.8	59.5	40.5	66.0	7.1	0.7	1.98	24.3	n.d.
L2	21200	9.8	5.6	57.4	42.6	66.5	4.7	0.7	0.56	27.6	n.a.
L3	21100	8.8	6.2	57.6	42.4	65.1	5.3	0.6	0.81	28.1	0.02
C1	18000	3.9	32.5	36.0	64.0	73.8	4.3	1.1	0.32	20.5	n.d.
C2	25000	1.5	23.0	50.6	49.4	78.3	6.7	1.1	0.67	13.2	0.01
C3	26700	3.7	9.8	35.9	64.1	77.2	5.2	2.0	0.72	14.9	0.02
C4	30400	1.6	9.4	38.7	61.3	81.9	5.2	1.6	2.67	8.3	0.30

W = water, A = ash, V = volatiles, C_{fix} = fixed carbon, n.a. = analysis not available, n.d. = not determinable
O calculated by difference: $\gamma_O = 1 - \gamma_C - \gamma_H - \gamma_N - \gamma_S - \gamma_{Cl}$ (all γ_i in daf state)

Used standards: NCV - DIN 51900-1 [195]; C_{fix} - DIN 51734 [196]; W - DIN 51718 [197]; A - DIN 51719 [198]; V - DIN 51720 [199]; C, H, N - DIN 51732 [200]; Cl - DIN 51727 [201]; S - DIN 51724-1 [202]; O - DIN 51733 [203]

typical Lusatian lignite quality for power production.

The high-volatile bituminous coals C1, C2[22], and C3 were used for experiments at the 20 kW BTS-VR rig for studies on the SO_3 formation in air and oxy-fuel operation. These three coals were supplied from Australia and are comparable[23] to the coal qualities previously tested by IHI [10] (air and oxy-fuel tests in 1.2 MW (thermal) scale, with flue gas recirculation) in the framework of the Callide oxy-fuel project. These three coals differ considerably in their ash and sulfur contents. The ash contents of coals C1, C2, and C3 are in a proportion of roughly 3 to 2 to 1, with coals C1 and C2 showing very high ash contents of $32.5 \cdot 10^{-2}\ \frac{kg}{kg}$ and $23.0 \cdot 10^{-2}\ \frac{kg}{kg}$. The sulfur contents are in a proportion of about 1 to 2 to 2 and are relatively low (approx. $0.3 \cdot 10^{-2}\ \frac{kg}{kg}$ and $0.7 \cdot 10^{-2}\ \frac{kg}{kg}$). The fuel C4 is a high sulfur and chlorine hard coal ($2.67 \cdot 10^{-2}\ \frac{kg}{kg}$ and $0.30 \cdot 10^{-2}\ \frac{kg}{kg}$, respectively), mined in the USA. This coal quality was selected for testing of DSI for SO_2, SO_3, as well as HCl control at IFK's 20 kW BTS-VR and 500 kW KSVA test rigs. In addition, with this coal a limited number of experiments investigating SO_3 formation were conducted at BTS-VR. An analysis of this fuel for water soluble anions showed besides the expected considerable content of chloride, no significant amounts of bromide, iodide, and fluoride.

All tested fuels were also analyzed for their main ash forming oxides[24], according to DIN 51729

[22] For a bituminous coal, coal C2 has a relatively high volatile content. Nonetheless, due to its high calorific value it is classified as such.

[23] Some differences in the compositions occurred, due to variations of the coals across the mine sites with time.

[24] I.e. Al_2O_3, BaO, CaO, Fe_2O_3, K_2O, MgO, Mn_2O, Na_2O, P_2O_5, SiO_2, SO_3, SrO_2, TiO_2.

Table 3.2: Analyses of the fuels used in this thesis for main ash forming elements by inductively coupled plasma optical emission spectrometry (ICP-OES).

	Al_2O_3	CaO	Fe_2O_3	K_2O	MgO	MnO	Na_2O	P_2O_5	SiO_2	SO_3	TiO_2
fuel	$10^{-2}\ \frac{kg}{kg}$, db										
L1	7.1	9.9	9.6	1.2	2.8	0.0	0.2	0.1	57.6	11.0	0.5
L2	3.9	28.1	25.4	0.7	9.1	n.a.	0.1	0.0	13.2	19.3	0.2
L3	3.9	20.5	20.3	0.7	8.2	0.2	0.3	n.d.	29.7	15.9	0.3
C1	26.2	1.2	6.8	0.4	0.7	n.a.	0.1	0.2	59.0	3.0	2.4
C2	21.5	0.4	1.2	0.4	0.7	n.a.	0.2	0.0	64.5	7.2	3.9
C3	22.1	6.7	10.9	0.9	1.7	n.a.	1.2	1.7	31.8	21.8	1.2
C4	20.6	3.8	14.6	2.4	1.0	0.0	0.7	0.2	52.5	3.0	1.1

n.a. = analysis not available, n.d. = not determinable

[204]. The results are shown in table 3.2. The ashes of the lignites L2 and L3 have a relatively high content of CaO, Fe_2O_3, SiO_2, and SO_3. These four compounds account for more than $85 \cdot 10^{-2}\ \frac{kg}{kg}$ of the ashes. The contents of earth alkalis (calcium, magnesium) in the ashes are responsible for the high sulfur self-retention potential of the fuels. The molar earth alkali ($\alpha_{(Ca+Mg)/S}$) and, to a lesser extent, alkali ($\alpha_{(Na_2+K_2)/S}$) to sulfur ratios can serve as indicators for the sulfur retention potential of the fuels. Those were calculated, according to equations 3.1 and 3.2, and they are listed in table 3.3.

$$\alpha_{(Ca+Mg)/S} = \frac{\gamma_{A,db}}{\gamma_{S,db}} \cdot M_{M,S} \cdot \left(\frac{x_{CaO,A}}{M_{M,CaO}} + \frac{x_{MgO,A}}{M_{M,MgO}} \right) \tag{3.1}$$

$$\alpha_{(Na_2+K_2)/S} = \frac{\gamma_{A,db}}{\gamma_{S,db}} \cdot M_{M,S} \cdot \left(\frac{x_{Na_2O,A}}{M_{M,Na_2O}} + \frac{x_{K_2O,A}}{M_{M,K_2O}} \right) \tag{3.2}$$

$$\gamma_{Ca+Mg,db} = \gamma_{A,db} \cdot \left(x_{CaO,A} \cdot \frac{M_{M,Ca}}{M_{M,CaO}} + x_{MgO,A} \cdot \frac{M_{M,Mg}}{M_{M,MgO}} \right) \tag{3.3}$$

$$\gamma_{K+Na,db} = \gamma_{A,db} \cdot 2 \cdot \left(x_{K_2O,A} \cdot \frac{M_{M,K}}{M_{M,K_2O}} + x_{Na_2O,A} \cdot \frac{M_{M,Na}}{M_{M,Na_2O}} \right) \tag{3.4}$$

$$\gamma_{Fe,db} = \gamma_{A,db} \cdot x_{Fe_2O_3,A} \cdot \frac{2 \cdot M_{M,Fe}}{M_{M,Fe_2O_3}} \tag{3.5}$$

$\alpha_{(Ca+Mg)/S}$ of the lignites L2 and L3 are 2.5 and 1.5, respectively. The ash of lignite L1 shows a similar character with a considerable CaO, Fe_2O_3, and SO_3 content. However, the ash of this fuel contains much more SiO_2 and Al_2O_3. Presumably, the reason for this is a contamination of

Table 3.3: (Ca+Mg)/S and (2Na+2K)/S ratios of the used fuels.

	L1	L2	L3	C1	C2	C3	C4
$\alpha_{(Ca+Mg)/S}$	0.9	2.5	1.5	1.9	0.4	0.8	0.1
$\alpha_{(Na_2+K_2)/S}$	0.06	0.03	0.03	0.28	0.11	0.14	0.05

the lignite by inerts, such as sand and clay. The higher sulfur content of lignite L1 leads to a lower but still considerable $\alpha_{(Ca+Mg)/S}$ ratio of 0.9.

All hard coals' ashes contain considerably higher amounts of Al_2O_3 than the lignite ashes, indicating a higher content of alumino-silicatic minerals. Such minerals as well as silicates frequently contain earth alkali and alkali elements. Alkalis and earth alkalis contained in silicates and alumino-silicates are often relatively stable and therefore, not or less available for sulfation reactions between the flues gas and the ash. This should be considered when assessing the $\alpha_{(Ca+Mg)/S}$ ratios of these fuels. It is possible that even though the hard coals C1 and C3 show considerable $\alpha_{(Ca+Mg)/S}$ ratios of 1.9 and 0.8, respectively, their sulfur retention potential may be low. This is particularly true for coal C1, the high $\alpha_{(Ca+Mg)/S}$ ratio of which is mainly caused by its very high ash and low sulfur content. The coals C2 and C4 have a very low sulfur self-retention potential with $\alpha_{(Ca+Mg)/S}$ ratios of only 0.4 and 0.1, respectively. This is positive in respect to the DSI tests performed with the C4 coal that can be assumed to be practically unaffected by SO_2 retention in the ash.

In addition to earth alkalis, also alkali compounds may react with SO_2 and SO_3. Due to the higher availability of earth alkalis, generally those dominate the desulfurization. However, for SO_3 capture also alkalis may be relevant. Therefore, for the hard coals for which SO_3 formation was studied, also the earth alkali $\gamma_{Ca+Mg,db}$ and in addition, the alkali $\gamma_{K+Na,db}$ contents were calculated, according to equations 3.3 and 3.4 (see table 3.4). One sees that coal C4 has the highest alkali content followed by coals C3, C1, and C2. Again it should be highlighted that particularly for the high ash coals C1 and C2, a considerable portion of the alkalis may be relatively stable within silicates and alumino-silicates and therefore, not accessible for desulfurization reactions. In respect to possible catalytic SO_3 formation, also the iron content of the fuels is of interest. The respective values were determined, according to equation 3.5, and can be found in table 3.4. Coal C1 has the highest iron content of $1.5 \cdot 10^{-2}\ \frac{kg}{kg}$, followed by coals C4, C3, and C2, with contents of $1.0 \cdot 10^{-2}\ \frac{kg}{kg}$, $0.7 \cdot 10^{-2}\ \frac{kg}{kg}$, and $0.2 \cdot 10^{-2}\ \frac{kg}{kg}$, respectively.

Table 3.4: Alkali, earth alkali, and iron contents of the tested hard coals.

	unit	C1	C2	C3	C4
$\gamma_{K+Na,db}$		0.12	0.10	0.15	0.22
$\gamma_{Ca+Mg,db}$	$10^{-2}\ \frac{kg}{kg}$, db	0.42	0.16	0.57	0.31
$\gamma_{Fe,db}$		1.5	0.2	0.7	1.0

3.2.2 Sorbents

Two different sorbents have been tested in experiments investigating SO_2, SO_3, and HCl control in air and oxy-fuel firing. Table 3.5 summarizes key characteristics of those sorbents. Both are industrial products for dry flue gas cleaning, i.e. finely milled limestone and highly porous hydrated lime. The sorbent analyses were provided by the sorbent manufacturer. Standards used for these analyses were not provided. Analyses of the sorbents used in the experiments showed that their moisture content was below $0.5 \cdot 10^{-2}\ \frac{\text{kg}}{\text{kg}}$, and thus, assuming dry sorbents in the calculation of $\alpha_{Ca/S}$ and $\alpha_{Ca/2Cl}$ is justified.

The tested sorbents $CaCO_3$ and $Ca(OH)_2$ are considerably differing in their composition and properties, with $CaCO_3$ being relatively fine (D_{90} of 24.2 µm) and $Ca(OH)_2$ being coarser (D_{90} = 39.3 µm). In contrast, the specific surface area of $Ca(OH)_2$ is 16 times the one of $CaCO_3$ and the porosity in the meso-porous range is by almost 2 orders of magnitude higher. The sorbents can be considered exemplary for a cheap, less advanced ($CaCO_3$) and a more expensive, advanced sorbent ($Ca(OH)_2$). It should be kept in mind that when $CaCO_3$ is injected into a furnace above its calcination temperature (approx. 780 °C and 880 °C in air and oxy-fuel firing, respectively), the sorbent calcines rapidly releasing CO_2. This release leads to the formation of a porous structure in and a fragmentation of the sorbent particles, increasing their reactive surface. Also $Ca(OH)_2$ calcines when injected at elevated temperatures, releasing H_2O ($Ca(OH)_2$ calcination at approx. 420 °C).

The two tested sorbents consist not entirely of $CaCO_3$ and $Ca(OH)_2$. While the $CaCO_3$ sorbent contains other components to an extent of $1.5 \cdot 10^{-2}\ \frac{\text{kg}}{\text{kg}}$, $Ca(OH)_2$ contains $0.4 \cdot 10^{-2}\ \frac{\text{kg}}{\text{kg}}$ of other compounds. Moreover, the two sorbents contain both, $CaCO_3$ and $Ca(OH)_2$. This leads to mass specific partial amounts of calcium $n_{Ca,Sorb}$ of the two sorbents that differ from the ones of the pure substances. The mass specific partial amount of calcium (i.e. $n_{Ca,Sorb} = N_{Ca,Sorb}/m_{Sorb}$) is

Table 3.5: Analyses of particle sizes, surface areas, porosities, and $CaCO_3$ and $Ca(OH)_2$ contents of the sorbents used in DSI experiments in this thesis.

sorbent	$CaCO_3$	$Ca(OH)_2$	D_{50}	D_{90}	$y_{D>32\mu m}$	a_{BET}	$v_{por,tot}$	$v_{por,meso}$	$\overline{D_{por}}$
	$10^{-2}\ \frac{\text{kg}}{\text{kg}}$, db		µm		$10^{-2}\ \frac{\text{m}^3}{\text{m}^3}$	$\frac{\text{m}^2}{\text{g}}$, db		$\frac{\text{cm}^3}{\text{g}}$, db		nm
$CaCO_3$	98.3	0.3	6.4	24.2	4.3	2	0.005	0.001	11.1
$Ca(OH)_2$	6.4	93.3	7.5	39.3	14.3	32	0.186	0.098	20.9

D_{50}/D_{90}: Diameter for which $50/90 \cdot 10^{-2}\ \frac{\text{m}^3}{\text{m}^3}$ of the particles of the sample have a smaller size
$y_{D>32\mu m}$: Volume fraction of particles of the sample that are bigger than 32 µm
a_{BET}: Specific surface area determined according to the BET method
$v_{por,tot}$: Total porous volume in the pore size range between 1.7 and 100 nm
$v_{por,meso}$: Porous volume of pores in the meso-porous size range between 10 and 30 nm
$\overline{D_{por}}$: Mean pore diameter

0.009 85 $\frac{\text{kmol}}{\text{kg}}$ for the $CaCO_3$ sorbent and 0.013 22 $\frac{\text{kmol}}{\text{kg}}$ for the $Ca(OH)_2$ sorbent. These values have been used for calculating the molar ratios $\alpha_{Ca/S}$ and $\alpha_{Ca/2Cl}$ (see section 3.3.3.6) that are important in respect to the DSI experiments.

3.3 Conducted experiments

The experiments that are presented in this thesis can be separated in three categories:

(i) Experiments studying the stability of sulfates in ashes and deposits of lignite combustion and the retention of sulfur in the ash that reduces emissions of SO_x with the flue gas: These tests were conducted in the electrically heated test furnace BTS-VR and at the KSVA test rig that is equipped with a flue gas recirculation system and hence, allows for experiments under industrially relevant air and oxy-fuel recycle conditions. In addition, some experiments involved Vattenfall's industrial scale oxy-fuel pilot plant "Schwarze Pumpe", from where ashes and deposits could be obtained.

(ii) Experiments investigating the application of DSI for control of acid gases in air and oxy-fuel combustion were conducted at the BTS-VR and at the KSVA test rigs.

(iii) Experiments that were conducted at BTS-VR focusing on the formation of SO_3 in air and simulated oxy-fuel combustion of different hard coal qualities.

The following sections describe details of all the mentioned experiments.

3.3.1 Experiments investigating sulfate stability in deposits

Dedicated experiments have been conducted at BTS-VR to assess the impact of high SO_2 concentration levels in oxy-fuel combustion conditions on the stability of sulfates in deposits. During these experiments, the lignite L2 was combusted maintaining a flue gas production of 11.5 $\frac{\text{m}^3}{\text{h}}$, *STP*, wet, to have comparable gas residence times in the furnace in the different experimental runs. The exit O_2 level was kept constant at approx. $2.7 \cdot 10^{-2}$ $\frac{\text{m}^3}{\text{m}^3}$, dry. To simulate oxy-fuel flue gas recirculation, the BTS-VR combustion rig's top-mounted burner was fed with a mix of dry CO_2 and O_2 with $28 \cdot 10^{-2}$ $\frac{\text{m}^3}{\text{m}^3}$ oxygen. For the investigation of the impact of high SO_2 concentrations under oxy-fuel combustion conditions on ash and deposits, the oxidant gas was doped with additional SO_2. The SO_2 concentrations reached $750 \cdot 10^{-6}$ $\frac{\text{m}^3}{\text{m}^3}$, wet ($850 \cdot 10^{-6}$ $\frac{\text{m}^3}{\text{m}^3}$, dry), when no additional SO_2 was injected to the oxidant gas and $5530 \cdot 10^{-6}$ $\frac{\text{m}^3}{\text{m}^3}$, wet ($6250 \cdot 10^{-6}$ m^3/m^3, dry), with injection of SO_2[25]. In the experiments with and without SO_2 addition, deposits were sampled at two locations inside the furnace, 1.5 m from the burner via a lateral port and 2.5 m from the burner via the furnace outlet, using an uncooled ceramic probe (sampling time: approx. 2 h). A schematic of the BTS-VR furnace can be found in figure 3.6a.

[25]Measured inside the furnace, 1.5 m from the burner, at 1200 °C.

The electrically heated furnace was operated so that at the two deposit sampling locations local temperatures of 1200 °C and 1100 °C were reached. The obtained deposit samples were subjected to scanning electron micro-probe analyses.

3.3.2 Experiments investigating SO_x retention in ash and deposits

3.3.2.1 Experimental parameters

Combustion parameters for the experiments studying SO_x retention in ash and deposits at the 500 kW KSVA and the 30 MW "Schwarze Pumpe" plants are summarized in table 3.6. In the oxy-fuel experiments, oxidant O_2 concentrations were between 25 and $28.9 \cdot 10^{-2}$ $\frac{m^3}{m^3}$, wet. In most oxy-fuel experiments, oxygen was mixed with the recirculated flue gas before injecting it via the burner. Only the oxy-fuel experiments with lignite L2 were conducted injecting pure oxygen through dedicated nozzles of the burner. In air fired experiments, the exit O_2 concentration was approx. 3.2 to $3.7 \cdot 10^{-2}$ $\frac{m^3}{m^3}$, dry, while in the oxy-fuel tests at KSVA it was 4.3 to $4.9 \cdot 10^{-2}$ $\frac{m^3}{m^3}$, dry, and in the 30 MW oxy-fuel experiment it was $6.9 \cdot 10^{-2}$ $\frac{m^3}{m^3}$, dry. The experiments represent typical air and oxy-fuel combustion conditions, and hence, the results are suitable for a comparative evaluation. The higher oxygen concentrations $\bar{y}_{O_2,oxid,wet}$ in the oxidant gas in oxy-fuel experiments correspond to increased flue gas residence times in

Table 3.6: Combustion parameters for experiments studying SO_x retention in ash and deposits at the 500 kW KSVA and the 30 MW "Schwarze Pumpe" pilot plant including mode of O_2 addition, thermal power $\bar{P}_{th}$, fuel feed $\bar{\dot{M}}_{RC}$, volumetric flow of clean CO_2 for sensor purging and fuel dosing $\bar{\dot{V}}_{CO_2}$, volumetric fraction of air leakage $\bar{y}_{leak,dry}$, and overall O_2 concentration in the oxidant $\bar{y}_{O_2,oxid,wet}$ and in the flue gas exiting the furnace $\bar{y}_{O_2,out,dry}$.

			$\bar{P}_{th}$	$\bar{\dot{M}}_{RC}$	$\bar{\dot{V}}_{CO_2}$	$\bar{y}_{leak,dry}$	$\bar{y}_{O_2,oxid,wet}$	$\bar{y}_{O_2,out,dry}$
fuel	mode	O_2 add.	MW	$\frac{t}{h}$	$\frac{m^3}{h}(STP)$		10^{-2} $\frac{m^3}{m^3}$	
L1	air	-	0.31	0.0606	-	-	20.9	3.2
	oxy	premixed	0.31	0.0611	33	6.1	28.9	4.6
L2	air	-	0.29	0.0490	-	-	20.9	3.5
	oxy	direct	0.29	0.0495	42	7.1	25.0	4.9
C4	air	-	0.33	0.0385	-	-	20.9	3.7
	oxy	premixed	0.33	0.0385	38	6.1	28.0	4.3
L3	oxy	premixed	22.6	3.8500	n.a.	n.a.	28.5	6.9

$y_{leak,dry}$ for KSVA tests estimated on basis of the measured H_2O and/or CO_2 concentrations in the flue gas

n.a. = analysis not available

the furnace[26]. In table 3.6 also information on the volumetric flow of clean CO_2 for sensor purging and fuel dosing $\bar{\dot{V}}_{CO_2}$, and the volumetric fraction of air leakage $\bar{y}_{leak,dry}$ is given, which is required for the calculation of sulfur retention in KSVA oxy-fuel experiments. For the experiments conducted at the 30 MW "Schwarze Pumpe" pilot plant, no information on $\dot{V}_{CO_2}$ and $y_{leak,dry}$ is available and those values could only be estimated.

3.3.2.2 Details on ash and deposit sampling

Ash and deposit samples and associated calculations: In experiments investigating SO_x retention in ash and deposits at the KSVA and the "Schwarze Pumpe" plants, process ashes were sampled from the facilities' air/gas preheater (GH), bottom ash (BA), and different ESP precipitation fields (E1, E2, E3). In addition, entrained ash and deposits were sampled at various locations in the furnaces of both facilities. Table 3.7 summarizes details on all samples of entrained ash (A) and cooled (C) and uncooled (UC) deposits included in this thesis. The sampling locations for the lignite fired experiments have been selected to represent flue gas

Table 3.7: List of and details on entrained ash (A) and cooled (C),and uncooled (UC) deposit samples from the 500 kW KSVA and the 30 MW "Schwarze Pumpe" pilot plant (i.e. fuels, combustion modes, sampling levels, distances from burner, and ϑ_{FG}).

			furn. level	bur. dist.		
plant	fuel	mode		m	ϑ_{FG}	samples
KSVA	L1	air	Lev11	1.99	1110 °C	U
			Lev15	2.67	1020 °C	U
			Lev26	5.67	750 °C	U
		oxy	Lev11	1.99	1125 °C	U
			Lev15	2.67	1035 °C	U
			Lev26	5.67	750 °C	U
KSVA	L2	air	Lev11	1.99	1095 °C	U, C, A
			Lev26	5.67	750 °C	U, C, A
		oxy	Lev11	1.99	1055 °C	U, C, A
			Lev26	5.67	730 °C	U, C, A
KSVA	C4	air	L20	3.63	915 °C	U, C
		oxy		3.63	895 °C	U
KSVA	C4, $Ca(OH)_2$ furn. inj.	air	L20	3.63	940 °C	U, C
		oxy		3.63	925 °C	U
OxyPP	L3	oxy	Lev4	≈ 5.5	1100 °C	U, A
			Lev8	≈ 10	750 °C	U, C, A

[26] On basis of the volume reduction, residence times in air firing can be estimated to be approx. 27 % (L1), 16 % (L2), 25 % (C4), and 27 % (L3) below those in oxy-fuel firing

temperatures in radiative (approx. 1100 °C) and convective sections (approx. 750 °C) of power boilers. Sampling locations for coal C4 have been selected to be about 1.5 m downstream the DSI sorbent injection location to allow for a comparison of the deposit composition with and without sorbent injection. The temperature at this location corresponds also to the convective section of a power boiler. Temperature controlled deposit samples, so called "cooled deposits", were collected using a probe whose surface was controlled to temperatures ϑ_{Probe} between 550 °C and 650 °C to simulate superheater surface temperatures. Entrained ash and uncooled deposits have been sampled at KSVA and the oxy-fuel pilot plant "Schwarze Pumpe" subsequently at the same measurement ports, while cooled deposits were collected at neighboring sampling ports at the same furnace levels. The obtained ash and deposit samples have been analyzed for their chemical composition (i.e. main ash-forming oxides) and in addition, selected samples were subjected to electron micro-probe analyses. Based on the chemical composition, the extent of sulfation of the samples can be evaluated. For this purpose, molar Ca/S, Mg/S, Na_2/S, and K_2/S ratios α_i are calculated, according to equations 3.6, 3.7, 3.8, and 3.9. In these calculations, $\gamma_{A,db}$ refers to the ash content determined for the ash and deposit samples to account for any unburned fuel in the samples.

$$\alpha_{Ca/S} = \frac{\gamma_{A,db}}{\gamma_{S,db}} \cdot M_{M,S} \cdot \frac{x_{CaO,A}}{M_{M,CaO}} \tag{3.6}$$

$$\alpha_{Mg/S} = \frac{\gamma_{A,db}}{\gamma_{S,db}} \cdot M_{M,S} \cdot \frac{x_{MgO,A}}{M_{M,MgO}} \tag{3.7}$$

$$\alpha_{Na_2/S} = \frac{\gamma_{A,db}}{\gamma_{S,db}} \cdot M_{M,S} \cdot \frac{x_{Na_2O,A}}{M_{M,Na_2O}} \tag{3.8}$$

$$\alpha_{K_2/S} = \frac{\gamma_{A,db}}{\gamma_{S,db}} \cdot M_{M,S} \cdot \frac{x_{K_2O,A}}{M_{M,K_2O}} \tag{3.9}$$

Limitations in respect to ash mass balances at KSVA: During the air and oxy-fuel experiments with lignites L1 and L2 and coal C4 at KSVA, process ashes from all ash drains (bottom ash, ash from gas preheater, ESP ash[27]) were collected and the sample masses were determined, summed up, and compared against the ash input with the fuel. The recovery ratios for the ash were relatively low (42-86 %) and deviations between corresponding air and oxy-fuel tests carried out subsequently within one test campaign were high (e.g. 50 vs. 69 % and 86 vs. 42 %, respectively). It can only be speculated for the reasons, e.g. too low sampling durations and considerable ash accumulation in furnace and flue gas ducts. It is known from the KSVA facility that several hours of experimental operation are required for the ashes in the system to be moved to the respective ash discharge systems. Those ash travel times are

[27] The mass of ash accumulated in the fabric filter over several hours of operation was non-existent or very low (few hundred grams) in the experiments and was not further considered.

impacted by changed flue gas flow rates and corresponding gas velocities in flue gas ducts in air and oxy-fuel operation. Changed gas velocities may also impact the ash fractionation between bottom ash, gas preheater ash, and the different ESP ashes, which is an uncertainty in the comparative assessment of the process ashes from air and oxy-fuel operation. Due to the low ash recovery ratios and the observed deviations between combustion modes, no experimentally determined process ash production rates etc. are included in this thesis. For the same reasons, the assessment of process ash compositions is focusing on qualitative changes in the character of sampled ashes, omitting a detailed quantitative evaluation. It should be highlighted that all process ashes included in this thesis were carefully sampled at the end of longer periods of stable operation (i.e. between 8 h and 20 h for all experiments except the air fired DSI experiments that had to be stopped after approx. 3.5 h, due to a mill damage). To avoid a possible contamination of the ash samples by carry-over of ash accumulated in the flue gas ducts during previous experiments, the samples were always obtained from the top of each ash container. In general, the qualitative results in respect to sulfur retention in ashes from the experiments at KSVA are in agreement to the findings based on more reliable flue gas concentration measurements.

3.3.3 Experiments investigating acid gas removal by DSI

Experiments investigating the control of the acid gases SO_2, SO_3, and HCl in air and oxy-fuel conditions have been conducted at BTS-VR and KSVA. All DSI experiments in this thesis were carried out combusting the coal C4. Initial experiments at the BTS-VR facility were conducted with a range of dry sorbents ($CaCO_3$, different $Ca(OH)_2$ qualities, mixtures of $Ca(OH)_2$ and activated carbon, and trona) to identify most promising sorbents and injection locations for subsequent tests at the KSVA facility that required much higher efforts. In this thesis, only the results for sorbents that were tested at both facilities (BTS-VR and KSVA) are reported (i.e. finely milled $CaCO_3$ and highly porous $Ca(OH)_2$). Results for other sorbents can be found in [37, 39].

3.3.3.1 Experimental parameters in BTS-VR DSI tests

In DSI experiments, the fuel C4 was injected to the furnace of BTS-VR using part of the oxidant gas as transport medium (approx. 1.5 $\frac{m^3}{h}$, *STP*, dry). The remaining oxidant gas was provided to the inner and outer annulus around the central fuel injection pipe in a split of 40 to 60 %, respectively. In all experiments, the flue gas production in the furnace was kept constant at approx. 11.5 $\frac{m^3}{h}$, *STP*, wet, requiring a combustion of approx. 1.3 $\frac{kg}{h}$ coal in air and 1.8 $\frac{kg}{h}$ in CO_2/O_2 firing. In experiments with sorbent injection to the furnace and upstream the filter, additional gas for sorbent injection (approx. 0.5 to 0.8 $\frac{m^3}{h}$, *STP*, dry) was added to the generated flue gas. About 10 $\frac{m^3}{h}$, *STP*, wet, of the gas leaving the furnace was extracted to the flue gas duct and filter of the BTS-VR system (measured after filter), with the rest being vented to a separate

exhaust system. In experiments with DSI upstream the filter, the gas flow through the filter was maintained at 10 $\frac{m^3}{h}$, *STP*, wet, and the flue gas extraction from the furnace exit was reduced by the amount of sorbent injection gas accordingly. Volumetric gas streams $\dot{V}_{FG}$ into which dry sorbents were injected were either continuously measured (flue gas flow measurement at filter outlet for experiments with sorbent injection upstream filter) or calculated based on oxidant gas feeds and fuel composition (co-injection with fuel and injection to furnace).
In air fired as well as in oxy-fuel experiments, the facility was operated to keep the excess oxygen concentration $y_{O_2,exc,dry}$ at the furnace exit at about $3 \cdot 10^{-2}$ $\frac{m^3}{m^3}$. This is equivalent to a combustion stoichiometry n_{air} of 1.17 and $n_{O_2,o-t}$ of 1.09. Since the BTS-VR system is not equipped with an actual flue gas recirculation system, oxy-fuel tests were carried out in a simulated oxy-fuel combustion atmosphere. In these experiments, an overall O_2 concentration in the oxidant gas of $28 \cdot 10^{-2}$ $\frac{m^3}{m^3}$, wet, was maintained, with the remainder being mainly CO_2 and additionally H_2O, NO, N_2, SO_2, and Hg. Similar to the experiments studying SO_3 formation (see section 3.3.4 for more details) a certain removal efficiency from the recirculated gas was assumed for the mentioned impurities. In the DSI experiments, SO_2, H_2O, and Hg[28] were added to the flue gas, simulating a removal of 80 % of the SO_2, 50 % of the H_2O, and 0 % of the Hg contained in the recirculated gas (i.e. recirculation of 20 % SO_2, 50 % H_2O, and 100 % Hg). In addition, NO was added to the oxidant gas to simulate a NO content of the recirculated flue gas $y_{NO,dry}$ of about $950 \cdot 10^{-6}$ $\frac{m^3}{m^3}$. N_2 was added only for sorbent injection purposes (see section 3.3.3.3). The required amounts of SO_2, H_2O, and Hg were calculated on basis of the fuel analysis. The experimental settings in the DSI tests with coal C4 are consistent to the ones in the experiments studying SO_3 formation with the same fuel (i.e. tests C4-A and C4-8S0H). More details on the experimental parameters can be found in tables 3.11 and 3.12.
In tests on DSI at the BTS-VR facility, the electrical heating zones of the furnace (see figure 3.6a) were operated according to table 3.8, with temperatures of 1300 °C at the first heating zone, where the facility's burner is located, and temperatures of 1150 °C and 1100 °C at the two last heating zones of the furnace, where sorbent was injected.
During the DSI tests, the BTS-VR's flue gas duct was heated by electrical trace heating to reduce heat losses and simulate a temperature and residence time profile comparable to an actual power plant. Indicative temperature profiles averaged over the air and CO_2/O_2 DSI

Table 3.8: Temperatures of the electrically heated BTS-VR furnace during all air and oxy-fuel DSI experiments.

ϑ_{BTS1}	ϑ_{BTS2}	ϑ_{BTS3}	ϑ_{BTS4}	ϑ_{BTS5}
1300 °C	1250 °C	1200 °C	1150 °C	1100 °C

[28] Hg is not relevant to this thesis and hence, is not covered here in greater detail. It can be assumed that the very low Hg concentration levels (maximum about $2.0 \cdot 10^{-9}$ $\frac{m^3}{m^3}$, dry) that were present in the oxidant gas during the DSI experiments did not influence the results in respect to acid gas capture.

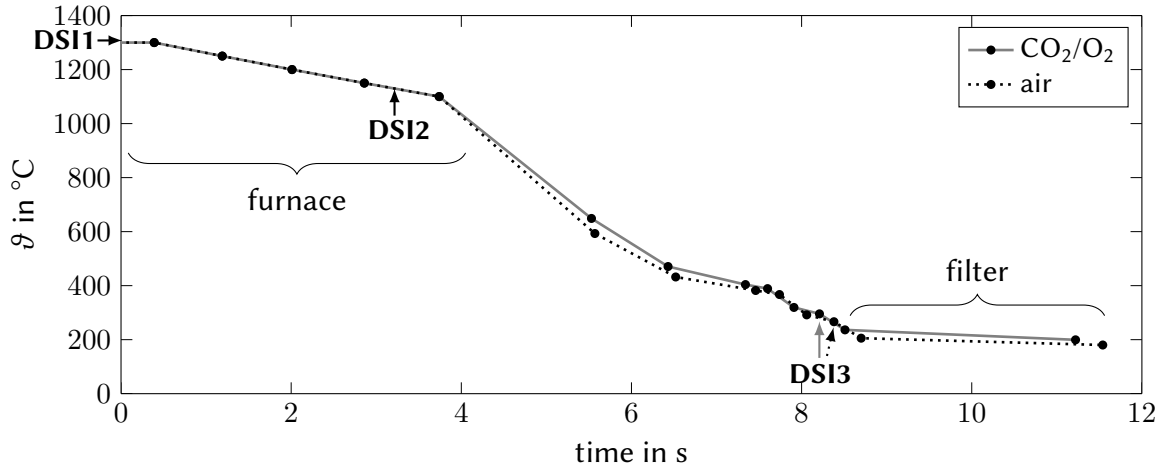

Figure 3.4: Indicative temperature profile along the furnace, flue gas duct, and filter of BTS-VR during air and CO_2/O_2 experiments studying DSI. The DSI locations are shown: DSI1: co-injection with fuels, DSI2: furnace injection, DSI3: Injection upstream filter.

experiments, respectively, are presented in figure 3.4[29]. Also the different sorbent injection locations are included. The temperatures and residence times that sorbents experience when traveling through a combustion system can have a considerable impact on the acid gas capture. However, in all reported DSI experiments the temperature and residence time profiles were similar and hence, all DSI experiments are assumed to be comparable.

The temperature profiles for the DSI experiments were obtained as described on page 71. As in the experiments investigating SO_3 formation (section 3.3.4.1), in CO_2/O_2 tests the temperatures in the gas ducts were somewhat higher than in air firing, with otherwise same settings in both modes. In DSI experiments, the average difference between air and CO_2/O_2 firing reached up to almost 50 °C at the flue gas duct inlet and reduced to approx. 20 °C at the filter outlet. As in the SO_3 experiments at BTS-VR, temperature variations along the flue gas duct were observed between individual tests. The flue gas duct inlet temperatures in the individual air fired DSI experiments were in a range of about 525 °C to 625 °C and temperatures at the filter inlet ranged from about 190 °C to 225 °C. In CO_2/O_2 experiments those temperature ranges were approx. 605 to 665 °C and 215 to 255 °C, respectively. An average temperature drop between filter in- and outlet of 25 °C and 35 °C was observed in the experiments.

3.3.3.2 Experimental parameters in KSVA DSI tests

For DSI experiments at the KSVA test facility, the same coal (C4) as at the BTS-VR test rig was used. The fuel was injected to the furnace of KSVA via the inner annulus of the burner using approx. 30 $\frac{m^3}{h}$, *STP*, dry, primary gas[30]. The remaining secondary oxidant gas[31] was provided to

[29] Lines between temperature measurements (indicated by black dots) are linearly interpolated and the temperature between burner and the first temperature measurement of the furnace ϑ_{BTS1} is assumed to be constant.
[30] Dry air or dry CO_2 in air and oxy-fuel firing, respectively.
[31] Air or recirculated flue gas mixed with oxygen.

the outer annulus. In all experiments, the fuel feed was kept constant at approx. 38.5 $\frac{kg}{h}$, which is equivalent to a thermal power of approx. 310 kW. In addition to the oxidant gases, other gases were fed to purge flame detectors (approx. 8 $\frac{m^3}{h}$, *STP* of dry air or dry CO_2) and to inject sorbents (approx. 10 to 13 $\frac{m^3}{h}$, *STP* of dry air or dry CO_2). The oxidant O_2 level in oxy-fuel firing was $28 \cdot 10^{-2}$ $\frac{m^3}{m^3}$, wet[32]. This corresponds to a flue gas recirculation ratio ξ_{rec} of about 50 %. When primary, purge, and sorbent injection gases[33] are included in the calculation of the recirculation ratio with a corresponding wet flue gas flow rate, the recirculation ratio for the conducted experiments is approx. 71 %. Recirculation ratios and volumetric gas streams $\dot{V}_{FG}$ at different locations of the KSVA facility (required to calculate $\alpha_{Ca/S}$ and $\alpha_{Ca/2Cl}$, see section 3.3.3.6) were determined using an Aspen Plus model (Version 8.6) of the test rig to calculate mass balances for the different air and oxy-fuel DSI experiments, on basis of all gas streams and the fuel feed entering the process. The model assumes a simplified fuel conversion to produce only CO_2, H_2O, SO_2, N_2, HCl, and Hg. The process flow diagram used for the calculations of the oxy-fuel configurations is schematically shown in figure 3.5. The air fired process flow diagram is omitted here since it does not include any particularities. By fixing fuel feed, primary CO_2, purge, and DSI gas streams (air/CO_2), air ingress, overall oxidant O_2 concentration, and the excess O_2 level, the required recirculation and O_2 feed gas streams were calculated.
The different oxidant O_2 levels in both combustion modes at a constant coal feed imply a change in the flue gas flow rate through the furnace. This value was approx. 352 $\frac{m^3}{h}$, *STP*, wet, in air

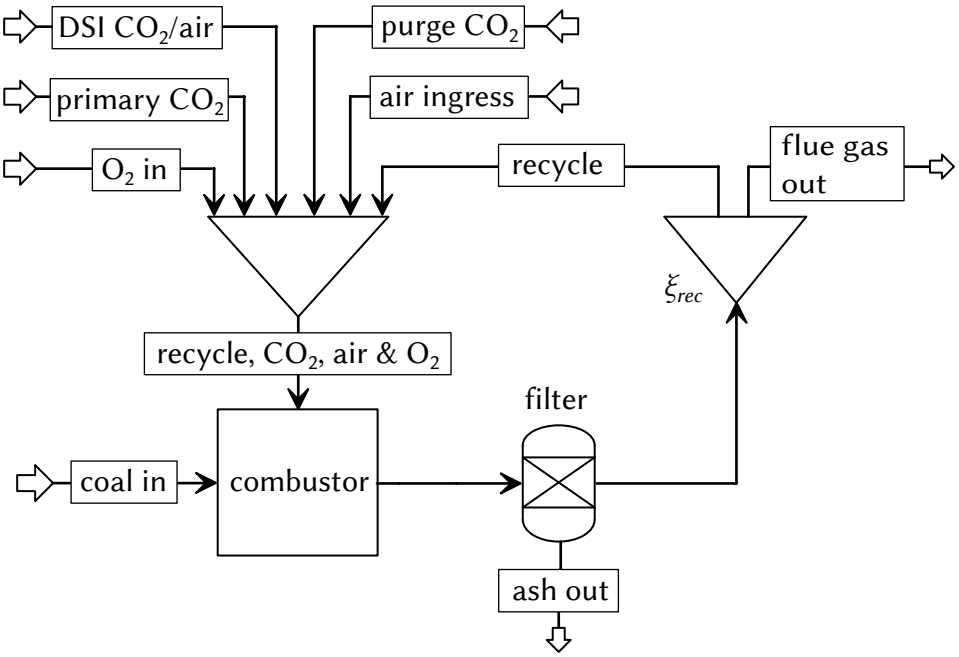

Figure 3.5: Schematic process flow diagram used in Aspen Plus models for balancing oxy-fuel process configurations for the DSI experiments at KSVA.

[32] Averaged over all feed gas streams, i.e. primary, secondary, purge, and sorbent injection gas.
[33] I.e. dry, clean, compressed air or CO_2 from tank.

firing and approx. 261 $\frac{m^3}{h}$, *STP*, wet, in oxy-fuel firing. The volumetric flue gas flow rate to the stack was about 125 $\frac{m^3}{h}$, *STP*, wet, in oxy-fuel operation. The differences in flue gas flow rates in the furnace and gas ducts are also associated to different residence times of the flue gases in the system in air and oxy-fuel experiments. Since the temperatures in the system were similar (see discussion below), the residence time in the air fired experiment can be estimated, being approx. 26 % shorter than the one in oxy-fuel firing. The flue gas residence time in the furnace of KSVA is estimated to be about 7.5 s in the conducted air and about 10 s in the oxy-fuel experiments. The DSI via a lateral port at the furnace was located after approximately 30 % of that gas travel time. The excess oxygen concentration of the combustion was kept at approx. $3 \cdot 10^{-2}$ $\frac{m^3}{m^3}$, dry, in air and at approx. $4 \cdot 10^{-2}$ $\frac{m^3}{m^3}$, dry, in oxy-fuel operation, equivalent to a combustion stoichiometry n_{air} of 1.17 in air and $n_{O_2,rec}$ of 1.04 and $n_{O_2,o-t}$ of 1.13 in oxy-fuel firing (see section 4.2.1.4 for details on $n_{O_2,rec}$ and $n_{O_2,o-t}$).

For the KSVA DSI experiments, a number of temperatures were continuously measured along the flue gas path during air and oxy-fuel DSI experiments (table 3.9). One observes certain differences between air and oxy-fuel conditions for ϑ_{Lev4}. It should be highlighted that this temperature measurement is at a position close to the flame in the furnace. At this location the temperature measurement is very sensitive to small fluctuations of the flame position that are known to occur when changing the combustion mode from air to oxy-fuel. One can also see that temperature ϑ_{Lev26} (close to the furnace outlet) and the temperatures measured at the ESP in- and outlet are very similar in both combustion modes. Moreover, they were observed to be very similar in individual air and oxy-fuel DSI experiments reported in this thesis. This highlights that the results of the DSI experiments should not be strongly influenced by altered temperatures between tests. In addition to the temperatures reported here, for dedicated DSI tests also temperature profiles in the furnace were determined (see section 4.2.2.3).

Table 3.9: Average temperatures at various locations in the furnace and at the ESP of KSVA measured during air and oxy-fuel DSI experiments.

Mode	ϑ_{Lev4}	ϑ_{Lev26}	$\vartheta_{ESP_{in}}$	$\vartheta_{ESP_{out}}$
	°C			
air	1020	780	219	181
oxy-fuel	802	800	205	179

ϑ_{Lev4}: Temperature measured in the KSVA furnace at level 4.
ϑ_{Lev26}: Temperature measured in the KSVA furnace at level 26.
$\vartheta_{ESP_{in}}$: Temperature measured at the inlet of KSVA's ESP.
$\vartheta_{ESP_{out}}$: Temperature measured at the outlet of KSVA's ESP.

3.3.3.3 Details on sorbent injection approaches

Air, CO_2/O_2, and oxy-fuel recycle DSI experiments at BTS-VR and KSVA were carried out with sorbent injection at 3 different locations: Sorbents were co-injected to the furnace together with the fuel, injected to the furnace at a temperature of about 1100 °C, and injected upstream the fabric filter of BTS-VR (ϑ = 206 to 236 °C) and the ESP of KSVA (ϑ = 205 to 219 °C). The positioning of the sorbent injection probes for furnace injection at both reactors is shown in figure 3.6. Since DSI sorbents tend to stick to the walls of transport and injection pipes with a strong deflection (e.g. by 90°) such configurations were avoided in the conducted experiments. This implies a different injection probe arrangement in BTS-VR and KSVA. At BTS-VR the sorbent was injected to the furnace counter-currently with the probe being introduced upwards via the furnace outlet, while at KSVA the sorbent had to be injected via a lateral port in

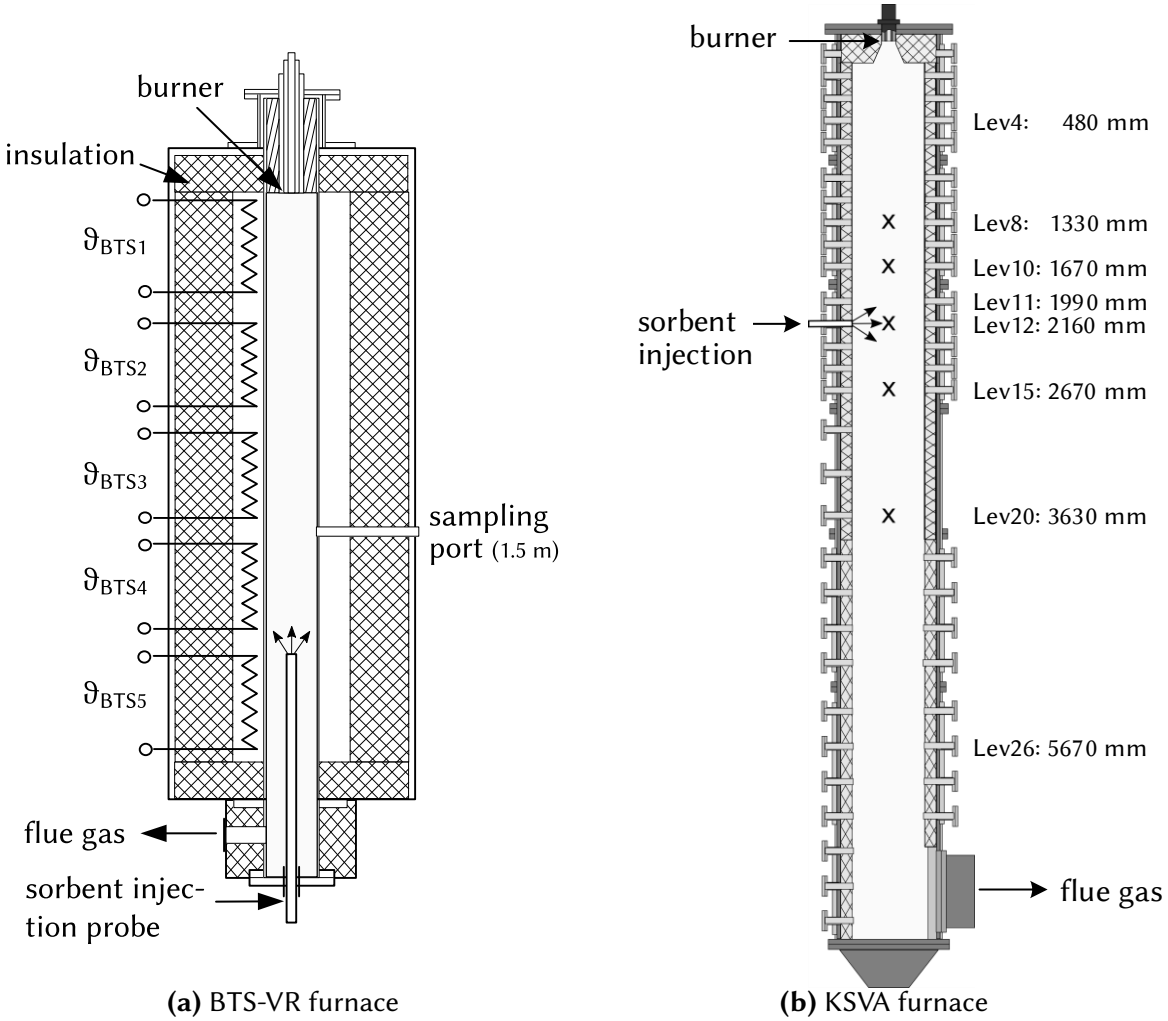

(a) BTS-VR furnace **(b)** KSVA furnace

Figure 3.6: Schematics of the furnaces of (a) BTS-VR and (b) KSVA. The placement of the sorbent injection probe at both furnaces is shown. Levels at which SO_2 concentration and temperature measurements inside the furnace of KSVA were conducted during DSI experiments are marked by "x". Also ports used for deposit sampling at both rigs are shown. The port specifications given refer to their distances from the burner.

orthogonal direction to the flue gas flow. Even though this has not been studied in detail, it can be assumed that sorbent dispersion in both reactors is not exactly the same. The counter-current injection might allow for a better and more homogeneous mixing of flue gases and sorbents. The sorbent injection upstream of the particle separation devices of BTS-VR and KSVA was arranged in a way so that the sorbent had a travel time of approx. 0.5 s before entering the separator.

The sorbent dosing and dispersion at the two experimental systems was done similarly. At BTS-VR, a volumetrically controlled sorbent feeder with a Venturi type powder dispersion system (Topas SAG 410) was used that was placed on a balance to record the loss-in-weight signal. For the experiments at KSVA, a Venturi nozzle was used for sorbent dispersion. However, this nozzle was fed by a gravimetrically controlled screw feeder. The gravimetric control of the screw feeder was working with an accuracy that was in a range of approx. +/-10 %. The measurement of the sorbent weight loss signal for the experiments at BTS-VR was done using a balance with a resolution of 0.05 g and a linearity of 0.5 g (Kern DS 8K0.05). Problems related to the detection of the weight loss signal at BTS-VR were due to the small sorbent feed rates required in some tests (down to below 10 $\frac{g}{h}$; see section A.6) and difficulties to reliably decouple forces induced by the sorbent feed line from the balance. The overall accuracy of weight loss signals from BTS-VR experiments, used in this thesis, is estimated to be in the range of +/-3 $\frac{g}{h}$. This highlights that experiments conducted at low sorbent feed rates are subject to a relatively high uncertainty in respect to the loss-in-weight signal. In some instances, the loss-in-weight signals recorded were not plausible, due to additional disturbances of the sorbent balance. In these cases, sorbent feed rates had to be estimated, according to the volumetric set-point of the sorbent feeder. For this estimation, a linear correlation between this set-point and the feed rate was assumed that was calibrated with data from more reliable tests. This is justified, since preliminary sorbent feeding and dispersion experiments showed such a linear correlation in a relevant range of set points. In those preliminary experiments also settings of the Venturi system for optimal sorbent dispersion were determined (i.e. dispersion gases and flow rates) using a cold model system that allowed for an optical assessment of the dispersion quality on a filter element. Optimized settings were selected for subsequent DSI experiments.

One observation that was made during the preliminary sorbent dispersion tests is that it is impossible to use CO_2 to feed $Ca(OH)_2$ based sorbents due to a rapid reaction between sorbent and gas (see section A.5). For this reason, in oxy-fuel and CO_2/O_2 experiments with $Ca(OH)_2$ injection, air or N_2 had to be used as sorbent dispersion gas. In the respective oxy-fuel experiments at KSVA with flue gas recirculation and in the sorbent CO_2/O_2 co-injection experiments at BTS-VR, air was used as $Ca(OH)_2$ dispersion gas, since in those experiments all or part of this gas passes through the flame so that oxygen can participate in the combustion, reducing the dilution by nitrogen. Oxy-fuel experiments with $CaCO_3$ injection at KSVA used CO_2 as dispersion gas. The used sorbent injection gases are listed in table 3.10. One peculiarity

Table 3.10: Sorbent injection gases used in DSI experiments at KSVA and BTS-VR.

		KSVA		BTS-VR	
Sorbent	Injection	Air	Oxy-Fuel	Air	CO_2/O_2
$CaCO_3$	co-injection	air	CO_2	air	air
	furnace/filter/ESP	air	CO_2	air	N_2
$Ca(OH)_2$	co-injection	air	air	air	air
	furnace/filter/ESP	air	air	air	N_2

of the Venturi dispersion principle is that the dispersion nozzle has to be allowed to suck in the sorbent together with ambient air. According to the manufacturer of the used dispersion nozzles (Topas GmbH) the ratio between pressurized transport gas for the Venturi nozzle and the absorbed air is approx. 2. This number matches well the flue gas dilution that was observed in DSI reference experiments[34]. On that basis, the total sorbent feed gas flow rate can be estimated. It was approx. 0.5 to 0.8 $\frac{m^3}{h}$, *STP*, dry, at BTS-VR and approx. 10 to 13 $\frac{m^3}{h}$, *STP*, dry, at KSVA.

3.3.3.4 Conducted measurements

The measurements of concentration levels $\bar{y}_i$ of the acid gas components (i.e. SO_2, SO_3, or HCl) in DSI experiments were conducted right after the fly ash separation devices of BTS-VR (fabric filter) and KSVA (ESP). In the DSI experiments, SO_2 and HCl were measured continuously and SO_3 discontinuously, with at least two, but in most cases three repetitive measurements that were used to calculate average SO_3 concentrations. At BTS-VR, the fabric filter was cleaned before each representative measurement period, so that at the start of this period the filter was freshly cleaned and then ash and sorbent was accumulating over the duration of the experiment. At KSVA, the ESP system was operated in automatic rapping mode.
Even though this thesis focuses on SO_x, the studies on DSI have been extended to the acid gas component HCl. The reason is that HCl may impact the sorbent reactions with gaseous SO_x, particularly when operating with a Cl rich fuel, such as C4 coal. Moreover, the control of HCl as a corrosive flue gas component has relevance to the oxy-fuel process. Due to the complexity of the DSI performance tests and efforts for discontinuous SO_3 measurements, only a limited number of such measurements could be performed in small and pilot scale DSI experiments. Fortunately, it was possible to use a FTIR analyzer for continuous HCl measurement during DSI tests in addition to the online SO_2 analysis. It allowed to derive a comprehensive dataset on the performance of DSI for HCl removal in air and oxy-fuel operation. The results on HCl may indirectly also give an indication in respect to the capture of SO_3 when injecting sorbents at low temperatures upstream filters or ESPs since it is generally assumed that in conditions that

[34]Experiments, in which gas injection was started, but no sorbent was fed.

allow for an efficient HCl removal also SO_3 that is more reactive (see: [162–164]) is captured to a large extent. The limited experimental data on SO_3 capture by DSI, available from the conducted experiments, supports this hypothesis.

3.3.3.5 Experimental procedure

Figure 3.7 shows exemplary the concentration trends for SO_2, CO_2, and O_2 measured downstream the ESP during $CaCO_3$ co-injection and oxy-fuel combustion of coal C4 at KSVA. At the start of the plot, a stable oxy-fuel operation has been established (approx. $5000 \cdot 10^{-6}$ $\frac{m^3}{m^3}$, dry, SO_2). At the time step indicated by "G", the CO_2 gas for sorbent injection is started leading to a dilution of the oxy-fuel flue gas by additional CO_2 and hence, a drop in the SO_2 level by approx. $350 \cdot 10^{-6}$ $\frac{m^3}{m^3}$, dry. The sorbent addition to the injection gas stream is started at the time step indicated by "I_1" and the sorbent mass flow is increased two times (i.e. time steps "I_2" and "I_3"). Each of these events is followed by a decrease in the measured SO_2 level. At the time step indicated by "S", the sorbent mass stream is stopped and the SO_2 level rises rapidly. To calculate DSI capture efficiencies, average SO_2 (and HCl) concentration levels have been determined for the different phases of the experiment, i.e. after start of injection gas, but without sorbent (i.e. reference SO_2, SO_3, or HCl concentration level $\bar{y}_{i,ref}$) and at each sorbent injection level (i.e. SO_2, SO_3, or HCl concentration level $\bar{y}_i$ during DSI). The procedure was analogue for all other DSI experiments at the BTS-VR and KSVA facilities. Certain injection settings (i.e. $Ca(OH)_2$ furnace injection at $\alpha_{Ca/S}$ = 1.0 and 1.1 in the two combustion modes) have been operated for

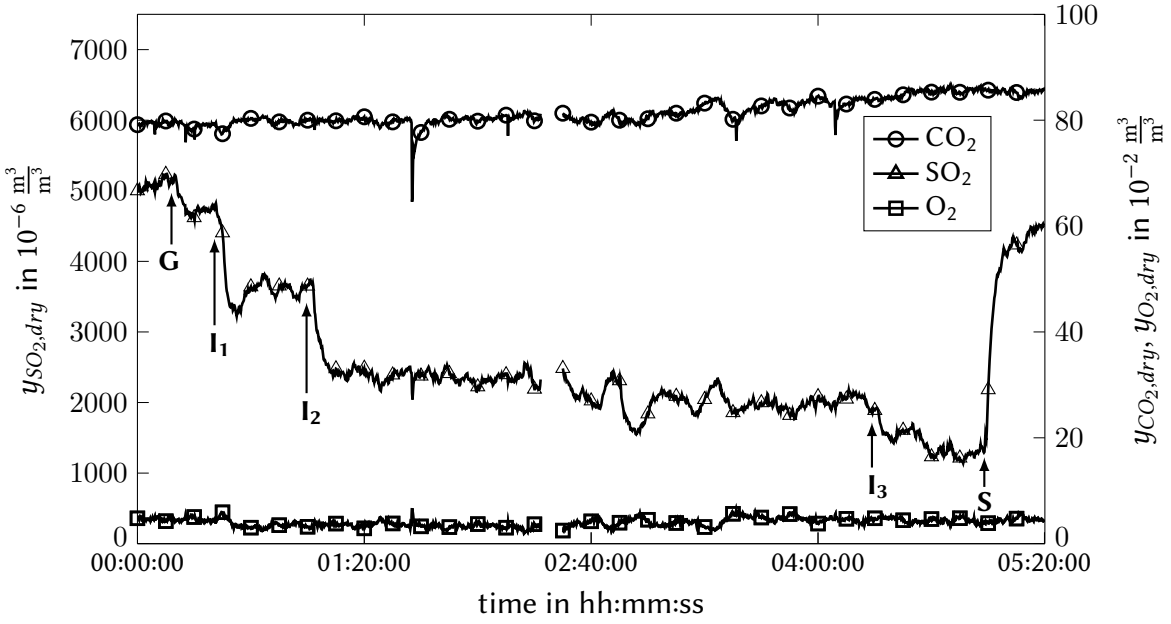

Figure 3.7: Exemplary concentration trends for SO_2, CO_2, and O_2 measured downstream the ESP in $CaCO_3$ oxy-fuel co-injection with coal C4 at KSVA; G: Start of dosing gas (CO_2), I_1: Start of sorbent injection ($\alpha_{Ca/S}$ = 0.9), I_2: Increase of sorbent injection ($\alpha_{Ca/S}$ = 2.1), I_3: Increase of sorbent injection ($\alpha_{Ca/S}$ = 3.0), S: Stop of sorbent injection.

longer durations to allow for sampling of process ashes and for conduction of measurements inside the furnace.

3.3.3.6 Data processing and presentation of results

Based on the reference concentration levels $\bar{y}_{i,ref}$ of the acid gas components (i.e. SO_2, SO_3, and HCl) measured after particulate control devices and the concentration levels $\bar{y}_i$ during individual DSI injection experiments (see section 3.3.3.5), acid gas removal efficiencies η_i can be calculated, according to equation 3.10.

$$\eta_i = \frac{\bar{y}_{i,ref} - \bar{y}_i}{\bar{y}_{i,ref}} \tag{3.10}$$

$$\alpha_{Ca/S} = \frac{\dot{N}_{Ca,inj}}{\dot{N}_{SO_2,FG}} = \dot{m}_{Sorb,inj} \cdot n_{Ca,Sorb} \cdot \frac{V_{mol}}{\bar{y}_{SO_2,ref,dry}\dot{V}_{FG,dry}} \tag{3.11}$$

$$\alpha_{Ca/2Cl} = \frac{\dot{N}_{Ca,inj}}{2 \cdot \dot{N}_{HCl,FG}} = \dot{m}_{Sorb,inj} \cdot n_{Ca,Sorb} \cdot \frac{V_{mol}}{2 \cdot \bar{y}_{HCl,ref,dry}\dot{V}_{FG,dry}} \tag{3.12}$$

To relate the acid gas removal performance to the sorbent feed that was injected, it is useful to calculate molar ratios of the injected amount of calcium to the amount of acid gas components that are present in the flue gas without sorbent injection, i.e. $\alpha_{Ca/S}$ and $\alpha_{Ca/2Cl}$. In section 4.2.2 of this thesis, η_i is commonly plotted versus α_i. The calculation of the molar ratios α_i is done in respect to the major acid gas species treated by DSI. Therefore, in this thesis it is generally calculated in respect to the gases SO_2 and HCl. Compared to the concentrations of SO_2 and HCl, SO_3 levels are very low. Since in the case of HCl two moles are reacting with one mole of calcium, in addition, a stoichiometric factor needs to be included in the calculation of $\alpha_{Ca/2Cl}$. $\alpha_{Ca/S}$ and $\alpha_{Ca/2Cl}$ are calculated on basis of the injected mass stream of sorbent $\dot{m}_{Sorb,inj}$, the mass specific partial amount of calcium (i.e. $n_{Ca,Sorb} = N_{Ca,Sorb}/m_{Sorb}$), the production of dry flue gas $\dot{V}_{FG,dry}$, and the dry concentration of SO_2 ($y_{SO_2,ref,dry}$) or HCl ($y_{HCl,ref,dry}$) in the flue gas for the respective reference experiments. This is done according to equations 3.11 and 3.12. As introduced in section 3.5, for the sorbents used in this thesis $n_{Ca,Sorb}$ is 0.009 85 $\frac{\text{kmol}}{\text{kg}}$ for $CaCO_3$ and 0.013 22 $\frac{\text{kmol}}{\text{kg}}$ for $Ca(OH)_2$. For calculation of the molar ratios α_i in oxy-fuel recycle combustion, it is important to select a representative volumetric flow $\dot{V}_{FG,dry}$: In recycle combustion conditions, the volumetric flow of flue gas leaving the combustion process (i.e. after recycle) is used. In this way, the molar flow of SO_2 and HCl passing through the system is considered, without regarding any impurities' cycling in the recirculation loop. In air and in O_2/CO_2 experiments that have no flue gas recirculation, the flue gas flow going to the stack is used. Values of $\dot{V}_{FG,dry}$ are given in sections 3.3.3.1 and 3.3.3.2.

For calculation of injection stoichiometries α_i and acid gas removal efficiencies η_i, acid gas concentrations have been corrected to certain reference oxygen levels $y_{O_2,ref,dry}$, to consider

dilution of flue gas by air ingress or by unreacted oxidant gas. The methodology for correction of gas concentrations is introduced in section 3.6.4. The reference oxygen corresponds always to the value used for calculation of the flue gas production $\dot{V}_{FG,dry}$ for the respective experiment. The corrections of acid gas concentrations in DSI experiments do not consider dilution of flue gases by sorbent injection gases in particular. Instead, the reference acid gas concentration level $\bar{y}_{i,ref}$ that is used for calculation of the injection stoichiometries α_i and acid gas removal efficiencies η_i has been determined during feeding of sorbent injection gas but without addition of sorbents. For all other DSI experiments, it is assumed that the sorbent injection gas stream, or more accurately, the ratio between the flue gas production and this stream was constant.
In the figures in section 4.2.2 of this thesis, showing results of DSI experiments, trendlines based on 2nd order polynomial fits are plotted for the sake of clarity. Even though this fitting approach yields a good agreement to the experimental results, it has not been optimized and its utilization does not imply a general principle describing the capture of acid gases by DSI.

3.3.4 Experiments at BTS-VR investigating SO_3 formation

3.3.4.1 Experimental parameters

The experiments in respect to the SO_3 formation and retention in the ash in a fabric filter under air and simulated oxy-fuel conditions were carried out combusting the coals C1, C2, C3, and C4. The fuels were injected to the furnace of BTS-VR using part of the oxidant gas as transport medium (approx. 1.5 $\frac{m^3}{h}$, *STP*, dry). The remaining oxidant gas was provided to the inner and outer annulus around the central fuel injection pipe in a split of 40 to 60 %, respectively. The flue gas production in the furnace was constant at approx. 11.5 $\frac{m^3}{h}$, *STP*, wet, requiring different fuel feed rates for the different coals and combustion atmospheres (see table 3.12). About 10 $\frac{m^3}{h}$, *STP*, wet, of the gas leaving the furnace was extracted to the main flue gas duct and filter of the BTS-VR reactor (measured after filter), with the rest being vented to a separate exhaust system. The BTS-VR system is not equipped with an actual flue gas recirculation system. Therefore, tests in respect to oxy-fuel combustion at this facility were carried out in simulated oxy-fuel atmospheres. The investigated combustion conditions in the experiments studying SO_3 formation included conventional air firing and a number of simulated oxy-fuel atmospheres, i.e. CO_2/O_2 combustion with and without additional injection of impurities (H_2O, NO, SO_2, and Hg^0). By variation of the impurity injection rate, different oxy-fuel recycle and once-through removal efficiencies from the recirculated gas of the impurities H_2O, SO_2, and Hg[35], between 0 and 100 %, were simulated (for more information on recycle and once-through removal efficiencies see section 4.1.3). In air fired and oxy-fuel experiments, the facility was operated at an excess oxygen concentration $y_{O_2,exc,dry}$ at the end of the furnace of about $3 \cdot 10^{-2}$ $\frac{m^3}{m^3}$.

[35]Hg is not relevant to this thesis and hence, is not covered here in greater detail. It can be assumed that the very low Hg concentration levels (maximum about $3.3 \cdot 10^{-9}$ $\frac{m^3}{m^3}$, dry) that were present in the oxidant gas, did not influence the results in respect to SO_3 formation.

In all oxy-fuel tests, an overall O_2 concentration in the oxidant gas of $28 \cdot 10^{-2}$ $\frac{m^3}{m^3}$, wet, was maintained, with the remainder being CO_2, H_2O, NO, SO_2, and Hg. This corresponds to simulated recirculation ratios of about 70 %.

To ease the identification of different air and oxy-fuel experiments studying SO_3 formation, all tests are labeled with a code allowing for identification of the experimental settings. In addition to air fired experiments (labeled "A"), in total eight different oxy-fuel settings, seven with injection of H_2O, NO, SO_2, and Hg^0, and one with combustion in pure CO_2/O_2 (i.e. removal of 100 % of all impurities; experiments labeled "CO2") were investigated. The fuels and recycle removal efficiencies for SO_2 and Hg in simulated oxy-fuel experiments are included in the labels of the respective experiments. For example, the label C3-O2S5H indicates an oxy-fuel experiment with coal C3 and simulated removal of about 20 % of the SO_2 (label: 2S) and of about 50 % of the Hg (label: 5H) from the recirculated gas. Coals C1, C2, and C3 were all tested under A, OC, and 2S5H conditions (approx. 20 % SO_2 and 50 % Hg removal) and coal C1 was

Table 3.11: List of indices denominating experimental settings for different fuels, combustion atmospheres, simulated recycle and once-through impurity removal efficiencies from the recirculated flue gas for H_2O, SO_2 and Hg, and simulated NO_x concentrations in the recirculated gas in experiments studying SO_3 formation at BTS-VR.

index	coal	air/oxy	sim. removal efficiencies in %						sim. $y_{NO,dry}$ in rec. flue gas in 10^{-6} $\frac{m^3}{m^3}$
			η_{H_2O}		η_{SO_2}		η_{Hg}		
			rec.	o.-t.	rec.	o.-t.	rec.	o.-t.	
C1-A	C1	air	-	-	-	-	-	-	-
C1-CO2		oxy	100	100	100	100	100	100	0
C1-5S5H		oxy	25	9	52	25	44	19	890
C1-2S5H		oxy	25	9	23	8	44	19	890
C1-2S0H		oxy	25	9	23	8	7	2	890
C1-2S8H		oxy	25	9	23	8	80	54	890
C1-0S5H		oxy	25	9	3	1	44	19	890
C1-0S0H		oxy	25	9	3	1	7	2	890
C2-A	C2	air	-	-	-	-	-	-	-
C2-CO2		oxy	100	100	100	100	100	100	0
C2-2S5H		oxy	26	9	24	8	52	24	860
C3-A	C3	air	-	-	-	-	-	-	-
C3-CO2		oxy	100	100	100	100	100	100	0
C3-2S5H		oxy	26	9	25	9	63	34	860
C4-A	C4	air	-	-	-	-	-	-	-
C4-8S0H		oxy	48	20	78	49	0	0	950

investigated with five additional oxy-fuel settings (permutations of approx. 0 %, 20 %, and 50 % SO_2 and approx. 0 %, 50 %, and 80 % Hg removal). Coal C4 was tested in air and one oxy-fuel setting (C4-8S0H: approx. 80 % SO_2 and 0 % Hg removal). Also moisture recirculation was simulated. For coals C1, C2, and C3 oxy-fuel experiments, approx. 25 % drying (recycle) of the recirculated gas and for coal C4, 50 % drying (recycle) was simulated. In addition, NO was added to the oxidant gases to simulate a NO content of the recirculated flue gas y_{NO} of between 860 and $950 \cdot 10^{-6}$ $\frac{m^3}{m^3}$, dry. Since H_2O and NO levels were kept constant in the simulated oxy-fuel experiments for each fuel, they are not considered in the labels of the experiments. Table 3.11 lists all experiments including their labels, the simulated oxy-fuel recycle and once-through impurity removal efficiencies, and simulated NO concentrations in the recirculated flue gas. Deviations from the desired SO_2 and Hg removal efficiencies, mentioned above, can be observed, but experiments with different coals and similar removal efficiencies are considered to represent comparable oxy-fuel setups. The oxy-fuel setting for experiments with coal C4 differs somewhat from the experiments with coals C1, C2, and C3, since these experiments have been conducted in a different research project with different focus. Nonetheless, they have been included here to complement the results obtained with coals C1, C2, and C3.

The recycle removal efficiencies mentioned above refer to calculated, theoretical concentration maxima for H_2O, SO_2, and Hg ($y_{i,max,oxy,dry}$ and $y_{H_2O,max,oxy,wet}$) in an oxy-fuel process with no impurity removal and no air ingress and an exit O_2 concentration of $3 \cdot 10^{-2}$ $\frac{m^3}{m^3}$, dry. Those maxima can be calculated, according to equations 3.13 (i: SO_2, Hg; j: S or Hg) and 3.14, on basis of the fuel analyses.

$$y_{i,max,oxy,dry} = \frac{\frac{\gamma_j}{M_{M,j}}}{\frac{1}{1 - y_{O_2,exc,dry}} \left(\frac{\gamma_S}{M_{M,S}} + \frac{\gamma_C}{M_{M,C}} + \frac{\gamma_N}{2M_{M,N}} \right)} \tag{3.13}$$

$$y_{H_2O,max,oxy,wet} = \frac{\frac{\gamma_H}{2M_{M,H}} + \frac{\gamma_W}{M_{M,W}}}{\frac{\gamma_W}{M_{M,W}} + \frac{\gamma_H}{2M_{M,H}} + \frac{1}{1 - y_{O_2,exc,dry}} \cdot \left(\frac{\gamma_S}{M_{M,S}} + \frac{\gamma_C}{M_{M,C}} + \frac{\gamma_N}{2M_{M,N}} \right)} \tag{3.14}$$

To simplify the determination of the operational conditions for the different experiments, Aspen Plus (Version 8.6) models for mass balancing of oxy-fuel recycle combustion systems with once-through impurity removal efficiencies, as listed in table 3.11, were prepared for the different fuels. In these models, a simplified fuel conversion, producing only CO_2, H_2O, SO_2, N_2, HCl, and Hg, is assumed. The recycle impurity removal efficiencies listed in table 3.11 can be calculated from the once-through ones and the recirculation ratio, according to equation 4.11. Figure 3.8 shows a schematic of the oxy-fuel model used for calculating the oxidant gas

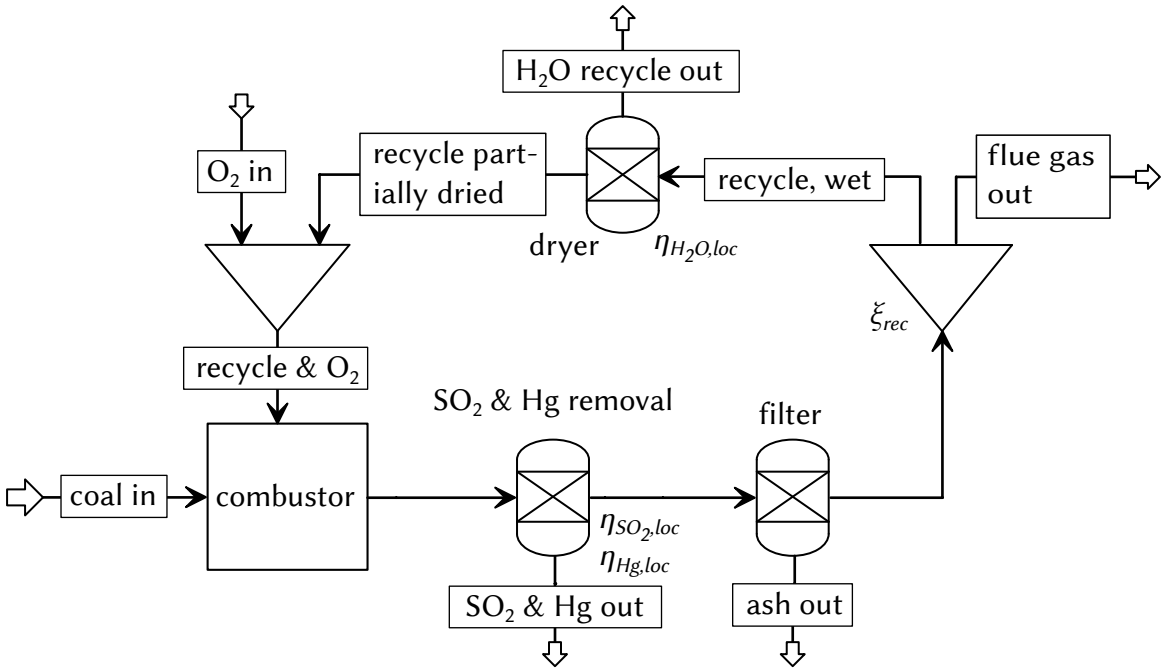

Figure 3.8: Schematic process flow diagram used in Aspen Plus models for balancing oxy-fuel process configurations for simulated oxy-fuel experiments at BTS-VR with different extents of recycle gas cleaning (i.e. η_{H_2O}, η_{SO_2}, and η_{Hg}).

compositions. The Aspen Plus model has been used to calculate the oxidant gas compositions for the different experiments and the corresponding recirculation ratios that would be required in actual oxy-fuel recycle combustion to maintain the desired oxidant O_2 concentration of $28 \cdot 10^{-2}$ $\frac{m^3}{m^3}$, wet. In table 3.12 the information on oxidant compositions, simulated recirculation ratios, and coal feeds is summarized.

During the experiments studying SO_3 formation with Australian coals (C1, C2, C3) at BTS-VR, the facility's electrically heated furnace was operated with a constant temperature of all five heating zones (i.e. ϑ_{BTS1} to ϑ_{BTS5} = 1350 °C). In experiments with coal C4, a temperature profile from 1300 °C to 1100 °C was applied (see table 3.8). The facility's flue gas duct was trace heated, to reduce heat losses and accomplish a temperature and residence time profile comparable to actual power plant systems. Indicative temperature profiles averaged over the individual air and CO_2/O_2 experiments investigating SO_3 formation with coals C1, C2, and C3, are presented in figure 3.9[36]. The temperatures and residence times in certain temperature ranges can impact the formation and capture of SO_3. However, in all experiments with coals C1, C2, and C3, the temperature and residence time profiles were similar and hence, the results of the experiments studying SO_3 are assumed to be comparable. Due to the lower furnace outlet temperature, with coal C4 the temperature profile is somewhat altered, compared to the other SO_3 formation experiments (see figure 3.4). However, along the flue gas path the temperature profiles for the different experiments converge more and more and reach very similar temperatures at the

[36]Lines between temperature measurements (indicated by black dots) are linearly interpolated, and the temperature between burner and first temperature measurement of the furnace ϑ_{BTS1} is assumed to be constant.

Table 3.12: Simulated recirculation ratios (ξ_{rec}), coal feeds ($\dot{M}_{coal}$), and oxidant compositions for studies on SO_3 formation at BTS-VR with coals C1, C2, C3, and C4.

			oxidant compositions						
	ξ_{rec}	$\dot{M}_{coal}$	y_{H_2O}	y_{O_2}	y_{O_2}	y_{CO_2}	y_{SO_2}	y_{NO_x}	c_{Hg}
index	$\frac{m^3}{m^3}$	$\frac{kg}{h}$	$10^{-2}\ \frac{m^3}{m^3}$				$10^{-6}\ \frac{m^3}{m^3}$		$\frac{\mu g}{m^3}$, STP
	-	-	wet	wet	dry	dry	dry	dry	dry
C1-A	-	2.1	-	20.9	20.9	-	-	-	-
C1-CO2	-	2.8	0	28.0	28.0	72.0	0	0	0
C1-5S5H	69.8	2.8	16.9	28.0	33.7	66.3	515	654	17.8
C1-2S5H	69.8	2.8	16.9	28.0	33.7	66.3	824	654	17.8
C1-2S0H	69.8	2.8	16.9	28.0	33.7	66.3	824	654	29.4
C1-2S8H	69.8	2.8	16.9	28.0	33.7	66.3	824	654	6.5
C1-0S5H	69.8	2.8	16.9	28.0	33.7	66.3	1030	654	17.8
C1-0S0H	69.8	2.8	16.9	28.0	33.7	66.3	1030	654	29.4
C2-A	-	1.5	-	20.9	20.9	-	-	-	-
C2-CO2	-	2.1	0	28.0	28.0	72.0	0	0	0
C2-2S5H	70.6	2.1	20.5	28.0	35.2	64.8	1569	631	8.9
C3-A	-	1.4	-	20.9	20.9	-	-	-	-
C3-CO2	-	1.9	0	28.0	28.0	72.0	0	0	0
C3-2S5H	70.5	1.9	17.5	28.0	34.0	66.0	1687	634	3.7
C4-A	-	1.3	-	20.9	20.9	-	-	-	-
C4-8S0H	73.1	1.7	12.1	28.0	31.9	68.1	1779	700	17.7

fabric filter inlet. Nonetheless, it should be considered that the different temperature profiles for coal C4 and the other coals (C1, C2, C3) may have impacted the results.

The temperature and residence time profile for coal C1, C2, and C3 experiments was determined on basis of the gas flow rates through the furnace, flue gas duct, and filter, the temperatures that were measured along the system, and its geometry. This calculation is subject to uncertainties in the assumptions (e.g. clean furnace and pipes) and differences in the actual temperatures that were reached in individual experiments. This approach was validated in an experiment using a tracer gas and a gas analyzer to determine the actual gas travel times along the furnace and flue gas duct in dedicated tests. A difference between measured residence times and calculated ones of +/- 15 % was observed, which gives an indication of the accuracy of the calculated temperature profiles. A general observation that was made in the air and simulated oxy-fuel experiments is that the temperatures in the flue gas duct in simulated oxy-fuel operation are somewhat higher than in air firing. This is related to the different thermal properties of the flue gases in both combustion modes. The difference is most pronounced at the inlet of the flue

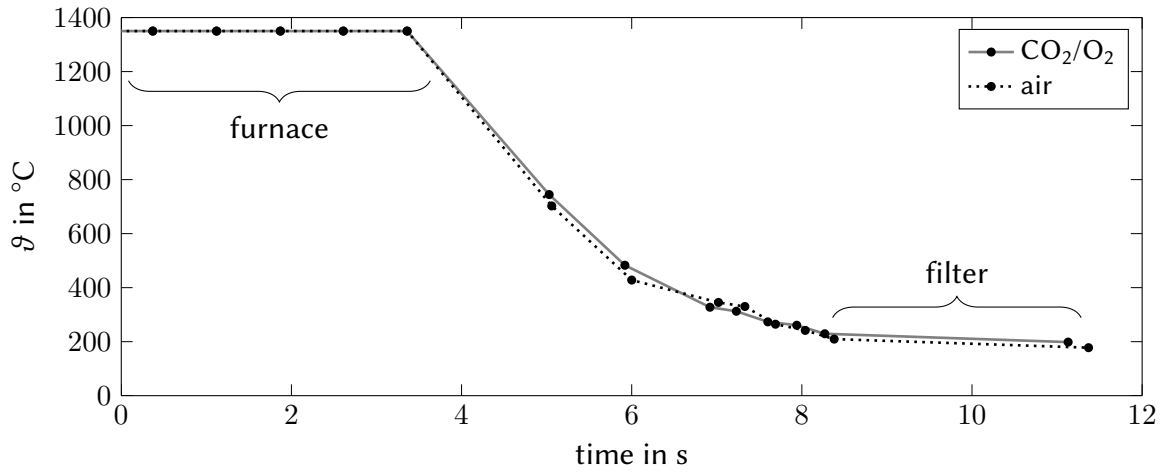

Figure 3.9: Indicative temperature profile along the furnace, flue gas duct, and filter of BTS-VR during air and CO_2/O_2 experiments studying SO_3 formation with coals C1, C2, and C3 (for coal C4, see figure 3.4).

gas duct where heat losses, due to the high temperature, are highest. The average temperature difference between both combustion modes reaches up to about 40 °C at the duct inlet and then reduces to approx. 20 °C at the filter outlet. For individual experiments, temperature variations along the flue gas duct were observed, with duct inlet temperatures in air firing ranging from about 630 °C to 765 °C and temperatures at the filter inlet between about 185 °C and 225 °C. In oxy-fuel experiments those temperature ranges were approx. 660 to 865 °C and 190 to 210 °C. The average temperature drop between filter in- and outlet ranged between 25 °C and 30 °C in both combustion modes.

3.3.4.2 Conducted measurements and data processing

In the experiments studying SO_3 formation at BTS-VR, O_2, CO_2, CO, SO_2, and NO_x were measured continuously before fabric filter. H_2O concentrations were calculated based on coal composition and water injection. SO_3 was measured discontinuously before and after the BTS-VR's fabric filter. This filter was cleaned before each individual SO_3 sampling. During the course of a measurement, the filter cleaning was discontinued. This implies an increase of the ash loading of the fabric filter during individual measurements as well as differing ash build-up rates for different coal feed rates and ash contents. Such conditions are similar to an actual power plant system, where ash build-up rates vary with the fuel. In the experiments investigating SO_3 formation at least two but in most cases three repetitive measurements were conducted that were used to calculate average SO_3 concentrations that are reported in this thesis.

Based on the SO_2 and SO_3 concentrations measured before the fabric filter of BTS-VR $\bar{y}_{SO_3,b.f.}$, SO_2 to SO_3 conversion ratios κ_{23} can be calculated. The calculation of κ_{23} was conducted, according to equation 3.15. This correlation is based on a well established standard to calculate

κ_{23} at SCR catalysts for NO_x reduction [205] and does not consider the concentration of SO_3 in the denominator. Due to the relatively low concentrations of SO_3 in combustion flue gases, compared to the SO_2 concentrations, the difference between the calculation of κ_{23} according to equation 3.15 and according to a correlation that also considers the concentration of SO_3 in the denominator is low and does not impact the interpretation of the results obtained. The SO_3 capture efficiency at BTS-VR's fabric filter $\eta_{SO_3,fil.}$ is calculated, according to equation 3.16, on basis of the average SO_3 concentrations measured before ($\bar{y}_{SO_3,b.f.}$) and after ($\bar{y}_{SO_3,a.f.}$) the filter.

$$\kappa_{23} = \frac{\bar{y}_{SO_3,b.f.}}{\bar{y}_{SO_2,b.f.}} \tag{3.15}$$

$$\eta_{SO_3,fil.} = \frac{\bar{y}_{SO_3,b.f.} - \bar{y}_{SO_3,a.f.}}{\bar{y}_{SO_3,b.f.}} \tag{3.16}$$

3.4 Deposit and ash sampling

A number of different sampling probes were used in the experiments of this project to collect fly ash and deposit samples. Fly ash (abbreviated in plots by "A") was sampled from furnaces using a cooled suction probe. In fly ash sampling, ashes (i.e. fly ash together with unburned carbon, etc.) are separated from the sample gas with a cyclone and sintered metal filter. Sampling was conducted for relatively short time periods (i.e. for several minutes to half an hour) until enough sample material was obtained for subsequent analyses. Also analyses of so called process ashes were conducted. Process ashes were sampled from the test facilities' ash discharge systems, i.e. bottom, filter, and ESP ash hoppers. Such samples were always taken at the end of an experiment and from the top of the ash accumulated in the ash hoppers.

Deposits were sampled using uncooled and temperature-controlled deposit sampling probes. So called "cooled deposits" (abbreviated in plots by "C") were collected using a probe whose surface temperature can be controlled by cooling air, e.g. to simulate surface temperatures of superheater tubes. The cooled deposit samples aim to represent the initial layer of heat exchanger deposits. The cooled deposition probe was kept inside the furnace for longer durations (i.e. approx. 20 and 72 h). Uncooled deposition probes use a ceramic sample carrier whose surface reaches the temperature of surrounding flue gases. The temperature of this kind of probe is not controlled. The obtained uncooled deposit (abbreviated in plots by "U") represents the outer deposit layer that builds up over an initial layer on heat exchanger surfaces. Uncooled deposits were sampled over periods of approx. 2 to 4 h. Even though, the sampled deposits give detailed insights to the characteristics of such materials in air and oxy-fuel combustion and have been used successfully in the past to understand deposition mechanisms etc. (e.g. [206]), they cannot fully represent actual deposits from power plant heat exchangers which experience much longer exposure times to furnace conditions and often in addition

multiple soot-blower cleaning cycles. Hence, certain characteristics of such deposits may not be fully covered by the deposit analyses included in this thesis.
Ashes and deposits sampled during experimental campaigns were analyzed for their composition and morphology by ICP-OES analysis and by scanning electron microscopy (SEM-EDX, SEM-WDX). Few ash oxide samples included in this thesis (i.e. extracted fly and bottom ash samples), also contained minor amounts of carbon in form of carbonates (observed only very rarely) and some unburned carbon. To render all ash analyses comparable, they were recalculated to an unburned carbon and carbonate free basis. In addition, all ash oxide analyses have been normalized to $100 \cdot 10^{-2} \frac{\text{kg}}{\text{kg}}$.

3.5 Analysis of solid samples

3.5.1 Chemical analysis of solid samples

Solid samples were analyzed for their contents of ash (DIN 51719 [198]), total organic and inorganic carbon in ash (DIN 19539, [207]), sulfur (DIN 51724-1, [202]), chlorine (only water soluble chlorine that constitutes the majority of chlorine in ash samples was analyzed, according to DIN 38414-4 [208] and DIN EN ISO 10304-1 [209]), and main ash-forming elements (DIN 51729-11, [210]). Ash and deposit samples obtained from air and oxy-fuel experiments have been analyzed directly (certain samples had to be milled previously to the analysis), without additional ashing of the samples. The aim of this is to avoid a loss of volatile compounds (e.g. alkali salts) in the standard laboratory ashing process that is conducted at 815 °C.

3.5.2 Scanning electron microscope analysis

A number of deposit samples have been analyzed by scanning electron microscopy (SEM) to study the samples' morphology and distribution of elements. This allows for an assessment of changes in the deposits obtained from different experimental conditions. Previously to the electron micro-probe analyses, the samples were embedded in a resin, cut, and polished. In the obtained micrographs, the resin that consists of molecules containing only carbon and hydrogen atoms appears black, while structures containing other atoms are plotted in shades of gray or in white, depending on the molecular weight (BSE micrographs) or the concentrations of selected atomic species (element maps). A CAMECA SX100 electron micro-probe was used for SEM analyses. The system has an energy dispersive X-ray detector (SEM-EDX) that was used to generate backscattered micrographs showing the sample morphology on a microscopic scale. Moreover, this detector was used to obtain the local elemental composition of selected points of the analyzed samples. In addition to the EDX system, the electron microscope has five wavelength dispersive X-ray spectrometers (SEM-WDX) that can be used to analyze the characteristic radiation that is emitted from the sample when irradiated by an electron beam.

An evaluation of this characteristic radiation allows for a quantitative and localized analysis of the elemental composition of the sample. With properly polished samples a resolution of the elemental distribution down to the scale of 1 µm is possible. The WDX system was used to generate maps of the distribution of selected elements (e.g. sulfur) on a certain area of interest of the sample. Sample analyses by SEM-EDX and SEM-WDX are very time consuming and hence, have only been conducted to analyze selected samples.

3.6 Gas measurement techniques

3.6.1 Standard online gas analysis

In case of continuous gas analysis for the components O_2, CO_2, CO, NO_x (sum of NO and NO_2), and SO_2, sample gas was extracted from flue gas ducts or furnaces, subjected to out-stack sample gas filtration, and a moisture removal, using a sample gas cooler operated at 4 °C. All sampling lines upstream the sample gas cooler as well as the filter for ash removal were heated to 180 °C. Flue gas sampling from KSVA's furnace to obtain SO_2 concentration profiles was conducted using a water cooled gas extraction probe, to quench reactions rapidly after the sampled gas enters the probe tip.

Table 3.13: Information on standard gas analyzers used at BTS-VR and KSVA.

Fuel/experiment	Measurement instrument	Component	Principle
KSVA, end of furnace			
L2 / combustion	ABB MAGNOS206	O_2	paramagnetism
	ABB URAS26	CO, CO_2, SO_2	IR photometry
	ECO Phys. CLD 700EL/EL ht	NO_x	chemiluminescence
L1 / combust.; C4 / combust. & DSI	ABB MAGNOS206	O_2	paramagnetism
	ABB URAS26	CO, CO_2	IR photometry
	ABB Limas11	SO_2, NO_x	UV photometry
KSVA, ESP & furnace profiles			
C4 / DSI	ABB MAGNOS206	O_2	paramagnetism
	ABB URAS26	CO, CO_2, SO_2	IR photometry
	ECO Physics CLD 700EL ht	NO_x	chemiluminescence
BTS-VR, end of furnace & filter			
C4 / DSI & SO_3; L2 / deposits; C1, C2, & C3 / SO_3	ABB MAGNOS206	O_2	paramagnetism
	ABB URAS26	CO, CO_2	IR photometry
	Siemens Ultramat 23	SO_2, (CO_2)	IR photometry
	ECO Phys. CLD 700EL/822s	NO_x	chemiluminescence

Table 3.13 summarizes information on the analyzers used at BTS-VR and KSVA for the different experimental campaigns and fuels as well as their measuring principles. The analyzers have been calibrated regularly[37] during experimental campaigns to ensure correct analysis results. In respect to the measurements conducted after ESP of the oxy-fuel pilot plant "Schwarze Pumpe" that are included in this thesis, only limited information is available. These measurements have been conducted by Vattenfall using a paramagnetic O_2 sensor and infrared photometry for other reported components. It can be assumed that the measuring equipment of this industrial oxy-fuel pilot plant was well maintained and calibrated, so that the measured gas concentrations are trustworthy. At the oxy-fuel pilot plant's furnace, also few local gas measurements were conducted at locations where deposits have been sampled. These measurements were performed using a mobile Testo 350 multi-component analyzer. This analyzer uses electrochemical analysis cells for O_2, CO, NO, and SO_2 and an NDIR sensor for CO_2.

3.6.2 FTIR online gas analysis

The HCl measurements in DSI experiments at KSVA and BTS-VR test rigs reported in this thesis were conducted using a "Gasmet DX 4000" continuous multi-component Fourier transform infrared radiation (FTIR) analyzer. The used analyzer has a 5 m[38] measuring cell that was heated to 180 °C allowing for the measurement of wet flue gas samples. The spectrometer has a spectral resolution of 8 $\frac{1}{\text{cm}}$ and a spectral range of 600 to 4200 $\frac{1}{\text{cm}}$. The analyzer leads infra red (IR) light from a wide spectral length IR source through a measuring cell containing sample gas. In the measuring cell, IR active gases can absorb part of this light. The sample gas is continuously extracted from the sampling location and fed to the measuring cell with help of a suitable gas sampling system (stainless steel and PTFE gas lines, pump, and particle filter heated to 180 °C). With help of an interferometer the intensity of the absorption over a certain spectral range can be measured by a detector. The detector signal is digitalized and Fourier transformed by a computer program which results in an IR absorption spectrum of the sample gas that gives the absorption for each wavelength in the spectral range of the detector. For measurements during DSI experiments, sampling frequencies of 0.2, 0.05, and 0.017 Hz (absorption spectrum scan times of 5, 20, and 60 s) were used.

The analysis of the IR absorption spectra was conducted using Gasmet's proprietary Calcmet software and suitable reference spectra for pure gas components of known concentrations that were provided by the German distributor of the FTIR analyzer, Ansyco. For each gas component, several reference spectra for different relevant concentrations have been used and these reference spectra have been linearized using the respective tool in the Calcmet software. Different gases can have absorption peaks close to each other, which may cause

[37] In most cases calibration was conducted daily and always when switching from air to oxy-fuel combustion and vice versa.

[38] This length is realized with help of mirror optics.

Table 3.14: Components and analysis areas used for FTIR absorption spectra evaluation.

Component	Analysis area 1	Analysis area 2
	$\frac{1}{cm}$	
H_2O	3200-3401	-
CO_2	926-1150	2000-2146
CO	2020-2210	2550-2600
NO	1875-2150	-
NO_2	2700-2950	-
HCl	2617-2880	2856-2879
SO_2	1050-1250	1200-1310
HF	2500-2600	4020-4250

interferences in their absorption. To minimize negative impacts of such interferences on the spectral evaluation, the user can select suitable analysis areas (i.e. wavenumber ranges) for each component. Table 3.14 lists the analysis areas that have been selected in this thesis on basis of Ansyco's recommendations, with certain modifications to minimize interferences between gas species in the sampled gases. To correct the slope of the baseline of the reference spectra that may have an impact on the analyzed gas concentrations if wide analysis areas are selected, the automatic baseline correction function of Calcmet was applied. The Calcmet software also offers a function to correct interferences between measured gases that cannot be avoided by a selection of suitable analysis areas. This feature was applied to all measured gas components using the automatic interference configuration mode of Calcmet.

Even though the FTIR analyzer can analyze the sample gas for a large number of IR-active species, in this thesis, only FTIR measurements of HCl are used extensively. In addition, few H_2O measurements of flue gases by this analyzer are reported. To validate the applicability of the FTIR analyzer for HCl analysis of flue gases, a number of comparative wet chemical HCl[39] measurements during combustion of different fuels have been conducted (i.e. extraction of sample gas and HCl absorption in water following DIN EN 1911 [211] and subsequent Cl^- analysis by ion chromatography, according to DIN EN ISO 10304 [209]), giving deviations in the range of +/- 10 % between both methods [37, 46]. On basis of that result and due to the fact that the FTIR method allows for continuous HCl measurements, which is not possible with the wet chemical method, the decision was made to conduct HCl measurements during DSI testing exclusively by FTIR analysis.

[39] More accurately, gaseous chloride measurements: It is assumed that the bulk of gaseous chlorides absorbed from the combustion flue gases with this method are present in form of HCl.

3.6.3 Wet chemical SO_3 measurement

In part of the experiments included in this thesis, SO_3 concentrations were measured before and after the fabric filters and ESP systems of different experimental facilities. The used method is based on the guideline VDI 2462 [212] with some modifications (slightly different condenser coil and in-stack filter) and uses the controlled condensation of liquid H_2SO_4 (that is formed quantitatively when cooling SO_3 in moist atmospheres) in a suitable condenser. A schematic of the sampling system used for SO_3 measurements of this thesis is shown in figure 3.10. Sample gas was extracted from a flue gas duct (1) via an in-stack filter cartridge (2) filled with quartz wool[40] using a glass sampling probe (3). The in-stack filter was always introduced to the flue gas duct and equilibrated to reach the temperature of the flue gas, and the filter cartridge was exchanged in-between individual samplings of SO_3 to minimize the impact of accumulated filter ash on the SO_3 measurements. Relevant sections of the flue gas duct and the sampling probe up to the point where it enters the H_2SO_4 condenser were heated with electrical heating bands and in addition with a hot air fan to reliably maintain the wall above the sulfuric acid dew point temperature. The sample gas was fed to the H_2SO_4 condenser (5) that was fully immersed in a water bath heated to a temperature well above the water dew point (i.e. about 90 °C). The extracted gas flow was regulated with a valve (7) to maintain a gas flow of about 4 to 8 $\frac{\text{l}}{\text{min}}$, which was measured using a variable area flow meter (8)[41]. A pressure sensor in the sampling line-up (6) allowed to notice blockages in the system. After the flow meter, the sampling gas was fed to a gas drier. The flue gas was extracted through the sampling system using a gas pump (10) and was supplied to a volumetric gas meter (12) that was equipped with a pressure and temperature measurement (11) to allow for recalculation of the measured SO_3 concentrations to standard conditions (DIN 1343 [213]: 0 °C, 1013.25 hPa). During SO_3

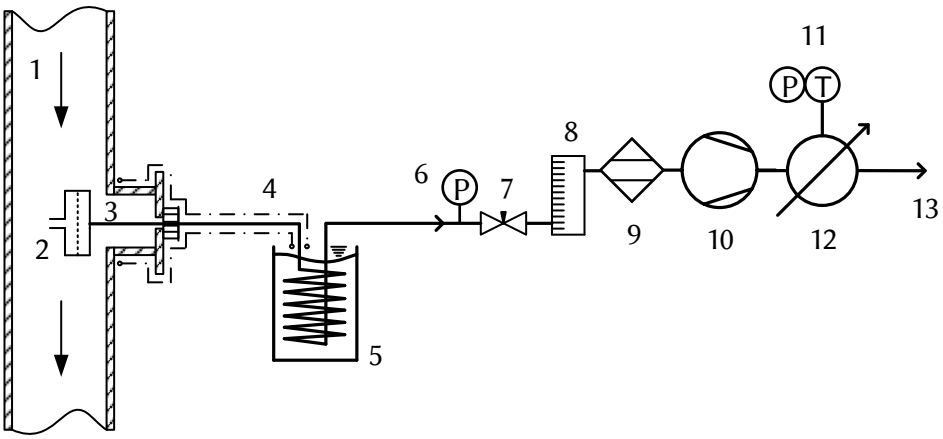

Figure 3.10: Schematic of the sampling system used for SO_3 measurements.

[40] The utilization of quartz wool filter materials is crucial since other materials, e.g. glass wool, were found to absorb SO_3 in significant quantities which leads to a negative bias of the measurement.

[41] Since the variable area flow meter's reading (8) is dependent on the gas density, the flow meter needs to be calibrated for air and oxy-fuel flue gas conditions, e.g. by using the volumetric gas meter (12).

measurements, the O_2 level was regularly measured at the sample gas outlet and compared to the O_2 level in the flue gas sampled at furnace exit or after filter/ESP, to ensure gas tightness of the sampling system. In case this difference was too high (i.e. above $0.5 \cdot 10^{-2}$ $\frac{m^3}{m^3}$, dry, O_2), SO_3 measurements were stopped and the system's tightness was improved accordingly. After completion of the gas sampling (depending on SO_3 levels, after sampling of 30 to 220 l of sample gas), the glass coil was disconnected and rinsed at least three times with deionized water and the obtained liquid was then filled up to a volume of 50 ml.

$$y_{SO_3,FG} = \frac{(c_{liq,SO_4} - c_{liq,SO_4,blank}) \cdot V_{liq} \cdot V_{mol}}{V_{sample} \cdot M_{M,SO_4}} \tag{3.17}$$

These liquid SO_3/H_2SO_4 samples were then analyzed for their sulfate content by ion chromatography (DIN EN ISO 10304 [209]) or by titration[42] (VDI 2462 [212]). On basis of the sulfate content in the liquid sample c_{liq,SO_4} and in a blank sample $c_{liq,SO_4,blank}$, the volume of the liquid sample V_{liq}, the sampled gas volume V_{sample}, the molecular weight of sulfate M_{M,SO_4}, and the molar volume V_{mol}, the SO_3 concentration in the flue gas $y_{SO_3,FG}$ can be calculated, according equation 3.17. All SO_3 values included in this thesis refer to dry gas and represent results averaged from minimum two but in most cases three individual SO_3 measurements.

3.6.4 Correction of gas concentrations to reference oxygen levels

Certain parts of this thesis (e.g. DSI experiments) require a direct comparison of gas concentrations measured in different experiments and combustion modes. Due to the size and complexity of the used experimental test rigs, it is not possible to keep all experimental parameters constant between different tests. This is particularly relevant in the context of slightly varying O_2 concentrations in the measured flue gases that imply a variation of the dilution of flue gases by unconverted oxidant gas or by air ingression to the process. For that reason, in several instances gas concentrations were corrected to certain O_2 concentration levels. Such corrections of gas concentrations are indicated in the results chapter. The corrections were done in different ways for the different combustion facilities and combustion modes (i.e. air, CO_2/O_2, oxy-fuel recycle).

For air fired combustion, acid gas concentrations were corrected to a reference O_2 level of $3 \cdot 10^{-2}$ $\frac{m^3}{m^3}$, dry, according to equation 3.18. This correction assumes that the flue gas is a mixture of air, combustion products (i.e. CO_2, SO_2, HCl), and unreacted oxidant air (simplified composition: $20.9 \cdot 10^{-2}$ $\frac{m^3}{m^3}$, dry, O_2 and $79.1 \cdot 10^{-2}$ $\frac{m^3}{m^3}$, dry, N_2). Since in this case oxidant gas and ambient air have the same composition, this correction calculation can cover varying flue gas dilution that is caused by false air ingress to the combustion process as well as by small

[42] Titration was only used for analysis of samples from lignite L1 air and oxy-fuel combustion at KSVA.

fluctuations in the fuel feed which affect the oxidant air consumption in the furnace.

$$\bar{y}_{i,dry,corr} = \frac{0.209 - 0.03}{0.209 - \bar{y}_{O_2,dry}} \cdot \bar{y}_{i,dry} \tag{3.18}$$

$$\bar{y}_{i,dry,corr} = \frac{y_{O_2,oxid,dry} - 0.03}{y_{O_2,oxid,dry} - \bar{y}_{O_2,dry}} \cdot \bar{y}_{i,dry} \tag{3.19}$$

$$\bar{y}_{i,dry,corr} = \frac{1 - y_{O_2,ref,dry}}{1 - \bar{y}_{O_2,dry}} \cdot \bar{y}_{i,dry} \tag{3.20}$$

This is different in CO_2/O_2 experiments that were conducted at BTS-VR. In those experiments, the oxidant gas contained different O_2 levels and hence, equation 3.18 would only be applicable if one assumes that fluctuations of the O_2 concentration in the flue gas are caused only by false air ingress and not by fluctuations in the fuel feed. Since during the CO_2/O_2 experiments at BTS-VR great care was put into avoiding false air ingress to the combustion process such an assumption is not justified. Instead, for the correction of such gas concentrations to a reference O_2 level, it is assumed that false air ingress was reliably avoided and therefore, fluctuations in the O_2 concentration of the flue gas are caused only by fluctuations in the fuel feed and hence, by dilution of the CO_2/O_2 combustion products (i.e. CO_2, SO_2, HCl) with unreacted oxidant gas of a certain oxygen concentration $y_{O_2,oxid,dry}$ (e.g. for coal C4 CO_2/O_2 exeriments at BTS-VR $y_{O_2,oxid,dry}$ = 31.9 $\cdot$ 10^{-2} $\frac{m^3}{m^3}$, dry). The gas concentrations can hence be corrected to a reference O_2 level of 3 $\cdot$ 10^{-2} $\frac{m^3}{m^3}$, according to equation 3.19.

The situation is more complicated in case of oxy-fuel recycle experiments at KSVA. In those experiments, air ingress could not fully be avoided (see table 3.6, $y_{leak,dry} \approx 6$ to 7 $\cdot$ 10^{-2} $\frac{m^3}{m^3}$) while also small fluctuations in the fuel feed occurred. In addition, in the different DSI experiments the SO_2 concentration in the oxidant gas (i.e. recirculated flue gas) was varying. A practical way to correct acid gas concentrations to a certain reference O_2 level is to consider only the dilution of the flue gas by unreacted oxygen. However, this assumption does not consider any effects caused by a varying false air ingress between different experiments. To minimize the effect that the correction of gas concentrations has on the results, a reference O_2 concentration is used which is close to the actual O_2 levels in the flue gas reached in all the oxy-fuel experiments. For the oxy-fuel DSI experiments at KSVA, a reference O_2 concentration $y_{O_2,ref,dry}$ of 4 $\cdot$ 10^{-2} $\frac{m^3}{m^3}$ was selected. In cases using other reference O_2 concentrations this is indicated. The correction of gas concentrations to the reference O_2 concentration $y_{O_2,ref,dry}$ for oxy-fuel recycle experiments at KSVA is calculated, according to equation 3.20.

3.7 Calculation of sulfuric acid dew point temperatures

From SO_3 and H_2O contained in the flue gas, gaseous sulfuric acid (H_2SO_4) forms when temperatures fall below about 400 °C. The gaseous sulfuric acid starts to condense when its dew point temperature is reached. The H_2SO_4 dew point temperature can be calculated on basis of the partial pressures of H_2O and SO_3/H_2SO_4 in the flue gas, according to empirical equations. Some well know correlations have been proposed by Verhoff and Banchero [121] and Okkes [122]. A more recent and more accurate correlation by ZareNehzhad [123] is used in this thesis (equation 3.21). In equation 3.21, the partial pressures p_{SO_3} and p_{H_2O} are used with the unit "mm_{HG}".

$$\vartheta_{H_2SO_4,dew} = 150 + 11.664ln(p_{SO_3}) + 8.1328ln(p_{H_2O}) - 0.383226ln(p_{SO_3})ln(p_{H_2O}) \quad (3.21)$$

3.8 Thermodynamic equilibrium simulation by FactSage and ChemSheet

3.8.1 Introduction to thermodynamic equilibrium simulation

In the past decades, various research groups and companies have developed software packages for the calculation of thermodynamic equilibrium conditions based on a minimization of the Gibbs energy and have collected thermodynamic data that serves as a basis for this calculation [214]. A popular program family has been developed around the application ChemSage. One of the most commonly used programs available from this family is FactSage that can be used to calculate complex multiphase and multicomponent equilibria in metallurgical and other process applications. FactSage also contains extensive thermodynamic databases. ChemSheet is another program of the ChemSage family that uses the FactSage Gibbs energy minimizer and thermodynamic databases. It is a Microsoft Excel macro allowing the calculation of thermodynamic equilibria within a spreadsheet [215].

3.8.2 Thermodynamic simulation in high temperature process engineering

Thermodynamic equilibrium simulation using FactSage has been applied by various research groups to study the behavior of problematic ash systems in high temperature environments and has helped to explain various effects in respect to ashes and deposits in combustion [206, 216–222]. It has to be considered that the equilibrium simulation approach uses highly idealized assumptions (i.e. perfect mixing and instantaneous equilibrium) and hence, the validity of the results should always be assessed on basis of experimental results and practical experiences. The equilibrium simulation work by others (e.g. [206, 216–222]) has been limited by the range

of functions and methods of visualization available in FactSage. The application of a thermodynamic equilibrium simulation program, such as ChemSheet, for two (or more) dimensional, thermodynamic phase mapping and other related applications and an efficient methodology for results evaluation and visualization, in contrast, allows a much more customized approach that can be adapted to virtually any given thermodynamic equilibrium simulation task. For this thesis, a thermodynamic phase mapping technique has been developed that will be introduced in detail in the following section. A similar approach was used by Ma et al. [223] to study slag formation from woody biomass under pressurized, entrained-flow gasification conditions.

3.8.3 Thermodynamic phase mapping using ChemSheet

For generation of the equilibrium data presented in this thesis, GTT's ChemSheet macro (originally developed by VTT in Finland) for Microsoft Excel was used. Since the ChemSheet macro alone is only capable of varying one parameter within a loop of simulations (e.g. temperature ϑ), an additional Excel macro was used to run a second loop varying an additional parameter (e.g. stoichiometric ratio n) and store the simulation results. In this way, equilibrium compositions of the system of interest can be obtained for different combinations of the two varied parameters (i.e. a two-dimensional table array containing all stable components and phases). It is also possible to add additional variation loops if desired. The obtained equilibrium compositions of the system can then be assessed in detail and parameters of interest can be plotted. Since the resulting data is extensive, an efficient means of data processing is required. MathWorks' MATLAB can be applied for this task. Moreover, MATLAB contains powerful applications for data visualization, which helps for further results analysis.

Figure 3.11 shows a schematic of the procedure for two dimensional thermodynamic phase mapping based on ChemSheet in combination with an additional Excel macro loop. In this thesis, the procedure is applied to study the behavior of two characteristic ash systems containing calcium and iron or calcium, iron, and silicon. Particles with such compositions were found in deposits sampled during oxy-fuel combustion of L3 lignite at Vattenfall's oxy-fuel pilot plant (see annex A.3 and [41, 42]). The behavior of these ash systems is studied in combustion atmospheres of an air and corresponding oxy-fuel fired system and at relevant temperatures. The approach is as follows: The elemental composition (elemental analysis plus moisture) of the L3 lignite combusted as well as the composition of characteristic deposit particles that were found in deposits is used as input data to the ChemSheet spreadsheet macro. Moreover, the system pressure (1 bar) is specified. For the system of interest, a thermodynamic database file is generated with FactSage and loaded to the ChemSheet macro. The thermodynamic databases FactPS and FTOxide of FactSage 7.0 were used for the simulation of equilibria. ChemSheet allows the variation of one so called "Stepindex". In this example, temperature is used as the "Stepindex" and varied between a minimum (ϑ_{min} = 250 °C) and a maximum (ϑ_{max} = 1750 °C) with a defined step width ($\Delta\vartheta$ = 2 °C). To vary the second dimension of interest (stoichiometric

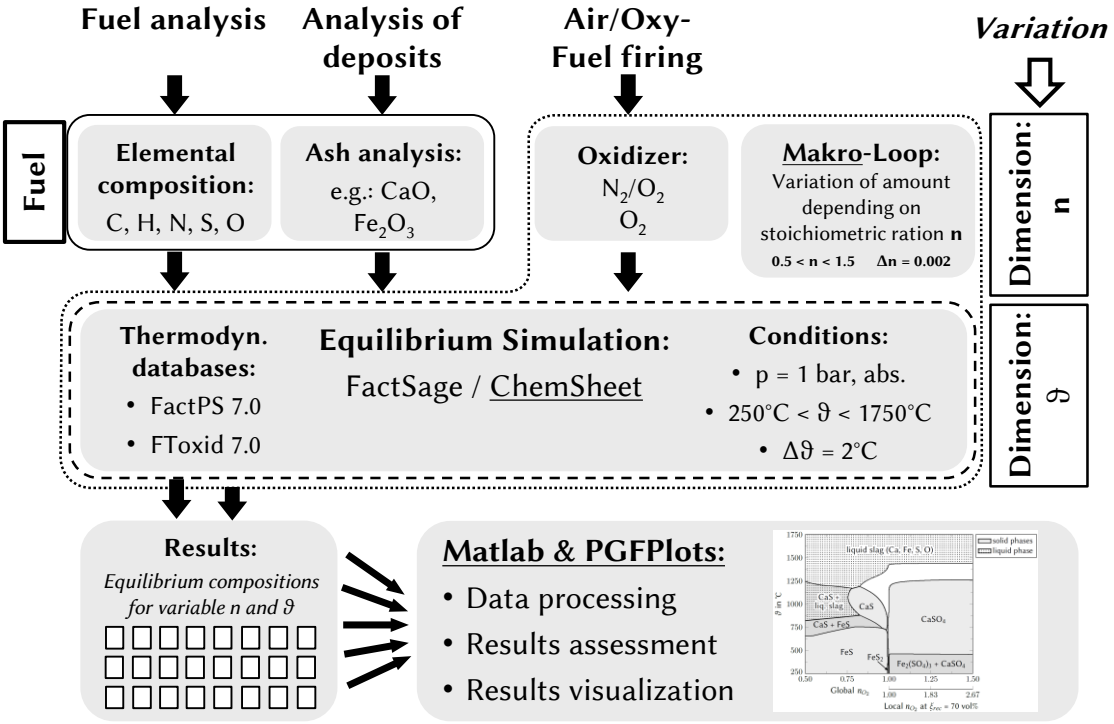

Figure 3.11: Schematic of the method used for two-dimensional thermodynamic phase mapping of ash/deposit systems in air and oxy-fuel atmospheres.

ratio n), the stoichiometric amount of O_2 required for combustion of the lignite was added to the ChemSheet spreadsheet[43]. Using an additional Excel macro, the input amount of O_2 for varying stoichiometric ratios is calculated between a minimum (n_{min} = 0.5) and maximum (n_{max} = 1.5) value with a defined step width (Δn = 0.002). Starting from the first input amount of O_2 for a certain stoichiometric ratio, the ChemSheet macro calculates the equilibrium composition of the system for all temperature steps between ϑ_{min} and ϑ_{max}. After completion of this, the input amount of O_2 is varied and the procedure is repeated. In this way a large number of individual thermodynamic equilibrium problems are solved. For the phase diagrams included in this thesis, 375000 individual equilibrium states (i.e. 750 stoichiometries times 500 temperatures) were evaluated. To obtain information on all relevant gas, solid, and liquid species, ChemSheet was set to store data for all possible species of this system (e.g. in a system of carbon, hydrogen, nitrogen, sulfur, oxygen, calcium, iron, silicon: 325 species).

The resulting data for each stoichiometry step is stored in a table listing the equilibrium amount of all possible components for all temperature steps. In this way, one obtains a large table array[44]. To be able to handle this data set, it is transferred into a three-dimensional results matrix (i.e. temperature × stoichiometric ratio × species amount) using MATLAB. During

[43] This description refers to oxy-fuel conditions. For air firing, N_2 needs to be added accordingly.

[44] For the system of carbon, hydrogen, nitrogen, sulfur, oxygen, calcium, iron, and silicon that was used to generate some of the phase diagrams included in this thesis, the table array contains more than 120 million individual values.

this transfer, also insignificant species (i.e. species that do not exist in relevant amounts for any of the studied temperatures and stoichiometric ratios) can be deleted to reduce the file size and hence, calculation times. The obtained matrix can now serve as a basis for further calculations. To generate phase diagrams, the matrix is scanned for stable phases and the areas in which certain phases are stable can be plotted using data visualization programs, such as MATLAB or the TeX/LaTeX macro package PGF/TikZ that was used in this thesis [224]. Based on the three-dimensional results matrix also other information, such as amounts of formed melt, concentrations of certain species, etc., can be extracted.

3.8.4 Thermodynamic equilibrium simulation by FactSage

Besides the thermodynamic phase mapping with ChemsSheet, also more conventional applications of the thermodynamic equilibrium simulation program FactSage and its databases are included in this thesis. Conventional phase diagrams (i.e. partial pressure versus temperature) and equilibrium temperatures have been obtained using the FactSage program package (version 7.0) and its “Equilib” and “Phase Diagram” modules. In these simulations, the pure substances “FACTPS” and the oxide compounds and oxide solutions “FToxid” (with base solution phase “FToxid-SLAGA”) FactSage databases were used.

4 Results and discussion

4.1 Theoretical considerations on impacts of oxy-fuel firing on SO_x and its capture

4.1.1 SO_2 concentration levels in air and oxy-fuel combustion

Based on a mole balance for air and oxy-fuel combustion, theoretical maximum concentrations of SO_2[45] and other flue gas species that are originating from components of the fuel (e.g. H_2O, CO_2, HCl, Hg) can be calculated. The equations 4.1 and 4.2 can be used to calculate the air and oxy-fuel SO_2 concentrations based on dry flue gas, while equations 4.3 and 4.4 give the concentrations based on wet flue gas[46].

$$y_{SO_2,max,air,dry} = \frac{\frac{\gamma_S}{M_{M,S}}}{\frac{\gamma_S}{M_{M,S}} + \frac{\gamma_C}{M_{M,C}} + \frac{\gamma_N}{2M_{M,N}} + \frac{0.791 + y_{O_2,exc,dry}}{0.209 - y_{O_2,exc,dry}}} \cdots cont. \cdots \tag{4.1}$$

$$\cdots cont. \cdots \frac{}{\cdot \left(\frac{\gamma_S}{M_{M,S}} + \frac{\gamma_C}{M_{M,C}} + \frac{\gamma_H}{4M_{M,H}} - \frac{\gamma_O}{2M_{M,O}} \right)}$$

$$y_{SO_2,max,oxy,dry} = \frac{\frac{\gamma_S}{M_{M,S}}}{\frac{1}{1 - y_{O_2,exc,dry} - y_{leak,dry}} \left(\frac{\gamma_S}{M_{M,S}} + \frac{\gamma_C}{M_{M,C}} + \frac{\gamma_N}{2M_{M,N}} + \frac{\dot{V}_{CO_2}}{\dot{M}_{RC} V_{mol}} \right)} \tag{4.2}$$

The calculations disregard the contribution of minor fuel components, such as chlorine, to the flue gas volume, which for common power plant fuels is not significant. The calculation of maximum oxy-fuel concentrations is based on a "practical" oxy-fuel recycle configuration (i.e. secondary recycle after ash separation and primary recycle after subsequent SO_x and H_2O

[45] Assuming that SO_2 is the only sulfur bearing component that is formed.
[46] All mass fractions γ_i in equations 4.1, 4.2, 4.3, and 4.4 are referring to the fuel state "raw".

removal[47]; this corresponds to recycle option a in figure 2.2). It is important to differentiate between wet and dry concentrations when discussing the differences between air and oxy-fuel operation. The reason for this is that commonly flue gas concentrations are measured and reported on a dry basis. Consequently, when comparing SO_2 concentration levels of air and oxy-fuel processes, concentrations on dry basis are commonly used (e.g. [1, 9, 10, 13]). However, for the thermodynamic stability of sulfates in furnaces the actual conditions in this unit are of relevance and hence, the SO_2 concentrations on a wet basis need to be considered. To discuss differences of SO_2 concentration levels between air and oxy-fuel firing, the ratio between $y_{SO_2,max,oxy}$ and $y_{SO_2,max,air}$ can be calculated (i.e. $\xi_{oxy/air,dry} = {y_{SO_2,max,oxy,dry}}/{y_{SO_2,max,air,dry}}$ and $\xi_{oxy/air,wet} = {y_{SO_2,max,oxy,wet}}/{y_{SO_2,max,air,wet}}$), giving the expected increase of wet and dry concentrations in oxy-fuel operation, compared to air firing.

$$y_{SO_2,max,air,wet} = \frac{\dfrac{\gamma_S}{M_{M,S}}}{\dfrac{\gamma_W}{M_{M,W}} + \dfrac{\gamma_H}{2M_{M,H}} + \dfrac{\gamma_S}{M_{M,S}} + \dfrac{\gamma_C}{M_{M,C}} + \dfrac{\gamma_N}{2M_{M,N}} + \dfrac{0.791 + y_{O_2,exc,dry}}{0.209 - y_{O_2,exc,dry}}} \cdots cont. \cdots$$

$$\cdots cont. \cdots \frac{}{\cdot \left(\dfrac{\gamma_S}{M_{M,S}} + \dfrac{\gamma_C}{M_{M,C}} + \dfrac{\gamma_H}{4M_{M,H}} - \dfrac{\gamma_O}{2M_{M,O}} \right)} \tag{4.3}$$

$$y_{SO_2,max,oxy,wet} = \frac{\dfrac{\gamma_S}{M_{M,S}}}{\dfrac{\gamma_W}{M_{M,W}} + \dfrac{\gamma_H}{2M_{M,H}} + \dfrac{1}{1 - y_{O_2,exc,dry} - y_{leak,dry}}} \cdots cont. \cdots$$

$$\cdots cont. \cdots \frac{}{\cdot \left(\dfrac{\gamma_S}{M_{M,S}} + \dfrac{\gamma_C}{M_{M,C}} + \dfrac{\gamma_N}{2M_{M,N}} + \dfrac{\dot{V}_{CO_2}}{\dot{M}_{RC} V_{mol}} \right)} \tag{4.4}$$

As can be seen from equations 4.1, 4.2, 4.3, and 4.4, for one fuel quality these $\xi_{oxy/air}$ ratios for wet and dry concentrations are influenced by the oxygen excess ($y_{O_2,exc,dry}$), the air ingress to the oxy-fuel process ($y_{leak,dry}$), and the specific volumetric flow of clean CO_2 (i.e. $v^*_{CO_2,dos} = {\dot{V}_{CO_2}}/{\dot{M}_{RC}}$) used for fuel dosing[48]. When comparing $\xi_{oxy/air}$ values for similar process conditions (i.e. same $y_{O_2,exc,dry}$, $y_{leak,dry}$, and $v^*_{CO_2,dos}$ ranges) but different fuel qualities, one sees that also the

[47] The cleaned primary recycle gas is considered in the calculations by assuming a certain fuel specific amount of clean CO_2 $v^*_{CO_2,dos}$ for fuel feeding.

[48] In the experiments at IFK's KSVA this is clean CO_2 from a tank. In industrial facilities (e.g. "Schwarze Pumpe" oxy-fuel pilot plant) it is cleaned flue gas that is recirculated.

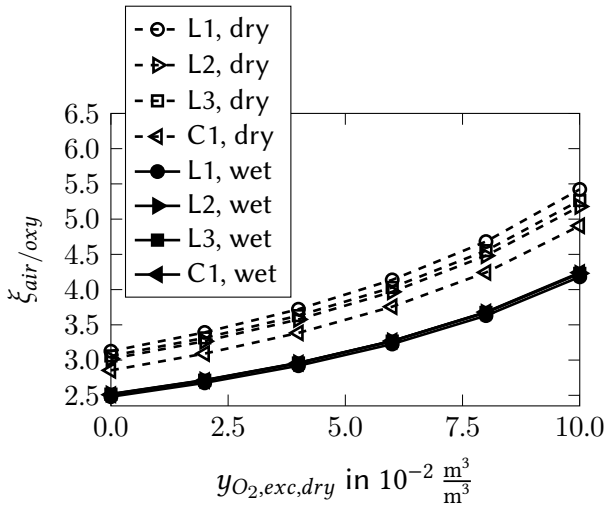

(a) Excess O_2: Lignites, coal C1

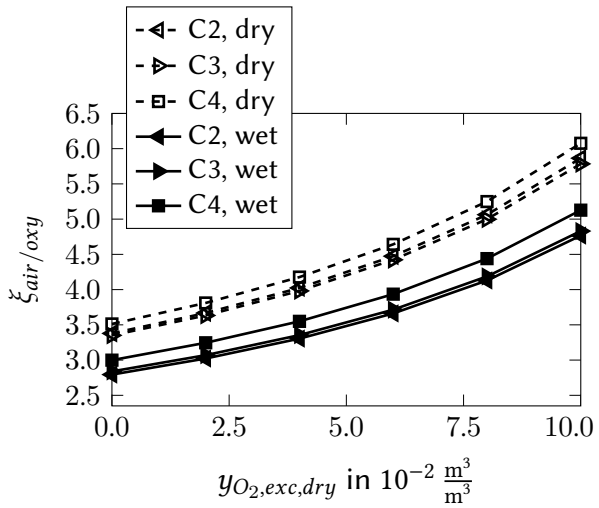

(b) Excess O_2: Coals C2, C3, C4

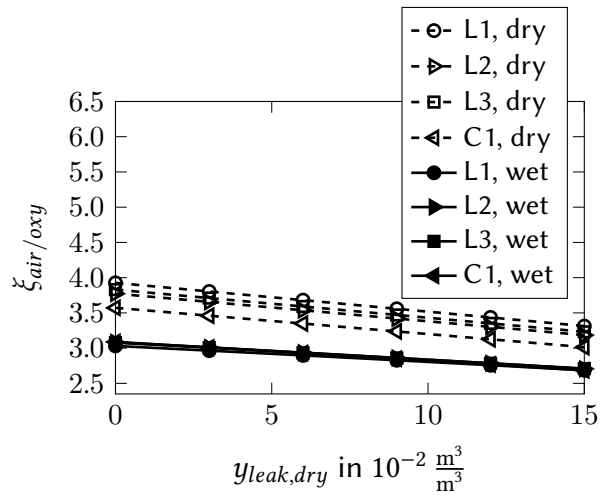

(c) Air ingress: Lignites, coal C1

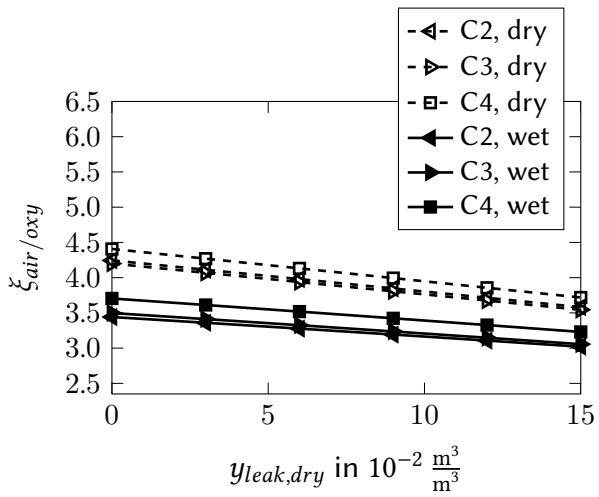

(d) Air ingress: Coals C2, C3, C4

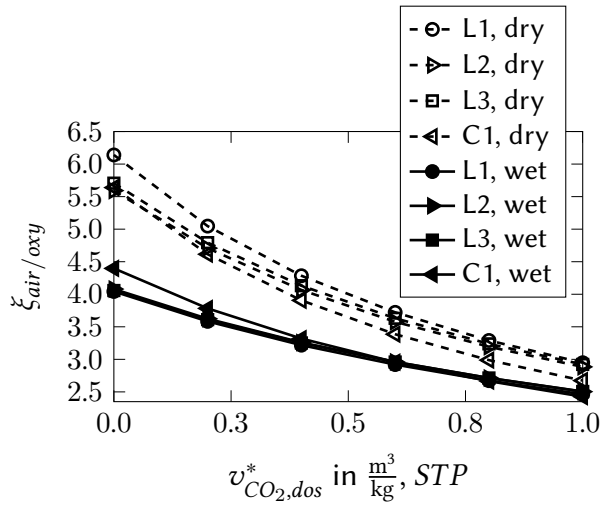

(e) Clean primary CO_2: Lignites, coal C1

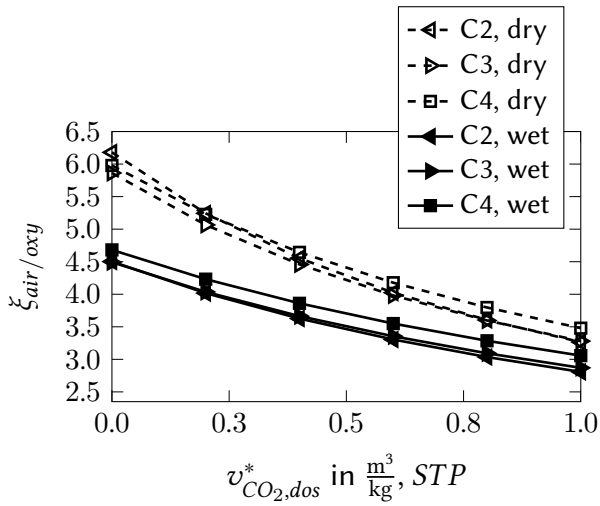

(f) Clean primary CO_2: Coals C2, C3, C4

Figure 4.1: $\xi_{oxy/air}$ ratios (wet and dry) between $y_{SO_2,max,oxy}$ and $y_{SO_2,max,air}$ calculated for the tested fuels and relevant ranges of the process parameters $y_{O_2,exc,dry}$, $y_{leak,dry}$, and $v^*_{CO_2,dos}$ (a, b: $y_{leak,dry}$= $5 \cdot 10^{-2}$ $\frac{m^3}{m^3}$, $v^*_{CO_2,dos}$= 0.6 $\frac{m^3}{kg}$; c, d: $y_{O_2,exc,dry}$= $4 \cdot 10^{-2}$ $\frac{m^3}{m^3}$, $v^*_{CO_2,dos}$= 0.6 $\frac{m^3}{kg}$; e, f: $y_{O_2,exc,dry}$= $4 \cdot 10^{-2}$ $\frac{m^3}{m^3}$, $y_{leak,dry}$= $5 \cdot 10^{-2}$ $\frac{m^3}{m^3}$).

fuel composition alters $\xi_{oxy/air}$ values. In this respect, $\xi_{oxy/air,wet}$ is strongly impacted by the moisture content of the fuel. The contents of carbon, oxygen, hydrogen, sulfur, and nitrogen in the fuel influence $\xi_{oxy/air,wet}$ as well as $\xi_{oxy/air,dry}$, even though, the impact of sulfur and nitrogen is generally low, due to their relatively low contents in most fuels.
To illustrate the ranges of $\xi_{oxy/air}$ expected in practice for the fuels tested in the framework of this thesis and for practically relevant ranges of $y_{O_2,exc,dry}$, $y_{leak,dry}$, and $v^*_{CO_2,dos}$, $\xi_{oxy/air}$ ratios are plotted in figure 4.1. It can be seen that the obtained $\xi_{oxy/air}$ ratios for all the lignites are similar, as their elemental compositions are. Due to its similar behavior, coal C1 is plotted in diagrams together with the lignites (figures 4.1a, 4.1c, and 4.1e). The $\xi_{oxy/air}$ ratios for the coals C2, C3, and C4 are similar and both, $\xi_{oxy/air,dry}$ and $\xi_{oxy/air,wet}$ ranges are higher than those of the lignites and coal C1, with coal C4 showing the highest difference between the SO_2 concentrations of air and oxy-fuel firing. Another observation is that $\xi_{oxy/air,wet}$ and therefore, the thermodynamically relevant increase between the air and oxy-fuel SO_2 levels is always lower than $\xi_{oxy/air,dry}$. This is due to the higher H_2O levels in wet recycle oxy-fuel firing, compared to air combustion that dilute concentrations of other components, such as SO_2. When comparing the plots of figure 4.1, it is obvious that $\xi_{oxy/air}$ is more sensitive towards changes of $y_{O_2,exc,dry}$ and of $v^*_{CO_2,dos}$ than towards changes of $y_{leak,dry}$. $\xi_{oxy/air}$ increases with $y_{O_2,exc,dry}$, while it drops with increasing $v^*_{CO_2,dos}$. The reason for this is that an increase of the excess oxygen in air firing goes along with additional dilution by airborne nitrogen, which is not the case in oxy-fuel conditions. In contrast, increasing the specific amount of clean CO_2 only dilutes the SO_2 concentrations in oxy-fuel operation, without any impact on the air fired concentration levels. For the tested fuels and an air and comparable practical oxy-fuel setup (i.e. non-ideal system with air ingress $y_{leak,dry}$ of $5 \cdot 10^{-2}$ $\frac{m^3}{m^3}$, cleaned primary recycle gas for milling/dosing of fuel $v^*_{CO_2,dos}$ of 0.6 $\frac{m^3}{kg}$, and an oxygen flue gas concentration $y_{O_2,exc,dry}$ of $4 \cdot 10^{-2}$ $\frac{m^3}{m^3}$), the SO_2 concentrations can be expected to increase by a factor of 3.4-4.2 referring to dry and of 2.9-3.5 for wet conditions. For an idealized oxy-fuel setup with no air ingress and no utilization of cleaned primary recycle gas for milling/dosing of fuel ($y_{O_2,exc,dry}$= $4 \cdot 10^{-2}$ $\frac{m^3}{m^3}$) the ranges for $\xi_{oxy/air,dry}$ and $\xi_{oxy/air,wet}$ are 5.9-6.5 and 4.2-4.9, respectively. The $\xi_{oxy/air,dry}$ ratios for a practical oxy-fuel setup compare well with those previously reported by others from experiments of 2-4 [1, 9, 13].

4.1.2 Stability of sulfates in air and oxy-fuel combustion

Investigations of this thesis, but also by others [19, 124, 126, 225, 226], indicate that due to the high SO_2 concentrations[49] (see section 4.1.1) increased sulfur contents in boiler deposits and process ashes are one important difference between air and oxy-fuel fired systems. The increased partial pressure of SO_2 stabilizes sulfates thermodynamically. Due to their composition, for most of the fuels and sorbents tested within this thesis, but also generally, $CaSO_4$ is the most

[49] If recirculated gases are not cleaned.

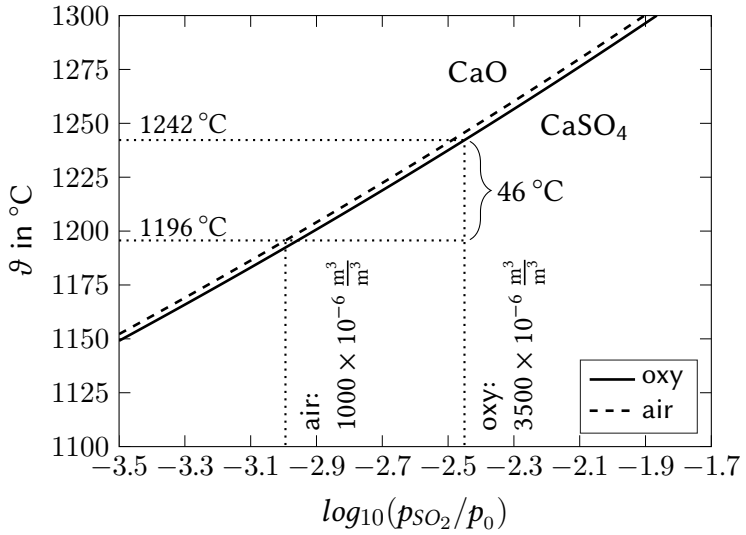

Figure 4.2: Phase boundary between CaO and $CaSO_4$ at variable temperature ϑ and SO_2 partial pressure p_{SO_2} for typical air and oxy-fuel atmospheres (p_{tot} = 1.013 25 · 10^5 Pa; air: $y_{N_2,wet} = 75.1 \cdot 10^{-2}\ \frac{m^3}{m^3}$, $y_{CO_2,wet} = 16.2 \cdot 10^{-2}\ \frac{m^3}{m^3}$, $y_{H_2O,wet} = 5.0 \cdot 10^{-2}\ \frac{m^3}{m^3}$, $y_{O_2,wet} = 3.8 \cdot 10^{-2}\ \frac{m^3}{m^3}$; oxy-fuel: $y_{CO_2,wet} = 76.8 \cdot 10^{-2}\ \frac{m^3}{m^3}$, $y_{H_2O,wet} = 20.0 \cdot 10^{-2}\ \frac{m^3}{m^3}$, $y_{O_2,wet} = 3.2 \cdot 10^{-2}\ \frac{m^3}{m^3}$) with the same $y_{O_2,dry} = 4 \cdot 10^{-2}\ \frac{m^3}{m^3}$. p_{SO_2} for complementary air and oxy-fuel fired settings and the expected rise of the $CaSO_4$ decomposition temperature are illustrated exemplary.

abundant sulfate species formed. To assess the effect of altered SO_2 concentrations on the stability of $CaSO_4$ in typical air and oxy-fuel flue gas atmospheres, CaO-$CaSO_4$ phase boundaries for the CaO-$CaSO_4$-flue-gas system in dependency of the SO_2 partial pressure (p_{SO_2}) are plotted in figure 4.2. This allows for a first estimation of the differences in $CaSO_4$ decomposition temperatures between combustion modes. Assuming a rise of p_{SO_2} (wet basis) by a factor of 3.5 (see discussion on $\xi_{oxy/air,wet}$ in section 4.1.1) and a wet based SO_2 concentration of $1000 \cdot 10^{-6}\ \frac{m^3}{m^3}$ in air firing, a complementary oxy-fuel system would have a SO_2 concentration of $3500 \cdot 10^{-6}\ \frac{m^3}{m^3}$, wet. From figure 4.2, one can determine that with this increase of p_{SO_2} the $CaSO_4$ decomposition temperature rises in a range of almost 50 °C. For different values of $\xi_{oxy/air,wet}$ this increase may be somewhat higher or lower.

The previous considerations were taking into account a simplified ash system consisting of pure CaO in a typical oxidizing air and oxy-fuel flue gas atmosphere. However, practical combustion systems are more complex. The ash contains additional compounds and the gas atmosphere that ash particles experience while traveling through a power plant is changing. Near the flame, particles experience high temperatures and an oxygen deficiency. Further downstream, better gas mixing and burnout air/O_2 addition lead to an excess of oxygen while heat extraction reduces the temperature. To cover the effects of these changing conditions on the thermodynamically stable phases of relevant ash forming elements, a method for two-dimensional thermodynamic phase mapping was developed (see section 3.8) and applied to

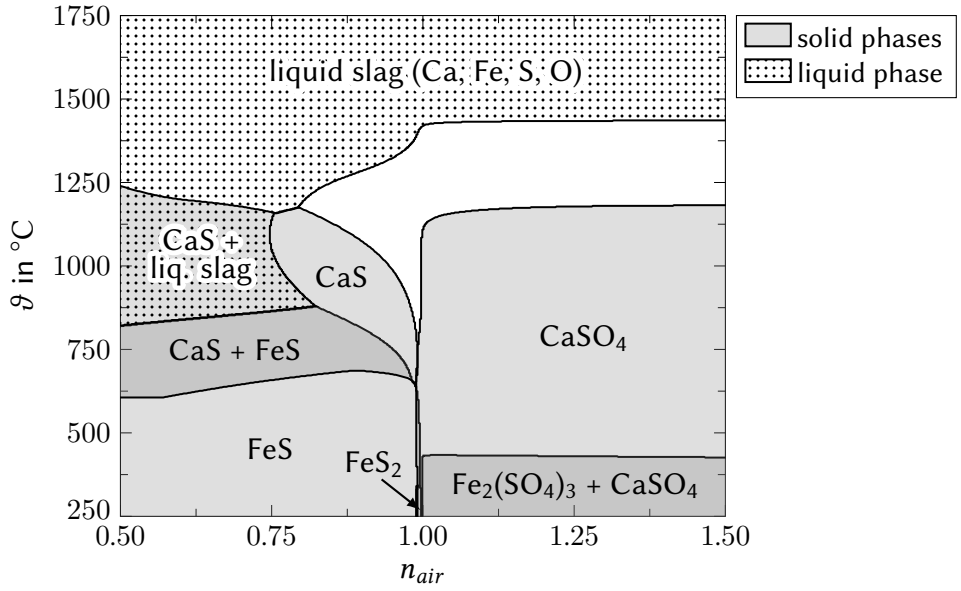

(a) Air

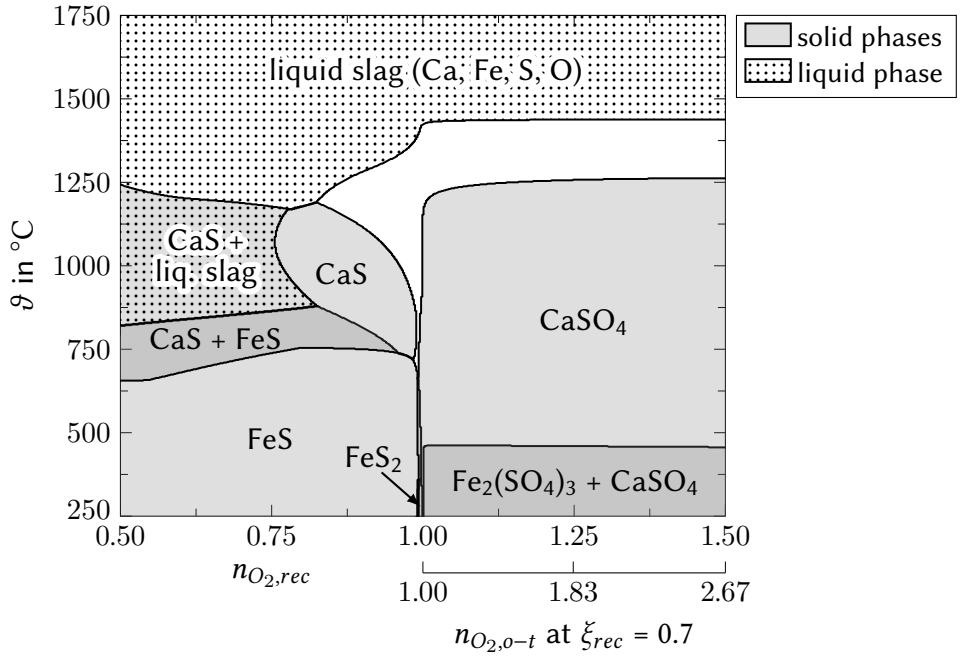

(b) Oxy-fuel

Figure 4.3: Thermodynamically stable solid and liquid phases containing sulfur in a system with **CaO** and **Fe_2O_3** in atmospheres of L3 lignite air and oxy-fuel combustion. (solid phases plotted with opacity, i.e. darker gray areas indicate coexisting solid phases; gaseous phases are not shown; white areas indicate that no sulfur is present in solid and liquid phases, i.e. it is in gas phase; for other stable solid phases: see annex, p. 168).

systems simulating air and oxy-fuel combustion of a fuel with the same elemental composition as the L3 lignite. This fuel was chosen since it was used in tests at Vattenfall's oxy-fuel pilot plant, for which deposits and ashes were sampled and analyzed in detail. Moreover, this fuel is similar to the L2 lignite, for which comparative studies on air and oxy-fuel ashes and deposits

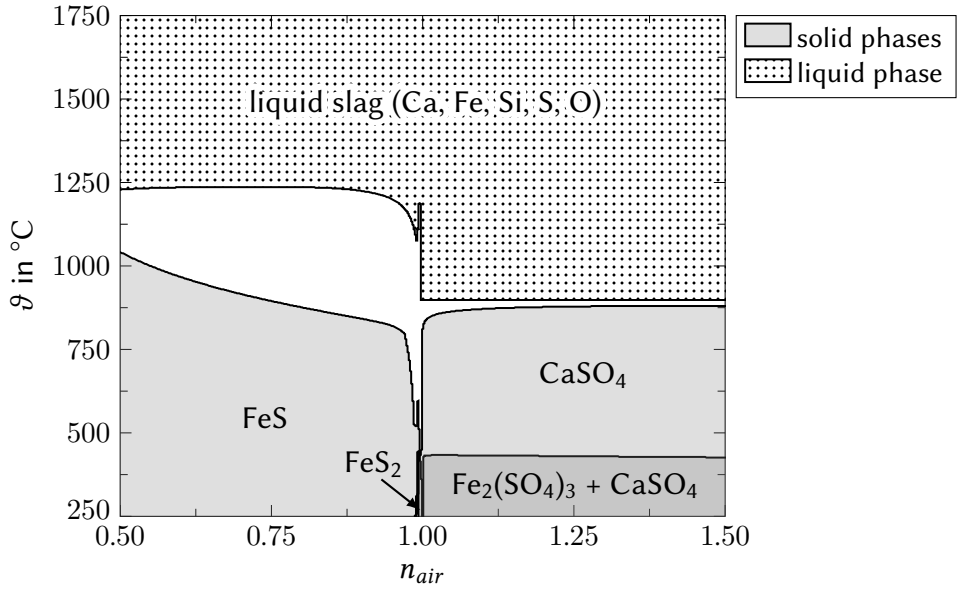

(a) Air

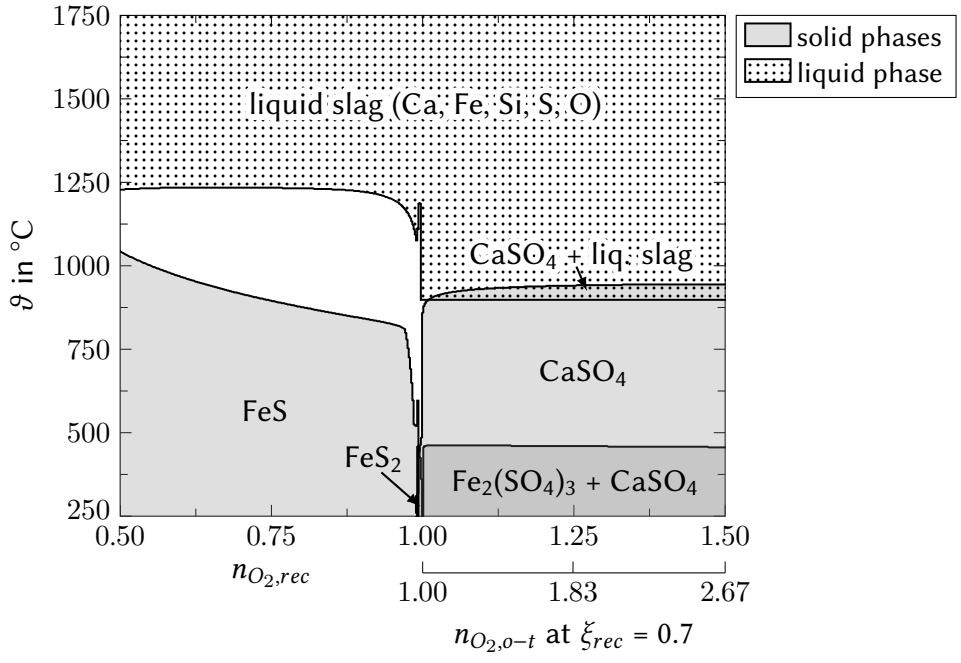

(b) Oxy-fuel

Figure 4.4: Thermodynamically stable solid and liquid phases containing sulfur in a system with **CaO**, **Fe_2O_3**, and **SiO_2** in atmospheres of L3 lignite air and oxy-fuel combustion (solid phases plotted with opacity, i.e. darker gray areas indicate coexisting solid phases; gaseous phases are not shown; white areas indicate that no sulfur is present in solid and liquid phases, i.e. it is in gas phase; for other stable solid phases: see annex, p. 169).

were carried out.

Phase diagrams for air and oxy-fuel combustion for two different ash systems relevant to the L3 lignite were prepared. The ash system compositions were selected on basis of typical particles detected in boiler deposits and fly ashes from the oxy-fuel pilot scale experiments (see also

section 4.2.1.3 and annex A.3). The combusted lignite's ash contains more than $85 \cdot 10^{-2}\ \frac{kg}{kg}$ of CaO, Fe_2O_3, SiO_2, and SO_3. Consequently, the elements calcium, iron, silicon, and sulfur were also found to play a determining role in the sampled ashes and deposits. Particles found in samples from Vattenfall's oxy-fuel pilot plant were categorized into main particle classes based on their composition[50]. The most abundant particles in deposits and fly ashes are spherical iron and calcium rich particles with a sulfur rich shell (see also figure 4.17). These particles contain a core with CaO and Fe_2O_3 in a ratio that is very similar to the ratio in the original fuel (see [42] for more details). In addition to those particles, also a particle category containing SiO_2 in addition to CaO and Fe_2O_3 was observed in greater abundance. For these particles, the ratio of CaO, Fe_2O_3, and SiO_2 was also similar to the ratio in the fuel. The CaO, Fe_2O_3, and SiO_2 rich particles contained much less sulfur than the CaO and Fe_2O_3 rich ones[51]. Due to the observation of these two dominating ash particle classes that are interacting with sulfur during combustion, systems with such compositions were further assessed in two-dimensional thermodynamic phase mapping. Phase mapping simulations were carried out with the following input: Elemental analysis of the fuel L3, ash that contains CaO and Fe_2O_3 ($20.5 \cdot 10^{-2}\ \frac{kg}{kg}$ and $20.3 \cdot 10^{-2}\ \frac{kg}{kg}$, daf) and ash containing CaO, Fe_2O_3 and SiO_2 ($20.5 \cdot 10^{-2}\ \frac{kg}{kg}$, $20.3 \cdot 10^{-2}\ \frac{kg}{kg}$, and $29.7 \cdot 10^{-2}\ \frac{kg}{kg}$, daf) in the same amounts as lignite L3, and a variable amount of oxygen/air (i.e. variation of stoichiometric ratio of combustion) as well as a temperature variation.
Figure 4.3 shows the stable sulfur containing, liquid and solid phases for an ash system with CaO and Fe_2O_3, while figure 4.4 was prepared for an ash system containing SiO_2 in addition to CaO and Fe_2O_3. Stable ash components that do not contain any sulfur are omitted in the phase diagrams presented here for readability reasons. The respective diagrams for such phases can be found in annex A.1. Stable, gaseous species were not further assessed in the thermodynamic equilibrium study and hence, are not presented. The phase diagrams for the two combustion modes are plotted versus the stoichiometric air (n_{air}) and oxy-fuel recycle O_2 ratios ($n_{O_2,rec}$), respectively. Since the recycle O_2 ratio for oxy-fuel firing does not properly represent the oxygen availability in the furnace of an oxy-fuel recycle system that also depends on the recirculation of oxygen together with part of the flue gas, an additional secondary abscissa showing the once-through O_2 ratio $n_{O_2,o-t}$ in a system with a flue gas recirculation ratio ξ_{rec} of 0.7 is presented (see p. 116 for more details on $n_{O_2,rec}$ and $n_{O_2,o-t}$). The calculation of once-through O_2 ratios is not meaningful for systems with an oxygen deficiency, since in practical oxy-fuel systems unburned solids are not recirculated in the same way as unburned oxygen is. Hence, this axis is not plotted for sub-stoichiometric conditions (i.e. $n < 1$).

[50] This was done through SEM-EDX analyses of individual particles in fly ash and deposits sampled during oxy-fuel operation from levels 4 and 8 of the furnace of the oxy-fuel pilot plant. More details on those analyses can be found in annex A.3.

[51] A third important particle class that is not further considered here consisted mainly of SiO_2. These particles seem to originate from sand in the lignite and pass through the furnace without interacting with other ash components and sulfur (see also p. 105 and p. 111).

When comparing the air and oxy-fuel phase diagrams for the two selected ash systems, one notes that the change in combustion conditions does not lead to a fundamental change in the stability of sulfur containing solid species and liquid slag. No new species are stable and no components disappear. Also the increased CO_2 partial pressures do not lead to considerable changes in the stability of carbonates, particularly in oxidizing atmospheres, in which SO_x reacts with available CaO to form sulfates instead of carbonates (see figures A.1 and A.2 in the annex). The most dominant change between air and oxy-fuel fired conditions is that the solid sulfates $CaSO_4$ and $Fe_2(SO_4)_3$ as well as solid FeS are stable up to higher temperatures in oxy-fuel combustion. Similar to the previous discussion on $CaSO_4$ stability (i.e. figure 4.2), the increased stability of these sulfur containing species can be associated to the increased sulfur activity in the simulated oxy-fuel atmospheres, where it is not diluted by airborne nitrogen.
The comparison between the systems with CaO and Fe_2O_3 and with CaO, Fe_2O_3, and SiO_2 shows that the addition of SiO_2 has a strong impact on a number of sulfur containing species in air, just as in oxy-fuel combustion conditions. Obviously, liquid and solid Ca-Si species are more stable at high temperatures and in sub-stoichiometric combustion environments than Ca-S species. Hence, under these conditions, calcium in the system is consumed by reactions with silicon and CaS completely disappears from the phase diagram, while the stability of $CaSO_4$ is shifted to lower temperatures. The stability of $Fe_2(SO_4)_3$ is not affected by the SiO_2 addition. Since the solid-solid reaction of Ca and Si is limited by the contact of these species, in practical combustion systems the formation of Ca-Si compounds likely does not proceed to the extent predicted by equilibrium simulations.
To allow for a better comparison of the stability of sulfates in air and oxy-fuel combustion environments, the phase boundaries for the sulfates $CaSO_4$ and $Fe_2(SO_4)_3$ in the two simulated ash systems (i.e. CaO and Fe_2O_3 and CaO, Fe_2O_3, and SiO_2) were extracted from data of figures 4.3 and 4.4 and plotted in figure 4.5. It should be highlighted that in practice, for the considered ash systems $CaSO_4$ is the dominating sulfate species. $Fe_2(SO_4)_3$ is plotted here for the sake of completeness. In addition to the phase boundaries obtained when simulating stable compounds for a system firing the L3 lignite ($\gamma_S = 0.81 \cdot 10^{-2}\ \frac{\mathrm{kg}}{\mathrm{kg}}$, daf), also the phase boundaries for a hypothetic lignite with a higher sulfur content γ_S of $3 \cdot 10^{-2}\ \frac{\mathrm{kg}}{\mathrm{kg}}$, daf (with accordingly balanced O content) and otherwise same composition is shown. The marked points in figure 4.5 exemplary illustrate conditions with the same excess oxygen concentration $y_{O_2,dry}$ of $4 \cdot 10^{-2}\ \frac{\mathrm{m}^3}{\mathrm{m}^3}$ for air and oxy-fuel operation. As can be seen from table 4.1, for these combustion conditions the $CaSO_4$ phase boundary temperature in oxy-fuel firing is 57 to 77 °C above the one in air firing, while for $Fe_2(SO_4)_3$ this range is between 32 and 61 °C. Similar results with somewhat lower differences in respect to the temperature regions for $CaSO_4$ stability between air and oxy-fuel combustion were obtained by Schnurrer et al. [19], who assessed a fuel with a different composition at an excess oxygen ratio $n_{O_2,rec}$ of 1.2.
For both ash systems, an increase in the fuel sulfur content also increases the difference of the

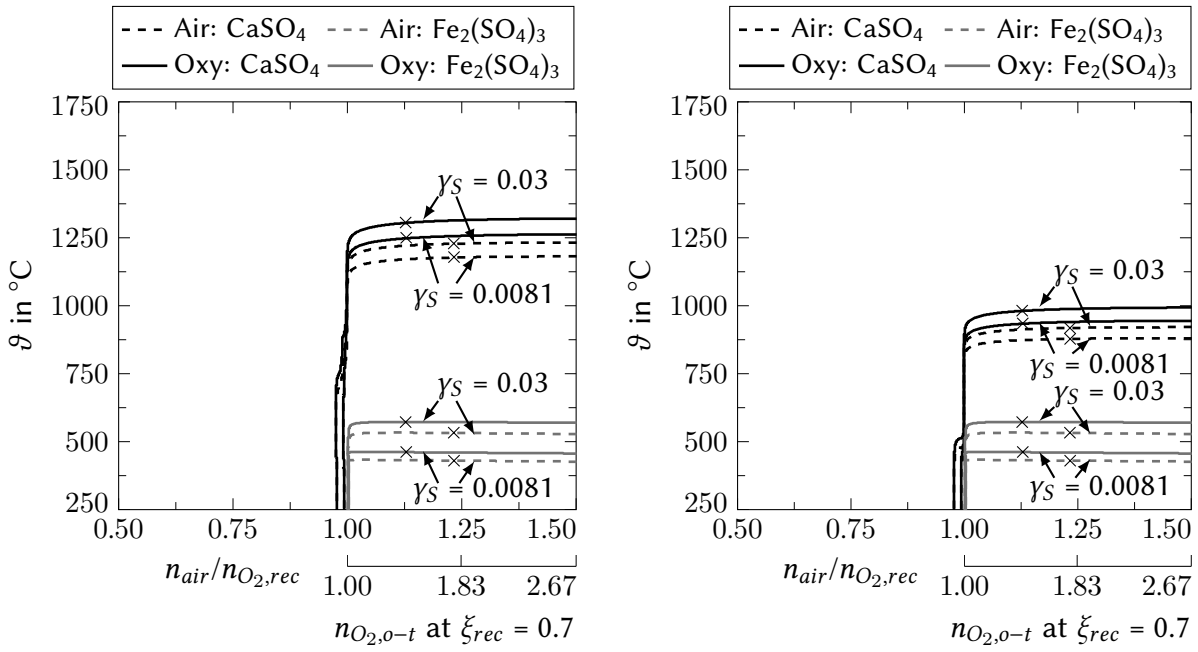

(a) CaO and **Fe_2O_3** **(b) CaO**, **Fe_2O_3**, and **SiO_2**

Figure 4.5: Phase boundaries of thermodynamically stable sulfates ($CaSO_4$ and $Fe_2(SO_4)_3$) in systems containing (a) CaO and Fe_2O_3 and (b) CaO, Fe_2O_3, and SiO_2. The simulated atmospheres consider air and oxy-fuel combustion of L3 lignite. The marked points represent combustion stoichiometries with the same outlet O_2 concentrations $y_{O_2,dry}$ of $4 \cdot 10^{-2}\ \frac{m^3}{m^3}$ for air and oxy-fuel conditions. In addition to simulations with this fuel's true sulfur content ($0.81 \cdot 10^{-2}\ \frac{kg}{kg}$, daf), combustion of a similar lignite with an increased sulfur content ($3 \cdot 10^{-2}\ \frac{kg}{kg}$, daf and appropriately adapted γ_O content) was examined.

maximum sulfate existence temperatures $\Delta\vartheta_{i,exist,air/oxy}$. This effect is more pronounced for $Fe_2(SO_4)_3$ than for $CaSO_4$. One notable peculiarity in figure 4.5 is that the maximum $CaSO_4$ existence temperatures for the low sulfur lignite ($0.81 \cdot 10^{-2}\ \frac{kg}{kg}$, daf) under oxy-fuel firing is in a similar range than for air firing of the high sulfur lignite ($3 \cdot 10^{-2}\ \frac{kg}{kg}$, daf). Since fouling issues induced by $CaSO_4$ formation can be handled in existing boilers firing similar high sulfur fuels,

Table 4.1: Differences of maximum sulfate existence temperatures $\Delta\vartheta_{i,exist,air/oxy}$ ($= \vartheta_{i,exist,oxy} - \vartheta_{i,exist,air}$) at the same $y_{O_2,dry}$ of $4 \cdot 10^{-2}\ \frac{m^3}{m^3}$ in systems containing CaO and Fe_2O_3 and CaO, Fe_2O_3, and SiO_2 for air and oxy-fuel conditions (temperatures extracted from figure 4.5 data).

		CaO/Fe_2O_3		$CaO/Fe_2O_3/SiO_2$	
		$\gamma_{S,daf}$ in $10^{-2}\ \frac{kg}{kg}$			
species	unit	0.81	3	0.81	3
$CaSO_4$	°C	71	77	57	64
$Fe_2(SO_4)_3$		32	61	32	61

potentially also oxy-fuel fired systems using low sulfur fuels that show a similar $CaSO_4$ stability may be operable using standard equipment (e.g. soot blowers). For higher sulfur fuels, without recycle gas cleaning, the $CaSO_4$ stability is considerably higher in oxy-fuel systems, than in conventional air fired systems, and hence, one must expect that undesired $CaSO_4$ deposits may form at higher temperature regions in a boiler were they are currently not observed. A positive aspect of the increased $CaSO_4$ stability that was discussed also by others (e.g. [11]) is that sulfur retention in calcium contained in fuel ash or in calcium based sorbents may be enhanced in oxy-fuel systems. However, also undesired $CaSO_4$ boiler deposits may be more sintered and calcium rich fuel ash will have an increased sulfur content with possible implications on ash utilization.

4.1.3 Impact of recycle combustion on SO_x capture

Wet SO_2 (or more generally SO_x) partial pressures that are relevant for diffusion of SO_2 to molecules in ashes or sorbents that can react with this component (e.g. calcium species) and for the desulfurization reactions, are significantly increased in oxy-fuel combustion by a factor of 2.9-3.5[52] (see p. 88). This has a positive impact on the efficiency of diffusion and desulfurization reactions. In addition, as explained in section 4.1.2 and also by others [11], the increased SO_2 level enhances the stability of sulfates, which allows for their formation at higher temperatures. This in turn has a positive impact on the available volume and hence, reaction time for the formation of such sulfates within a furnace which also has a positive impact on the efficiency of diffusion and desulfurization reactions. However, in practical oxy-fuel combustion systems that require a recirculation of flue gases, the correlation is more complex. In the following, the issue is explained on basis of a sulfur balance of the PF oxy-fuel combustion process with flue gas recirculation (see figure 4.6). Similar correlations were introduced in papers by Liu and various coworkers [11, 104, 105, 190–192], even though, their presentation was less illustrative. Since the correlations in this section are only based on material balances, they disregard impacts on the desulfurization caused by changing process conditions that occur when varying the

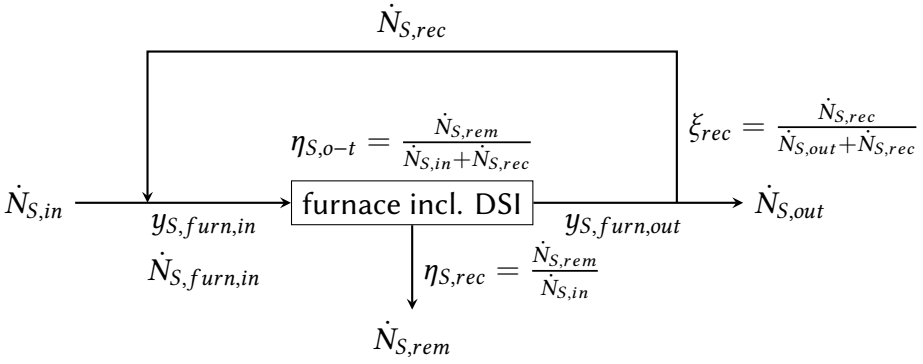

Figure 4.6: Schematic of the molar sulfur balance in oxy-fuel recycle combustion.

[52] For Cl species, such as HCl, the correlation applies analog.

recirculation ratio (e.g. changing residence times, temperatures, etc.). Sulfur is selected in this discussion exemplary, referring to the sum of all sulfur species in the system. In practice, this is mainly SO_2 and sulfates bound in ash and/or sorbents. Assuming no transformation of a recirculated species to other gaseous compounds, the correlation applies also to individual gas species (e.g. SO_2 and HCl). The correlations introduced in this section apply generally to sulfur retention in the ash as well as to sulfur capture by dedicated desulfurization systems (e.g. DSI).

$$\eta_{S,rec} = \frac{\dot{N}_{S,rem}}{\dot{N}_{S,in}} = \frac{\dot{N}_{S,rem}}{\dot{N}_{S,rem} + \dot{N}_{S,out}} \tag{4.5}$$

$$\eta_{S,o-t} = \frac{\dot{N}_{S,rem}}{\dot{N}_{S,in} + \dot{N}_{S,rec}} \tag{4.6}$$

$$\xi_{rec} = \frac{\dot{N}_{S,rec}}{\dot{N}_{S,out} + \dot{N}_{S,rec}} = \frac{\dot{N}_{FG,rec}}{\dot{N}_{FG,out} + \dot{N}_{FG,rec}} = \frac{\dot{N}_{FG,rec}}{\dot{N}_{FG,furn}} \tag{4.7}$$

$$\eta_{S,rec} = \frac{(\dot{N}_{S,in} + \dot{N}_{S,rec})\eta_{S,o-t}}{\dot{N}_{S,in}} \tag{4.8}$$

$$\dot{N}_{S,rec} = (\dot{N}_{S,in} + \dot{N}_{S,rec})(1 - \eta_{S,o-t})\xi_{rec} \tag{4.9}$$

$$\dot{N}_{S,rec} = \frac{\dot{N}_{S,in}(1 - \eta_{S,o-t})\xi_{rec}}{1 - (1 - \eta_{S,o-t})\xi_{rec}} \tag{4.10}$$

$$\eta_{S,rec} = \frac{\eta_{S,o-t}}{1 - (1 - \eta_{S,o-t})\xi_{rec}} \tag{4.11}$$

$$\eta_{S,o-t} = \frac{\eta_{S,rec}(1 - \xi_{rec})}{1 - \xi_{rec}\eta_{S,rec}} \tag{4.12}$$

As for systems without a flue gas recycle (i.e. conventional air firing), the recycle desulfurization efficiency $\eta_{S,rec}$ can be expressed as the quotient between sulfur removed from the flue gas $\dot{N}_{S,rem}$ and the amount of sulfur fed to the system $\dot{N}_{S,in}$ (see equation 4.5). When part of the flue gas and the contained sulfur species are recirculated with a recirculation ratio ξ_{rec} (see equation 4.7), this recycle adds additional sulfur $\dot{N}_{S,rec}$ to the sulfur entering the furnace ($\dot{N}_{S,furn,in} = \dot{N}_{S,in} + \dot{N}_{S,rec}$) and hence, also a once-through desulfurization efficiency $\eta_{S,o-t}$ can be defined (equation 4.6). The once-through and recycle desulfurization efficiencies can also be related to each other by solving equation 4.6 for $\dot{N}_{S,rem}$ and inserting this to equation 4.5, which gives equation 4.8. On basis of a sulfur balance of the recycle loop, the flux of recirculated sulfur $\dot{N}_{S,rec}$ can be expressed, according to equation 4.9. This relation can be solved for $\dot{N}_{S,rec}$ giving equation 4.10. Substitution of $\dot{N}_{S,rec}$ in equation 4.8 yields equation 4.11, which correlates recycle and once-through desulfurization efficiencies and the recirculation ratio independently of other variables. Equation 4.12 gives the same correlation solved for $\eta_{S,o-t}$.

Neglecting the change of the molar flux of flue gas $\dot{N}_{FG,furn}$ through the furnace by desulfurization, this molar flux can be expressed, according to equation 4.13. The molar sulfur fraction at the furnace inlet $y_{S,furn,in}$ can be calculated, according to equation 4.14. The different

reformulations can be obtained with help of equations 4.10, 4.13, and 4.12. The molar sulfur fraction at the process outlet $y_{S,out}$ ($= y_{S,furn,out}$) can be calculated, according to equation 4.15 that can be reformulated to the different presented forms with help of equation 4.5. It is worth noting that the first factor $\dot{N}_{S,in}/\dot{N}_{FG,out}$ in equations 4.14 and 4.15 is equivalent to the molar fraction of sulfur in the flue gas of the combustion process without any gas cleaning.

$$\dot{N}_{FG,furn} = \frac{\dot{N}_{FG,out}}{1-\xi_{rec}} \tag{4.13}$$

$$y_{S,furn,in} = \frac{\dot{N}_{S,in}+\dot{N}_{S,rec}}{\dot{N}_{FG,furn}} = \frac{\dot{N}_{S,in}}{\dot{N}_{FG,out}}\frac{1-\xi_{rec}}{1-(1-\eta_{S,o-t})\xi_{rec}} = \frac{\dot{N}_{S,in}}{\dot{N}_{FG,out}}(1-\xi_{rec}\eta_{S,rec}) \tag{4.14}$$

$$y_{S,out} = \frac{\dot{N}_{S,out}}{\dot{N}_{FG,out}} = \frac{\dot{N}_{S,in}-\dot{N}_{S,out}}{\dot{N}_{FG,out}} = \frac{\dot{N}_{S,in}}{\dot{N}_{FG,out}}(1-\eta_{S,rec}) \tag{4.15}$$

Based on equation 4.11, in figure 4.7, $\eta_{S,rec}$ is plotted versus ξ_{rec} (a) and $\eta_{S,o-t}$ (b) for selected values of $\eta_{S,o-t}$ and ξ_{rec}, respectively. For the purpose of generalization, in figure 4.8a, which is a plot of equations 4.14 and 4.15 at a fixed recycle desulfurization efficiency ($\eta_{S,rec} = 80$ %), normalized molar fractions $y_{S,furn,in,*}$ and $y_{S,furn,out,*}$ are presented (i.e. the factor $\dot{N}_{S,out}/\dot{N}_{FG,out}$ equals 1). Figure 4.8b is a plot of equation 4.12 and shows the dependency of $\eta_{S,o-t}$ on ξ_{rec} at a fixed value of $\eta_{S,rec}$ of 80 %.

On basis of the equations introduced above and figures 4.7 and 4.8, the correlation of the desulfurization efficiencies $\eta_{S,rec}$ and $\eta_{S,o-t}$ and ξ_{rec} in a recycle system can be assessed. Obviously, without recirculation, $\eta_{S,rec}$ and $\eta_{S,o-t}$ are equal, while also at recirculation ratios close to 100 % both desulfurization efficiencies converge to the same value. Between those extremes

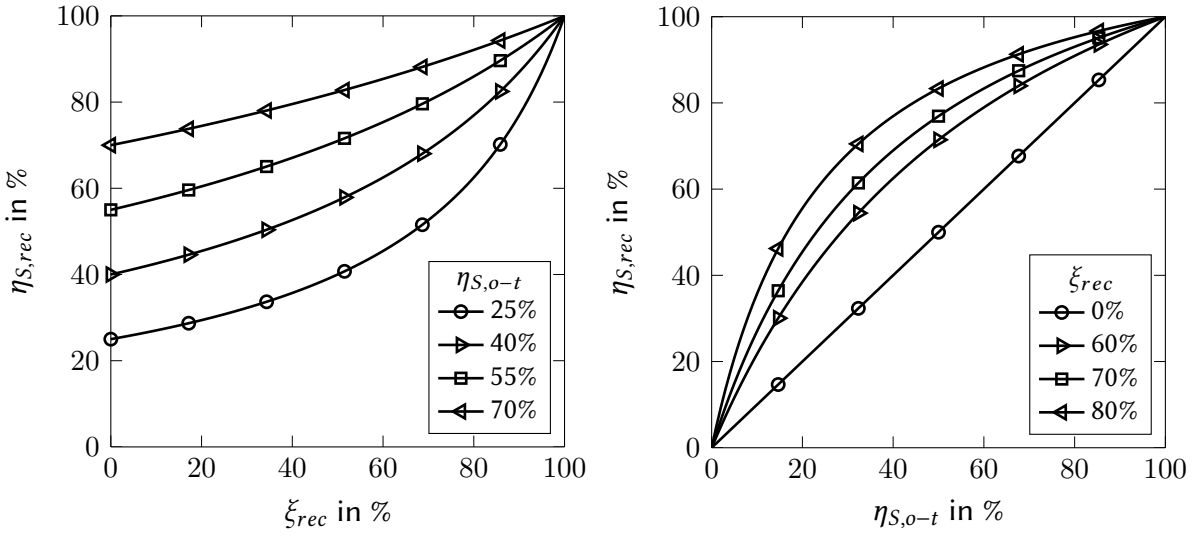

(a) $\eta_{S,rec}$ versus ξ_{rec} **(b)** $\eta_{S,rec}$ versus $\eta_{S,o-t}$

Figure 4.7: Dependency of the recycle desulfurization efficiency $\eta_{S,rec}$ on (a) the recirculation ratio ξ_{rec} and (b) the once-through desulfurization efficiency $\eta_{S,o-t}$ at discrete values of $\eta_{S,o-t}$ and ξ_{rec}, respectively (plots of equation 4.11).

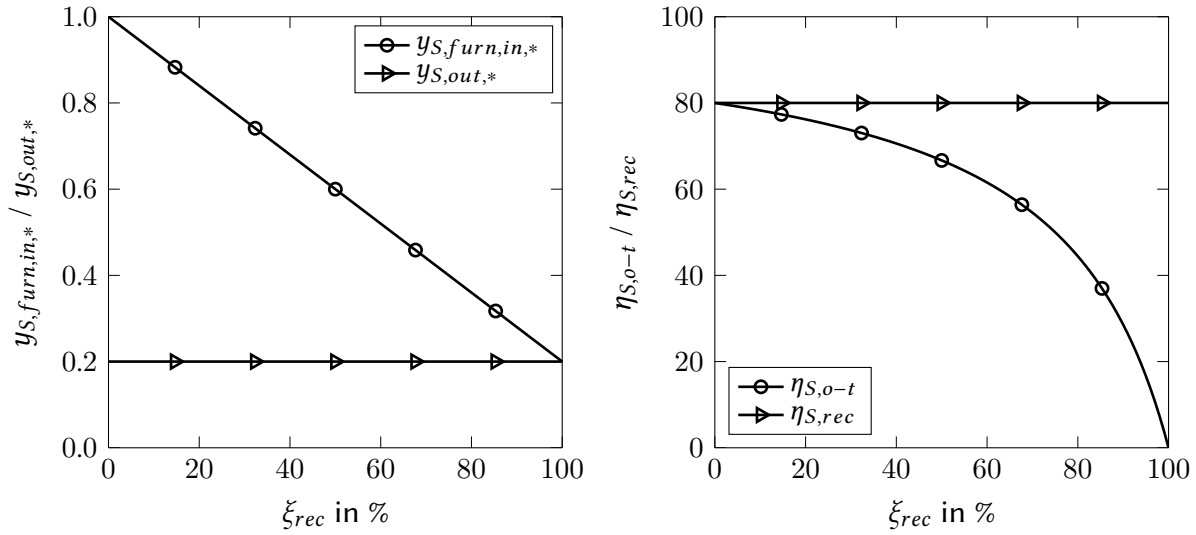

(a) $y_{S,furn,in,*}$ and $y_{S,furn,out,*}$ versus ξ_{rec} **(b)** $\eta_{S,rec}$ and $\eta_{S,o-t}$ versus ξ_{rec}

Figure 4.8: Normalized molar sulfur fractions at the recycle combustion process' in- and outlet $y_{S,furn,in,*}$ and $y_{S,furn,out,*}$ and recycle and once-through desulfurization efficiencies $\eta_{S,rec}$ and $\eta_{S,o-t}$ versus the recirculation ratio ξ_{rec} at a fixed recycle desulfurization efficiency $\eta_{S,rec}$ of 80 % (plots of equations 4.14, 4.15, and 4.12).

the interpretation of the correlation is more complex. As can be seen in figure 4.7, at high recirculation ratios, lower once-through desulfurization efficiencies $\eta_{S,o-t}$ are sufficient to reach high recycle desulfurization efficiencies $\eta_{S,rec}$, while at lower recirculation ratios $\eta_{S,rec}$ is much stronger impacted by $\eta_{S,o-t}$. This effect can also be observed in figure 4.8. At a fixed recycle desulfurization efficiency $\eta_{S,rec}$, an increase of the recirculation ratio ξ_{rec} is equivalent to an increasing dilution of the flue gases at the furnace inlet by desulfurized flue gas from the furnace outlet. This reduces the sulfur level at the furnace inlet (i.e. $y_{S,furn,in,*}$) and affects the once-through desulfurization efficiency $\eta_{S,o-t}$ negatively. However, this is compensated by a larger flux of sulfur compounds to the furnace (i.e. $\dot{N}_{S,furn,in}$). More illustrative, sulfur compounds that are not captured when passing the furnace are returned to its inlet at a ratio ξ_{rec} and hence, are exposed again to an environment that allows for their capture. In this system, ξ_{rec} and $\eta_{S,o-t}$ compensate each other, as can also be seen in equations 4.11 and 4.12.
Based on figure 4.7b, another feature of the recycle combustion system in respect to desulfurization can be noted. Flue gas recirculation is most beneficial for desulfurization technologies that have a relatively low once-through desulfurization efficiency (e.g. DSI). This is illustrated by the large difference between $\eta_{S,rec}$ and $\eta_{S,o-t}$ at lower desulfurization efficiencies (e.g. at $\xi_{rec} = 70$ %: $\eta_{S,rec} = 45$ % at $\eta_{S,o-t} = 20$ %). For technologies that are already very efficient in a once-through configuration (e.g. wet or semi-dry desulfurization systems), the benefit of flue gas recirculation is less pronounced (e.g. at $\xi_{rec} = 70$ %: $\eta_{S,rec} = 97$ % at $\eta_{S,o-t} = 90$ %).
The discussion in this section is purely based on material balances for desulfurization in a recycle loop assuming that no restrictions of the combustion process and the desulfurization reactions exist, which is not true in practice. For example, the volume of a boiler is a fixed

parameter and a change in ξ_{rec} is corresponding to an altered volumetric flow of flue gas through the furnace and hence, a different flue gas residence time in that unit (with higher recirculation ratios giving lower residence times). In addition, variations in ξ_{rec} also impact the heat transfer in the boiler and hence, the flue gas temperature profile in the system. Those aspects can have a considerable impact on the once-through desulfurization efficiency $\eta_{S,o-t}$ that is reached within the recycle loop. Without a complete redesign of pulverized power boilers, in practice, due to temperature and heat transfer restrictions, ξ_{rec} is limited to a range between about 60 % and 80 %. As can be seen in figure 4.7a, in that range the impact of ξ_{rec} on the desulfurization efficiency is considerable and even at moderate once-through desulfurization efficiencies $\eta_{S,o-t}$, relatively high recycle desulfurization efficiencies $\eta_{S,rec}$ can be accomplished.
The calculation of $\eta_{S,o-t}$ (i.e. once-through $DeSO_x$ efficiency), on basis of actual furnace inlet SO_2 levels in oxy-fuel recycle DSI experiments and, calculated on basis of those levels, the once-through molar Ca/S ratios ($\alpha_{Ca/S,o-t}$) allow to compare the desulfurization performance in air fired experiments to those of corresponding oxy-fuel tests, since the impact of flue gas recirculation is eliminated. An evaluation of experimental data in that way was conducted and can be found in section 4.2.2.3.

4.2 Experiments studying the behavior of sulfur oxides

4.2.1 Sulfur oxides in ashes and deposits

4.2.1.1 Impact of increased SO_2 levels on sulfates in deposits

In section 4.1.2, the impact of increased SO_2 concentrations on the stability of sulfates (especially $CaSO_4$) was described. To validate these theoretical considerations, a set of experiments at the BTS-VR combustion test rig was designed. In these tests, the impact of increased SO_2 partial pressures on the occurrence of sulfates in deposits sampled from the furnace fired with L2 lignite was determined. The combustion was operated with a $72 \cdot 10^{-2}\ \frac{m^3}{m^3}$, dry, CO_2 and $28 \cdot 10^{-2}\ \frac{m^3}{m^3}$, dry, O_2 oxidizer and an excess O_2 concentration of approx. $2.7 \cdot 10^{-2}\ \frac{m^3}{m^3}$, dry. In one experiment additional SO_2 was doped to the oxidant gas mix while in the other it was not. This resulted in SO_2 concentrations of $750 \cdot 10^{-6}\ \frac{m^3}{m^3}$, wet ($850 \cdot 10^{-6}\ \frac{m^3}{m^3}$, dry), in the undoped and $5530 \cdot 10^{-6}\ \frac{m^3}{m^3}$, wet ($6250 \cdot 10^{-6}\ m^3/m^3$, dry), in the doped test[53]. A factor $\xi_{oxy/air,wet}$ of approx. 7.4 between these concentration levels that is considerably larger than the one between air and complementary "practical" oxy-fuel conditions (see p. 88: $\xi_{oxy/air,wet} \approx 2.9 - 3.5$), was selected to ensure significant experimental results. In these two flue gas atmospheres, deposits were sampled at two different temperatures. The sampling temperatures of 1200 °C (1.5 m from burner) and 1100 °C (2.5 m from burner) were selected closely above and below the $CaSO_4$ decomposition temperature at the two different SO_2 concentrations. In figure 4.9, all four

[53] Measured inside the furnace, 1.5 m from the burner, at 1200 °C.

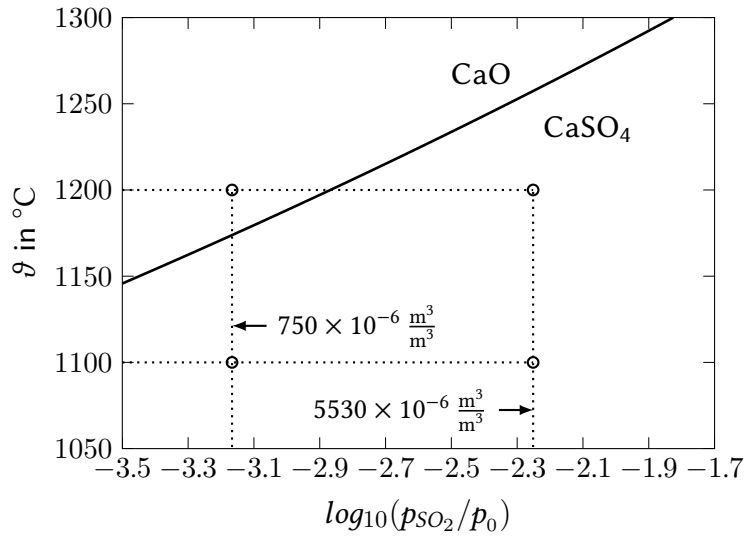

Figure 4.9: Deposit sampling conditions (ϑ_{Probe} = 1100 °C, 1200 °C; $y_{SO_2,wet} = 750 \cdot 10^{-6}\ \frac{m^3}{m^3}$, $5530 \cdot 10^{-6}\ \frac{m^3}{m^3}$) plotted in a CaO/$CaSO_4$ phase diagram for a flue gas matrix as in the performed experiments (i.e. $p_{tot} = 1.013\,25 \cdot 10^5$ Pa, $y_{CO_2,wet} = 85.8 \cdot 10^{-2}\ \frac{m^3}{m^3}$, $y_{H_2O,wet} = 11.5 \cdot 10^{-2}\ \frac{m^3}{m^3}$, $y_{O_2,wet} = 2.7 \cdot 10^{-2}\ \frac{m^3}{m^3}$).

deposit sampling conditions are plotted together with the CaO-$CaSO_4$ phase boundary that was calculated for a flue gas matrix similar to the one in the performed experiments. The deposit sampling was performed using ceramic deposition probes that can be assumed to reach quickly the bulk flue gas temperature when being exposed to the furnace atmosphere. The flue gas temperatures were set up by adjusting the control temperatures[54] of the heating zones upstream and at the sampling locations. In previous tests with help of a suction pyrometer it was determined that the heating zone control and flue gas temperatures (outside the flame zone) are similar. Hence, in this study, the deposit sampling temperatures are assumed to be equivalent to the respective furnace control temperatures.

Figure 4.10 shows BSE images of and the distribution of sulfur in (by SEM-WDX)[55] the deposit samples obtained from these experiments. The BSE images at each sampling temperature show a very similar morphology of the deposits, irrespective of the SO_2 level. At 1200 °C (figures 4.10 b and d) deformed and fused deposits are obvious, indicating that partially molten ash particles hit the sampling probe. At 1100 °C deformation during impaction and fusion of molten ash particles is not obvious. The 1100 °C samples (figures 4.10 a and c) are dominated by spherical calcium and iron rich ash particles that are surrounded by a sulfur rich shell. Such a deposit character was also observed in samples from 500 kW and 30 MW scale experimental facilities when firing Lusatian lignites (see chapter 4.2.1.3). The SEM-WDX sulfur maps demonstrate clearly that increased SO_2 concentrations stabilize sulfates in the deposits of calcium rich lignite ash under furnace conditions. The sample from the experiment with an SO_2 level of

[54]Each furnace heating zone uses temperatures measured at the furnace wall for temperature control.
[55]More detailed SEM-WDX maps for other elements can be found in annex A.2.

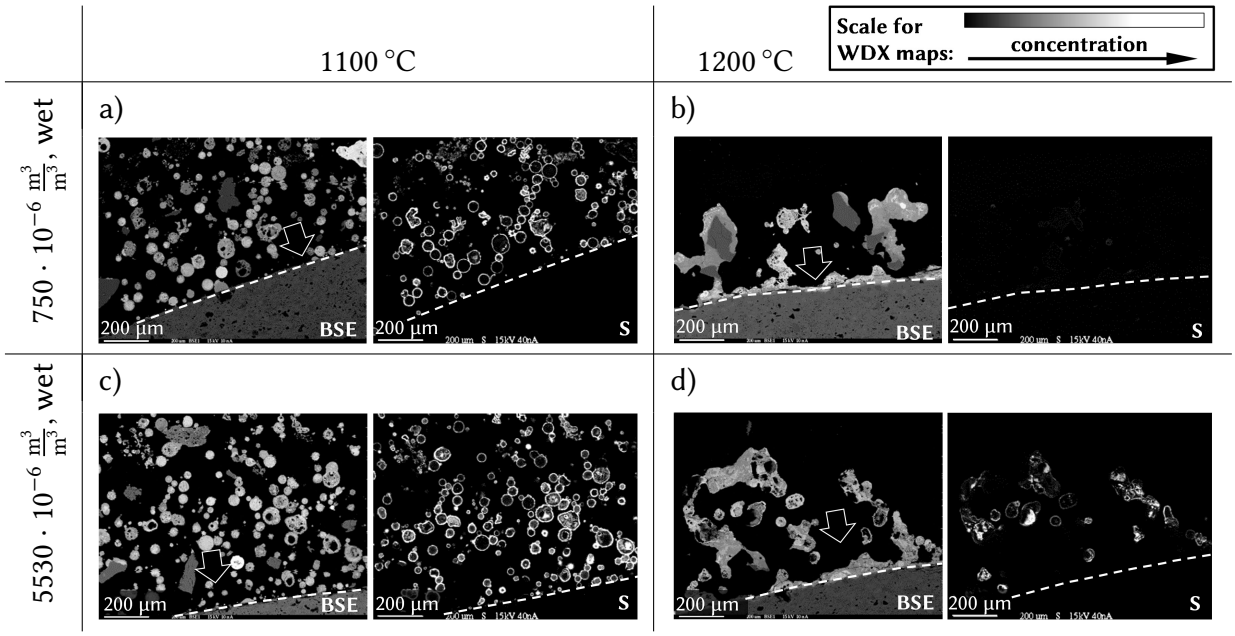

Figure 4.10: BSE images and SEM-WDX sulfur maps of uncooled deposits sampled at 1100 °C (a, c) and 1200 °C (b, d) with a SO_2 concentration of $750 \cdot 10^{-6}$ $\frac{m^3}{m^3}$, wet (a, b), and $5530 \cdot 10^{-6}$ $\frac{m^3}{m^3}$, wet (c, d) (white dashed lines indicate sampling probe surfaces, arrows indicate flue gas flow directions).

$750 \cdot 10^{-6}$ $\frac{m^3}{m^3}$, wet, shows at 1200 °C hardly any sulfur in the deposit, while at $5530 \cdot 10^{-6}$ $\frac{m^3}{m^3}$, wet, the retention of sulfur in the deposited ash is obvious. At a deposit sampling temperature of 1100 °C sulfur capture can be observed in samples for both SO_2 levels. Nonetheless, the sulfur retention is more distinct at the higher SO_2 concentration level.

4.2.1.2 SO_x retention in ash in air and oxy-fuel combustion

Analyses of measured SO_2 emissions: A number of comparative experiments studying sulfur retention in the ash in corresponding air and oxy-fuel recycle experiments was carried out at the 500 kW combustion test facility KSVA. Two lignites (L1 and L2) and one hard coal (C4) were used in these tests. In addition, results for oxy-fuel combustion of lignite L3 (similar to L2) at Vattenfall's 30 MW oxy-fuel pilot plant are available. Table 4.2 lists gas concentrations measured in air and oxy-fuel combustion and values in respect to sulfur retention calculated on that basis. The exit O_2 levels in oxy-fuel experiments at KSVA were 0.6 to $1.4 \cdot 10^{-2}$ $\frac{m^3}{m^3}$, dry, higher than in air fired operation, which is necessary to maintain the combustion stoichiometries in similar ranges. In oxy-fuel firing, CO_2 levels of 88 to $89 \cdot 10^{-2}$ $\frac{m^3}{m^3}$, dry, at KSVA and of $82.4 \cdot 10^{-2}$ $\frac{m^3}{m^3}$, dry, at OxyPP indicate that air ingress to the facilities was low. For both combustion regimes and all four fuels, relatively low average CO levels were measured (air: < 8 to $74 \cdot 10^{-6}$ $\frac{m^3}{m^3}$, dry, oxy-fuel: < 80 to $218 \cdot 10^{-6}$ $\frac{m^3}{m^3}$, dry). However, in oxy-fuel experiments with lignite L1 at KSVA and in the experiments with lignite L3 at the pilot plant "Schwarze Pumpe", CO peaks exceeding the measurement range of the analyzers

Table 4.2: Measured flue gas composition at the furnace exit of KSVA for L1, L2, and C4 air and oxy-fuel combustion (y_{H_2O} for L2 calculated based on mass balances) and calculated sulfur retention in ash. In addition, the gas compositions after ESP during oxy-fuel combustion of lignite L3 at the pilot plant "Schwarze Pumpe" are given.

		$\bar{y}_{O_2}$	$\bar{y}_{CO_2}$	$\bar{y}_{H_2O}$	$\bar{y}_{CO}$	$\bar{y}_{NO_x}$	$\bar{y}_{SO_2}$	S retention
		$10^{-2}\ \frac{m^3}{m^3}$		$10^{-2}\ \frac{m^3}{m^3}$	$10^{-6}\ \frac{m^3}{m^3}$			
fuel	mode	dry		wet	dry			%
L1	air	3.2	16.3	7.4	26	210	1657	4
	oxy-fuel	4.6	88.8	21.8	218	539	5358	14
L2	air	3.5	15.9	(8.3)	<10	397	346	35
	oxy-fuel	4.9	87.9	(21.9)	32	795	818	47
C4	air	3.7	15.1	7.5	74	620	1801	3
	oxy-fuel	4.3	89.0	15.0	77	1036	5753	8
L3	oxy-fuel	6.9	82.4	28.0	81	345	2085	(20-30)†

† Sulfur retention is an estimation based on available data from the experimental campaign, assumptions in respect to the amount and composition of cleaned primary gas, and a material balance conducted using the process simulation package AspenPlus.

(i.e. $> 5000 \cdot 10^{-6}\ \frac{m^3}{m^3}$, dry) and above $700 \cdot 10^{-6}\ \frac{m^3}{m^3}$, dry, respectively, have been observed. This indicates that certain combustion instabilities occurred that also may have influenced the sulfur retention in the ash.

SO_2 concentrations in oxy-fuel operation were approx. 3.2 (L1), 2.3 (L2), and 3.2 (C4) times higher than during air firing. Based on the measured SO_2 concentrations and theoretical maximum gas concentrations (according to equations 4.1 and 4.2), the sulfur retention efficiency was calculated for experiments conducted at KSVA assuming that the difference between both values corresponds to the sulfur retained in ash and deposits. During oxy-fuel operation, the retention of sulfur was enhanced considerably by 10 (L1) and 12 (L2) percentage points for both, the sulfur rich and the sulfur lean lignite, respectively that have an ash containing considerable quantities of calcium and magnesium. For oxy-fuel combustion of the sulfur rich lignite L1 ($\alpha_{(Ca+Mg)/S}$ = 0.9), 14 % of the sulfur introduced with the fuel could be retained in the ash, while for the sulfur lean lignite L2 ($\alpha_{(Ca+Mg)/S}$ = 2.5) almost half of the sulfur was captured. The sulfur retention in the ash of the sulfur lean lignite L2 in these experiments was somewhat lower than the one observed by Fleig et al. [12] with a similar fuel. Nonetheless, the observed trend in respect to an enhanced sulfur retention in oxy-fuel operation is similar and corresponds also to the observations reported by other researchers [1, 10, 54, 109]. Due to missing data on the cleaned primary gas amount and composition for the experiments at the pilot plant "Schwarze Pumpe", the sulfur retention could only be estimated on basis of assumptions in respect to those parameters. Hence, this value is only indicative. The much

higher SO_2 concentration level measured with lignite L3, compared to the similar lignite L2 (factor 2.55 higher), is partly caused by the sulfur content of lignite L3 that is by a factor of 1.45 higher than that of lignite L2. In addition to that, at KSVA, presumably a considerably higher specific clean CO_2 gas stream $v^*_{CO_2,dos}$ was used as primary gas for fuel injection, compared to the oxy-fuel pilot plant (i.e. 0.54 to 0.99 $\frac{m^3}{kg}$, *STP*, dry, at KSVA versus an estimated 0.3 to 0.4 $\frac{m^3}{kg}$, *STP*, dry, at OxyPP. This corresponds to solid loadings of about 1 to 1.85 $\frac{kg}{m^3}$, *STP*, dry and about 3 $\frac{kg}{m^3}$, *STP*, dry, respectively.). As introduced in section 4.1.1, this impacts the SO_2 concentration and can explain in the range of about 20-35 % of the higher emissions at OxyPP. The remaining difference is to be explained by relatively poor SO_2 retention in the ash in the L3 experiment, compared to the oxy-fuel combustion of lignite L2. This is likely related to the lower sulfur retention potential of L3 lignite ($\alpha_{(Ca+Mg)/S}$ = 1.5), compared to lignite L2 ($\alpha_{(Ca+Mg)/S}$ = 2.5) and to non-ideal sulfur capture at the oxy-fuel pilot plant "Schwarze Pumpe", due to the aforementioned combustion instabilities that may have had a detrimental effect on the desulfurization reactions.
For the high sulfur hard coal C4 containing considerably less earth alkalis than the lignites and having a high sulfur content ($\alpha_{(Ca+Mg)/S}$ = 0.1), the sulfur retention was generally low and only increased by about 5 percentage points between both combustion modes. Differences in the SO_2 levels measured during a large number of conducted combustion experiments (without sorbent injection) suggest that the sulfur level of that fuel is inherently fluctuating in the range of about 5 %. Hence, the differences in air and oxy-fuel operation that can be observed in table 4.2 might not necessarily only be related to a change in the combustion atmosphere and an enhanced sulfur retention in oxy-fuel firing.

Analyses of process ashes: During the comparative air and oxy-fuel experiments at KSVA as well as in oxy-fuel combustion at the "Schwarze Pumpe" pilot plant, process ashes were sampled from air/gas preheater (GH), bottom ash (BA), and different ESP precipitation fields (E1, E2, E3) and analyzed for their main ash-forming elements' contents. Figures 4.11, 4.12, and 4.14 show the compositions of the process ashes[56] obtained at KSVA and molar Ca/S, Mg/S, K_2/S, and Na_2/S ratios α_i, for the two lignites and the C4 hard coal, respectively. When assessing analyses from process ashes of the KSVA facility, one should keep in mind general limitations that are associated with those samples (see p. 56). Due to such limitations, in the following only a qualitative discussion of process ashes from different experiments is included. In addition to the comparison of air and oxy-fuel ashes produced at KSVA, figure 4.13 shows the same data comparatively for process ashes obtained from oxy-fuel combustion of the similar lignite qualities L2 and L3 at the combustion test facility KSVA and at Vattenfall's oxy-fuel pilot plant, respectively. For process ashes from the "Schwarze Pumpe" pilot plant, also only a qualitative assessment can be conducted since no data is available in respect to the ash mass flows exiting

[56]I.e. SO_3, SiO_2, MgO, Fe_2O_3, CaO, Al_2O_3, Rest = K_2O, Na_2O, P_2O_5, TiO_2, SrO_2, BaO, Mn_2O.

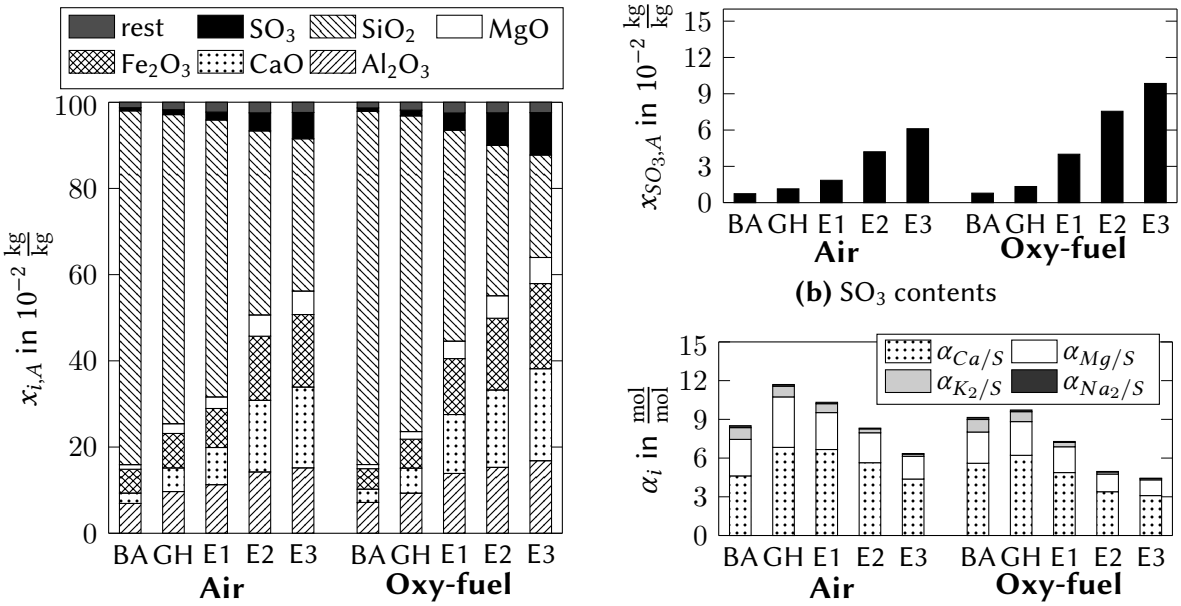

(a) Composition of process ashes

(b) SO_3 contents

(c) Molar Ca, Mg, K_2, and Na_2 to S ratios α_i

Figure 4.11: (a) Composition of process ashes from lignite L1 air and oxy-fuel combustion (BA: bottom ash; GH: air/gas preheater; E1, E2, E3: ESP ashes), (b) SO_3 contents, and (c) Molar Ca/S, Mg/S, K_2/S, and Na_2/S ratios α_i of the ashes.

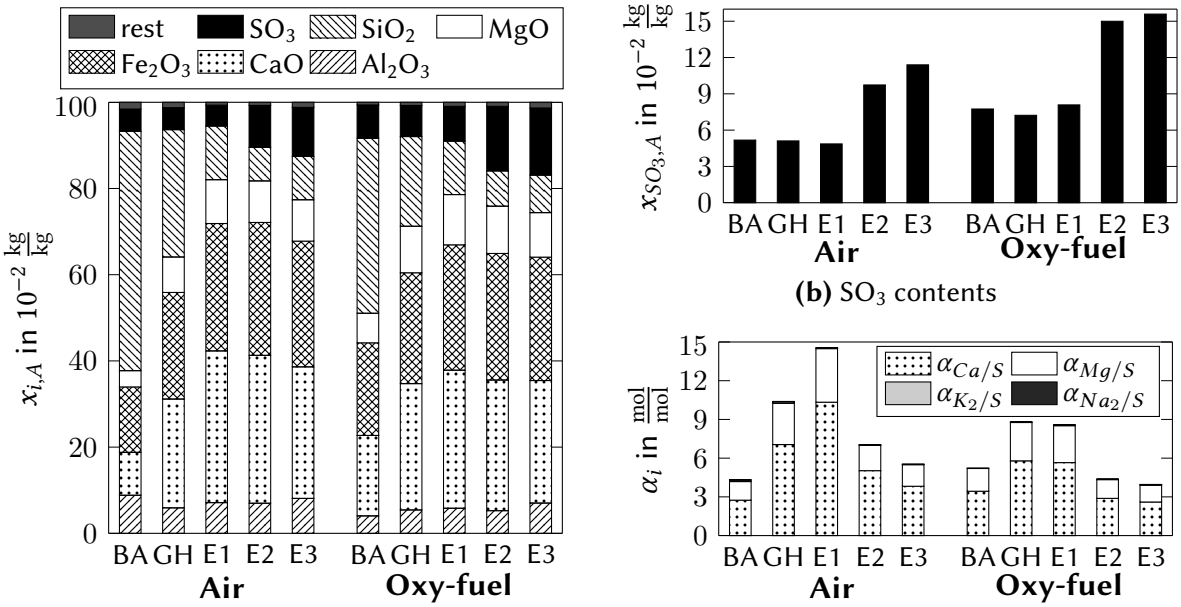

(a) Composition of process ashes

(b) SO_3 contents

(c) Molar Ca, Mg, K_2, and Na_2 to S ratios α_i

Figure 4.12: (a) Composition of process ashes from lignite L2 air and oxy-fuel combustion (BA: bottom ash; GH: air/gas preheater; E1, E2, E3: ESP ashes), (b) SO_3 contents, and (c) Molar Ca/S, Mg/S, K_2/S, and Na_2/S ratios α_i of the ashes.

the process via the different ash drains.

In entrained flow combustors, one commonly can observe a size fractionation of ashes between the different ash drains, with coarser particles being preferentially separated further upstream in the plant (e.g. bottom ash) and finer particles removed to a larger extent in downstream

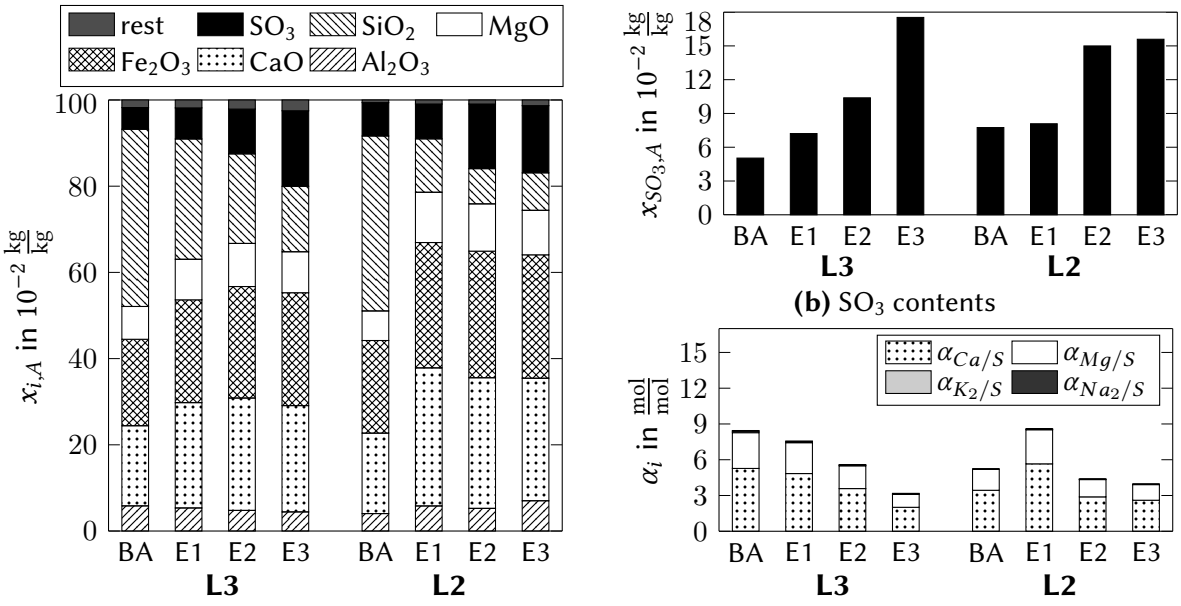

(a) Composition of process ashes **(b)** SO_3 contents **(c)** Molar Ca, Mg, K_2, and Na_2 to S ratios α_i

Figure 4.13: (a) Composition of process ashes from lignites L2 and L3 oxy-fuel combustion (BA: bottom ash, for L3: of 1st draft; GH: air/gas preheater; E1, E2, E3: ESP ashes), (b) SO_3 contents, and (c) Molar Ca/S, Mg/S, K_2/S, and Na_2/S ratios α_i of the ashes.

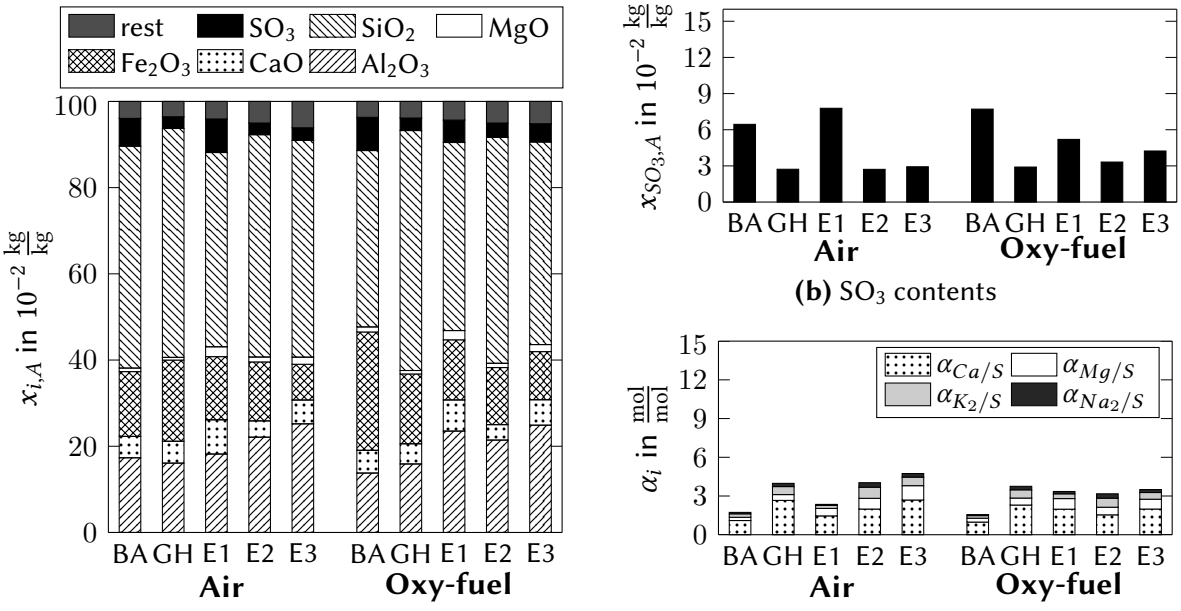

(a) Composition of process ashes **(b)** SO_3 contents **(c)** Molar Ca, Mg, K_2, and Na_2 to S ratios α_i

Figure 4.14: (a) Composition of process ashes from C4 coal air and oxy-fuel combustion (BA: bottom ash; GH: air/gas preheater; E1, E2, E3: ESP ashes), (b)SO_3 contents, and (c) Molar Ca/S, Mg/S, K_2/S, and Na_2/S ratios α_i of the ashes.

particle control devices (e.g. ESP). The same behavior did also occur in lignite combustion experiments at KSVA and at the oxy-fuel pilot plant "Schwarze Pumpe". The lignite that was combusted in those plants presumably contained part of the ash in form of coarse SiO_2 rich sand. The preferential separation of these particles in the bottom ash explains the increased

SiO_2 content of this fraction. In contrast to SiO_2, other elements, such as MgO, Fe_2O_3, and CaO, show an enrichment in finer ESP ashes, while for Al_2O_3 no clear trend is observed.
For the lignites L1, L2, and L3, the decreasing particle size from ESP precipitation field E1 to E3 goes along with increasing SO_3 but also K_2O and Na_2O contents of the ash. For lignite L1, also CaO and MgO contents are increasing from E1 to E3. It can be seen that the SO_3 content in the process ashes from lignite L1 and L2 combustion is clearly increased in oxy-fuel operation. This behavior is pronounced for the ashes sampled from the ESP. The molar Ca/S, Mg/S, K_2/S, and Na_2/S ratios α_i of the process ashes allow for an evaluation of the degree of sulfation of these ashes. One sees a trend of decreasing α_i ratios from the first to the last ESP field (E1 to E3) that likely is related to the decreasing ash particle size and thus, a higher activity of the ash for sulfation. For both lignites combusted at KSVA, the α_i ratios of the ESP and GH ashes are decreasing considerably when switching from air to oxy-fuel combustion. This must be linked to the enhanced sulfur retention in oxy-fuel combustion. The trend in respect to lower α_i ratios in oxy-fuel, compared to air fired combustion, is not observed for the bottom ash. However, this ash contains only little CaO, compared to process ashes sampled further downstream, which limits its sulfur retention capacity. When comparing oxy-fuel process ash samples from KSVA and from the oxy-fuel pilot plant "Schwarze Pumpe" (figure 4.13), one recognizes differences in the compositions of corresponding ash samples. This is likely related to a somewhat different fuel and ash composition of lignites L2 and L3 and a different ash fractionation behavior of the two facilities that are differing in the design of their furnaces, flue gas ducts, and precipitators. Nonetheless, process ashes from both oxy-fuel experiments show relatively high SO_3 contents. In contrast to the lignite experiments, for hard coal C4 that showed only low sulfur retention on basis of the measured flue gas compositions and only a minor increase thereof in oxy-fuel combustion, the variations in the molar α_i ratios between both combustion modes are low, as is the increase of the SO_3 content in the process ashes.

Assessment of results in respect to SO_2 emissions and process ashes: The observations from air and oxy-fuel combustion experiments with different fuels can be summarized as follows: For fuels that have a considerable sulfur capture potential (i.e. high $\alpha_{(Ca+Mg)/S}$), under oxy-fuel combustion conditions, a significant increase in the sulfur retention in the ash was observed that translates into reduced SO_2 emissions. Higher sulfur levels in ashes and deposits and lower sulfur to SO_2 conversion ratios in oxy-fuel combustion were also reported by other researchers [9, 12, 126]. For a fuel with a low $\alpha_{(Ca+Mg)/S}$ level (i.e. coal C4), no systematic differences in the SO_2 emission behavior (i.e. in $\frac{mg}{MJ}$) and in the composition of process ashes was observed[57]. The observation with this fuel is consistent to the findings of Tan et al. [16] for a low alkali and earth alkali fuel.
The main reason for the increased sulfur retention with the lignites is most likely the en-

[57] Only a slight increase of the sulfur retention was observed.

hanced sulfate stability under oxy-fuel fired conditions and the extended residence time of SO_2 molecules in the oxy-fuel recycle system, due to a reduced volumetric flue gas flow through the boiler and the recirculation of flue gases (see sections 3.3.2.1 and 4.1.3). It should be also considered that changes in the furnace temperature profile between air and oxy-fuel combustion can play a determining role in sulfur capture. However, the oxy-fuel experiments were conducted with oxidant O_2 levels high enough to yield similar combustion temperatures than in the corresponding air fired experiments. As presented in table 3.6, temperatures at various locations in the furnace were similar in corresponding air and oxy-fuel tests. Thus, the impact of temperatures on the presented results is most likely limited. An impact that has influenced results on sulfur retention in oxy-fuel combustion of lignite L1 and potentially also lignite L3, is an unstable combustion that might have caused local deficiencies of oxygen in the furnace and hence, may have negatively impacted sulfur capture reactions (see also section 4.2.1.4).
The enhanced self-retention of sulfur in oxy-fuel fired systems using fuels that contain significant amounts of earth alkali elements leads to lower energy based SO_2 emissions (i.e. in $\frac{mg}{MJ}$) of the oxy-fuel process, compared to an air fired system, and hence, reduces the necessary efforts for flue gas desulfurization in downstream units. However, it should be highlighted that this can also have implications on the utilization of process ashes. For example, according to the standard EN 450-1 [63], the application of coal fly ash in concrete is limited to fly ashes with SO_3 contents below $3 \cdot 10^{-2}$ $\frac{kg}{kg}$. Hence, for low calcium and magnesium hard coals, such as the tested C4, whose ashes would[58] generally qualify for utilization in concrete, a slight increase in the SO_3 content in oxy-fuel combustion may render the fly ash unsuitable for a application in concrete. This may cause additional efforts for ash processing and upgrading or allow only less profitable utilization routes (e.g. application in cement production, according to EN 197-1 [64]).

4.2.1.3 Sulfates in deposits in air and oxy-fuel combustion

Analyses of deposit samples: In the air and oxy-fuel experiments at KSVA and in the oxy-fuel fired tests at the "Schwarze Pumpe" pilot plant, fly ashes as well as deposits (uncooled and cooled) have been sampled in the furnaces at different flue gas temperatures representing radiative (KSVA: Lev11; OxyPP: Lev4) and convective boiler sections (KSVA: Lev15, Lev26; OxyPP: Lev8). These samples have been analyzed for their chemical composition. Selected uncooled deposits sampled from KSVA's level 11 during air and oxy-fuel combustion of lignite L2 and from Lev4 of the "Schwarze Pumpe" pilot plant's furnace during oxy-fuel combustion of lignite L3 have also been analyzed by SEM to assess their morphology and elemental distribution.
Figure 4.15 presents comparatively the chemical composition (i.e. main ash forming oxides) and molar alkali and earth alkali to sulfur ratios α_i for ash and deposit samples from air and oxy-fuel combustion of lignite L2. When comparing the different samples for each combustion mode,

[58] Due to their favorable contents of Al, Ca, Fe, and Si.

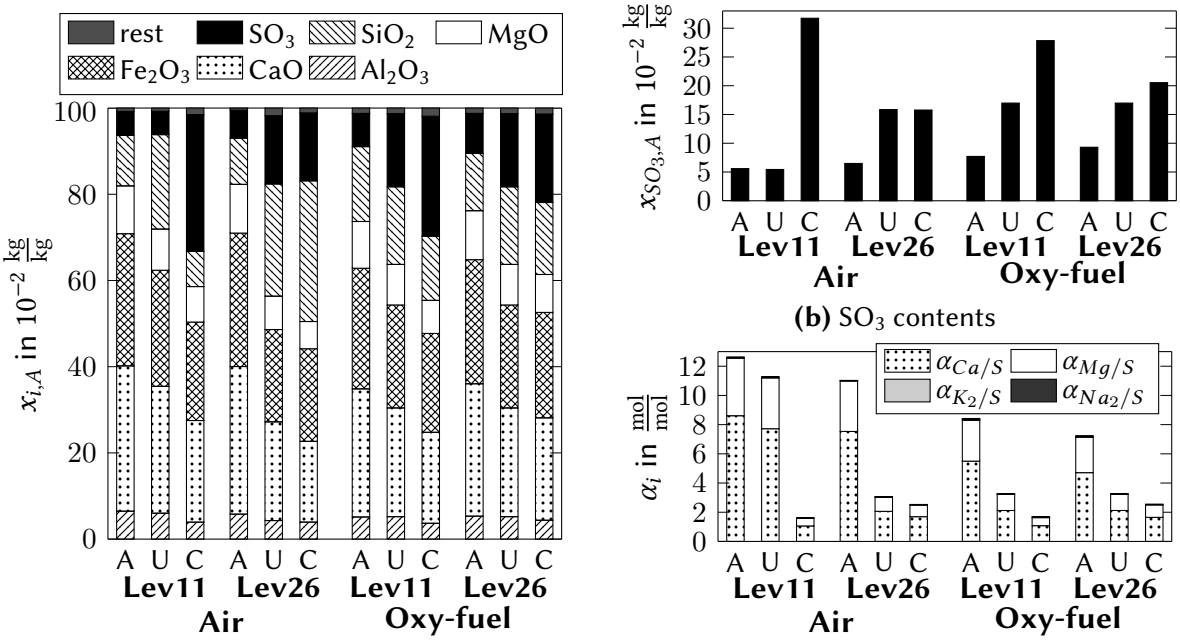

(a) Composition of ash and deposits

(b) SO_3 contents

(c) Molar Ca, Mg, K_2, and Na_2 to S ratios α_i

Figure 4.15: (a) Composition of entrained ashes (A) and uncooled (U) and cooled (C) deposits for lignite L2 air and oxy-fuel combustion, (b) SO_3 content, and (c) Molar Ca/S, Mg/S, K_2/S, and Na_2/S ratios α_i of the samples.

one can notice an increase of the SO_3 content from entrained ash samples to uncooled deposits and further to cooled deposits, with certain variations for the air fired experiments. Those variations seem to be linked to the SiO_2 contents in ashes and deposits for this experiment. The variations were not reproduced in the oxy-fuel tests. If SiO_2 contents are recalculated to similar levels for the samples from air firing, the SO_3 concentration increase pattern for the different locations and combustion modes would be more consistent. The increase in SO_3 can be explained by a longer gas-solids contact time that the deposit samples experienced, compared to the extracted entrained ash. The cooling of the deposit sample seems to shift the deposit temperature to a level that is more favorable for sulfate formation. For other ash elements, no distinct and characteristic change of the ash component's distribution can be observed (besides the SiO_2 variations mentioned above).

When the samples from air and oxy-fuel firing are compared, the most pronounced differences are in the SO_3 levels. The uncooled deposit from Lev11 and the entrained ash samples from both levels, Lev11 and Lev26, clearly show a higher extent of sulfation (i.e. lower levels of α_i). In contrast, the sulfation of cooled deposit samples and of the uncooled sample from Lev26 are very similar. These findings can be interpreted as follows: The sulfation of ashes and deposits seems to be generally limited by the reaction time which hinders entrained ash from capturing more sulfur and by too high temperatures which generally hinder sulfation, due to the SO_2 concentration dependent thermodynamic stability of sulfates. The cooled deposit and the uncooled samples from Lev26 in both combustion modes seem to have had a sufficient reaction

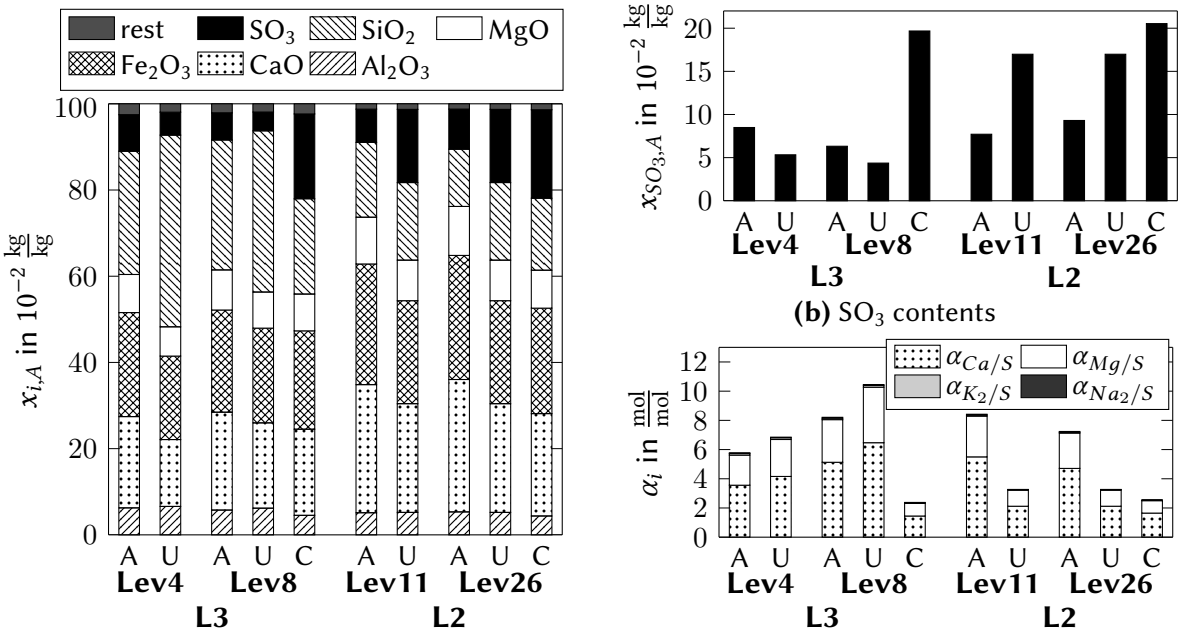

(a) Composition of ash and deposits

(b) SO_3 contents

(c) Molar Ca, Mg, K_2, and Na_2 to S ratios α_i

Figure 4.16: (a) Composition of entrained ashes (A) and uncooled (U) and cooled (C) deposits from lignite L3 (OxyPP) and L2 (KSVA) oxy-fuel combustion, (b) SO_3 contents, and (c) Molar Ca/S, Mg/S, K_2/S, and Na_2/S ratios α_i of the samples.

time at low enough temperatures so that sulfation could progress until the alkali and earth alkali compounds in the deposits were sulfated to a large extent (i.e. α_i around 2 or lower). For the other samples, limitations of the sulfation reactions in air firing by residence time and temperature were reduced in the oxy-fuel experiment due to a lower volumetric flue gas flow rate through the furnace (see section 3.3.2.1) and higher SO_2 partial pressures that enhance the sulfate stability and the rate of sulfation. This consequently leads to higher degrees of sulfation. Figure 4.16 presents analyses of cooled and uncooled deposits and entrained ashes sampled under comparable conditions (i.e. oxy-fuel combustion, similar fuels, and sampling temperatures) in the furnaces of KSVA and the oxy-fuel pilot plant "Schwarze Pumpe". The cooled deposit samples from KSVA and OxyPP (Lev8 and Lev26, respectively) show a very similar degree of sulfation. Different to the samples from KSVA that show increasing extents of sulfation from entrained ashes to uncooled deposits, the samples from OxyPP show the opposite behavior. This is unexpected since one would assume that the uncooled deposits that were sampled over times of approx. 2 h show more sulfation than entrained ash sampled at the same location. It should however be considered that ashes and deposits have been sampled subsequently and hence, they are subject to variations of the local process conditions that may have occurred during the different sampling periods. A reason for the relatively poor sulfation of uncooled deposits from L3 combustion and the unexpectedly higher degrees of sulfation of the entrained ash samples compared to the uncooled deposits, may also be found in combustion instabilities that have been observed at the "Schwarze Pumpe" pilot plant. CO concentration peaks at

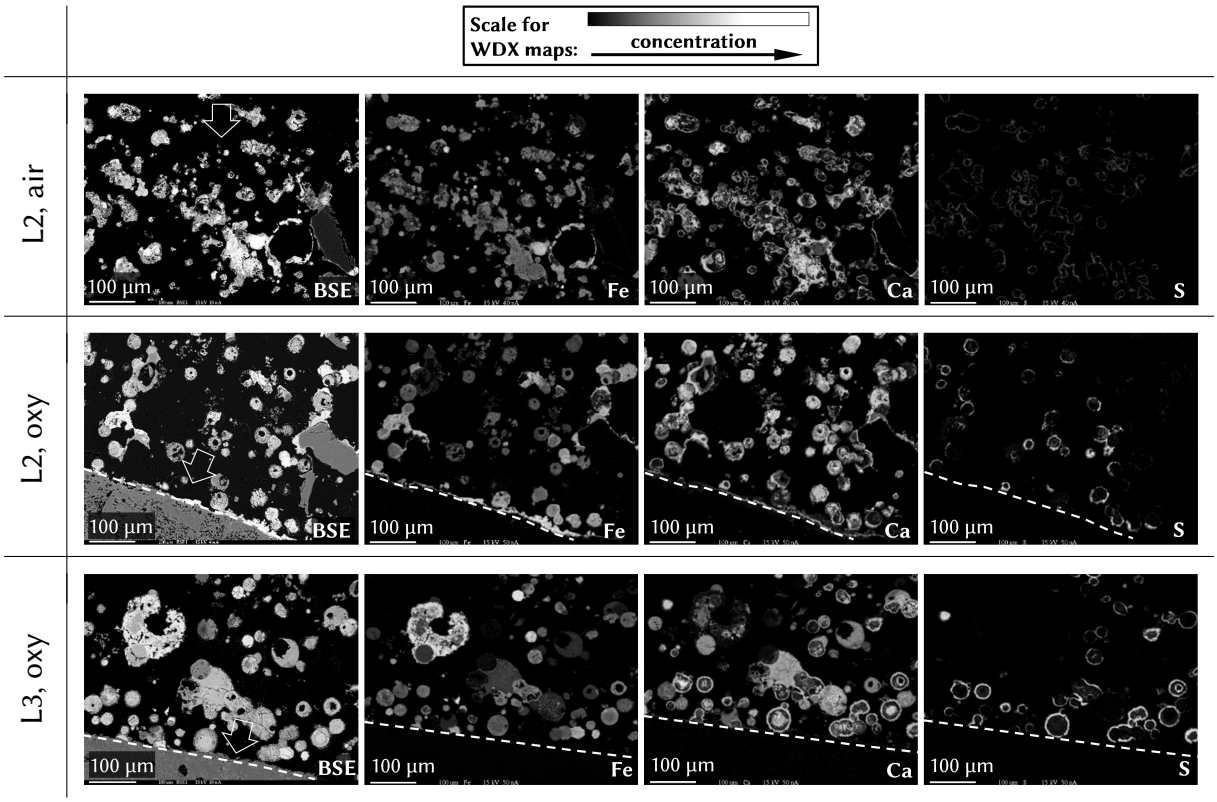

Figure 4.17: BSE images and SEM-WDX iron, calcium, and sulfur maps of uncooled deposits sampled at flue gas temperatures ϑ_{FG} of 1095 °C (L2, air), 1055 °C (L2, oxy), and 1100 °C (L3, oxy) in air and oxy-fuel experiments at Lev11 of KSVA (lignite L2) and Lev4 of the oxy-fuel pilot plant "Schwarze Pumpe" (lignite L3) (white dashed lines indicate sampling probe surfaces; arrows indicate flue gas flow direction).

Level 4 were reaching up to about $16\,300 \cdot 10^{-6}\ \frac{m^3}{m^3}$, dry, and at Level 8 up to about $7200 \cdot 10^{-6}\ \frac{m^3}{m^3}$, dry. Sub-stoichiometric combustion conditions (i.e. an oxygen deficit) can lead to a reduced sulfur retention in the ash, since the sulfation reaction requires oxygen. Potentially, such conditions even lead to a release of sulfur that has been captured in form of sulfates. The sulfation of the cooled deposit seems to be favored by longer residence times and lower deposit temperatures and sulfates may be stabilized in that way, explaining the considerably higher degree of sulfation.

In Figure 4.17 BSE images and the distribution of iron, calcium, and sulfur (by SEM-WDX)[59] of the uncooled deposit samples obtained from Lev11 of KSVA (air and oxy-fuel) and Lev4 of the oxy-fuel pilot plant "Schwarze Pumpe" are shown. In all three samples, irregular and spherical iron and calcium rich particles dominate the deposits[60], without a strong difference between different combustion modes and facilities, even though the sample from air fired combustion seems somewhat more fused. The spherical iron and calcium rich particles have a sulfur rich shell that is more pronounced in oxy-fuel deposits, highlighting their stronger

[59] More detailed SEM-WDX maps of L2 deposits including other elements can be found in annex A.2.

[60] The abundance of these iron and calcium rich particles is typical for the Lusatian lignite that was fired and has been also identified in deposits from BTS-VR experiments (see figure 4.9).

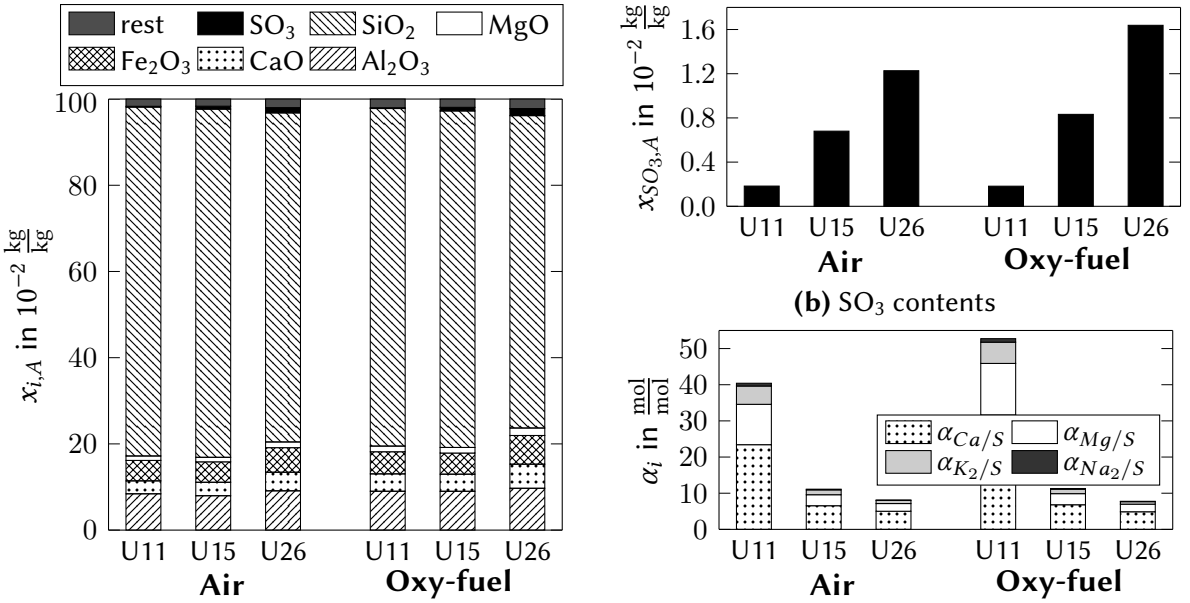

(a) Composition of deposits

(b) SO_3 contents

(c) Molar Ca, Mg, K_2, and Na_2 to S ratios α_i

Figure 4.18: (a) Composition of uncooled deposits sampled from levels 11 (UD11), 15 (UD15), and 26 (UD26) during lignite L1 air and oxy-fuel combustion, (b) SO_3 contents, and (c) Molar Ca/S, Mg/S, K_2/S, and Na_2/S ratios α_i of the samples.

sulfation, compared to air fired conditions. In addition to these particles, also a number of unsulfated particles can be observed. Those are either almost pure Fe_2O_3 or SiO_2 or contain in contrast to the sulfated particles, in addition to calcium and iron, higher amounts of silicon (see also annex A.3).

Figure 4.18 shows the compositions in respect to main ash forming elements of uncooled deposit samples from Lev11, Lev15, and Lev26 obtained in air and oxy-fuel combustion of the sulfur and ash rich lignite L1. The deposits of experiments with this lignite quality are dominated by the SiO_2 content of the fuel's ash ($57.6 \cdot 10^{-2}$ $\frac{kg}{kg}$) that dilutes all other ash components. As with samples of lignite L2, one observes increased SO_3 contents in the oxy-fuel, compared to the air fired samples. However, even though the combustion of the sulfur rich lignite yielded much higher SO_2 concentrations in both combustion modes, the extent of sulfation of the deposits is relatively low, compared to the samples from lignite L2 combustion. This may be linked to non-optimal combustion conditions in experiments with lignite L1 that are believed to be responsible for a generally lower sulfur retention in the ash in these experiments (see p. 107 and section 4.2.1.4). The extent of sulfation of the air and oxy-fuel Lev15 and Lev26 samples is similar, while the Lev11 sample from oxy-fuel firing shows even less sulfation, compared to the air fired one. However, for Lev11 samples, the SO_3 contents in the deposits are very low and the large difference in α_i may be caused by only minimal variations in the SO_3 and earth alkali contents and hence, should not be overrated.

A limited number of deposit samples were obtained for combustion tests with C4 coal with and without injection of $Ca(OH)_2$ to the furnace. Compositions of those samples are presented

and discussed on page 148.

Summary and interpretation of findings: To conclude this section, it can be summarized that in oxy-fuel combustion deposits from the furnace can show higher SO_3 contents and higher extents of sulfation of alkali and earth alkali compounds. In addition, it was observed on basis of uncooled deposit samples representing outer deposit layers of heat exchanger tubes that sulfatic deposits can be considerably more sulfated at higher temperatures that occur in the radiative section of a boiler and the inlet of the convective section. As also indicated by the thermodynamic equilibrium studies (section 4.1.2), this illustrates that sulfates in oxy-fuel systems are stable at higher temperatures and that the temperature range in which fouling by sulfates occurs and may be problematic, can be shifted to higher temperatures. Due to the higher degree of sulfation at higher temperatures in oxy-fuel firing, in such locations deposits may also be more sintered and therefore, more difficult to remove.
For cooled deposit samples that represent inner deposit layers on heat exchanger tubes, no pronounced increase in the degree of sulfation was observed. It should however be considered that cooled deposit samples from both combustion modes showed a relatively high extent of sulfation that was close to full sulfation of all alkalis and earth alkalis in the deposit. This highlights that especially if the sulfation of deposits in air firing is already high, for a complementary oxy-fuel combustion system, no significant differences in the extent of sulfation of the inner deposit layers are expected.
It needs also to be highlighted that for a fuel with low sulfur retention potential (C4 coal, see p. 148) and for combustion conditions that limit the sulfur retention (experiments with lignite L1), uncooled deposits showed only a relatively low content of SO_3 and no considerable changes in the extent of sulfation between air and oxy-fuel combustion. This indicates that changes in the formation of sulfatic deposits between air and oxy-fuel firing are highly fuel and combustion system related and will not necessarily occur to a considerable extent in all oxy-fuel fired systems.

4.2.1.4 Impacts of combustion instabilities on SO_2 emissions in oxy-fuel combustion

Unstable SO_2 emission behavior in oxy-fuel combustion: Section 4.2.1.2 introduced that combustion instabilities were observed during oxy-fuel combustion experiments with the sulfur rich lignite L1 at the KSVA test rig and, to a lesser extent, during combustion of lignite L3 at "Schwarze Pumpe" pilot plant. Those led to the emission of increased levels of CO in form of short term concentration peaks. The CO peaks were also linked to SO_2 concentration peaks of the firing systems and a reduced sulfur retention in the ash. In figure 4.19, SO_2 and CO concentrations measured at the end of KSVA's furnace in L1 air and oxy-fuel combustion tests are plotted versus O_2 concentrations. Figure 4.20 shows a similar plot for emissions measured downstream the ESP during oxy-fuel combustion of lignite L3 at the "Schwarze Pumpe" pilot

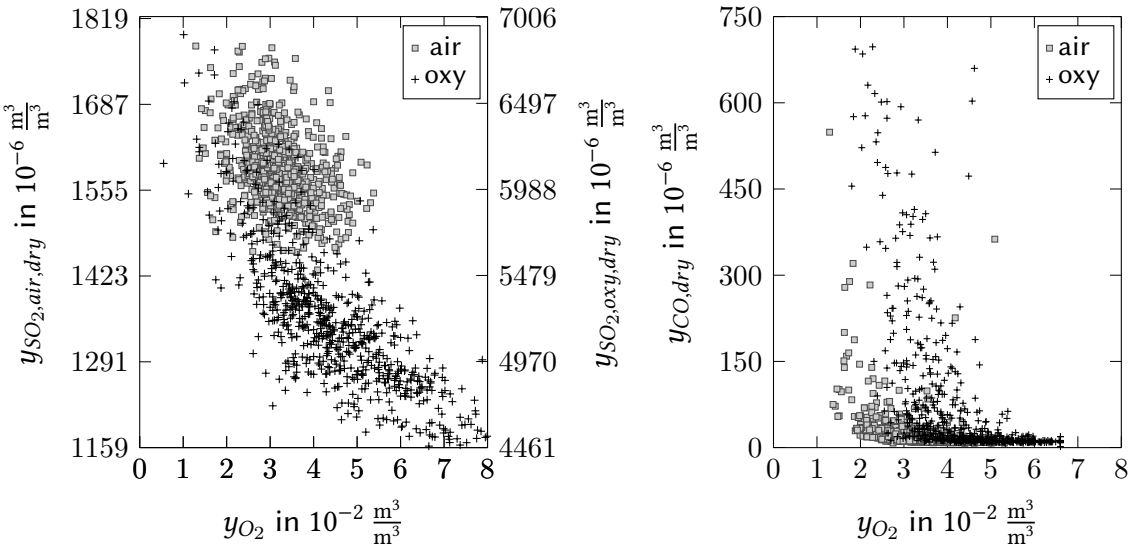

(a) SO_2 vs. O_2 **(b)** CO vs. O_2

Figure 4.19: Scatter plots of y_{SO_2} (a) and y_{CO} (b) vs. y_{O_2} measured at KSVA's furnace exit in lignite L1 air and oxy-fuel combustion. Plots show data of approx. 2 h of operation for each experiment[61]. y_{SO_2} and y_{CO} are recalculated to the same $y_{O_2,dry}$ of $4 \cdot 10^{-2}$ $\frac{m^3}{m^3}$. Figures A.10, A.11, and A.12 in the annex show the same plots with uncorrected concentrations and the concentration trends over time on which these scatter plots are based.

plant. Both figures, 4.19 and 4.20, show data for 2 h of operation for each experiment. To compensate effects by flue gas dilution, the concentrations y_{SO_2} and y_{CO} in these figures were recalculated to O_2 concentrations that were selected in the range of the mean O_2 level during the measurement period of the individual oxy-fuel tests. For the experiments with lignite L1, a reference O_2 level $y_{O_2,ref,dry}$ of $4 \cdot 10^{-2}$ $\frac{m^3}{m^3}$ was selected, while for the oxy-fuel trial with lignite L3, a reference O_2 level of $7 \cdot 10^{-2}$ $\frac{m^3}{m^3}$, dry, was used. These recalculations were done as described in section 3.6.4 (equation 3.20).

The SO_2 axis in figure 4.19a represents a concentration range of 70 % and 110 % of the theoretical maximum SO_2 concentrations $y_{SO_2,max,air,dry}$ (see equation 4.1) and $y_{SO_2,max,oxy,dry}$ (see equation 4.2) for air and oxy-fuel operation, respectively. It can be seen that the fluctuations of the SO_2 concentration relative to the theoretical maximum values are in air firing less pronounced than in oxy-fuel operation. Besides that, it can be noticed that very high SO_2 concentration peaks are preferentially reached when the O_2 concentration falls below a certain level. For the presented experiments with lignite L1, this threshold level lies at around $5 \cdot 10^{-2}$ $\frac{m^3}{m^3}$, dry, O_2 in oxy-fuel operation. Above that level, SO_2 concentrations rise slowly with decreasing oxygen, i.e. from about $4500 \cdot 10^{-6}$ $\frac{m^3}{m^3}$, dry, at $8 \cdot 10^{-2}$ $\frac{m^3}{m^3}$, dry, to about $5000 \cdot 10^{-6}$ $\frac{m^3}{m^3}$, dry, at $5 \cdot 10^{-2}$ $\frac{m^3}{m^3}$, dry. Below $5 \cdot 10^{-2}$ $\frac{m^3}{m^3}$, dry, O_2, this rise of SO_2 concentrations is much steeper and a similar reduction of O_2 by $3 \cdot 10^{-2}$ $\frac{m^3}{m^3}$, dry (to a O_2 level of $2 \cdot 10^{-2}$ $\frac{m^3}{m^3}$, dry), leads to an increase of SO_2

[61] y_{SO_2} axes are scaled to represent between 70 % and 110 % of the theoretical maximum SO_2 concentrations in lignite L1 air and oxy-fuel combustion with an outlet O_2 level of $4 \cdot 10^{-2}$ $\frac{m^3}{m^3}$, dry.

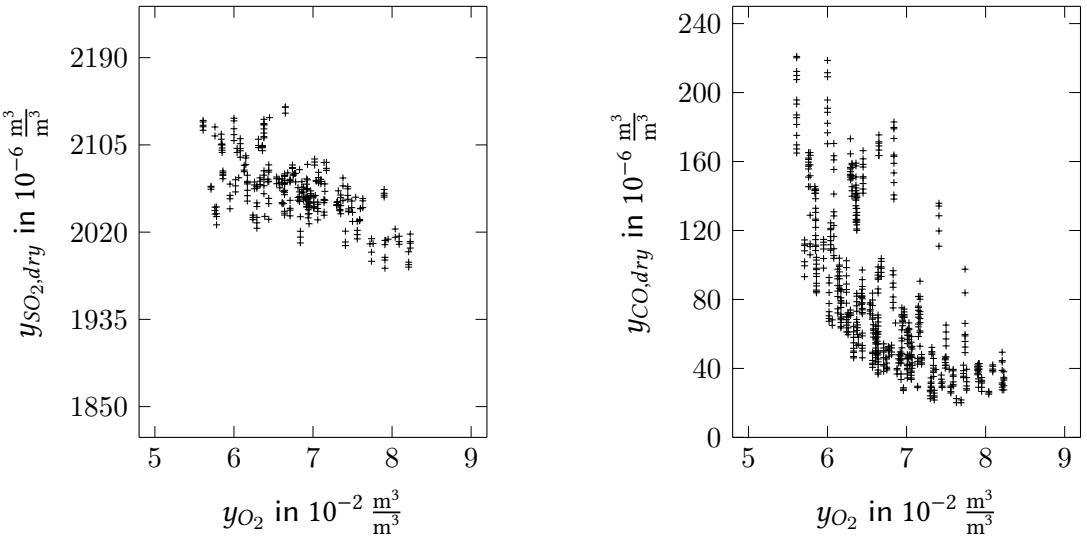

(a) SO_2 vs. O_2 **(b)** CO vs. O_2

Figure 4.20: Scatter plots of y_{SO_2} (a) and y_{CO} (b) vs. y_{O_2} measured after ESP in lignite L3 oxy-fuel combustion at the "Schwarze Pumpe" pilot plant. Plot shows data of approx. 2 h of operation[62]. All concentrations y_{SO_2} and y_{CO} are recalculated to the same $y_{O_2,dry} = 7 \cdot 10^{-2}\ \frac{m^3}{m^3}$. Figures A.13 and A.14 in the annex display the same plots with uncorrected concentrations and the concentration trends over time on which these scatter plots are based.

to approx. $6400 \cdot 10^{-6}\ \frac{m^3}{m^3}$, dry. In air fired operation the effect is much less distinct and the threshold is shifted to somewhat lower O_2 concentrations (approx. $4 \cdot 10^{-2}\ \frac{m^3}{m^3}$, dry).
In figure 4.19b, a similar trend as for SO_2 can be observed for the formation of CO. It can be noticed that in oxy-fuel combustion, CO concentration peaks are higher and occur already at higher excess O_2 concentrations, compared to air firing. The CO peaks at excess O_2 concentrations lower than about $4 \cdot 10^{-2}\ \frac{m^3}{m^3}$, dry in oxy-fuel and $3 \cdot 10^{-2}\ \frac{m^3}{m^3}$, dry in air firing indicate local, short term, near or sub-stoichiometric combustion conditions in the furnace. The oxy-fuel firing obviously responds more sensitive to short term fluctuations in the operating conditions. Presumably, one important parameter in this respect[63] is a fluctuation in the fuel feed. As discussed in detail in the next part of this section, due to the lower available amount of excess oxygen in oxy-fuel combustion (with oxidant O_2 levels above the ones in air) at similar excess O_2 concentrations, the same small, short term fluctuations of the fuel feed can easier lead to a short term oxygen depletion in the furnace, compared to air fired operation. The effect of reduced sulfur retention and an increased sensitivity of this reduction at higher oxidant O_2 levels is to some extent consistent to the one that was observed by Hu et al. [100] and is introduced on page 19, even tough, Hu's experiments were considerably different.
In figure 4.20, a similar dependency between SO_2 and CO levels and the oxygen excess can

[62] y_{SO_2} axes are scaled to represent between 65 % and 80 % of the theoretical maximum SO_2 concentrations in oxy-fuel combustion of lignite L3 with an outlet O_2 level of $7 \cdot 10^{-2}\ \frac{m^3}{m^3}$, dry.
[63] Particularly in a single burner furnace, such as KSVA or the oxy-fuel pilot plant "Schwarze Pumpe".

be observed in emission data obtained from the "Schwarze Pumpe" pilot plant. However, the effect is much less pronounced there. It must be noted that the SO_2 axis represents a smaller concentration range of 65 % to 80 % of the theoretical maximum SO_2 concentration[64]. The less pronounced effect in respect to the increase of SO_2 emissions at lower excess O_2 levels is probably also related to the measuring location that was, different to the KSVA experiments, placed further downstream the furnace, just after ESP. Therefore, flue gases experienced a longer residence time and more turbulent mixing when traveling through the boiler and flue gas ducts, which has most likely damped concentration peaks of SO_2 and CO. This assumption is supported by the much higher CO peaks that were observed during short term flue gas measurements at levels 4 and 8 of the boiler (see p. 110). Nonetheless, the observations from the oxy-fuel pilot plant "Schwarze Pumpe" highlight that the effect of instabilities in the SO_2 emission behavior and increasing overall SO_2 emissions at lower excess O_2 concentrations does also occur in larger oxy-fuel boilers.

Discussion on O_2 availability and unstable SO_2 emissions in oxy-fuel combustion: The reason for the greater sensitivity of the SO_2 emissions to combustion instabilities in oxy-fuel firing can be found in the overall O_2 availability that is, depending on the O_2 level in the oxidant $y_{O_2,oxid}$ (or equivalently the recirculation ratio ξ_{rec}), in practical oxy-fuel combustion (i.e. $y_{O_2,oxid} > y_{O_2,air}$) lower than in air fired systems, as long as the level of excess O_2 in the flue gas $y_{O_2,exc}$ is not adapted. This effect has also been described by Wild et al. [89]. O_2 is required for the desulfurization reaction between SO_2 in the flue gas and CaO in the ash (reaction 2.3). The availability of O_2 of a firing system can be expressed in terms of the combustion stoichiometry ($n_{O_2,rec}/n_{O_2,o-t}/n_{air}$) that relates the O_2 supply to the fuel specific stoichiometric O_2 demand $n_{O_2,stoic}$ (equation 4.16) that the combustible species in a fuel require to be fully oxidized. Similar to the definition of the once-through desulfurization efficiency in oxy-fuel recycle combustion (see section 4.1.3), a once-through combustion stoichiometry ($n_{O_2,o-t}$) can be defined.

$$n_{O_2,stoic} = \frac{\gamma_S}{M_{M,S}} + \frac{\gamma_C}{M_{M,C}} + \frac{\gamma_H}{4M_{M,H}} - \frac{\gamma_O}{2M_{M,O}} \tag{4.16}$$

$$n_{O_2,rec} = \frac{n_{O_2,in}}{n_{O_2,stoic}} = n_{O_2,o-t} - \xi_{rec}(n_{O_2,o-t} - 1) \tag{4.17}$$

$$n_{O_2,o-t} = \frac{n_{O_2,furn,in}}{n_{O_2,stoic}} = \frac{n_{O_2,in} + n_{O_2,rec}}{n_{O_2,stoic}} = \frac{n_{O_2,rec} - \xi_{rec}}{1 - \xi_{rec}} \tag{4.18}$$

[64] Due to a lack of operational data from the "Schwarze Pumpe" pilot plant, $y_{SO_2,max,oxy,dry}$ for the combustion test with lignite L3 could only be roughly estimated to be around $2800 \cdot 10^{-6}$ $\frac{m^3}{m^3}$, dry.

$n_{O_2,o-t}$ can be related to the recycle combustion stoichiometry ($n_{O_2,rec}$), according to equations 4.17 and 4.18 (indices used below are consistent with the ones in figure 4.6)[65].
In figure 4.21b, $n_{O_2,rec}$ is plotted versus $n_{O_2,o-t}$ for a range of different recirculation ratios ξ_{rec}. One sees that due to the recirculation of oxygen together with the recirculated flue gas, $n_{O_2,o-t}$ is generally larger than $n_{O_2,rec}$ and that this effect is growing with ξ_{rec}. When comparing air and oxy-fuel combustion stoichiometries in respect to the oxygen availability in the furnace, one should always use $n_{O_2,o-t}$, which considers both sources of oxygen supplied to the furnace, the freshly added O_2 ($n_{O_2,in}$) and the O_2 contained in the flue gas that is recirculated to the furnace ($n_{O_2,rec}$). In contrast to $n_{O_2,o-t}$, $n_{O_2,rec}$ considers only the feed of fresh O_2, provided to the process from tanks or an ASU ($n_{O_2,in}$). Hence, this value is particularly useful when the total oxygen consumption of an oxy-fuel process is considered but not to characterize the oxygen availability in a furnace. Since in an oxy-fuel system, oxygen losses with the flue gas are related to a considerable oxygen production cost, power plant operators are interested to minimize $n_{O_2,rec}$ by operating at low excess oxygen levels $y_{O_2,exc}$ in the flue gas [227]. For the combustion environment in the furnace, this is connected to a reduction of the oxygen availability (i.e. $n_{O_2,o-t}$). Depending on the recirculation ratio ξ_{rec} and the excess oxygen level $y_{O_2,exc}$, $n_{O_2,o-t}$ in typically used oxy-fuel combustion conditions may be lower than combustion stoichiometries that are commonly used in air fired pulverized fuel systems (i.e. $n_{air} \approx$ 1.15-1.3, [53]). This effect has also been previously discussed by others [92, 227]. For a given fuel (i.e. given stoichiometric O_2 consumption $n_{O_2,stoic}$ and dry flue gas production $n_{FG,stoic,dry}$; see equation 4.19), the excess oxygen level $y_{O_2,exc,dry}$ in oxy-fuel combustion can be calculated in dependence of ξ_{rec} and $n_{O_2,o-t}$, according to equation 4.20.

$$n_{FG,stoic,dry} = \frac{\gamma_S}{M_{M,S}} + \frac{\gamma_C}{M_{M,C}} + \frac{\gamma_N}{2M_{M,N}} \tag{4.19}$$

$$\begin{aligned} y_{O_2,exc,dry} &= \frac{(n_{O_2,rec} - 1)n_{O_2,stoic}}{(n_{O_2,rec} - 1)n_{O_2,stoic} + n_{FG,stoic}} = \\ &= \frac{(n_{O_2,o-t} - \xi_{rec}(n_{O_2,o-t} - 1) - 1)n_{O_2,stoic}}{(n_{O_2,o-t} - \xi_{rec}(n_{O_2,o-t} - 1) - 1)n_{O_2,stoic} + n_{FG,stoic}} \end{aligned} \tag{4.20}$$

In figure 4.21a, $y_{O_2,exc,dry}$ is plotted versus $n_{O_2,o-t}$ for lignite L1 combustion. One sees that depending on ξ_{rec}, relatively high excess oxygen levels are required to reach similar once-through combustion stoichiometries as in typical air fired systems. For a recirculation ratio of approx. 71.1 %, as in the combustion experiments with lignite L1, once-through combustion stoichiometries between 1.15 and 1.3 require excess O_2 concentrations between $4.9 \cdot 10^{-2}$ $\frac{m^3}{m^3}$, dry, and $9.3 \cdot 10^{-2}$ $\frac{m^3}{m^3}$, dry.
The considerations in respect to the once-through combustion stoichiometry in oxy-fuel firing highlight that in practice (i.e. when operated at relatively low excess O_2 levels), oxy-fuel

[65] It should be noted that equations 4.17 and 4.18 are only valid for stoichiometries above 1.

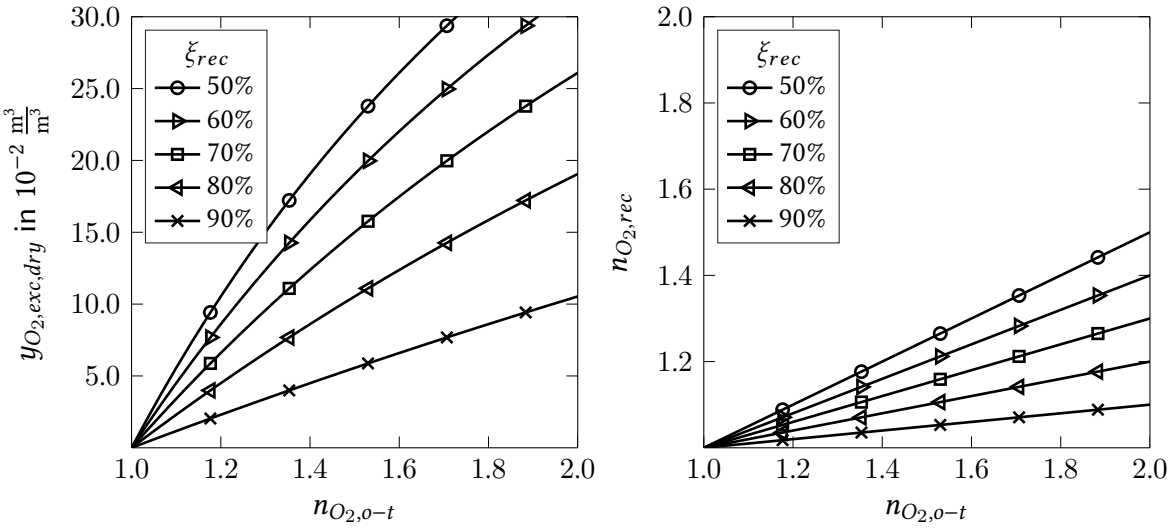

(a) $y_{O_2,exc,dry}$ versus $n_{O_2,o-t}$ **(b)** $n_{O_2,rec}$ versus $n_{O_2,o-t}$

Figure 4.21: Relation of (a) the excess oxygen level $y_{O_2,exc,dry}$ and (b) the recycle combustion stoichiometry $n_{O_2,rec}$ to the once-through combustion stoichiometry $n_{O_2,o-t}$ for various flue gas recirculation ratios ξ_{rec} (plots of equations 4.17 and 4.20, respectively). $y_{O_2,exc,dry}$ is calculated for lignite L1 combustion.

systems are more sensitive towards O_2 deficiencies. This is an issue to be considered in combustion system design and operation to achieve an optimal oxy-fuel system performance. The conducted experiments showed that in oxy-fuel firing combustion instabilities may not only lead to increased CO emissions but also to instabilities in the SO_2 emission behavior and to a reduced sulfur retention in the ash. A low O_2 excess that is desired for economic reasons, may lead to a significant increase in short term SO_2 peaks with associated negative consequences. This increases the importance of a good combustion performance in an oxy-fuel boiler. It should be highlighted that pronounced instabilities in the SO_2 emission behavior under oxy-fuel conditions were only observed in certain cases when the combustion performance was not optimal. In all other experiments, SO_2 levels at furnace outlet were relatively stable independently of the combustion mode. This shows that it is possible to operate an oxy-fuel fired system at low excess O_2 levels without formation of significant SO_2 concentration peaks. In some instances, it may however be beneficial to slightly increase the excess O_2 concentration, compared to air firing, to achieve an optimal SO_2 emission behavior.

The greater extent of SO_2 emission fluctuations in oxy-fuel combustion must be related to the higher capture of sulfur species in ashes and deposits in oxy-fuel, compared to air firing. If, due to an oxygen deficiency, the sulfur capture becomes ineffective, the additional release of SO_2 is consequently higher in oxy-fuel combustion. For example, in the air fired experiment with lignite L1, on average above 96 % of the fuel-sulfur can be found in the flue gas as SO_2. A rising sulfur release due to combustion instabilities can therefore only lead to relatively low additional SO_2 emissions. In addition, also sulfur that has been captured in deposits may become instable and may be released to the flue gas to some extent. Also in this context,

generally, a higher degree of sulfation of deposits in oxy-fuel combustion may be linked to a greater release of SO_2 when combustion instabilities occur. It can be expected that fuels with a low sulfur retention potential in their ash show a relatively stable SO_2 emission behavior in oxy-fuel firing, even in unstable combustion conditions (i.e. with CO emission peaks). Since for such fuels sulfur retention is already low, no considerable deterioration due to oxygen deficiencies can be expected.
In oxy-fuel firing with DSI, combustion instabilities may cause considerable fluctuations in SO_2 emissions. In the conducted DSI experiments at KSVA (see section 4.2.2.3), such a behavior was not observed, due to the very stable combustion performance.

4.2.2 Acid gas removal by DSI in air and oxy-fuel combustion

4.2.2.1 Considerations on dry SO_x removal in oxy-fuel combustion

DSI systems are well known and widely applied for emission reduction in industry. Due to the stringent emission regulations for large coal and lignite fired power plants in Germany and other developed countries and due to the limited acid gas capture efficiency at practically relevant sorbent injection rates, this technology's application in conventional power plants is limited. Nonetheless, a utilization of DSI technologies in oxy-fuel fired power plants may be an interesting solution. Such facilities have a very different emission profile and current emission regulations that focus on a limitation of the concentrations of pollutants within large flue gas streams that are emitted are likely less relevant to an oxy-fuel power plant that emits only relatively low gas flows to the atmosphere (e.g. vent gases of the CPU). Yet, also in the oxy-fuel process, acid gases contained in the flue gas need to be controlled since they may cause hot and low temperature corrosion and may induce fouling problems in power boilers. Moreover, eventually all acid gases need to be removed from the CO_2 rich oxy-fuel flue gas, down to very low concentrations. Therefore, a removal of most of the acid gases by an economic gas cleaning process followed by a gas polishing to maintain downstream gas quality requirements is foreseen in most oxy-fuel concepts. A DSI system can be a solution for such an economic acid gas cleaning system that can be installed within the oxy-fuel recycle to capture a large quantity of the acid gases without excessive recycle gas cooling and to purposely control the levels of acid gases, such as SO_2, SO_3, and HCl, within the boiler and recycle loop in order to limit acid gas induced corrosion. The findings of previous sections and other researchers [11, 104, 105] highlight that during oxy-fuel combustion higher sulfur retention in ash and in injected sorbents can be expected (see also section 4.1.3). Even though oxy-fuel desulfurization models highlight the great potential of the technology [11], its performance has not been studied experimentally in significant scales and in actual oxy-fuel recycle combustion. Experimental studies within this thesis focus on the application of DSI for SO_2, SO_3, and HCl control and assess DSI in air and oxy-fuel combustion comparatively. The results are presented in the

following sections.

4.2.2.2 DSI in air and simulated oxy-fuel atmospheres

In experiments at the BTS-VR test facility, the performance of DSI for acid gas control was tested comparatively for different sorbents ($CaCO_3$ and $Ca(OH)_2$), injection locations (co-injection with fuel, injection to the furnace at approx. 1100 °C, and upstream of a fabric filter), and combustion atmospheres (coal C4 combustion in air and simulated oxy-fuel conditions, labeled

Table 4.3: Gas concentrations (after filter, recalculated to $3 \cdot 10^{-2}$ $\frac{m^3}{m^3}$, dry, O_2) and removal efficiencies for SO_2 and HCl determined for $CaCO_3$ DSI experiments at BTS-VR.

Sorb.	Injec.	Mode	$\alpha_{Ca/S}$	$\alpha_{Ca/2Cl}$	$\bar{y}_{SO_2,dry}$	$\bar{y}_{HCl,dry}$	$\bar{y}_{SO_3,dry}$	η_{SO_2}	η_{HCl}	η_{SO_3}
			$\frac{mol}{mol}$			10^{-6} $\frac{m^3}{m^3}$				
$CaCO_3$	co-injection	air	0.0	0.0	1685.0	225.8	-	-	-	-
			0.5	2.0	1418.9	221.2	-	16 %	2 %	-
			1.3	5.0	1200.2	212.5	-	29 %	6 %	-
			2.0	7.5	1099.6	207.1	-	35 %	8 %	-
			2.5	9.3	952.9	199.3	-	43 %	12 %	-
			4.1	15.5	654.3	162.9	-	61 %	28 %	-
		O_2/CO_2	0.0	0.0	4956.9	450.9	-	-	-	-
			0.2	1.2	4504.2	445.4	-	9 %	1 %	-
			0.5	2.7	4167.4	442.8	-	16 %	2 %	-
			0.9	4.7	3304.8	417.6	-	33 %	7 %	-
			1.5	8.0	2947.5	400.7	-	41 %	11 %	-
	furnace	air	0.0	0.0	1597.0	205.7	-	-	-	-
			0.4	1.5	1400.8	202.6	-	12 %	1 %	-
			0.7	2.7	1201.4	198.3	-	25 %	4 %	-
			1.5	5.7	825.2	174.1	-	48 %	15 %	-
			1.8	7.0	690.3	167.4	-	57 %	19 %	-
			2.3	8.8	550.3	167.6	-	66 %	19 %	-
		O_2/CO_2	0.0	0.0	4376.0	366.7	17.2	-	-	-
			0.2	1.3	3909.8	375.9	-	11 %	0 %	-
			0.3	2.0	3672.0	380.6	-	16 %	0 %	-
			0.5	3.2	3365.4	370.9	-	23 %	0 %	-
			0.8	4.9	2992.6	363.8	-	32 %	1 %	-
			1.4	8.5	2311.3	341.4	-	47 %	7 %	-
			1.8	10.5	2111.5	336.3	-	52 %	8 %	-
			2.2	13.1	1748.7	326.2	0.6	60 %	11 %	97 %

Table 4.4: Gas concentrations (after filter, recalculated to $3 \cdot 10^{-2}$ $\frac{m^3}{m^3}$, dry, O_2) and removal efficiencies for SO_2, HCl, and SO_3 determined for $Ca(OH)_2$ DSI experiments at BTS-VR.

Sorb.	Injec.	Mode	$\alpha_{Ca/S}$	$\alpha_{Ca/2Cl}$	$\bar{y}_{SO_2,dry}$	$\bar{y}_{HCl,dry}$	$\bar{y}_{SO_3,dry}$	η_{SO_2}	η_{HCl}	η_{SO_3}
			$\frac{mol}{mol}$			10^{-6} $\frac{m^3}{m^3}$				
$Ca(OH)_2$	co-injection	air	0.0	0.0	1616.6	231.4	-	-	-	-
			0.4	1.6	1526.3	230.9	-	6 %	0 %	-
			1.2	4.3	1417.0	226.1	-	12 %	2 %	-
			2.0	7.5	1224.2	218.1	-	24 %	6 %	-
			2.5	9.1	1128.6	213.7	-	30 %	8 %	-
		O_2/CO_2	0.0	0.0	4855.0	393.2	-	-	-	-
			0.2	1.2	4722.7	394.1	-	3 %	0 %	-
			0.5	3.0	4499.3	394.9	-	7 %	0 %	-
			0.8	4.9	4161.2	392.8	-	14 %	0 %	-
			1.2	7.5	3968.7	387.7	-	18 %	1 %	-
	furnace	air	0.0	0.0	1696.1	197.4	-	-	-	-
			0.4	1.6	1334.7	187.6	-	21 %	5 %	-
			0.8	3.2	1041.7	167.4	-	39 %	15 %	-
			1.2	5.1	790.0	158.6	-	53 %	20 %	-
			1.5	6.4	610.2	148.4	-	64 %	25 %	-
			2.3	9.9	280.3	110.8	-	83 %	44 %	-
			2.3	10.0	178.2	95.5	-	89 %	52 %	-
			2.7	11.4	160.6	88.8	-	91 %	55 %	-
		O_2/CO_2	0.0	0.0	4427.4	376.4	17.2	-	-	-
			0.2	1.3	3659.3	367.8	-	17 %	2 %	-
			0.3	1.6	3471.9	365.1	13.0	22 %	3 %	24 %
			0.5	3.2	3046.1	346.6	-	31 %	8 %	-
			0.7	4.1	2772.7	341.9	-	37 %	9 %	-
			0.9	5.1	2510.5	337.3	-	43 %	10 %	-
			1.2	6.9	2162.9	331.6	3.1	51 %	12 %	82 %

"CO_2/O_2" below). Different to oxy-fuel recycle combustion (e.g. at the KSVA facility), the BTS-VR system cannot reproduce certain characteristics of the oxy-fuel recycle combustion (i.e. no longer average SO_2 reaction time), and the addition of surplus SO_2 doped to the oxidant gas needs to be considered in the calculation of the sorbent injection stoichiometries $\alpha_{Ca/S}$ and $\alpha_{Ca/2Cl}$ which hence, is done differently to the DSI tests at the KSVA test rig (see p. 66).

Tables 4.3, 4.4, and 4.5 summarize key parameters and results for all DSI experiments conducted at BTS-VR (i.e. used sorbents, injection locations, combustion modes, sorbent injection stoi-

Table 4.5: Gas concentrations (after filter, recalculated to $3 \cdot 10^{-2}$ $\frac{m^3}{m^3}$, dry, O_2) and removal efficiencies for SO_2, HCl, and SO_3 determined for $Ca(OH)_2$ DSI experiments at BTS-VR.

Sorb.	Injec.	Mode	$\alpha_{Ca/S}$	$\alpha_{Ca/2Cl}$	$\bar{y}_{SO_2,dry}$	$\bar{y}_{HCl,dry}$	$\bar{y}_{SO_3,dry}$	η_{SO_2}	η_{HCl}	η_{SO_3}
			$\frac{mol}{mol}$			10^{-6} $\frac{m^3}{m^3}$				
$Ca(OH)_2$	filter	air	0.0	0.0	1723.8	215.1	-	-	-	-
			0.1	0.3	1721.5	149.1	-	0 %	31 %	-
			0.2	0.7	1702.1	103.3	-	1 %	52 %	-
			0.3	1.0	1689.6	85.6	-	2 %	60 %	-
			0.4	1.5	1634.4	51.5	-	5 %	76 %	-
			0.8	3.0	1516.3	3.5	-	12 %	98 %	-
			1.5	5.9	1265.6	0.2	-	27 %	100 %	-
		O_2/CO_2	0.0	0.0	4576.2	392.7	17.2	-	-	-
			0.03	0.2	4394.5	331.7	-	4 %	16 %	-
			0.05	0.3	4397.9	277.5	1.4	4 %	29 %	92 %

chiometries $\alpha_{Ca/S}$ and $\alpha_{Ca/2Cl}$, acid gas concentrations y_{SO_2}, y_{HCl}, and y_{SO_3}, and corresponding acid gas removal efficiencies η_{SO_2}, η_{HCl}, and η_{SO_3})[66]. This data has been used to generate the plots of this subsection. Additional data on sorbent feed rates and not O_2 corrected acid gas concentrations y_{SO_2}, y_{HCl}, and y_{SO_3} can be found in the annex in tables A.1, A.2, and A.3.

Figure 4.22 shows SO_2 removal efficiencies η_{SO_2} versus the molar Ca/S ratios $\alpha_{Ca/S}$ for the sorbents (a) $CaCO_3$ and (b) $Ca(OH)_2$ and different injection locations. While the injection of sorbents into the furnace gives a similar SO_2 removal at comparable values of $\alpha_{Ca/S}$ in air and CO_2/O_2 combustion atmospheres, a co-injection of the sorbent together with the fuel yields a more efficient capture performance in CO_2/O_2 combustion. An explanation for this behavior could be related to the addition of SO_2 to the oxidant gas that increases the reference SO_2 concentration from approx. 1600 to 1700 $\cdot 10^{-6}$ $\frac{m^3}{m^3}$, dry, in air firing to 4500 to 5000 $\cdot 10^{-6}$ $\frac{m^3}{m^3}$, dry, in CO_2/O_2 combustion. This increase in the partial pressure stabilizes sulfates (see also section 4.1.2), leading to $CaSO_4$ decomposition temperatures of approx. 1225 °C and 1260 °C in air and CO_2/O_2 combustion, respectively. When sorbent is co-injected with the fuel, its sulfation can start earlier in conditions with higher SO_2 partial pressures. This effect was also mentioned by Liu et al. [11]. Based on the temperature profile set in the electrically heated reactor, its geometry, and the volumetric flue gas production, the sulfation reaction in CO_2/O_2 combustion can be estimated to start approx. 0.8 s earlier than in air firing, giving total reaction times in the furnace of approx. 3.4 s and 2.6 s for the two combustion modes. The desulfurization may also be enhanced by an increased porosity of the limestone sorbent when

[66] $y_{SO_3,dry}$ in CO_2/O_2 combustion under reference conditions (i.e. without sorbent injection) was only measured in an experiment separate to the DSI tests. This reference $y_{SO_3,dry}$ value is used in all relevant BTS-VR experiments for calculation of η_{SO_3}.

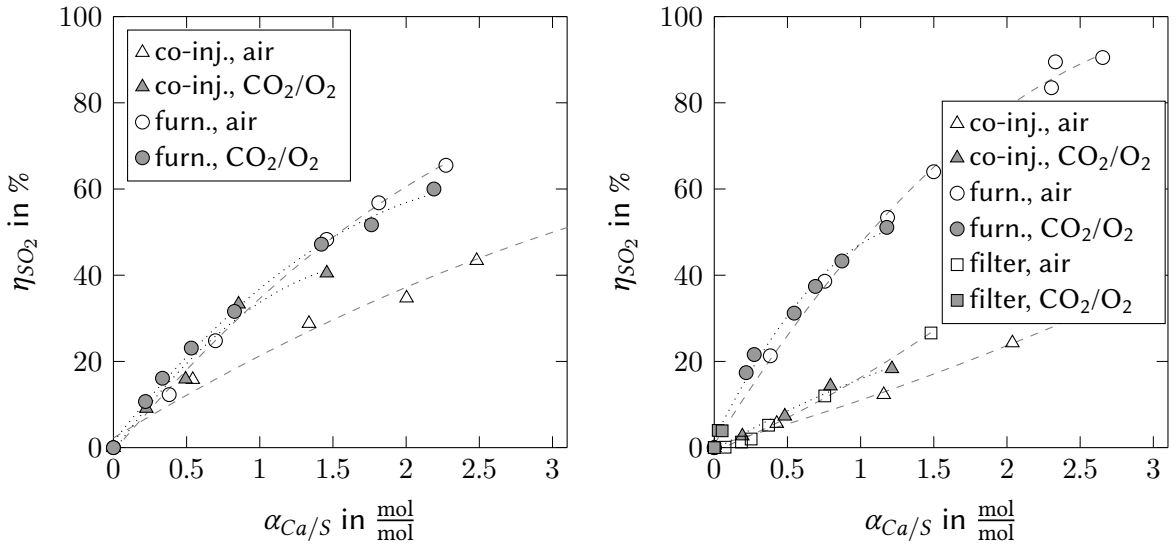

(a) η_{SO_2} for $CaCO_3$ injection

(b) η_{SO_2} for $Ca(OH)_2$ injection

Figure 4.22: η_{SO_2} versus $\alpha_{Ca/S}$ in air and CO_2/O_2 combustion of C4 coal at BTS-VR for (a) $CaCO_3$ and (b) $Ca(OH)_2$ co-injection together with fuel (triangles), injection to the furnace (circles), and injection upstream the fabric filter (squares). Dashed (air) and dotted (CO_2/O_2) trendlines were approximated by a 2nd order polynomial fit.

calcined at elevated CO_2 levels that has been reported by others [25, 107, 108].

An enhanced SO_2 removal performance in CO_2/O_2 combustion cannot be observed in furnace injection experiments. This may be explained by the fact that in these tests, the sorbents were injected at the same location, at a local temperature of 1100 °C, and hence, the time for sorbent sulfation in the furnace was the same in both combustion modes (approx. 1 s). This observation highlights that neither a change of the atmosphere from N_2 to CO_2, nor the increase in the H_2O and SO_2 levels seem to have a considerable impact on the SO_2 capture in furnace conditions when reaction times and temperatures are comparable. Obviously, a positive effect of an increased SO_2 partial pressure on rate limiting steps of the desulfurization reaction (e.g. diffusion) that may be expected seems to be limited in the conducted experiments. This might be related to the relatively high SO_2 capture efficiencies in both combustion modes.

In air firing, for both sorbents furnace injection yields a considerably higher SO_2 removal efficiency than the co-injection of sorbent together with the fuel. The reason for this can likely be found in detrimental effects of sorbent sintering that is known to occur at temperatures above approx. 1100 °C and decreases the sorbent's porosity and reactive surface area [53]. When sorbents are co-injected with the fuel, they are passing through the flame zone in which such temperatures occur. The lower $DeSO_x$ performance of the co-injection with fuel, compared to the furnace injection, is more pronounced for $Ca(OH)_2$ which is characterized by a very high initial surface area. A performance loss compared to furnace injection of up to about 60 percentage points was observed for co-injection of $Ca(OH)_2$ in air firing, compared to approx. 20 percentage points for $CaCO_3$. For $Ca(OH)_2$, the anticipated loss of reactive surface area relates

to a much higher initial level, compared to the $CaCO_3$ sorbent. The loss of sorbent performance in co-injection experiments in CO_2/O_2 is lower than in air firing. This is potentially due to the aforementioned longer time available for sorbent sulfation. For $CaCO_3$ and CO_2/O_2 conditions, η_{SO_2} of co-injection reaches close to the values observed for furnace injection. It should be highlighted that the injection of both sorbents to the furnace at 1100 °C gave a very good SO_2 capture performance. For example, in air firing, 66 % SO_2 capture was reached for $CaCO_3$ (at $\alpha_{Ca/S}$ = 2.3) and 83-89 % for $Ca(OH)_2$ (at $\alpha_{Ca/S}$ = 2.3). These SO_2 capture performances are significantly better than those observed by others in pilot scale experiments [58] where at similar stoichiometries removal efficiencies of about 30-40 % and 50-60 % were observed for $CaCO_3$ and $Ca(OH)_2$ furnace injection, respectively. However, the sorbents in those studies from the late 1980s were potentially less developed than the ones used here and the sorbent dispersion might have been less homogeneous than in the small scale BTS-VR experiments. The high removal efficiencies that might be close to maximum achievable ones in an optimized PF combustion setup indicate that at the BTS-VR facility sorbent dispersion and distribution was very good.

Compared to furnace injection, $Ca(OH)_2$ injection upstream the fabric filter yields only a relatively low SO_2 capture. This is assumed to be caused by a slower reaction of the sorbent with SO_2 at low temperatures, compared to the reactions with HCl and SO_3 that occur preferentially under these conditions. Due to a failure of test equipment, the data basis for $Ca(OH)_2$ injection upstream of the fabric filter in CO_2/O_2 atmospheres is limited to only few experiments at a relatively low $\alpha_{Ca/S}$. η_{SO_2} for these tests is significantly better than for corresponding air fired experiments. This may be related to the much higher SO_2 partial pressures in the CO_2/O_2 experiments. Relatively low SO_2 removal efficiencies for DSI before filter may, to some degree, be also negatively impacted by the high injection and filter temperatures far above the water dew point (see p. 40 for more background information).

Figure 4.23 shows HCl removal efficiencies η_{HCl} determined in the DSI experiments at BTS-VR versus the molar Ca/2Cl ratios $\alpha_{Ca/2Cl}$ for the sorbents (a) $CaCO_3$ and (b) $Ca(OH)_2$ and different injection locations. Obviously, the injection of sorbents to the furnace or co-injection together with the fuel are much less efficient for HCl capture than an injection upstream the fabric filter. While $Ca(OH)_2$ injection upstream the filter gave an almost complete removal of HCl in air fired conditions when $\alpha_{Ca/2Cl}$ was greater than 3, co-injection accomplished only about 6 % in air ($\alpha_{Ca/2Cl}$ = 7.5) and about 1 % ($\alpha_{Ca/2Cl}$ = 7.5) in CO_2/O_2 combustion. $Ca(OH)_2$ injection into the furnace at approx. 1100 °C was somewhat more efficient for controlling HCl, removing in air firing 20 % ($\alpha_{Ca/2Cl}$ = 5.1) and in CO_2/O_2 firing 10 % ($\alpha_{Ca/2Cl}$ = 5.1) of the HCl. The performance of $CaCO_3$ for HCl removal was in both combustion atmospheres for co-injection somewhat higher and for furnace injection somewhat lower than the performance of $Ca(OH)_2$. The HCl removal efficiencies obtained in air firing with injection of $Ca(OH)_2$ upstream the filter are similar but slightly lower than the ones reported by Fitzgerald [164], who used the

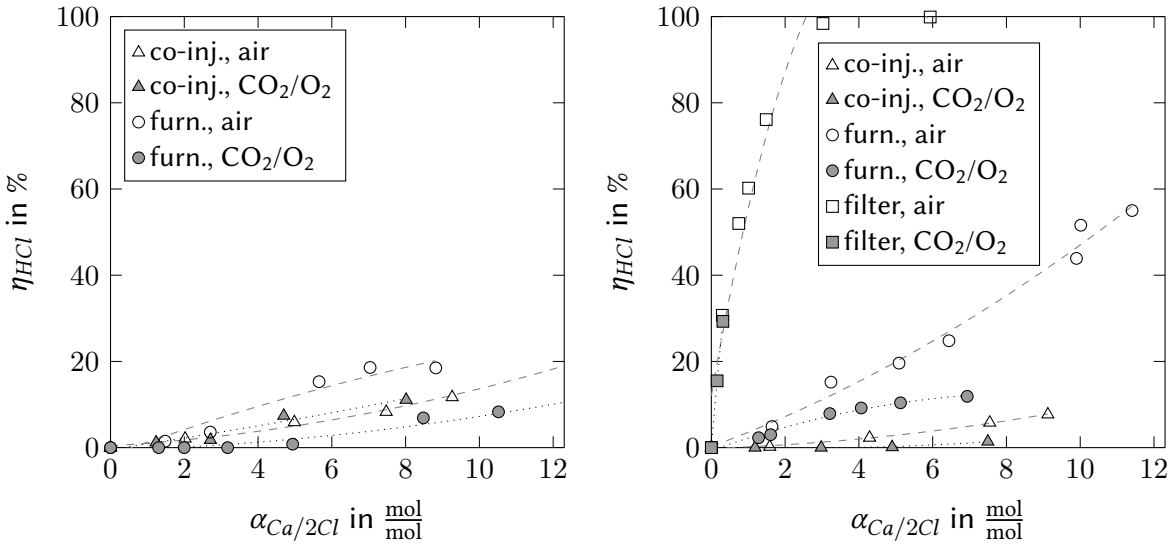

(a) η_{HCl} for $CaCO_3$ injection **(b)** η_{HCl} for $Ca(OH)_2$ injection

Figure 4.23: η_{HCl} versus $\alpha_{Ca/2Cl}$ in air and CO_2/O_2 combustion of C4 coal at BTS-VR for (a) $CaCO_3$ and (b) $Ca(OH)_2$ co-injection together with fuel (triangles), injection to the furnace (circles), and injection upstream the fabric filter (squares). Dashed (air) and dotted (CO_2/O_2) trendlines were approximated by a 2nd order polynomial fit.

same sorbent but potentially had lower SO_2 levels in the gas.

HCl capture is most efficient when injecting the sorbent upstream the fabric filter. At this location, η_{HCl} in both combustion environments is similar. For sorbent co-injection with fuel, where HCl capture is least efficient, the differences between the combustion atmospheres indicate for the $Ca(OH)_2$ based sorbent a slightly better HCl removal performance in air firing while for $CaCO_3$, the capture performances in both combustion modes are similar. For furnace injection, both sorbents showed a much better HCl removal behavior in air fired combustion than in the CO_2/O_2 tests. For $CaCO_3$, the HCl capture performance in air firing is 12 percentage points higher than in CO_2/O_2 combustion (at $\alpha_{Ca/2Cl} \approx$ 8.5-8.8) while for $Ca(OH)_2$, it is by 10 percentage points higher (at $\alpha_{Ca/2Cl}$ = 5.1). The better performance in the air fired experiments may be related to the way the experiments were conducted. In the CO_2/O_2 combustion tests, the oxidant gas was doped with SO_2 but not with HCl. Assuming that SO_2 and HCl are competing for reactions with the sorbent, the considerably increased SO_2 level favors a comparatively faster reaction of this component in the CO_2/O_2 compared to the air experiments. Hence, in the CO_2/O_2 tests more sorbent can be consumed by reactions of SO_2, leaving less unreacted sorbent for capture of HCl. This effect is likely not relevant to actual oxy-fuel recycle combustion. Another observation is that for sorbent co- and furnace injection, the HCl capture becomes more active once the injection stoichiometry exceeds $\alpha_{Ca/S}$ values of approx. 1 (in these experiments $\alpha_{Ca/2Cl}$ was greater 2-5). Presumably, unreacted sorbent that is required for capture of HCl is only available when a certain sorbent excess in respect to SO_2 is provided.

During the DSI experiments at BTS-VR, also a limited number of SO_3 measurements has

been conducted which allows for an assessment of the SO_3 capture performance of DSI in CO_2/O_2 fired conditions. For $Ca(OH)_2$ furnace injection, a SO_3 removal of 24 % and 82 % (equivalent to a $\vartheta_{H_2SO_4,dew}$ reduction of 3 and 17 °C, from $\vartheta_{H_2SO_4,dew}$ of 146 °C without DSI) was observed at $\alpha_{Ca/S}$ = 0.3 and 1.2, respectively. For injection upstream the filter, 92 % SO_3 removal (equivalent to a $\vartheta_{H_2SO_4,dew}$ reduction of 24 °C) was accomplished at $\alpha_{Ca/S}$ = 0.05[67]. Compared to the capture efficiencies given by Blythe and Paradis [171] for air fired operation (i.e. 60-80 % SO_3 removal at a molar Ca/SO_3 ratio of 8-17, depending on lime quality), this capture efficiency is relatively good. $CaCO_3$ furnace injection at $\alpha_{Ca/S}$ = 2.2[68] in CO_2/O_2 combustion yielded a SO_3 removal efficiency of 97 % (equivalent to a $\vartheta_{H_2SO_4,dew}$ reduction by 32 °C). These results indicate that if the main focus of DSI is to control SO_3 levels while maintaining a minimal sorbent consumption, $Ca(OH)_2$ should be injected upstream a filter. When sorbents are injected to the furnace, an excess of sorbent in respect to SO_2 is required to obtain high SO_3 removal efficiencies. Additional experiments by the author of this thesis with other $Ca(OH)_2$ based sorbents showed an analog behavior (see [37]). The observations in respect to SO_3 are similar to the ones concerning HCl capture. In the conducted tests at BTS-VR, a high SO_3 capture (above 65 %) was always found when at the same time HCl capture was significant (i.e. above 10-30 %). With a fuel, such as coal C4 that contains a significant amount of chlorine, HCl capture efficiency (that is much easier to determine than SO_3 capture) could serve as an indication to control the sorbent injection rate towards SO_3. Such an approach is also supported by the higher reactivity of SO_3 with the injected calcium based sorbents, compared to HCl that has been reported by others [162–164].

Summary of small scale test results on SO_2, SO_3, and HCl capture: To conclude this section on DSI tests for SO_2, SO_3, and HCl removal at BTS-VR, it can be stated that the capture of different acid gases by DSI should always be comprehensively evaluated, since competing reactions may otherwise cause misinterpretations. For a coal that is rich in sulfur and chlorine, such as the one used in this study, the measurement of both major acid gas components, SO_2 and HCl, is important to obtain a full picture of the acid gas removal performance. It was shown that SO_2 capture is most efficient at high temperatures (i.e. furnace injection at 1100 °C) and hence, if SO_2 is the target component, injection at lower temperatures may be less suitable. The opposite is true for the control of HCl and SO_3. Nonetheless, one can expect to remove all mentioned acid gases at any of the injection locations, e.g. efficient SO_2 capture for furnace injection and at the same time a significant HCl and SO_3 removal as a co-benefit.
Similar to the modeling results by Liu et al. [11], the experiments at BTS-VR showed that increased SO_2 concentration levels can have a beneficial effect on the SO_2 removal efficiency in CO_2/O_2 combustion. This effect seems to be related to the increased sulfate stability at high SO_2 partial pressures. It was only effective in the sorbent co-injection experiments

[67] $\alpha_{Ca/S}$ relates to SO_2 not to SO_3 in the flue gas. On a SO_3 basis the value is about 4.4.
[68] $\alpha_{Ca/S}$ relates to SO_2 not to SO_3 in the flue gas.

where an increased sulfate stability relates to an extended sulfation time. DSI to the furnace experiments, in which the reaction time in both experimental conditions were effectively the same, yielded very similar SO_2 removal efficiencies for air and CO_2/O_2 combustion, indicating that altered flue gas atmospheres and particularly the increased SO_2 levels are not significantly impacting the SO_2 removal efficiency for this injection point. This also implies that oxy-fuel combustion systems with a low flue gas recirculation ratio or without flue gas recirculation[69] that apply DSI to the furnace at around 1100 °C may not benefit to a large extent from higher SO_2 concentrations that are present in such systems (with a significant flue gas recycle this is different, see section 4.2.2.3). Depending on the available reaction time for desulfurization in such combustion systems, the desulfurization performance might be similar or only slightly better than in corresponding air fired systems.
The differences between combustion modes observed in respect to HCl capture (i.e. better performance in air firing) are likely related to the experimental methodology, simulating oxy-fuel recycle combustion by SO_2 but not HCl addition to the oxidant gas and should not be overrated. Results on SO_2 capture performances from experiments with CO_2/O_2 combustion cannot be directly compared to oxy-fuel recycle combustion since in the BTS-VR test rig flue gas was not recirculated. In the conducted experiments, acid gas capture by DSI has no feedback to the initial acid gas concentrations in the furnace and practical reaction times of acid gas molecules are not comparable to an oxy-fuel recycle system.
Investigations in respect to SO_3 removal by DSI showed that the technique can be a very effective measure to control this problematic component and the corresponding H_2SO_4 dew point temperature. It was observed that for the used high chlorine coal a high SO_3 capture efficiency was always associated to a significant HCl capture (i.e. above 10-30 %).

4.2.2.3 DSI in air and oxy-fuel recycle combustion

SO_2, HCl, and SO_3 control: To obtain information on the performance of DSI in oxy-fuel recycle combustion, experiments have been carried out at the KSVA facility. In these tests, the same sorbents ($CaCO_3$ and $Ca(OH)_2$) and comparable injection locations as at the smaller BTS-VR facility were used (i.e. co-injection with fuel, injection to the furnace at approx. 1100 °C, and injection upstream an ESP system). The DSI experiments were carried out under air and oxy-fuel recycle conditions firing the coal C4. Due to the results from small scale tests, focus was put on furnace injection for SO_2 control and low temperature injection before ESP for HCl capture. In addition, co-injection of $CaCO_3$ for SO_2 control was tested.
Table 4.6 summarizes key parameters and results of all DSI experiments conducted at KSVA (i.e. used sorbents, injection locations, combustion modes, sorbent injection stoichiometries $\alpha_{Ca/S}$ and $\alpha_{Ca/2Cl}$, acid gas concentrations y_{SO_2}, y_{HCl}, and y_{SO_3}, and corresponding acid gas

[69] E.g. staged oxy-fuel combustion concepts.

Table 4.6: Gas concentrations (after ESP, recalculated to 3 / 4 · 10^{-2} $\frac{m^3}{m^3}$, dry, O_2 for air / oxy; see p. 80) and removal efficiencies for SO_2, HCl, and SO_3 in DSI experiments at KSVA.

Sorb.	Injec.	Mode	$\alpha_{Ca/S}$	$\alpha_{Ca/2Cl}$	$\bar{y}_{SO_2,dry}$	$\bar{y}_{HCl,dry}$	$\bar{y}_{SO_3,dry}$	η_{SO_2}	η_{HCl}	η_{SO_3}
			$\frac{mol}{mol}$			10^{-6} $\frac{m^3}{m^3}$				
$CaCO_3$	co-injection	air	0.0	0.0	1607.2	213.0	-	-	-	-
			0.8	3.2	1285.0	219.4	-	20 %	0 %	-
			1.9	7.1	970.4	202.5	-	40 %	5 %	-
			2.7	10.3	740.2	197.3	-	54 %	7 %	-
		oxy	0.0	0.0	4739.0	615.7	-	-	-	-
			0.9	3.5	3582.9	583.8	-	24 %	5 %	-
			2.1	7.9	2317.4	520.8	-	51 %	15 %	-
			3.0	11.5	1276.6	509.1	-	73 %	17 %	-
	furnace	air	0.0	0.0	1537.5	226.5	-	-	-	-
			0.9	3.0	1181.2	218.4	-	23 %	4 %	-
			2.0	6.7	815.4	195.6	-	47 %	14 %	-
			2.9	9.7	664.1	188.8	-	57 %	17 %	-
		oxy	0.0	0.0	4801.9	555.5	-	-	-	-
			0.9	3.9	2985.3	523.6	-	38 %	6 %	-
			2.0	8.8	1533.2	487.7	-	68 %	12 %	-
			2.9	12.7	859.5	423.8	-	82 %	24 %	-
$Ca(OH)_2$	furnace	air	0.0	0.0	1511.0	212.0	5.9	-	-	-
			0.4	1.6	1242.9	209.4	-	18 %	1 %	-
			1.0	3.6	971.5	203.6	0.4	36 %	4 %	94 %
			1.6	5.8	848.0	195.6	-	44 %	8 %	-
		oxy	0.0	0.0	4617.6	533.1	4.3	-	-	-
			0.5	-	3290.1	-	-	29 %	-	-
			1.1	4.6	1861.8	487.2	0.8	60 %	9 %	82 %
			1.7	7.4	1236.2	462.5	-	73 %	13 %	-
	ESP	air	0.0	0.0	1583.4	241.2	5.9	-	-	-
			0.2	0.8	1570.0	140.8	-	1 %	42 %	-
			0.3	1.1	1546.4	80.9	0.5	2 %	66 %	92 %
			0.5	1.7	1508.2	52.6	-	5 %	78 %	-
		oxy	0.0	0.0	5023.1	524.2	-	-	-	-
			0.3	1.3	5017.4	245.5	-	0 %	53 %	-
			0.4	1.9	4802.1	125.8	-	4 %	76 %	-
			0.6	2.8	4095.2	78.8	-	18 %	85 %	-

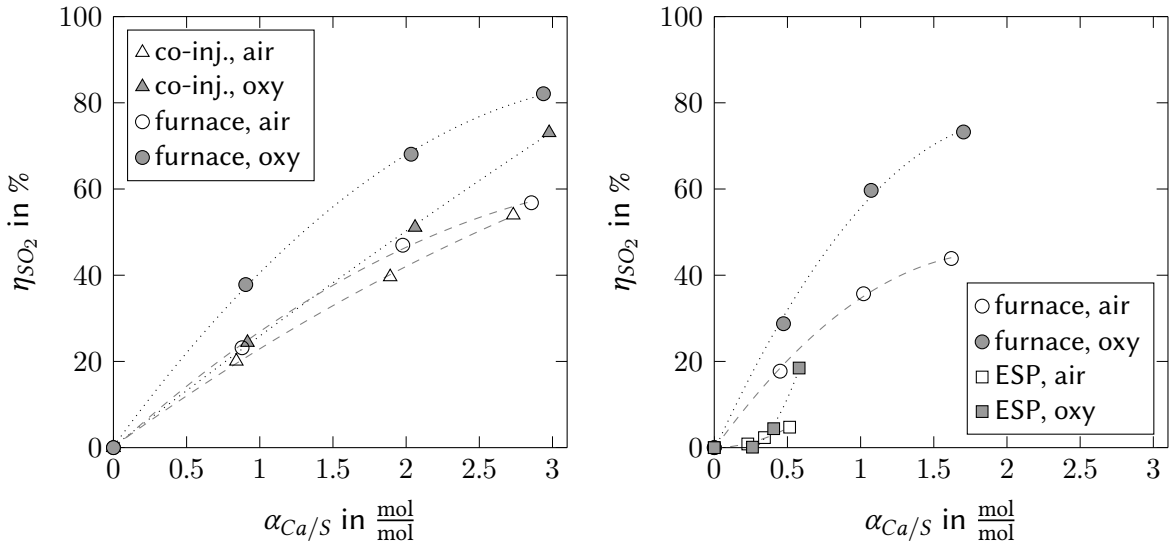

(a) η_{SO_2} for $CaCO_3$ injection

(b) η_{SO_2} for $Ca(OH)_2$ injection

Figure 4.24: η_{SO_2} versus $\alpha_{Ca/S}$ in air and oxy-fuel recycle combustion of coal C4 at KSVA for (a) $CaCO_3$ co-injection together with fuel and injection to the furnace and (b) $Ca(OH)_2$ injection to the furnace and upstream ESP. Dashed (air) and dotted (oxy-fuel) trendlines were approximated by a 2nd order polynomial fit.

removal efficiencies η_{SO_2}, η_{HCl}, and η_{SO_2})[70]. This data has been used to generate the plots of this subsection. Additional data on sorbent feed rates and not O_2 corrected acid gas concentrations y_{SO_2}, y_{HCl}, and y_{SO_3} can be found in the annex in table A.4.

Figure 4.24 shows η_{SO_2} versus $\alpha_{Ca/S}$ results for the sorbents (a) $CaCO_3$ and (b) $Ca(OH)_2$ for different injection locations and for air and oxy-fuel recycle combustion. It is obvious that in all experiments SO_2 capture in oxy-fuel was significantly better than in air firing. This performance gain of DSI under oxy-fuel conditions is likely related to the beneficial effect that the recycle combustion has on gas cleaning processes (see section 4.1.3). For $CaCO_3$ and $Ca(OH)_2$ furnace injection, η_{SO_2} was increased by up to 25 (at $\alpha_{Ca/S}$ = 2.9) and 29 percentage points (at $\alpha_{Ca/S}$ = 1.7), respectively, while for co-injection of $CaCO_3$ with the fuel, the enhancement amounted up to 19 percentage points (at $\alpha_{Ca/S}$ = 2.7-3.0). The SO_2 capture performance at KSVA in air firing was significantly lower than at BTS-VR (see more detailed discussion on p. 133) which may likely be related to an imperfect sorbent dispersion at the KSVA rig. However, the $DeSO_x$ performances for in-furnace injection of $Ca(OH)_2$ were within the ranges reported in the late 1980s by Muzio et al. [57] and Often et al. [58] from pilot scale DSI tests. The results of this thesis with $CaCO_3$ injection to the furnace at approx. 1100 °C are somewhat higher than the performances reported by these authors (i.e. at $\alpha_{Ca/S}$ = 2: 47 % vs. 20-40 %). The results in respect to $CaCO_3$ co-injection in air firing obtained in this thesis are better than the ones reported from tests at a full scale pulverized lignite fired boiler by Kirchen [102] (i.e.

[70] $y_{SO_3,dry}$ in air firing under reference conditions (i.e. without sorbent injection) was only measured in the $Ca(OH)_2$ ESP injection reference experiment. For calculation of η_{SO_3} in the air fired experiment with $Ca(OH)_2$ furnace injection, the same $y_{SO_3,dry}$ reference is used.

at $\alpha_{Ca/S}$ = 1.9: 40 % vs. approx. 30 %). Despite potentially non-optimal sorbent injection, a very efficient SO_2 removal, even at moderate $\alpha_{Ca/S}$ ratios, was observed under oxy-fuel recycle conditions, reaching desulfurization efficiencies of 51 % ($CaCO_3$ co-injection at $\alpha_{Ca/S}$ = 2.1), 68 % ($CaCO_3$ furnace injection at $\alpha_{Ca/S}$ = 2.0), and 73 % ($Ca(OH)_2$ furnace injection at $\alpha_{Ca/S}$ = 1.7). The highest SO_2 removal efficiency that could be demonstrated under oxy-fuel conditions reached 82 % ($CaCO_3$ furnace injection at $\alpha_{Ca/S}$ = 2.9).

As in the experiments at BTS-VR, injection of $Ca(OH)_2$ to the furnace yielded a better desulfurization performance than $CaCO_3$. It was by 13 and 22 percentage points better in air and oxy-fuel firing, respectively, at a low $\alpha_{Ca/S}$ of 0.9-1.1. At higher values of $\alpha_{Ca/S}$ of 1.6-2.0, the performance gain was less significant with only 3-5 percentage points. However, these results may also be negatively influenced by the non-optimal sorbent dispersion during in-furnace injection. The non-optimal dispersion might be more pronounced for $Ca(OH)_2$ since this sorbent is more sticky and more difficult to disperse, compared to $CaCO_3$. From an economic point of view, utilization of $CaCO_3$ in DSI might be very interesting for oxy-fuel recycle operation due to its relatively good desulfurization performance, its lower price compared to $Ca(OH)_2$, and to the possibility to inject it using CO_2 as carrier gas. Nonetheless, specific benefits of $Ca(OH)_2$, such as a lower sorbent consumption and a lower generation of by-products to reach a specific degree of desulfurization, remain similar to conventional air firing. Moreover, the maximum desulfurization that can be reached with $Ca(OH)_2$ at moderate sorbent injection stoichiometries (i.e. $\alpha_{Ca/S}$ up to approx. 3-4) is likely somewhat higher.

Similarly to the observations during the experiments at BTS-VR, co-injection of $CaCO_3$ is less efficient in respect to SO_2 removal than injection to the furnace. This is likely related to a reduction of the sorbent's reactive surface by sintering reactions that take place at high temperatures when sorbent particles pass the flame zone. The difference between both injection locations in air firing is less pronounced (i.e. 3-7 percentage points) than in oxy-fuel recycle combustion (9-17 percentage points). This may be related to the imperfect sorbent dispersion that is assumed for the injection to the furnace (see p. 133). Co-injection with the fuel presumably did not suffer from this issue. In oxy-fuel combustion, the non-optimal sorbent dispersion seems to be compensated to some extent by the beneficial effects that the recycle combustion has on the desulfurization performance (see section 4.1.3).

The injection of $Ca(OH)_2$ upstream the KSVA's ESP system was only tested up to relatively low values of $\alpha_{Ca/S}$ of 0.5-0.6. The reason for this is that the main focus of the DSI experiments at this injection location was HCl capture which, due to the HCl levels, requires less sorbent. One can observe that SO_2 removal has only been considerable when a certain excess of sorbent in respect to HCl (i.e. $\alpha_{Ca/2Cl}$ > 1.5) was used. This trend is similar in air and oxy-fuel combustion. Given the very effective HCl removal at low $\alpha_{Ca/2Cl}$ values (see fig. 4.25 and 4.27), the explanation for this behavior is likely that with such low injection stoichiometries most of the sorbent is consumed by HCl capture and almost no reactive sorbent is left for the capture of SO_2. At

higher $\alpha_{Ca/2Cl}$ values, enough unreacted sorbent is available to allow for a more efficient SO_2 removal. For a fairer comparative assessment of the conducted experiments with $Ca(OH)_2$ injection to the furnace and upstream ESP for SO_2 removal, the assumption of a certain offset in respect to the $\alpha_{Ca/S}$ stoichiometry in the tests with injection upstream the ESP (in the range of $\alpha_{Ca/S} \approx 0.4$) may be sensible. Since no experiments have been conducted at higher $\alpha_{Ca/S}$ levels, no reliable statement can be given in respect to a more extensive SO_2 removal at this injection location. The relatively high SO_2 removal efficiency of 18 % at $\alpha_{Ca/S}$ = 0.6 in oxy-fuel recycle conditions might however indicate a more efficient SO_2 capture than in the BTS-VR experiments with $Ca(OH)_2$ injection upstream the fabric filter. As at BTS-VR, at KSVA, the SO_2 removal efficiency was possibly also negatively impacted by the relatively high injection and ESP temperatures far above the water dew point ($\vartheta_{ESP_{in}}$: air - 205 °C; oxy-fuel - 219 °C; see also p. 40 for more background information).

Figure 4.25 shows η_{HCl} levels in air and oxy-fuel combustion versus $\alpha_{Ca/2Cl}$ for the sorbents (a) $CaCO_3$ and (b) $Ca(OH)_2$ and different injection locations. As indicated above, the injection of $Ca(OH)_2$ upstream ESP has been very efficient for HCl removal in both combustion modes, reaching HCl removal efficiencies of 78 % (at $\alpha_{Ca/2Cl}$ = 1.7) and 76 % (at $\alpha_{Ca/2Cl}$ = 1.9) in air and oxy-fuel operation, respectively. The HCl capture performance in the air fired experiment was similar but slightly lower than the one reported by Fitzgerald for the same sorbent [164]. The difference is likely related to the different experimental conditions. The maximum HCl removal efficiency measured during oxy-fuel combustion was 85 % (at $\alpha_{Ca/2Cl}$ = 2.8) and the capture behavior in respect to the injection stoichiometry indicates that removal efficiencies higher than

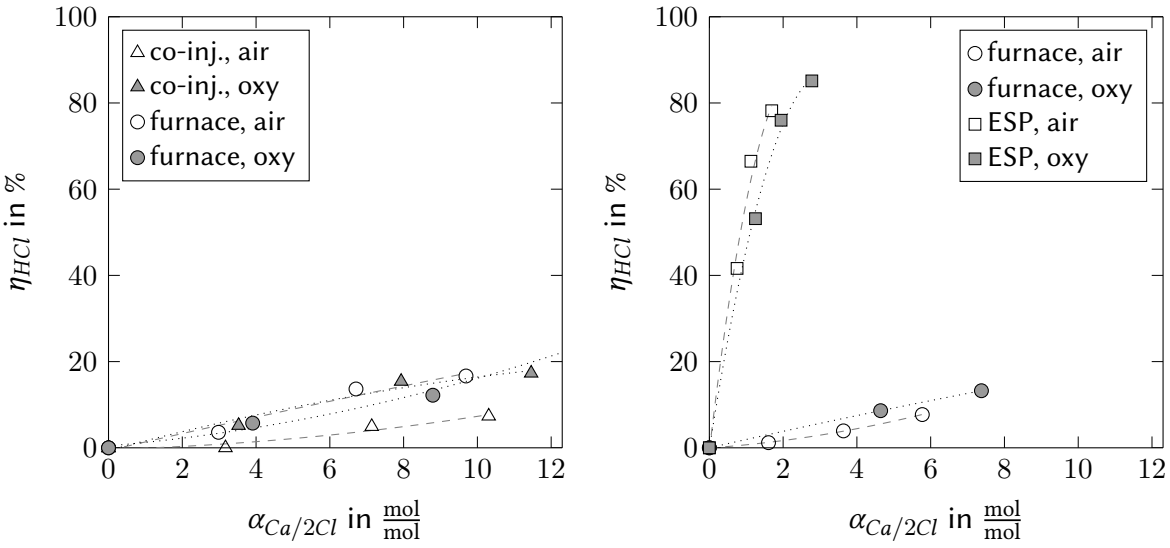

(a) η_{HCl} for $CaCO_3$ injection **(b)** η_{HCl} for $Ca(OH)_2$ injection

Figure 4.25: η_{HCl} versus $\alpha_{Ca/2Cl}$ in air and oxy-fuel recycle combustion of coal C4 at KSVA for (a) $CaCO_3$ co-injection together with fuel and injection to the furnace and (b) $Ca(OH)_2$ injection to the furnace and upstream ESP. Dashed (air) and dotted (oxy-fuel) trendlines were approximated by a 2nd order polynomial fit.

90 % are possible in air and oxy-fuel conditions when injecting moderately more sorbent (i.e. $\alpha_{Ca/2Cl}$ up to approx. 4). For the $Ca(OH)_2$ injection upstream ESP, no considerable difference in HCl capture was observed between air and oxy-fuel recycle combustion (the difference between both experiments is not considered significant in comparison to experimental uncertainties; See section 3.3.3.3). It might be that the HCl capture with the tested sorbent is close to its practical maximum (i.e. further reaction is hindered by large diffusional resistances). Potentially this is the reason why, different to other injection locations and SO_2 capture, no enhancement of the HCl removal performance by oxy-fuel recycle combustion was observed.

Injection of $Ca(OH)_2$ and $CaCO_3$ to the furnace of KSVA yielded a relatively low HCl removal efficiency since the majority of the sorbent seems to be consumed by reactions with SO_2. This is in agreement with observations by Partanen et al. [180] in TGA and Lin and Chyang [181] in fixed bed studies, even though, in these tests only temperatures up to 850 °C were considered. The HCl capture performance of furnace injection of $CaCO_3$ was superior to $Ca(OH)_2$. In air firing, $CaCO_3$ and $Ca(OH)_2$ reached 14 % (at $\alpha_{Ca/2Cl}$ = 6.7) and 8 % (at $\alpha_{Ca/2Cl}$ = 5.8) HCl removal, while under oxy-fuel fired conditions 12 % (at $\alpha_{Ca/2Cl}$ = 8.8) and 13 % (at $\alpha_{Ca/2Cl}$ = 7.4) were reached. The better performance of $CaCO_3$ furnace injection for HCl capture may be related to this sorbent's lower desulfurization efficiency that leaves more unreacted CaO for reactions with HCl that take place downstream of the furnace. This implies that under certain conditions that the sorbent experiences, while traveling along the flue gas path, important steps of HCl capture (i.e. diffusion through pores and product layers, reaction with CaO) are more efficient than corresponding ones for SO_2. The co-injection of $CaCO_3$ together with the fuel yielded a lower HCl capture efficiency than furnace injection, reaching 5 % (at $\alpha_{Ca/2Cl}$ = 7.1) and 15 % (at $\alpha_{Ca/2Cl}$ = 7.9) capture in air and oxy-fuel combustion, respectively. In all experiments with co-injection and furnace injection of sorbents, a tendency of better HCl removal under oxy-fuel conditions was observed that is again likely related to the beneficial effect that recycle combustion has on DSI performance (see section 4.1.3).

During some of the DSI experiments at KSVA, also SO_3 reduction has been assessed. It was found that SO_3 can be efficiently reduced (capture > 80 %) as a co-benefit when injecting $Ca(OH)_2$ to the furnace ($\alpha_{Ca/S}$ = 1.0-1.1) and upstream ESP ($\alpha_{Ca/2Cl}$ = 1.1) for SO_2 and HCl capture. However, in all these experiments, very high molar Ca/SO_3 ratios were used (the lowest α_{Ca/SO_3} level - for injection upstream ESP - was about 94, but the target in these tests was HCl at much higher levels than SO_3). The limited availability of experimental results does not allow for a reliable conclusion whether the performance of DSI for SO_3 control is significantly different in air and oxy-fuel operation. It is however obvious that if SO_3 is the main target component to be controlled by DSI, one should focus on DSI before the ESP system since this allows for a maximum SO_3 capture at a moderate sorbent consumption. At the various tested injection locations and combustion modes, DSI of $Ca(OH)_2$ allowed to reduce SO_3 from a level of $5.9 \cdot 10^{-6}$ $\frac{m^3}{m^3}$, dry, (equivalent to $\vartheta_{H_2SO_4,dew}$ = 128 °C) and $4.3 \cdot 10^{-6}$ $\frac{m^3}{m^3}$, dry, (equivalent to

$\vartheta_{H_2SO_4,dew}$ = 129 °C) in air and oxy-fuel conditions, respectively, down to below $1 \cdot 10^{-6}$ $\frac{m^3}{m^3}$, dry. The reduction was equivalent to lowering $\vartheta_{H_2SO_4,dew}$ in the flue gas by 26 to 28 °C in air and by 17 °C in oxy-fuel firing.

Summary of pilot scale results on SO_2, SO_3, and HCl capture: To sum up the results on DSI in air and oxy-fuel recycle combustion, it can be stated that, similar to the small scale experiments, for removal of SO_2 an injection of sorbents to the furnace or together with the fuel is most effective in both combustion modes, while an injection at lower temperatures is more suitable for controlling HCl and SO_3. Nonetheless, a considerable removal of all three acid gases was observed at any of the injection locations. One of the most important results of the comparative air and oxy-fuel recycle experiments is that the removal of SO_2 in oxy-fuel recycle combustion is considerably enhanced, compared to air firing. This is consistent to the predictions in section 4.1.3 and by others [11]. An improvement of η_{SO_2} by as much as 29 percentage points has been found in the experiments. Particularly, the SO_2 capture by DSI of $CaCO_3$ and $Ca(OH)_2$ together with the fuel or to the furnace under oxy-fuel combustion conditions has been proven to be very effective, allowing a capture of 50 % to more than 80 % of the SO_2 with moderate $\alpha_{Ca/S}$ levels between 1.1 and 2.9. Even the co-injection of $CaCO_3$ together with the fuel, which is potentially one of the simplest, cheapest, and expectedly least effective methods for DSI, reached a SO_2 capture efficiency of 73 % (at $\alpha_{Ca/S}$ = 3). This illustrates the large potential that the DSI technology has for acid gas control in oxy-fuel recycle combustion. Besides a reduction of SO_2 levels, also HCl and SO_3 can be controlled very efficiently, either as a co-benefit when reducing SO_2 levels by co-injection and injection to the furnace, or by a dedicated HCl control via DSI upstream an ESP system, which yielded in the range of 76-78 % HCl reduction in air and in oxy-fuel combustion (at $\alpha_{Ca/2Cl}$ = 1.7-1.9). Injection of $Ca(OH)_2$ to the furnace and upstream the ESP allowed for a reduction of SO_3 levels in air and oxy-fuel combustion down to below $1 \cdot 10^{-6}$ $\frac{m^3}{m^3}$, dry, with corresponding $\vartheta_{H_2SO_4,dew}$ levels below 112 °C. This is well in the range of $\vartheta_{H_2SO_4,dew}$ values that can be coped with in existing air fired power plants.

Comparative assessment of air fired DSI performance at BTS-VR and KSVA: At both facilities, KSVA and BTS-VR, flue gas residence times and temperature profiles were different, with longer flue gas residence times in the furnace of KSVA. This may have influenced the observed DSI performances. Nonetheless, results from the relatively similar air fired DSI experiments from both facilities are compared in the following. In figures 4.26 and 4.27, the SO_2 and HCl removal performances for injection of $CaCO_3$ and $Ca(OH)_2$ at various locations in air firing of C4 coal at the 500 kW facility KSVA and the 20 kW facility BTS-VR are plotted for direct comparison.

One can observe different trends for the different injection locations. While co-injection of $CaCO_3$ with the fuel yields a similar performance in both reactors, with slightly better η_{SO_2}

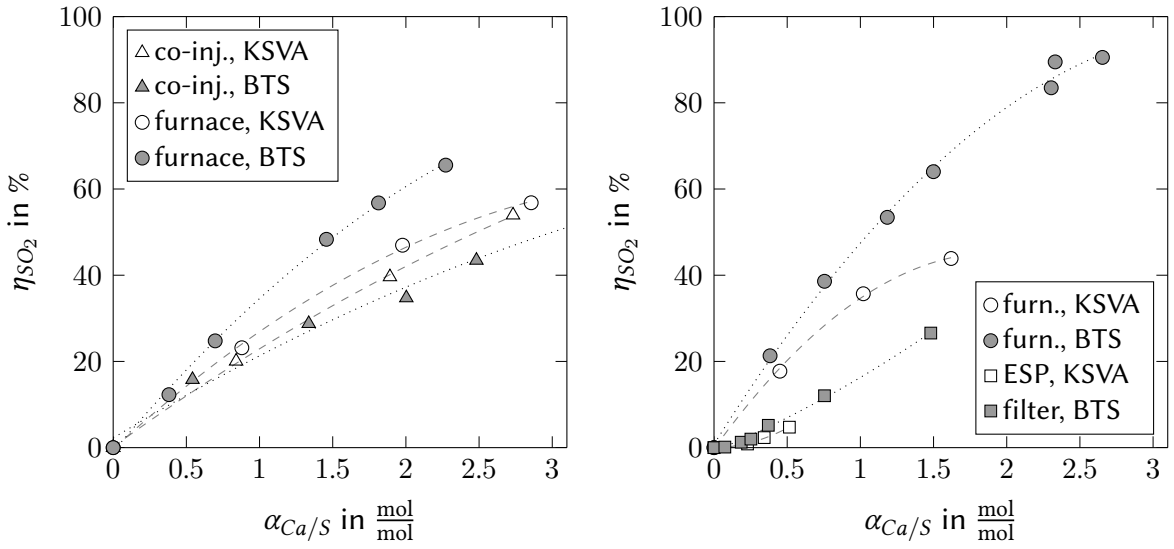

(a) η_{SO_2} for $CaCO_3$ injection **(b)** η_{SO_2} for $Ca(OH)_2$ injection

Figure 4.26: Comparison of η_{SO_2} versus $\alpha_{Ca/S}$ values from air firing of coal C4 at KSVA and BTS-VR for (a) $CaCO_3$ co-injection together with fuel and injection to the furnace and (b) $Ca(OH)_2$ injection to the furnace and upstream ESP (KSVA) or fabric filter (BTS). Dashed (KSVA) and dotted (BTS-VR) trendlines were approximated by a 2nd order polynomial fit.

at KSVA, with in-furnace injection at BTS-VR, generally, a significantly better SO_2 removal performance (10-30 percentage points) than at KSVA was accomplished. Also the HCl removal at a similar $\alpha_{Ca/2Cl}$ when injecting $Ca(OH)_2$ to the furnace was much more efficient at BTS-VR. Most likely, the reason for the differences in the two very similar experiments was a less homogeneous sorbent dispersion for furnace injection at KSVA, compared to BTS-VR. Due to the differences in size and accessibility of the two test furnaces, the sorbents could not be injected in exactly the same way. While at BTS-VR, the sorbent was injected to the furnace in counter-current flow direction with the sorbent probe introduced upwards via the furnace exit, at KSVA the sorbent had to be injected via a lateral port in orthogonal direction in respect to the flue gas flow. Even though this has not been studied in detail, it can be assumed that the counter-current injection leads to a better and more homogeneous mixing of flue gas and sorbent which ultimately gives a better SO_2 removal performance. The results highlight that proper sorbent dispersion is very important for an optimal acid gas removal by DSI. An explanation for the similar SO_2 capture performance at KSVA and BTS-VR when co-injecting $CaCO_3$ together with the fuel can be found in a similar quality of dispersion in those experiments in which sorbents were fed in a very similar way.

An interesting observation can be made when comparing η_{HCl} with $Ca(OH)_2$ injection upstream the ash removal devices of KSVA and BTS-VR (figure 4.27). Even though, both facilities use different ash removal equipment (i.e. ESP at KSVA, fabric filter at BTS-VR), the HCl removal performance at both systems is very similar. This may indicate that if sufficiently active sorbent is available upstream of the dust separation system, the HCl capture proceeds very rapidly in

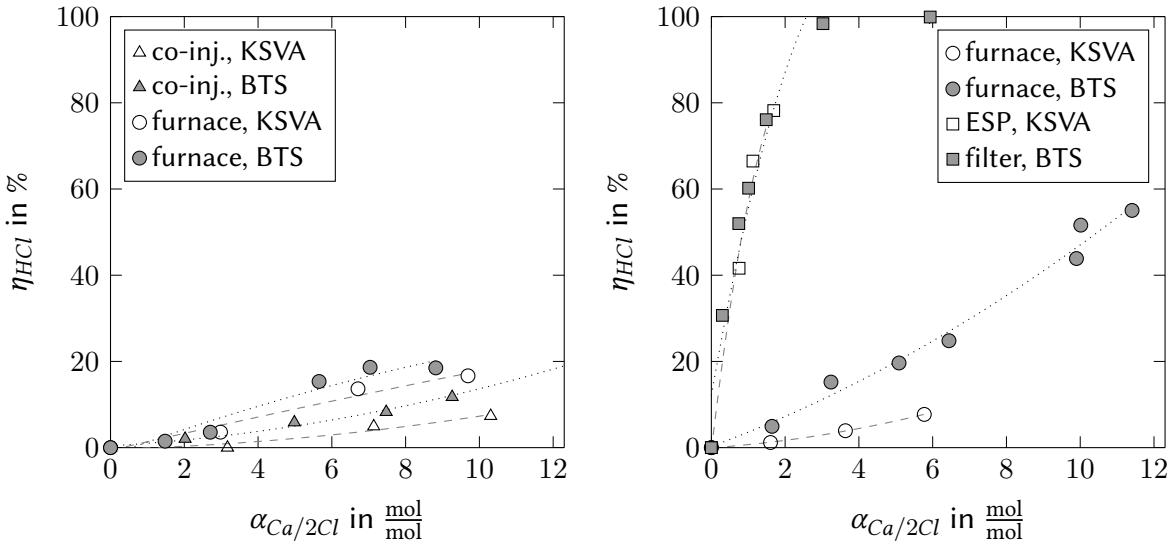

(a) η_{HCl} for $CaCO_3$ injection **(b)** η_{HCl} for $Ca(OH)_2$ injection

Figure 4.27: Comparison of η_{HCl} versus $\alpha_{Ca/2Cl}$ values from air firing of coal C4 at KSVA and BTS-VR for (a) $CaCO_3$ co-injection together with fuel and injection to the furnace and (b) $Ca(OH)_2$ injection to the furnace and upstream ESP (KSVA) or fabric filter (BTS). Dashed (KSVA) and dotted (BTS-VR) trendlines were approximated by a 2nd order polynomial fit.

entrained conditions rather than after precipitation or deposition of the particles. Otherwise, the similarly efficient HCl separation at a fabric filter and at an ESP system that allows only for a minimal contact of particles deposited at collector plates and HCl in the gas, can hardly be explained. This is also in agreement with observations in respect to the dynamics of HCl capture at BTS-VR's fabric filter. When injecting $Ca(OH)_2$ to this unit, a constant HCl concentration level (e.g. 60 % reduction from the initial level) was reached very rapidly after approx. 1 min, and after stopping the sorbent injection, the initial HCl level was established also with only a small delay (below 5 min). This indicates that $Ca(OH)_2$ deposited on the filter plays only a minor role in the HCl capture and most of the capture happens very rapidly, presumably, while the sorbent is still entrained in the flue gas. Experiments at BTS-VR with finely milled Trona (a sodium carbonate mineral) showed a very different behavior than with $Ca(OH)_2$ requiring a relatively long time to reach stable HCl concentrations at the filter outlet. This indicates a much slower reaction that also takes place to a large extent with sorbent deposited on the filter (see: [37, 48]).

Comparison of air and oxy-fuel once-through desulfurization performance at KSVA: In section 4.1.3, fundamentals of desulfurization in oxy-fuel recycle environments were introduced. Amongst other details, the concept of a once-through desulfurization efficiency $\eta_{S,o-t}$ (equation 4.12), the variability of the sulfur level at the furnace inlet $y_{S,furn,in}$ (equation 4.14) depending on the extent of sulfur removal, and a once-through molar Ca/S ratio $\alpha_{Ca/S,o-t}$ that is

Table 4.7: Equivalent SO_2 concentrations at furnace inlet $y_{SO_2,furn,in}$ (recalculated to 3 / $4 \cdot 10^{-2}$ $\frac{m^3}{m^3}$, dry, O_2 for air / oxy-fuel; see p. 80), once-through and recycle SO_2 removal efficiencies $\eta_{S,o-t}/\eta_{S,rec}$ (air: $\eta_{S,o-t} = \eta_{S,rec}$), and once-through and recycle molar Ca/S ratios $\alpha_{Ca/S,o-t}/\alpha_{Ca/S,rec}$ (air: $\alpha_{Ca/S,o-t} = \alpha_{Ca/S,rec}$) determined for DSI experiments at KSVA.

Sorbent	Injection	air			oxy-fuel				
		$\alpha_{Ca/S,o-t}$		$y_{SO_2,furn,in}$	$\alpha_{Ca/S,rec}$		$\alpha_{Ca/S,o-t}$		$y_{SO_2,furn,in}$
		$\frac{mol}{mol}$	$\eta_{S,o-t}$	10^{-6} $\frac{m^3}{m^3}$, dry	$\frac{mol}{mol}$	$\eta_{S,rec}$	$\frac{mol}{mol}$	$\eta_{S,o-t}$	10^{-6} $\frac{m^3}{m^3}$, dry
$CaCO_3$	co-injection	0.0	-	1607.2	0.0	-	0.0	-	4739.0
		0.8	20 %		0.9	24 %	0.5	14 %	4161.0
		1.9	40 %		2.1	51 %	1.3	34 %	3528.2
		2.7	54 %		3.0	73 %	2.2	58 %	3007.8
	furnace	0.0	-	1607.2	0.0	-	0.0	-	4801.9
		0.9	23 %		0.9	38 %	0.5	23 %	3893.6
		2.0	47 %		2.0	68 %	1.5	52 %	3167.5
		2.9	57 %		2.9	82 %	2.4	70 %	2830.7
$Ca(OH)_2$	furnace	0.0	-	1607.2	0.0	-	0.0	-	4617.6
		0.4	18 %		0.5	29 %	0.3	17 %	3953.8
		1.0	36 %		1.1	60 %	0.7	43 %	3239.7
		1.6	44 %		1.7	73 %	1.3	58 %	2926.9
	ESP	0.0	-	1607.2	0.0	-	0.0	-	5023.1
		0.2	1 %		0.3	0 %	0.1	0 %	5020.3
		0.3	2 %		0.4	4 %	0.2	2 %	4912.6
		0.5	5 %		0.6	18 %	0.3	10 %	4559.1

calculated on basis of $y_{S,furn,in}$[71] were introduced. Those parameters allow for a comparison of the performance of DSI in air and oxy-fuel conditions without the effect of flue gas recirculation. Table 4.7 lists those once-through parameters[72] together with the recycle values of $\alpha_{Ca/S,rec}$ and $\eta_{S,rec}$. In addition, corresponding data obtained in air fired experiments is included in the table to allow for a direct comparison. For the calculation of $y_{SO_2,furn,in,dry}$, the factor $\dot{N}_{S,in}/\dot{N}_{FG,out}$ in equation 4.14 was set to the dry reference SO_2 concentrations[73] measured in the individual experiments, without DSI (i.e. at $\alpha_{Ca/S} = 0$). It should be noted that the parameter $y_{SO_2,furn,in}$ is a theoretical value that expresses the total amount of sulfur that enters the furnace in form

[71] The molar Ca/S ratio $\alpha_{Ca/S,o-t}$ is determined based on the injected molar calcium and the molar sulfur feed at furnace inlet that considers $y_{S,furn,in}$ (equation 4.14) and the flue gas flow through the furnace.

[72] As introduced in section 3.3.3.2, a flue gas recirculation ratio ξ_{rec} of about 50 % was used in the DSI experiments and hence, was considered in the calculations.

[73] This assumes no desulfurization in such tests so that $\dot{N}_{S,in}/\dot{N}_{FG,out} = \dot{N}_{S,out}/\dot{N}_{FG,out}$.

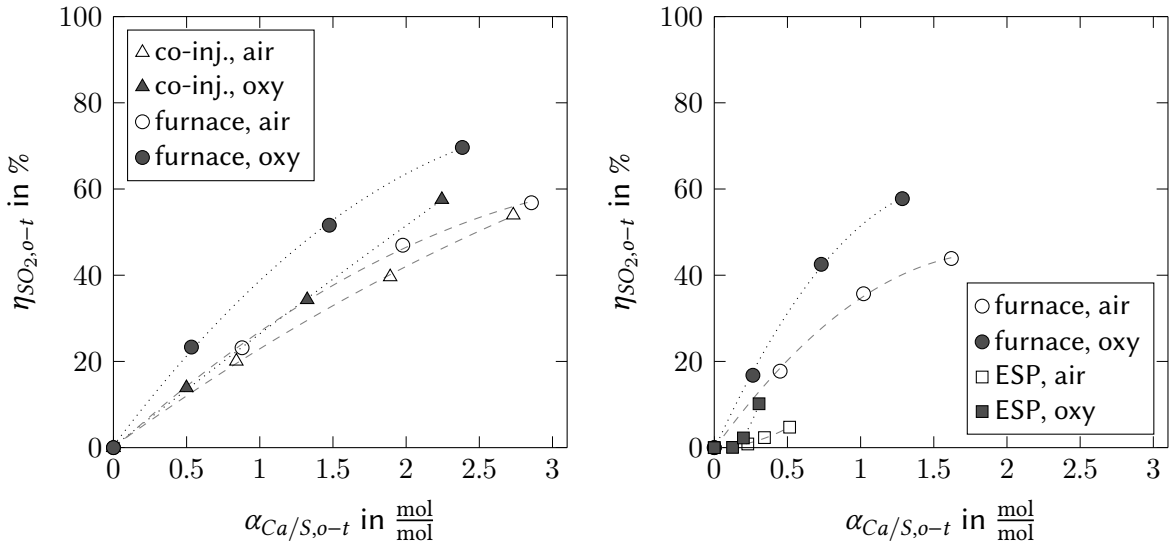

(a) η_{SO_2} for $CaCO_3$ injection **(b)** η_{SO_2} for $Ca(OH)_2$ injection

Figure 4.28: Local SO_2 capture efficiency $\eta_{SO_2,o-t}$ versus $\alpha_{Ca/S,o-t}$. in C4 air and oxy-fuel recycle combustion at KSVA for (a) $CaCO_3$ co-injection together with fuel and injection to the furnace and (b) $Ca(OH)_2$ injection to the furnace and upstream ESP. Dashed (air) and dotted (oxy-fuel) trendlines were approximated by a 2nd order polynomial fit.

of SO_2[74].

Figure 4.28 presents the experimental results from air and oxy-fuel operation with DSI at the KSVA test facility in respect to once-through desulfurization efficiency $\eta_{S,o-t}$ (in air firing: $\eta_{S,o-t} = \eta_{S,rec}$). It can be seen that in all experiments $\eta_{S,o-t}$ in oxy-fuel combustion exceeds the values obtained in air firing at the same molar Ca/S ratio $\alpha_{Ca/S,o-t}$. In the experiments with furnace injection of $CaCO_3$ and $Ca(OH)_2$, this difference is relatively big (up to about 20 percentage points). The differences indicate that the once-through SO_2 capture in the oxy-fuel recycle experiments is considerably better than in the corresponding air fired experiments. Possible explanations for this may be related to the longer flue gas residence times (about 25 % increased, see section 3.3.3.2) in the oxy-fuel experiments due to the reduced volumetric flue gas flow rate through the furnace. Another parameter that may be responsible for the differences is the increased SO_2 level in the furnace in the oxy-fuel experiments (i.e. $y_{SO_2,furn,in}$). This may beneficially influence diffusion and desulfurization reactions as well as sulfate stability. A comparison of results in respect to $\eta_{S,o-t}$ from KSVA and desulfurization performance of CO_2/O_2 experiments at BTS-VR is problematic due to different SO_2 levels in the furnace[75], different flue gas residence times, and anticipated differences in the sorbent dispersion quality in both reactors (see p. 132).

[74]The assumption made does not consider sulfur that is captured by the fuel's ash. As presented in table 4.2, this is only a small fraction of the total amount of sulfur (approx. 3 % in air and 8 % in oxy-fuel operation).

[75]KSVA: $y_{SO_2,furn,in}$ < approx. $4000 \cdot 10^{-6}$ $\frac{m^3}{m^3}$, dry; BTS: $y_{SO_2,furn,in} \approx 4500$ to $5000 \cdot 10^{-6}$ $\frac{m^3}{m^3}$, dry.

Temperature and SO_2 concentration profiles in the furnace: In the air and oxy-fuel recycle experiments at KSVA with injection of $Ca(OH)_2$ to the furnace and during the corresponding air and oxy-fuel recycle reference experiments without sorbent injection, y_{SO_2} and ϑ_{FG} have been measured at various locations inside the furnace upstream and downstream of the sorbent injection position. Based on these point measurements, ϑ_{FG} and y_{SO_2} profiles in this section of the furnace have been generated by interpolation[76]. These profiles can give a better insight to the conditions that were established during those experiments. Figure 4.29 shows the interpolated temperature profiles of the KSVA furnace during air and oxy-fuel combustion of C4 coal with and without $Ca(OH)_2$ furnace injection, while figure 4.30 shows the corresponding interpolated y_{SO_2} profiles. It should be highlighted that the spline interpolation used in the generation of the gas and temperature profiles does not consider the flue gas flow direction which is the reason for certain artifacts, such as an apparent spreading of the sorbent against the gas flow that is visible in the y_{SO_2} profiles. To avoid misleading interpretations caused by these artifacts, in the following, temperatures and concentrations are discussed on basis of positions at which actual temperature and SO_2 measurements were conducted.

One sees that in air as well as oxy-fuel experiments, similar temperatures in the range of approx. 1050 °C to 1100 °C were reached at the injection location 2160 mm from the burner, with slightly higher temperatures (approx. 40 °C) during oxy-fuel combustion. When comparing air and oxy-fuel experiments with and without $Ca(OH)_2$ injection, a temperature drop in the center of the furnace (i.e. 0 mm from the burner axis) at the position at which the sorbent is injected can be observed. This is due to the injection of cold carrier gas (air) together with the sorbent at this location and also due to the endothermic $Ca(OH)_2$ calcination reaction that is expected to occur as soon as the sorbent temperature reaches the $Ca(OH)_2$ calcination temperature (approx. 420 °C). Downstream the sorbent injection position, the temperature is further dropping, due to heat transfer via the furnace walls, so that at a distance of 3600 mm from the burner 900 °C is reached. The temperature difference 3600 mm from the burner between the air and oxy-fuel experiments with sorbent injection reduces to only approx. 5 °C. This highlights that the temperature conditions in the relevant area of the furnace for desulfurization in air and oxy-fuel experiments were similar and it justifies the comparability of the experiments in respect to this important parameter. Due to restrictions of the experimental time at the KSVA system, such dedicated measurements inside the furnace could not be conducted for other DSI experiments. Since the combustion conditions were the same in all air and oxy-fuel experiments, it can be assumed that comparable air and oxy-fuel temperature profiles were established also during other tests.

In figure 4.30 that shows the y_{SO_2} profiles, the effect of $Ca(OH)_2$ injection to the furnace 2160 mm from the burner can clearly be observed. In these experiments, $Ca(OH)_2$ was injected with a

[76] Profiles were interpolated mirroring the data points on the central axis, assuming symmetry within the cylindrical furnace and using the thin plate spline method, according to Donato and Belongie [228], provided by the software program Origin Pro 2015, without smoothing and extrapolation of data.

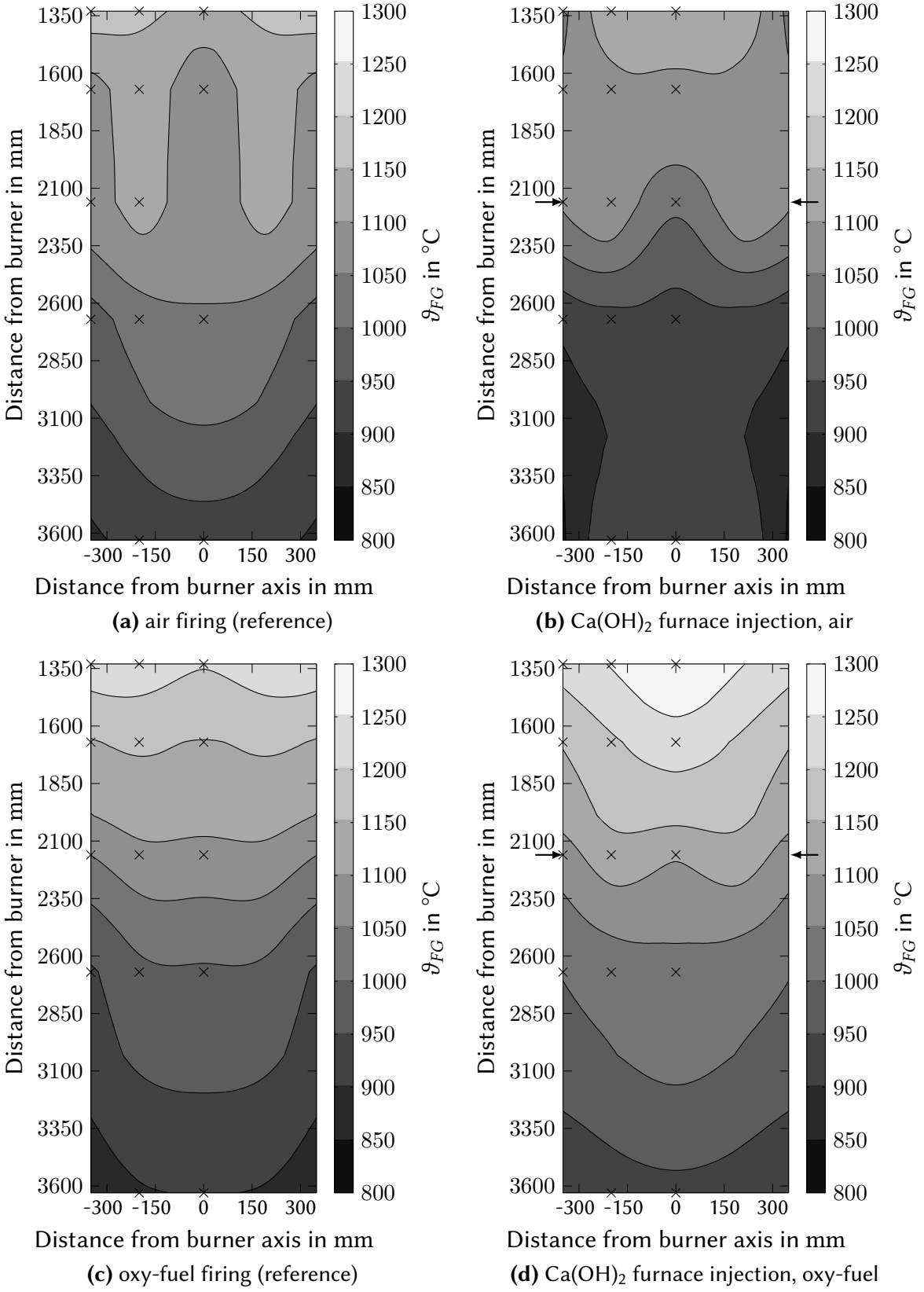

(a) air firing (reference)

(b) $Ca(OH)_2$ furnace injection, air

(c) oxy-fuel firing (reference)

(d) $Ca(OH)_2$ furnace injection, oxy-fuel

Figure 4.29: Interpolated temperature profiles in the KSVA furnace in air (a, b) and oxy-fuel (c, d) combustion of C4 coal with (b, d) and without (a, c) $Ca(OH)_2$ furnace injection ($\alpha_{Ca/S}$: 1.0/1.1 in air/oxy-fuel). The position of $Ca(OH)_2$ injection is indicated by arrows and the actual measurement points of the interpolated data by "x".

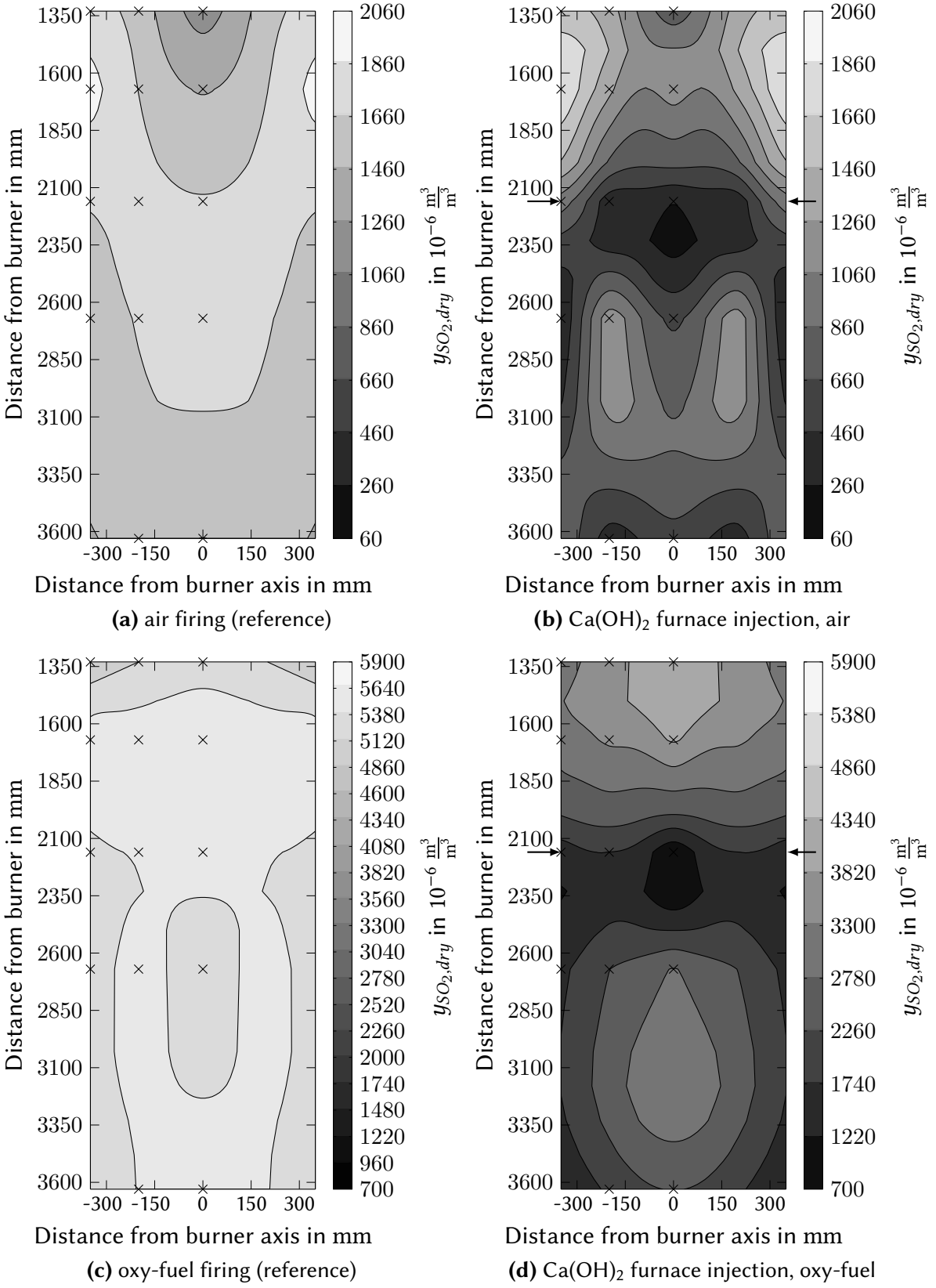

(a) air firing (reference)

(b) $Ca(OH)_2$ furnace injection, air

(c) oxy-fuel firing (reference)

(d) $Ca(OH)_2$ furnace injection, oxy-fuel

Figure 4.30: Interpolated y_{SO_2} profiles in the KSVA furnace in air (a, b) and oxy-fuel (c, d) combustion of C4 coal with (b, d) and without (a, c) $Ca(OH)_2$ furnace injection ($\alpha_{Ca/S}$: 1.0/1.1 in air/oxy-fuel). The position of $Ca(OH)_2$ injection is indicated by arrows and the actual measurement points of the interpolated data by "x".

value of $\alpha_{Ca/S}$ of 1.0 in air and 1.1 in oxy-fuel conditions, reducing y_{SO_2} from $1511 \cdot 10^{-6}$ $\frac{m^3}{m^3}$, dry, to $972 \cdot 10^{-6}$ $\frac{m^3}{m^3}$, dry, in air and from $4618 \cdot 10^{-6}$ $\frac{m^3}{m^3}$, dry, to $1862 \cdot 10^{-6}$ $\frac{m^3}{m^3}$, dry, in oxy-fuel operation, respectively. It should be highlighted that even though in oxy-fuel operation the SO_2 levels are much higher than in air firing, in the air and oxy-fuel DSI experiments discussed here the injected sorbent (1.7 $\frac{kg}{h}$) and coal feed rates (38.5 $\frac{kg}{h}$) were the same. y_{SO_2} profiles without sorbent injection are relatively homogeneous in air as well as in oxy-fuel experiments, with a difference of the average y_{SO_2} level[77] between 2160 mm (i.e. the level at which sorbent was injected) and 3600 mm from the burner of $306 \cdot 10^{-6}$ $\frac{m^3}{m^3}$, dry, and $361 \cdot 10^{-6}$ $\frac{m^3}{m^3}$, dry, in air and oxy-fuel operation, respectively. With sorbent injection this spread increases to $987 \cdot 10^{-6}$ $\frac{m^3}{m^3}$, dry, and $2485 \cdot 10^{-6}$ $\frac{m^3}{m^3}$, dry, respectively. This is due to the sorbent injection that generates a local minimum of the SO_2 concentration at the injection level. The average y_{SO_2} concentration[77] at the injection level during DSI was $534 \cdot 10^{-6}$ $\frac{m^3}{m^3}$, dry, in air and $1866 \cdot 10^{-6}$ $\frac{m^3}{m^3}$, dry, in oxy-fuel operation. Potentially also some bias of the y_{SO_2} measurement when extracting flue gases at locations with a very high loading of fresh sorbent may play a role. This issue was not further assessed.

An interesting effect that can be observed in the y_{SO_2} profiles is that in the oxy-fuel tests DSI has also a strong impact on the SO_2 levels upstream sorbent injection. For example at a position 1670 mm from the burner, well upstream of the sorbent injection, the average y_{SO_2} level[77] with sorbent injection is $3402 \cdot 10^{-6}$ $\frac{m^3}{m^3}$, dry, while without sorbent injection it is $5511 \cdot 10^{-6}$ $\frac{m^3}{m^3}$, dry, (i.e. 38 % reduction). The reason for this can be found in the recirculation of flue gases to the burner which creates a feedback loop in respect to the desulfurization effect of DSI. This is in good agreement with the expectations described in section 4.1.3 and the prediction of $y_{SO_2,furn,in}$ ($3240 \cdot 10^{-6}$ $\frac{m^3}{m^3}$, dry, see table 4.7) and highlights that of the total reduction of SO_2 of 60 % measured after ESP (i.e. from $4618 \cdot 10^{-6}$ $\frac{m^3}{m^3}$, dry, to $1862 \cdot 10^{-6}$ $\frac{m^3}{m^3}$, dry,) a large fraction is caused indirectly via recirculation of flue gas.

4.2.2.4 Discussion of the application of DSI for acid gas control

In the previous sections, very promising experimental results in respect to acid gas control by DSI were introduced, providing information on acid gas removal efficiencies that can be reached with different sorbents, injection locations, and combustion modes. This data may be used as a reference, when designing DSI systems, which is particularly useful for oxy-fuel fired processes, for which there is no other experience on DSI available. In the following, exemplary application cases for DSI are introduced and data in respect to sorbent consumption and by-products generation is presented. To complement the experimental data on acid gas removal efficiencies, also results in respect to the composition of boiler deposits and process ashes that were obtained in KSVA sorbent tests with $Ca(OH)_2$ furnace injection are presented

[77] In this subsection, y_{SO_2} averages refer to values averaged along the radius of the furnace (i.e. 0 mm to 350 mm from the burner axis).

the following.

Introduction to calculations used for DSI application examples: For discussion of the sorbent consumption and the production of DSI related by-products (i.e. unreacted sorbent and sorbent converted to CaO, $CaSO_4$, and $CaCl_2$), the sorbent utilization efficiency η_{sorb} (equation 4.23) is a useful parameter.

$$\eta_{sorb,CaSO_4} = \frac{\dot{N}_{Ca,reac,SO_2}}{\dot{N}_{Ca,inj}} = \frac{\dot{N}_{SO_2,rem}}{\dot{N}_{Ca,inj}} = \frac{\eta_{SO_2}}{\alpha_{Ca/S}} \tag{4.21}$$

$$\eta_{sorb,CaCl_2} = \frac{\dot{N}_{Ca,reac,HCl}}{\dot{N}_{Ca,inj}} = \frac{\dot{N}_{HCl,rem}}{\dot{N}_{Ca,inj}} = \frac{\eta_{HCl}}{\alpha_{Ca/2Cl}} \tag{4.22}$$

$$\eta_{sorb} = \eta_{sorb,CaSO_4} + \eta_{sorb,CaCl_2} \tag{4.23}$$

$$\xi_{sorb} = \frac{\dot{M}_{sorb}}{\dot{M}_{fuel}} \tag{4.24}$$

$$\xi_{byprod,i} = \frac{\eta_{sorb,i}\dot{M}_{sorb}}{\dot{M}_{fuel}} \frac{M_{M,sorb}}{M_{M,byprod,i}} \tag{4.25}$$

It relates the molar flow of calcium from the sorbent feed ($\dot{N}_{Ca,reac,i}$) that is consumed by reactions with SO_2 and HCl, forming $CaSO_4$ and $CaCl_2$, to the total feed of injected sorbent $\dot{N}_{Ca,inj}$. $\eta_{sorb,i}$ can be calculated on basis of $\alpha_{Ca/S}$, η_{SO_2}, $\alpha_{Ca/2Cl}$, and η_{HCl}, according to equations 4.21 and 4.22. η_{sorb,SO_3} can be calculated in an equivalent way. However, due to the relatively small concentrations of SO_3, its contribution to sorbent consumption and by-products generation is not significant and hence, it is not included in the discussion here. Sorbent that has not reacted with the target acid gas can be assumed to be the remainder of the injected material and, depending on injection temperature, may be present as $Ca(OH)_2$ or CaO.
$\eta_{sorb,i}$ can be used to calculate the generation of by-products i (i: $Ca(OH)_2$, $CaCO_3$, $CaCl_2$) by DSI for the conducted experiments (equation 4.25), which is done in the following for the two examples, $Ca(OH)_2$ injection upstream the ESP for SO_3 and HCl control and $Ca(OH)_2$ furnace injection for control of the SO_2 level in an oxy-fuel boiler firing coal C4. The fuel specific sorbent consumption ξ_{sorb} can be calculated on basis of equation 4.24.
In this section, the sorbent consumption and production of by-products are calculated on basis of the coal feed which eases upscaling of these parameters to a larger plant. Another option to obtain results on ξ_{sorb} and $\xi_{byprod,i}$ that can be used more generally and is not related to a particular fuel composition is to relate the sorbent consumption and by-products generation to the production of SO_2 in a combustion system. More details and selected results in this respect can be found in annex A.7. When assessing results on sorbent consumption and by-products generation of this thesis, it should be taken into account that the used coal C4 is relatively rich in sulfur and chlorine ($\gamma_{S,daf} = 2.67 \cdot 10^{-2}\ \frac{kg}{kg}$, $\gamma_{Cl,daf} = 0.3 \cdot 10^{-2}\ \frac{kg}{kg}$). With lower sulfur and chlorine fuels, ξ_{sorb} and $\xi_{byprod,i}$ would be considerably lower than the numbers presented here.

$Ca(OH)_2$ injection before ESP for HCl and SO_3 control: It has been demonstrated experimentally that DSI is efficient for controlling HCl and SO_3 levels in air and oxy-fuel combustion, particularly, when sorbents are injected at a lower temperature, upstream particulate control devices. Even though, no SO_3 measurements were conducted in oxy-fuel operation when sorbent was injected upstream the ESP, the SO_3 capture efficiency in air firing and the HCl capture performance in air and oxy-fuel operation indicate that relatively low sorbent injection rates are sufficient for an extensive SO_3 and HCl removal. In the conducted air fired experiment, a fuel specific injection of $Ca(OH)_2$ ξ_{sorb} of $1.6 \cdot 10^{-2}$ $\frac{kg}{kg}$ (i.e. $\alpha_{Ca/2Cl}$ = 1.1) led to a reduction of SO_2 by 2.3 %, of SO_3 by 92 %, and of HCl by 66 %. Based on $\eta_{Sorb,CaSO_4}$ (= 6.8 %) and $\eta_{Sorb,CaCl_2}$ (=59 %)[78] and assuming a conversion to $CaSO_4$ and $CaCl_2$, respectively, with the rest of the sorbent remaining as $Ca(OH)_2$[79], also the generation of the different by-product species can be estimated. The same can be done on basis of the experimental data from oxy-fuel trials with a fuel specific injection ξ_{sorb} of $Ca(OH)_2$ upstream ESP of $1.8 \cdot 10^{-2}$ $\frac{kg}{kg}$ (i.e. $\alpha_{Ca/2Cl}$ = 1.9) that yielded a removal of SO_2 of 4.4 % and of HCl of 76 % (i.e. $\eta_{Sorb,CaSO_4}$ = 10.8 %, $\eta_{Sorb,CaCl_2}$ = 39.1 %). The results on fuel specific sorbent consumption and by-product generation for both combustion modes are summarized in table 4.8. For comparison, the fuel specific ash production ξ_A of approx. $9.3 \cdot 10^{-2}$ $\frac{kg}{kg}$ can be considered. One sees that for DSI upstream ESP at the discussed moderate sorbent injection stoichiometries, the total amount of solid residue produced in the combustion process is increased by 23 % and 25 % for the air and oxy-fuel experiment, respectively.

Exemplary estimations on sorbent consumption and by-product generation in a potential oxy-fuel demonstration plant with a thermal power of 600 MW (C4 coal consumption of approx. 71 $\frac{t}{h}$) are presented in table 4.9. The data relates to an injection stoichiometry of $\alpha_{Ca/S}$ = 0.4, $\alpha_{Ca/2Cl}$ = 1.9. The estimated sorbent requirement and residue generation for such a demonstration plant are considerable but still in a range that conventional power plants are used to. Hence, it can be expected that those additional solid by-product loads can be handled with standard power plant equipment without major modifications. Additional investment

Table 4.8: Exemplary summary of data on fuel specific sorbent consumption ξ_{sorb} and by-products generation $\xi_{byprod,i}$ for air and oxy-fuel $Ca(OH)_2$ injection upstream ESP at moderate injection stoichiometries (calculated on basis of KSVA tests; air: $\alpha_{Ca/2Cl}$ = 1.1; oxy-fuel: $\alpha_{Ca/2Cl}$ = 1.9). In addition, values of η_i are given.

	η_{SO_2}	η_{SO_3}	η_{HCl}	ξ_{sorb}	$\xi_{byprod,CaSO_4}$	$\xi_{byprod,CaCl_2}$	$\xi_{byprod,Ca(OH)_2}$	$\xi_{byprod,tot}$
Mode		%				10^{-2} $\frac{kg}{kg}$		
air	2.3	92	66	1.6	0.2	1.4	0.5	2.1
oxy	4.4	-	76	1.8	0.4	1.1	0.9	2.3

[78] SO_3 capture is not considered here since its contribution to the sorbent conversion is minimal.
[79] I.e. "non-utilization efficiency": $\eta_{Ca(OH)_2} = 100\ \% - \eta_{Sorb,CaSO_4} - \eta_{Sorb,CaCl_2}$

Table 4.9: Estimation of sorbent consumption $\dot{M}_{sorb}$ and by-product generation $\dot{M}_{byprod,i}$ for $Ca(OH)_2$ injection upstream ESP in a 600 MW (thermal) oxy-fuel demonstration plant firing C4 coal (calculated on basis of KSVA tests with $\alpha_{Ca/2Cl}$ = 1.9). In addition, values of η_i and ash generation $\dot{M}_{ash}$ are given.

η_{SO_2}	η_{SO_3}	η_{HCl}	$\dot{M}_{sorb}$	$\dot{M}_{byprod,CaSO_4}$	$\dot{M}_{byprod,CaCl_2}$	$\dot{M}_{byprod,Ca(OH)_2}$	$\dot{M}_{byprod,tot}$	$\dot{M}_{ash}$
	%				$\frac{t}{h}$			
4.4	(92)†	76	1.3	0.3	0.8	0.6	1.7	6.6

† There is no SO_3 data available from the oxy-fuel trial. Therefore, the corresponding result from the air fired experiment with $Ca(OH)_2$ injection upstream ESP at a slightly lower injection stoichiometry (i.e. $\alpha_{Ca/2Cl}$ = 1.1) is given as a rough approximation.

and operational costs for sorbent injection and by-product handling may be tolerable since in turn problems caused by SO_3 and HCl in respect to low temperature acid corrosion may be avoided. It is important to note that when using fuels containing less Cl than coal C4, a considerably lower sorbent feed and hence, by-product generation can be expected to remove a large fraction of the SO_3 in the flue gas.

$Ca(OH)_2$ injection to the furnace for SO_2 control: The application of DSI for SO_2 control is particularly interesting for oxy-fuel combustion for which very good SO_2 capture performances were observed in pilot scale experiments. This goes along with a relatively high sorbent utilization efficiency. In experiments with $Ca(OH)_2$ injection to the furnace and injection stoichiometries of $\alpha_{Ca/S}$ = 1.0 and 1.1 in air and oxy-fuel operation, η_{sorb} reached 36 % and 58 %, respectively. At higher values of $\alpha_{Ca/S}$ (air/oxy-fuel: 1.6/1.7), η_{sorb} decreased to 28 % and 45 %. Higher sorbent utilization efficiencies in oxy-fuel combustion go along with a reduced specific sorbent consumption ξ_{sorb} to reach a desired degree of desulfurization. On basis of the experimental results for injection of $Ca(OH)_2$ to the furnace of the KSVA facility, in figure 4.31, the fuel specific sorbent consumption in air and oxy-fuel operation is plotted versus the SO_2 capture efficiency η_{SO_2}.

As for the previous example on low temperature DSI, the sorbent utilization efficiency $\eta_{sorb,i}$ can be linked to the specific generation of the by-products $CaSO_4$, $CaCl_2$, and CaO[80]. In figure 4.32, the specific by-product generation $\xi_{byprod,i}$ of these components is plotted versus η_{SO_2} for injection of $Ca(OH)_2$ to the furnace of KSVA in C4 air and oxy-fuel recycle combustion. For comparison, in figure 4.32, also the specific production of ash ξ_A is plotted. Extrapolated data in figures 4.31 and 4.32 for higher η_{SO_2} values than the ones tested in experiments should be used carefully since the extrapolation model is not optimized and not validated.

[80] When $Ca(OH)_2$ is injected at temperatures above its calcination temperature, it decomposes to CaO and H_2O. Assuming a low carbonation efficiency of the generated CaO (due to the loss of reactive surface by reactions with SO_2 and HCl), sorbent that does not react with acid gases is expected to be present as CaO in by-products. The "non-utilization efficiency" for this component is defined as $\eta_{CaO} = 100\% - \eta_{Sorb,CaSO_4} - \eta_{Sorb,CaCl_2}$.

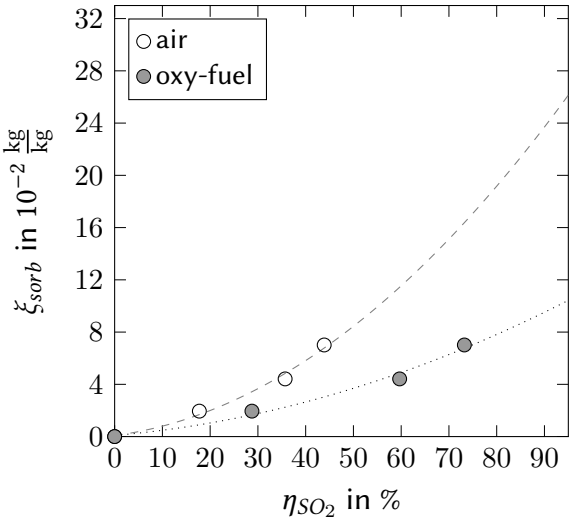

Figure 4.31: Fuel specific sorbent consumption ξ_{sorb} versus η_{SO_2} for $Ca(OH)_2$ furnace injection at KSVA in coal C4 air and oxy-fuel combustion. ξ_{sorb} values obtained from experimental data are marked by symbols. Dashed (air) and dotted (oxy-fuel) trendlines were approximated by a 2nd order polynomial fit of these results.

One sees clearly that the higher sorbent utilization efficiency in oxy-fuel operation is also linked to a considerably lower generation of by-products, compared to the air fired case. For example in oxy-fuel operation, accepting a doubling of the ash/by-product load, compared to an operation without DSI, would allow for a reduction of the SO_2 concentration at the furnace outlet by about 78 %. In air firing, under the same precondition, only 52 % reduction of the SO_2 concentration would be possible.

Also for the $Ca(OH)_2$ furnace injection that can efficiently control SO_2 levels, an estimation in respect to sorbent consumption and by-product generation in an oxy-fuel demonstration plant (i.e. 600 MW thermal power, C4 coal consumption of approx. 71 $\frac{t}{h}$) was conducted on basis of the DSI results from KSVA. The results are summarized in table 4.10. The dry sorbent application in this example increases the total load of solid residues (ash and DSI by-products) by about 65 % while allowing a considerable reduction of SO_2 and SO_3 and a minor reduction of HCl. As previously mentioned, the coal used for DSI experiments within this thesis was very rich in sulfur ($x_{S,daf} = 2.67 \cdot 10^{-2}$ $\frac{kg}{kg}$). With a lower sulfur fuel, the by-products generation by

Table 4.10: Estimation of sorbent consumption $\dot{M}_{sorb}$ and by-products generation $\dot{M}_{byprod,i}$ for $Ca(OH)_2$ furnace injection in a 600 MW (thermal) oxy-fuel demonstration plant (calculated on basis of the KSVA tests with $\alpha_{Ca/S} = 1.1$). In addition, also values of acid gas removal efficiencies η_i and ash generation $\dot{M}_{ash}$ are given.

η_{SO_2}	η_{SO_3}	η_{HCl}	$\dot{M}_{sorb}$	$\dot{M}_{byprod,CaSO_4}$	$\dot{M}_{byprod,CaCl_2}$	$\dot{M}_{byprod,CaO}$	$\dot{M}_{byprod,tot}$	$\dot{M}_{ash}$
	%				$\frac{t}{h}$			
60	82	9	3.1	3.2	0.1	1.0	4.3	6.6

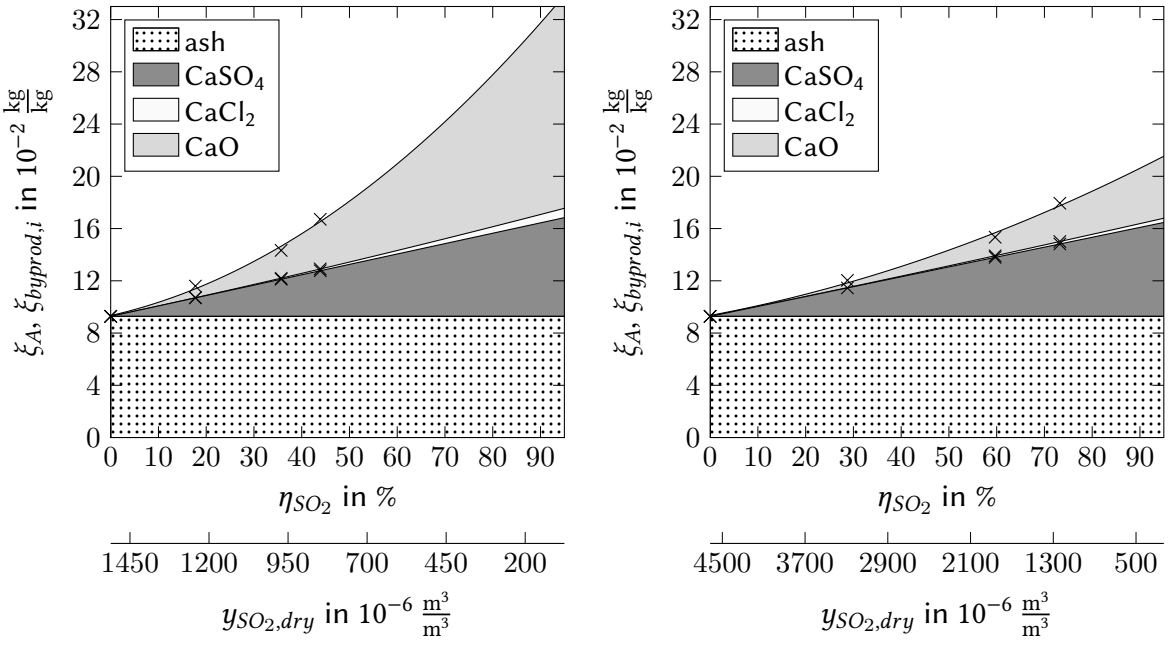

(a) $\xi_{byprod,i}$ and ξ_A in air firing **(b)** $\xi_{byprod,i}$ and ξ_A in oxy-fuel firing

Figure 4.32: Fuel specific by-product $\xi_{byprod,i}$ generation versus η_{SO_2} and associated outlet $y_{SO_2,dry}$ levels for injection of $Ca(OH)_2$ to the furnace of KSVA in (a) air and (b) oxy-fuel recycle combustion of C4 coal. In addition, the specific production of ash ξ_A is plotted. $\xi_{byprod,i}$ values obtained from experimental data are marked by "x". The plotted trends were approximated by a 2nd order polynomial fit of the experimental results.

DSI would be proportionally smaller. For example, for a coal with a sulfur content of $1 \cdot 10^{-2}$ $\frac{kg}{kg}$, daf, the increase of the solid residues at the same SO_2 capture efficiency of 60 % can be estimated to be only around 25 %, compared to the system without DSI. The additional solid residues from DSI will obviously increase efforts to remove solids from the flue gas and will require more efforts for their disposal. However, since no dedicated desulfurization system is required, the technology offers a possibility to control acid gases effectively in an oxy-fuel recycle combustion system with relatively low capital investment while still reaching a relatively high sorbent conversion and desulfurization efficiency. As can be seen from figure 4.32b, even though also higher degrees of desulfurization are possible in oxy-fuel operation, the sorbent conversion efficiency η_{sorb} reduces more and more with increasing desulfurization (e.g. from 61 % to 58 % to 45 % at η_{SO_2} values of 29 %, 60 %, and 73 %). This decrease is associated with more and more unconverted sorbent in the ash and a disproportionately higher sorbent consumption and DSI by-product generation when high desulfurization efficiencies are targeted. This may hinder the application of DSI for very high degrees of desulfurization. However, in an oxy-fuel system, there will also be a CPU system with additional options for acid gas removal. Depending on the sulfur content of the fuel, a combination of DSI and additional purification in the CPU may be a good solution that can avoid a wet scrubbing system. Moreover, DSI injection to the furnace of an oxy-fuel plant will give plant operators a handle to control sulfur levels in the boiler, SO_3

levels in the GPH and recirculation line, and to balance fluctuating SO_2 concentrations in the flue gas.

Impact of dry sorbent injection on process ash composition: It should be noted that the focus of the conducted DSI experiments was on the acid gas removal performance rather than on the effects of DSI on ashes and deposits. Therefore, the time to investigate ash and deposit behavior was limited and only for the reference experiments without DSI and for the air and oxy-fuel experiments with injection of $Ca(OH)_2$ into the furnace ($\alpha_{Ca/S}$ = 1.0 and 1.1, respectively), deposits and ashes have been sampled and analyzed. Those settings were operated continuously for longer durations without changing $\alpha_{Ca/S}$ (approx. 3.5 h in air and approx. 8 h in oxy-fuel). In the following, a qualitative characterization of process ashes and deposits from the different experiments is included.

During the air and oxy-fuel experiments, process ashes were sampled from air/gas preheater (GH), bottom ash (BA), and ESP precipitation fields 1, 2, and 3 (E1, E2, E3) and analyzed for their main ash-forming elements' contents. Figures 4.33 and 4.34 show the compositions of the sampled process ashes and molar Ca/S, Mg/S, K_2/S, and Na_2/S ratios α_i for the air and oxy-fuel experiments with and without DSI[81].

As expected, one observes increased CaO and SO_3 contents in the ash samples from DSI experiments when comparing them with ashes from the reference tests. This increase in CaO

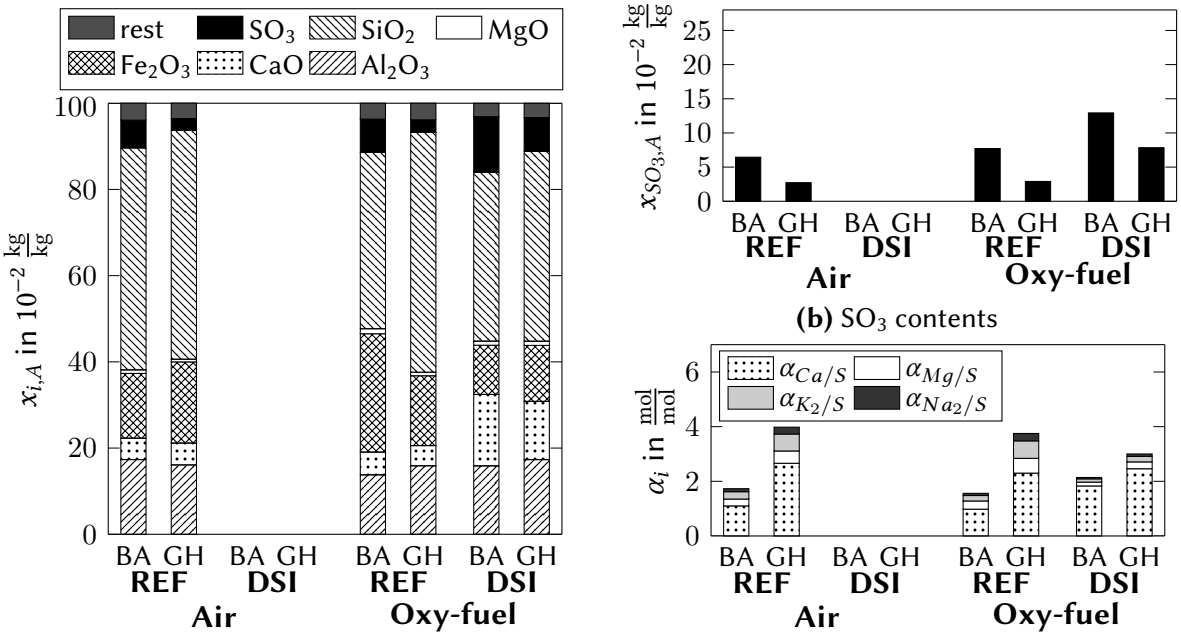

(a) Composition of process ashes

(b) SO_3 contents

(c) Molar Ca, Mg, K_2, and Na_2 to S ratios α_i

Figure 4.33: (a) Composition of bottom (BA) and gas preheater (GH) ash from C4 air and oxy-fuel combustion with (DSI) and without (REF) $Ca(OH)_2$ furnace injection, (b) SO_3 contents, and (c) Molar Ca/S, Mg/S, K_2/S, and Na_2/S ratios α_i of the ashes.

[81] Air preheater (GH) and bottom ash (BA) samples are not available from the air fired DSI experiment.

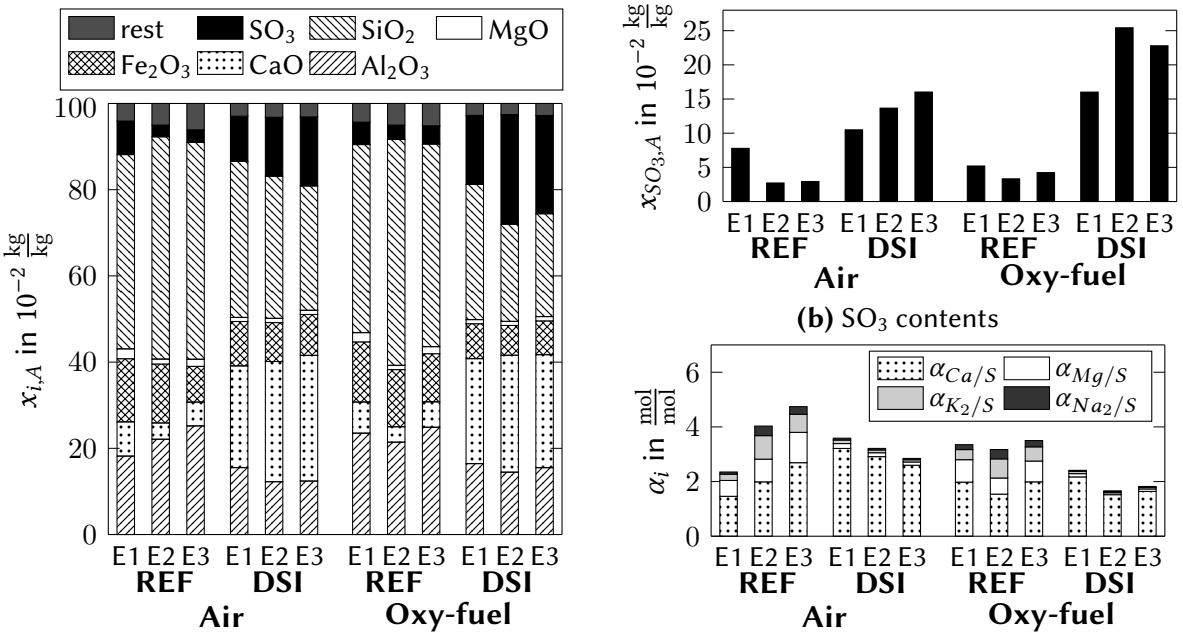

(a) Composition of process ashes

(b) SO_3 contents

(c) Molar Ca, Mg, K_2, and Na_2 to S ratios α_i

Figure 4.34: (a) Composition of ESP ashes (E1, E2, E3) from C4 air and oxy-fuel combustion with (DSI) and without (REF) $Ca(OH)_2$ furnace injection, (b) SO_3 contents, and (c) Molar Ca/S, Mg/S, K_2/S, and Na_2/S ratios α_i of the ashes.

.

and SO_3 is more pronounced for the ESP ashes, compared to the bottom and gas preheater ashes. In air firing without DSI, ESP ashes contained 3.8 to $7.9 \cdot 10^{-2}$ $\frac{kg}{kg}$ CaO and 2.7 to $7.8 \cdot 10^{-2}$ $\frac{kg}{kg}$ SO_3. In oxy-fuel combustion, the ESP ash composition was relatively similar (i.e. 3.6 to $7.2 \cdot 10^{-2}$ $\frac{kg}{kg}$ CaO and 3.3 to $5.2 \cdot 10^{-2}$ $\frac{kg}{kg}$ SO_3). In contrast, with injection of $Ca(OH)_2$ to the furnace, CaO contents rose to 23.6 to $29.2 \cdot 10^{-2}$ $\frac{kg}{kg}$ in air and 24.4 to $27.1 \cdot 10^{-2}$ $\frac{kg}{kg}$ oxy-fuel firing, and the SO_3 contents in ESP ashes reached 10.5 to $16.0 \cdot 10^{-2}$ $\frac{kg}{kg}$ and 16.0 to $25.4 \cdot 10^{-2}$ $\frac{kg}{kg}$, respectively. Even though this was not analyzed, one can assume that part of the calcium in the ash represents unreacted sorbent most likely in the form of (free/reactive) lime. The additional CaO and SO_3 diluted the other ash components, so that in DSI experiments the sum of SiO_2, Fe_2O_3, and Al_2O_3 in the ash fell from values above $78 \cdot 10^{-2}$ $\frac{kg}{kg}$ to 44 to $62 \cdot 10^{-2}$ $\frac{kg}{kg}$, which is below the minimum specification (i.e. $70 \cdot 10^{-2}$ $\frac{kg}{kg}$) that allows for utilization of the fly ash in concrete (see EN 450-1, [63]). In addition to that, the limit in respect to the SO_3 content of the ash (i.e. $3 \cdot 10^{-2}$ $\frac{kg}{kg}$) of EN 450-1 was by far exceeded, while in the reference experiments without DSI it was kept or only slightly exceeded in some process ash fractions. Also the SO_3 maximum for ash utilization in cement (i.e. $4 \cdot 10^{-2}$ $\frac{kg}{kg}$, according to EN 197-1 [64]) was clearly violated.
Even though specifications for certain ash utilization routes are exceeded, there may still be a use for ashes from DSI applications in the construction sector when they are blended with other ashes. For example reactive lime that is expected to be contained in ashes from DSI applications, is a desired component for utilization as calcerous fly ash in cement (i.e. 10 to

$15 \cdot 10^{-2}\ \frac{kg}{kg}$ reactive lime required, according to EN 197-1 [64]). Moreover, if only small amounts of sorbents are injected (i.e. when using DSI to control gaseous SO_3 emissions), the impact of the sorbent and its by-products on the ash composition would be much less pronounced. DSI will impact the utilization of process ashes and can render ashes unsuitable for utilization in high value applications, such as concrete or cement. This may cause additional efforts for ash processing or upgrading, allow only less profitable utilization routes, or may lead to a need to landfill such ashes, which will be associated to disposal costs.

Impact of dry sorbent injection on deposit composition: In figure 4.35, the compositions of uncooled and cooled deposits from the $Ca(OH)_2$ furnace injection and the reference experiments with coal C4 sampled at level 20 (3.63 m from the burner and 1.47 m from the DSI location) are shown. No cooled deposit samples are available from the oxy-fuel experiments, since the sampled deposits were very loose and were lost when extracting the sampling probe. When comparing uncooled air and oxy-fuel deposits without sorbent injection, their composition and degree of sulfation is very similar, even though, the SO_2 levels were much higher in the oxy-fuel experiment. When $Ca(OH)_2$ was injected to the furnace some differences can be observed in the CaO content of the samples. Since the same mass flow of sorbent and fuel was injected in air and oxy-fuel operation, this effect may be linked to an inhomogeneous sorbent distribution in the furnace. It is unlikely, but cannot be ruled out on basis of the available

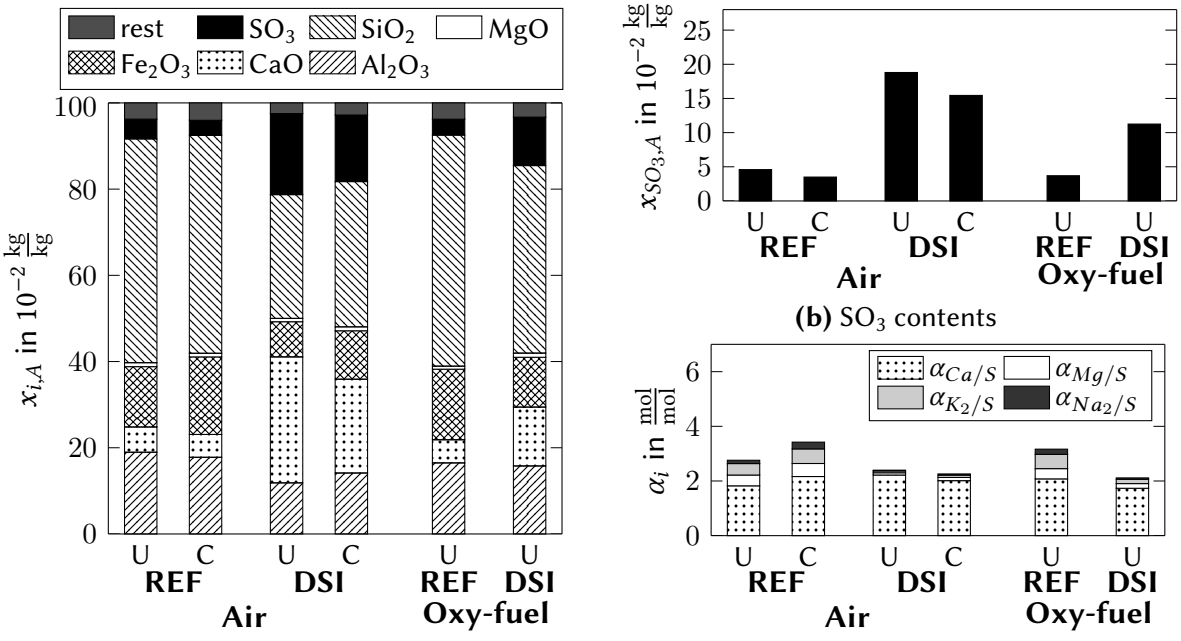

(a) Composition of ash and deposits

(b) SO_3 contents

(c) Molar Ca, Mg, K_2, and Na_2 to S ratios α_i

Figure 4.35: (a) Composition of uncooled (U) and cooled (C) deposits from C4 air and oxy-fuel combustion with (DSI) and without (REF) $Ca(OH)_2$ furnace injection sampled at Level 20 (3.63 m from the burner), (b) SO_3 contents, and (c) Molar Ca/S, Mg/S, K_2/S, and Na_2/S ratios α_i of the deposits.

deposit samples that this effect is due to differences in the deposit build up in both combustion modes. As for the process ashes, one observes a distinct increase of CaO and SO_3 when comparing the experiments with and without DSI. CaO rises from about 5.3 to $5.9 \cdot 10^{-2}$ $\frac{kg}{kg}$ without DSI, to values between 13.7 and $29.2 \cdot 10^{-2}$ $\frac{kg}{kg}$ and SO_3 form about 3.7 to $4.6 \cdot 10^{-2}$ $\frac{kg}{kg}$ to 11.2 to $18.8 \cdot 10^{-2}$ $\frac{kg}{kg}$. According to the molar Ca/S, Mg/S, K_2/S, and Na_2/S ratios α_i calculated based on the compositions of the deposit samples all samples had reached similarly high degrees of sulfation, with only a low potential to further react with gaseous sulfur species. None of the deposit samples appeared particularly sintered and hard. Nonetheless, during longer times of exposure to a furnace environment with DSI, more pronounced deposit sintering via sulfation and sintering of $CaSO_4$ may occur. In combination with the increased particle loading in the boiler, this indicates that there may be a potential for the formation of problematic sulfate deposits. This can however neither be confirmed nor ruled out on basis of the conducted experiments.

4.2.3 SO_3 formation and retention in ash in air and oxy-fuel firing

Experiments investigating SO_3 formation and retention on a filter were conducted in air and simulated oxy-fuel configurations at the BTS-VR system to study alterations in respect to SO_3 between both combustion modes. The results of this study are presented in the following sections.

4.2.3.1 Flue gas compositions in air and simulated oxy-fuel firing

Tables 4.11 and 4.12 list measured[82] and calculated concentrations of O_2, H_2O, NO_x, and SO_2 for experiments investigating SO_3 formation and retention. In all experiments, O_2 concentrations were about $3 \cdot 10^{-2}$ $\frac{m^3}{m^3}$, dry and in all simulated oxy-fuel experiments, CO_2 concentrations higher

Table 4.11: Flue gas composition measured at furnace exit of BTS-VR in air and simulated oxy-fuel experiments studying SO_3 formation and retention on a filter with coal C1 (y_{H_2O} calculated based on fuel composition and steam injection to the oxidant).

			coal C1							
species	unit	dry/wet	C1-A	C1-CO2	C1-5S5H	C1-2S5H	C1-2S0H	C1-2S8H	C1-0S5H	C1-0S0H
$\bar{y}_{O_2}$	10^{-2} $\frac{m^3}{m^3}$	dry	3.0	3.4	3.1	3.6	2.7	3.0	3.2	2.9
$\bar{y}_{H_2O}$		wet	6.4	8.7	23.5	23.5	23.5	23.5	23.5	23.5
$\bar{y}_{NO_x}$	10^{-6} $\frac{m^3}{m^3}$	dry	846	1380	1433	1410	1878	1547	1491	1784
$\bar{y}_{SO_2}$		dry	199	283	871	1235	1243	1228	1464	1531

[82] The concentrations of O_2, NO_x, and SO_2 represent values averaged on basis of measured concentrations from minimum 10 min of representative operation.

Table 4.12: Flue gas composition measured at furnace exit of BTS-VR in air and simulated oxy-fuel experiments studying SO_3 formation and retention on a filter with coals C2, C3, and C4 (y_{H_2O} calculated based on fuel composition and steam injection to the oxidant).

			coal C2			coal C3			coal C4	
species	unit	dry/wet	C2-A	C2-CO2	C2-2S5H	C3-A	C3-CO2	C3-2S5H	C4-A	C4-8S0H
$\bar{y}_{O_2}$	$10^{-2}\ \frac{m^3}{m^3}$	dry	3.1	3.2	3.0	3.1	2.8	3.1	3.0	3.2
$\bar{y}_{H_2O}$		wet	7.6	10.4	28.5	6.6	9.1	24.3	6.0	19.6
$\bar{y}_{NO_x}$	$10^{-6}\ \frac{m^3}{m^3}$	dry	862	939	1479	880	1487	1838	873	1247
$\bar{y}_{SO_2}$		dry	367	498	2578	444	603	2802	1605	4534

than $94 \cdot 10^{-2}\ \frac{m^3}{m^3}$, dry, were reached, proving a minimum amount of air ingress. Average CO concentrations were below $90 \cdot 10^{-6}\ \frac{m^3}{m^3}$, dry, in all experiments. Different fuel sulfur contents and different fuel feed rates at a constant flue gas production rate in air (A) and in combustion in pure CO_2/O_2 (labeled: CO2, $y_{O_2,oxid} = 28 \cdot 10^{-2}\ \frac{m^3}{m^3}$) are directly represented in the different SO_2 levels. In the flue gases, no considerable amounts of NO_2 were measured. Therefore, it can be assumed that the influence of SO_2 oxidation by NO_2 in the experiments was limited.

4.2.3.2 Measured SO_3 concentrations before and after filter

Figure 4.36 shows average concentrations of SO_3 measured upstream and downstream of BTS-VR's fabric filter. The lower and upper error bars represent the measured minimum and maximum SO_3 concentrations. The results for each coal are ordered from low to high SO_2 concentrations in the flue gas, i.e. from high to low simulated SO_2 removal rates (CO_2 - 100 %, 8S - 80 %, 5S - 50 %, 2S - 20 %, and OS - 0 % SO_2 removal).

Before filter, increasing SO_3 concentrations can be observed when comparing settings lean in SO_2, such as air and pure CO_2/O_2 combustion, to the oxy-fuel settings with additional SO_2 injection. Since the Hg concentrations in the flue gas are several orders of magnitude below those of SO_3 and Hg is not known to influence the SO_3 formation, it can be assumed that the variations in Hg concentrations (i.e. 5H - 50 %, 8H - 80 %, and OH - 0 % Hg removal) that had been set in cases with constant SO_2 removal rates have no, or only minimal impact on SO_3 concentrations. Therefore, the fact that for cases with the same SO_2 but differing Hg removal rates (i.e. C1-2S5H, C1-2S8H, and C1-2S0H; C1-0S5H and C1-0S0H), similar SO_3 concentrations were measured before filter, proves the repeatability of the SO_3 measurements at this location. After filter, this repeatability could not be established since experiments C1-O2S5H, C1-O0S0H, and C2-CO2 show unexpectedly high SO_3 concentrations (i.e. low SO_3 retention). This may be related to variations in filter inlet (+/-30 °C) and outlet (+/-15 °C) temperatures in the different experiments. SO_3 sorption on the ash can be sensitive at temperatures close to the H_2SO_4 due

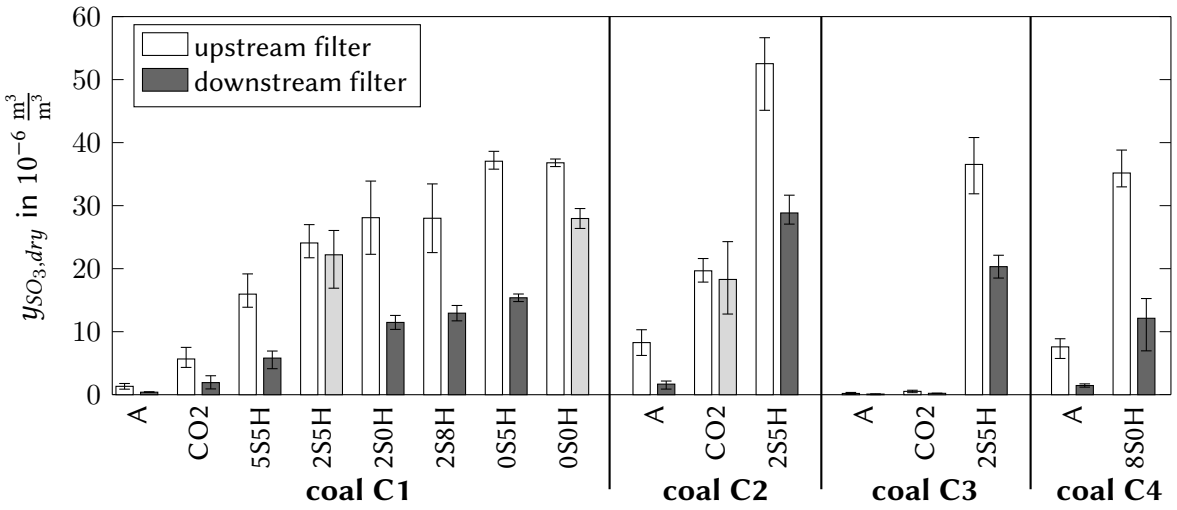

Figure 4.36: SO_3 concentrations measured upstream and downstream the BTS-VR's filter in air (indicated by "A") and simulated oxy-fuel combustion tests with coals C1, C2, C3, and C4 (error bars indicate measured min. and max. concentrations).

point temperature (see Cao et al. [117]). Therefore, the SO_3/H_2SO_4 sorption or condensation on the ash may have been influenced by small differences in the filter temperatures in different experiments, even though, they were always maintained well above the H_2SO_4 due point temperature and temperatures at filter in- and outlet were relatively similar in the conducted experiments.

As expected, in all tests, SO_3 was captured on the fabric filter and concentrations after the filter were considerably lower than those before the filter. For coals C1 and C3 barely any SO_3 was detected downstream the filter under air fired conditions and coal C3 generated only measurable SO_3 concentrations in the oxy-fuel experiment with SO_2 addition to the oxidant gas.

4.2.3.3 Assessment of measured SO_3 concentrations

The extent of the available experimental data from air simulated oxy-fuel operation with four different coals allows for a more detailed evaluation in respect to parameters that may have influenced the SO_3 generation and interactions with fly ash on the fabric filter of the BTS-VR system. Due to the scale and the nature of the performed experiments, it is however not possible to completely separate the impacts of all parameters that potentially influence the sulfur transformation in the system and hence, the experimental evaluation can in several instances not give unambiguous results.

Interactions between SO_2 and SO_3 gases and comparison to published data: Figure 4.37 presents the results of the SO_3 measurements performed before BTS-VR's fabric filter with coals C1, C2, C3, and C4 and before ESP during air and oxy-fuel recycle experiments at the

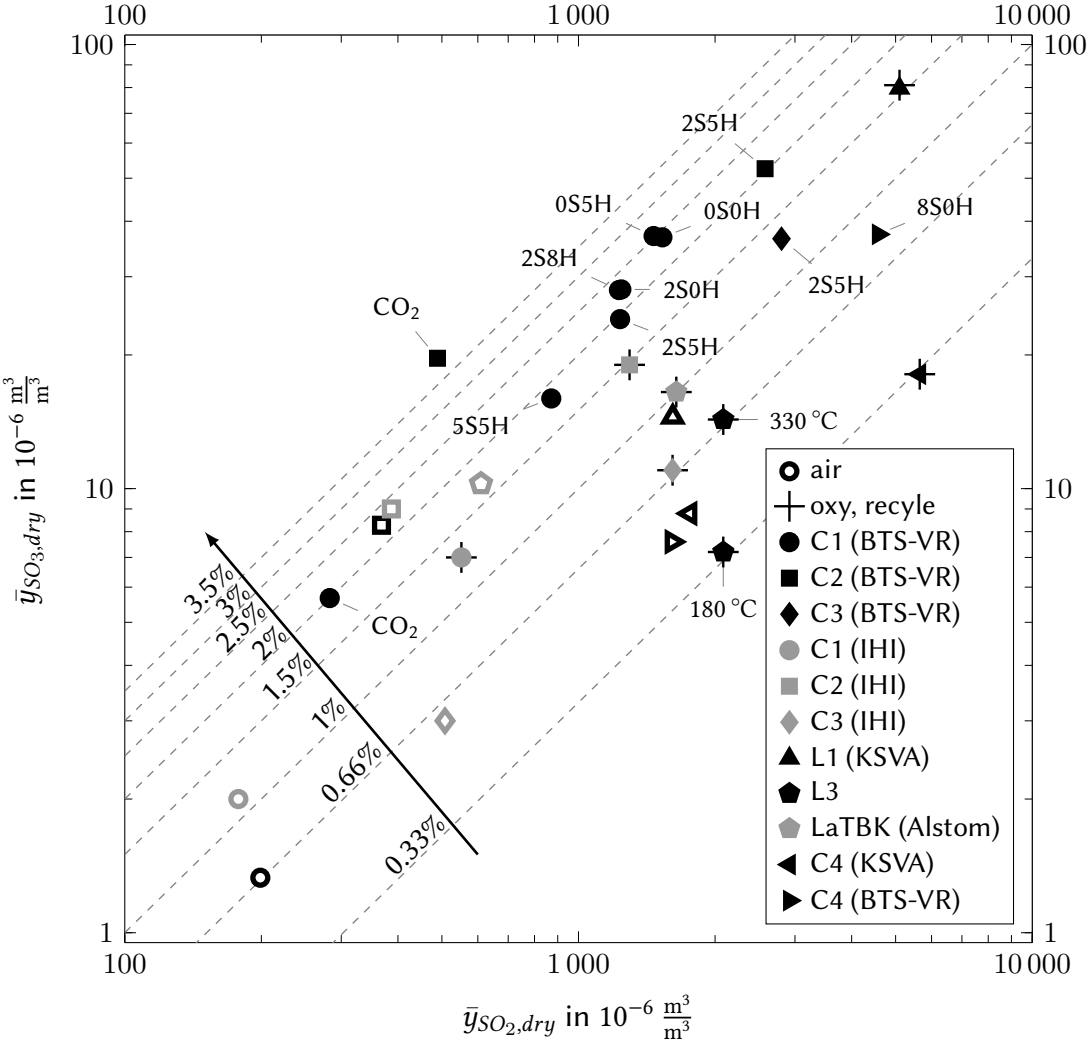

Figure 4.37: $\bar{y}_{SO_2}$ versus $\bar{y}_{SO_3}$ of various air and oxy-fuel experiments performed with fuels C1, C2, C3, L1, L3, and C4 (measurements before filter of BTS-VR/ESP of KSVA and L3; at the pilot plant "Schwarze Pumpe", SO_3 has been sampled at two locations/temperatures upstream the ESP). The concentrations are plotted in comparison to results from IHI's combustion test facility in Japan (combustion of coals C1, C2, and C3 [10]) and Alstom's oxy-fuel pilot system in the USA [229] (combustion of Lusatian pre-dried lignite similar to fuels L2 and L3 of this thesis). The results by others are plotted in gray color. Concentrations measured in air firing are shown as empty symbols and results from actual oxy-fuel recycle combustion are highlighted by a "+" symbol. The dashed lines represent SO_2 to SO_3 conversion ratios.

KSVA and the "Schwarze Pumpe" pilot plant[83] with the fuels L3, L1, and C4[84]. For comparison, SO_3 concentrations generated with similar coal qualities at IHI's combustion test facility in Japan (combustion of coals C1, C2, and C3 [10]) and in combustion of Lusatian pre-dried lignite (qualities similar to fuels L2 and L3 of this thesis) at Alstom's oxy-fuel pilot system in the USA

[83]For "Schwarze Pumpe" pilot plant, $\bar{y}_{SO_3}$ values for two sampling locations upstream ESP with flue gas temperatures of 180 °C and 330 °C are included.

[84]Details on the flue gas compositions during those tests can be found in table 4.2.

[229] are included in figure 4.37. Obviously, there is considerable scatter when measuring SO_3 at different combustion rigs, under different conditions, and with different coals.
SO_2 to SO_3 conversion ratios κ_{23} between approx. 0.3 and 4 % were observed in this dissertation project, with most values being between 0.3 and 2.5 %. This is in the range of data on SO_3 formation from other sources [10, 118, 229, 230]. Similar to the work of Fleig et al. [26], also in this thesis no consistent trend in respect to changes of κ_{23} between air and oxy-fuel firing was observed. However, for most experiments included in this thesis, somewhat higher SO_2 to SO_3 conversion ratios were found in oxy-fuel, compared to air combustion. When comparing $\bar{y}_{SO_2}$ and $\bar{y}_{SO_3}$ from air firing measured in this study with values generated at IHI's combustion test rig [10] a good agreement in the measured levels can be noticed for coals C1, C2, and with a somewhat greater deviation, for coal C[85]. Nonetheless, the comparability of the oxy-fuel results from the two plants may be limited by differences in the test facilities and experimental approaches. At IHI, CO_2 concentrations in the dry flue gas were relatively low (approx. 65 to $75 \cdot 10^{-2}$ $\frac{m^3}{m^3}$, dry) which indicates a considerable extent of air ingress and therefore, flue gas dilution, while at BTS-VR, CO_2 concentrations above $94 \cdot 10^{-2}$ $\frac{m^3}{m^3}$, dry, could be reliably kept during all experiments and hence, measured concentrations are undiluted. In addition, even though the coals were very similar, ash and sulfur contents in the different coal batches used by IHI and at BTS-VR were considerably different. The air and oxy-fuel κ_{23} results obtained in this study for the three Australian coals with simulated impurity recirculation (O2S5H experiments), and those from IHI's oxy-fuel experiments with actual flue gas recirculation, lay all in a band between approx. 0.7 and 2.5 %. Differences at BTS-VR and IHI's plant between comparable experiments (i.e. air vs. air and O2S5H vs. oxy-fuel) are below 0.7 %.
The results from this dissertation project show clearly that y_{SO_3} is very significantly influenced by y_{SO_2} in the flue gas, with increasing y_{SO_3} as y_{SO_2} increases. This will obviously lead to considerably increased y_{SO_3} levels in oxy-fuel combustion where y_{SO_2} increases by a factor of around 3.5-4 (dry basis, see p. 88). The only fuel, for which the same batch has been tested at BTS-VR and at KSVA is coal C4. For this fuel, the SO_3 levels and κ_{23} in air firing were very similar[86], while between the oxy-fuel recycle and the simulated oxy-fuel experiments there was some difference[87]. Similar to the experiments with coals C1, C2, and C3 and the related experiments by IHI, this difference might, to some extent, be due to the experimental setup that was different at the BTS-VR and KSVA test rigs (i.e. real recycle vs. simulated recycle).
In figure 4.38, κ_{23} calculated on basis of SO_3 measurements at filter inlet of BTS-VR are plotted versus alkali (γ_{K+Na}), earth alkali (γ_{Ca+Mg}), and iron γ_{Fe} contents of coals C1, C2, C3, and C4.

[85] Coal C1: IFK - $\bar{y}_{SO_3,dry} = 1.3 \cdot 10^{-6}$ $\frac{m^3}{m^3}$, IHI - $\bar{y}_{SO_3,dry} = 2 \cdot 10^{-6}$ $\frac{m^3}{m^3}$; coal C2: IFK - $\bar{y}_{SO_3,dry} = 8 \cdot 10^{-6}$ $\frac{m^3}{m^3}$, IHI - $\bar{y}_{SO_3,dry} = 9 \cdot 10^{-6}$ $\frac{m^3}{m^3}$; coal C3: IFK - $\bar{y}_{SO_3,dry} = 0.2 \cdot 10^{-6}$ $\frac{m^3}{m^3}$, IHI - $\bar{y}_{SO_3,dry} = 3 \cdot 10^{-6}$ $\frac{m^3}{m^3}$.
[86] BTS-VR: $\bar{y}_{SO_3} = 7.6 \cdot 10^{-6}$ $\frac{m^3}{m^3}$, dry, $\kappa_{23} = 0.5$ %, $\bar{y}_{SO_2} = 1609 \cdot 10^{-6}$ $\frac{m^3}{m^3}$, dry; KSVA: $\bar{y}_{SO_3} = 8.8 \cdot 10^{-6}$ $\frac{m^3}{m^3}$, dry, $\kappa_{23} = 0.5$ %, $\bar{y}_{SO_2} = 1760 \cdot 10^{-6}$ $\frac{m^3}{m^3}$, dry.
[87] BTS-VR: $\bar{y}_{SO_3} = 37.4 \cdot 10^{-6}$ $\frac{m^3}{m^3}$, dry, $\kappa_{23} = 0.8$ %, $\bar{y}_{SO_2} = 4579 \cdot 10^{-6}$ $\frac{m^3}{m^3}$, dry; KSVA: $\bar{y}_{SO_3} = 18.1 \cdot 10^{-6}$ $\frac{m^3}{m^3}$, dry, $\kappa_{23} = 0.3$ %, $\bar{y}_{SO_2} = 5651 \cdot 10^{-6}$ $\frac{m^3}{m^3}$, dry.

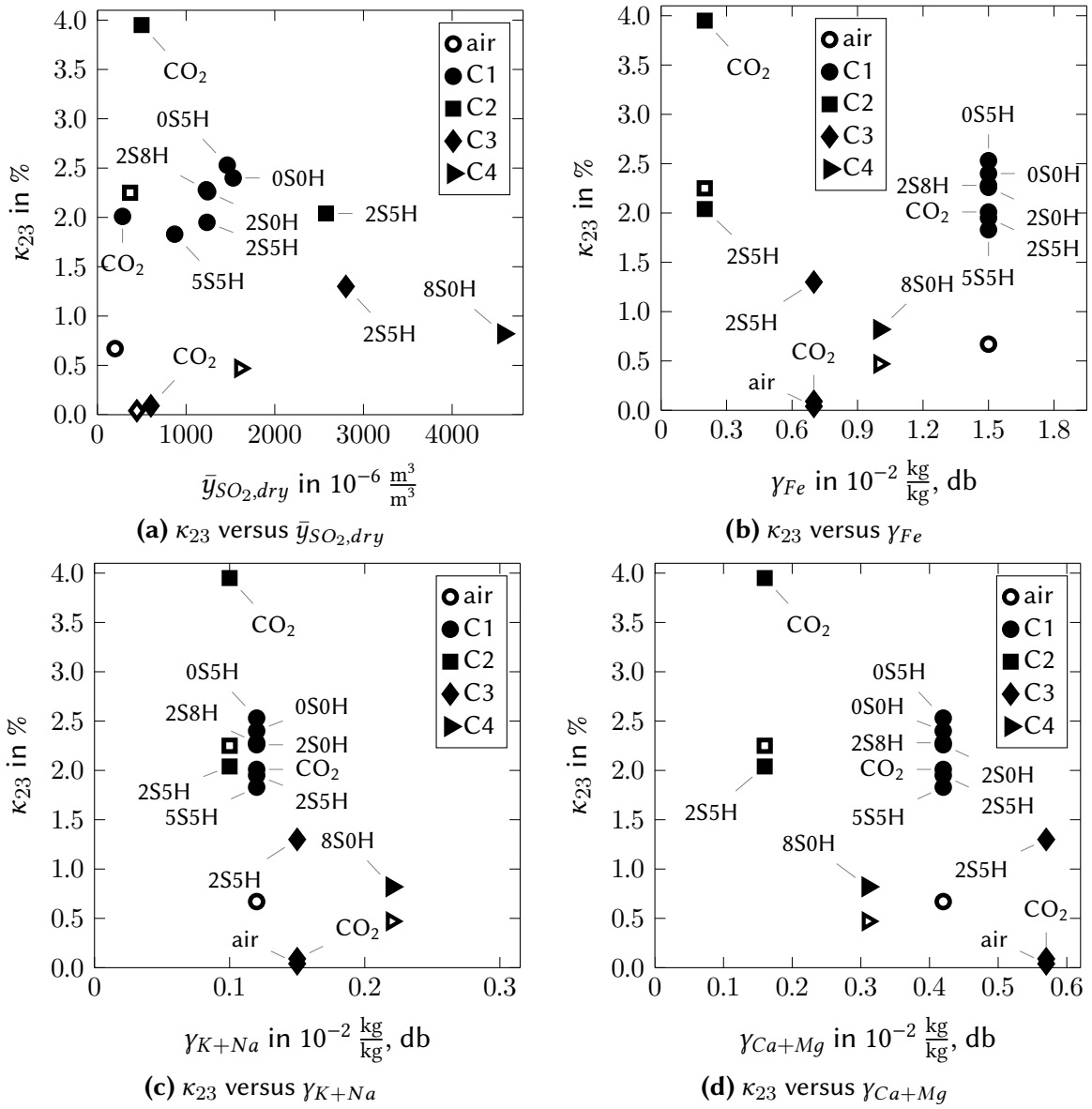

(a) κ_{23} versus $\bar{y}_{SO_2,dry}$

(b) κ_{23} versus γ_{Fe}

(c) κ_{23} versus γ_{K+Na}

(d) κ_{23} versus γ_{Ca+Mg}

Figure 4.38: SO_2/SO_3 conversion ratios κ_{23} (upstream filter) measured in air (empty symbols) and simulated oxy-fuel combustion experiments with coals C1, C2, C3, and C4 at BTS-VR versus (a) $\bar{y}_{SO_2}$ at filter inlet, (b) iron γ_{Fe}, (c) alkali (γ_{K+Na}), and (d) earth alkali (γ_{Ca+Mg}) contents of coals. Empty symbols designate results from air firing.

Those parameters are considered to be relevant to the conversion of SO_2 to SO_3 in combustion processes (see section 2.2.2.1). In addition, κ_{23} is plotted versus $\bar{y}_{SO_2}$ in this figure. The results in figure 4.38 highlight that for individual fuels there seems to be a trend of increasing κ_{23} with increasing SO_2 levels. This statement is supported by the results for coal C1 that was tested under similar simulated oxy-fuel conditions, but with different levels of SO_2 in the flue gas (i.e. experiments 5S5H, 2S5H, 2S8H, 0S5H, and 0S0H). Hence, between those tests, the only significant difference was the SO_2 level. Another observation that can be made is that, even though the trend is not consistent, there seems to be a tendency of higher κ_{23} values in the simulated oxy-fuel combustion, compared to air firing. The effect may be related to the higher

SO_2 levels in the oxy-fuel experiments, rather than to the change in the combustion mode.
It should be highlighted that the correlation of κ_{23} to the alkali (γ_{K+Na}), earth alkali (γ_{Ca+Mg}), and iron γ_{Fe} contents of coals C1, C2, C3, and C4 in figure 4.38 is simplifying an important aspect of ash interactions with SO_x. On basis of the bulk ash chemical analysis, no information is available in respect to the forms in which the different elements are present in the ash and on their reactivity and availability for reactions with SO_2 and SO_3. It is for example possible that iron is present in forms that are not catalytically active for the SO_2 to SO_3 conversion. Nonetheless, the respective plots are included here to put the obtained results in context to some general statements in literature in respect to the SO_3 formation in coal combustion and its dependency from the coal ash composition (see also section 2.2.2.1). For instance, a positive effect of the iron content in coal ashes on κ_{23} that has been mentioned by others [29, 111–113], cannot be observed in figure 4.38b. Even if only experiments with relatively similar SO_2 levels in the flue gas are compared (e.g. C1-A, C2-A, and C3-A; C4-A, 2S5H, 2S8H, 0S5H, and 0S0H; C3-2S5H and C2-2S5H), the response of κ_{23} on γ_{Fe} is mixed[88]. This is similar for the correlation of γ_{Ca+Mg} and κ_{23} that also gives a mixed response and does not allow to conclude whether a high content of earth alkalis in the ash causes always low conversion ratios κ_{23}. The only ash component, for which a negative correlation with κ_{23} can be observed consistently in all experiments is the fuels' alkali content γ_{K+Na}. It seems that a high content of alkalis is always related to low κ_{23} values.
Figure 4.38a gives some additional insight to the SO_2 to SO_3 conversion behavior. The available data indicates that for certain fuels, a relatively high $\bar{y}_{SO_2}$ level is required in order to generate SO_3 in greater quantity. At lower $\bar{y}_{SO_2}$ levels, $\bar{y}_{SO_3}$ seem to be offset potentially by capture of SO_3 either via reactions with ash while in suspension or on the in-stack ash filter that was used. This is most prominent for coal C3. In experiments with low SO_2 levels (i.e. air firing and combustion with pure CO_2/O_2), virtually no SO_3 was measured (see figure 4.36), while at a higher SO_2 concentration, SO_3 was detected in a significant amount. It seems that for coal C3, a certain y_{SO_2} level needs to be reached to generate measurable quantities of SO_3. The behavior is potentially linked to the coal's ash that is relatively rich in alkaline and earth alkaline compounds, compared to the ashes of coals C1 and C2. At low y_{SO_2} levels, the generated SO_3 may efficiently be captured by the ash of coal C3, removing virtually all generated SO_3 from the gas so that no SO_3 can be measured. When the SO_2 and in connection to that the SO_3 concentrations rise, the ash becomes more and more saturated or inactivated/sulfated so that SO_3 cannot be fully retained in the ash and therefore, SO_3 can be found in the flue gas. The proposed effect of ash deactivation by sulfation would be governed by the extent of consumption of alkali and earth alkali elements in the ash by reactions with SO_2 and SO_3, which in turn would be influenced by the level of SO_2 and SO_3. With this mechanism, the

[88] E.g. Coal C2 with the lowest iron content showed similar or higher SO_2 to SO_3 conversion ratios as coal C1 with the highest iron content. Coal C3 with a iron content 3.5 times higher than coal C2 showed the lowest κ_{23} values.

apparent (net) SO_2 to SO_3 conversion ratios κ_{23} that can be measured at a combustion system would be affected by the gross SO_3 formation (i.e. without SO_3 retention in the ash) and the deactivation of ash components that can capture SO_3, by reactions with both, SO_2 and SO_3. Unfortunately, the extent of these reaction steps can hardly be quantified in actual combustion environments with the available analytical tools and hence, it is difficult to proof the proposed mechanism, especially since it may occur to different extents with different fuels, depending on their ash. The proposed mechanism may also be an explanation for the relatively low SO_2 to SO_3 conversion efficiencies of 1.3 and 0.8 % in the C3-2S5H and C4-8S0H experiments with coals C3 and C4, respectively. κ_{23} in the coal C3 and C4 CO_2/O_2 experiments with SO_2 addition are considerably lower than the ones for coals C1 and C2 (with high SO_2 levels, i.e. $\bar{y}_{SO_2} > 1000 \cdot 10^{-6} \frac{m^3}{m^3}$, dry) that were around 2-2.5 %. These low conversion ratios may be related to the ash of coals C3 and C4 that contain more alkalis, and for coal C3 also earth alkalis, than coals C1 and C2. This may be responsible for a more effective capture of part of the generated SO_3 in the ash in the C3-2S5H and C4-8S0H experiments. The reason why in contrast to coal C3, SO_3 can be measured in considerable quantities in air firing of coal C4 may be the much higher sulfur content of this fuel and hence, much higher y_{SO_2} (and potentially gross y_{SO_3}) levels in air firing that are sufficient to overcome the SO_3 retention potential of coal C4's ash. Also the trend of increasing κ_{23} values with increasing SO_2 levels that was observed for coal C1 under comparable oxy-fuel conditions, but with different levels of SO_2 in the flue gas (i.e. experiments 5S5H, 2S5H, 2S8H, 0S5H, and 0S0H) may be associated with a saturation of the ash by sulfation leading to a higher net SO_3 generation at higher y_{SO_2}. Assuming that a change in the combustion environment has no significant impact on the gross SO_3 generation but mainly alters the activity of the ash for sulfur retention, due to a more complete sulfation of the ash, similar considerations in respect to the increasing values of κ_{23} at increasing y_{SO_2} could be also true for coals C3 and C4 that showed higher values of κ_{23} in the high SO_2 CO_2/O_2 experiments with SO_2 addition, compared to the low SO_2 air firing. Coal C2 that has an ash with very low contents of alkaline and earth alkaline elements behaves very different to the other fuels and showed a relatively high SO_2 to SO_3 conversion ratio in air and in pure CO_2 combustion, even at low levels of SO_2. In the 2S5H experiments, the measured κ_{23} value was lower than in the pure CO_2 experiment which cannot be explained on basis of the proposed mechanism.

Summary and outlook in respect to SO_2 to SO_3 conversion in air and oxy-fuel firing: For the application of the oxy-fuel combustion process, the observed coal specific increase of the SO_2 to SO_3 conversion ratios κ_{23} with increasing y_{SO_2} may have the following implication. In oxy-fuel combustion (without $DeSO_x$ of the recirculated gas), y_{SO_2} is by a factor of around 3.4-4.2 higher than in air firing (on dry basis, see p. 88). The observed SO_3 emission behavior implies that due to a considerable increase in the SO_2 levels, the SO_2 to SO_3 conversion ratio κ_{23} may also increase for coals that are under conventional air fired conditions unproblematic

in respect to SO_3 formation (e.g. low S, high Ca coals). The effect should be related to the content and reactivity of alkaline and potentially also earth alkaline compounds in a coal's ash and will likely not be important for coals without considerable contents of those elements if those fuels show already a relatively high SO_2 to SO_3 conversion κ_{23} in air firing (i.e. for such fuels, net SO_3 formation is expected to be not significantly impacted by retention of SO_3 in the ash). To validate the hypothesis that alkalis play a dominant role in the apparent (net) SO_2 to SO_3 conversion efficiency and that a certain SO_3 capture potential in the ash can be offset by high enough levels of SO_2 and SO_3, the following experiment may be worthwhile: One could test a fuel, such as coal C2, and add alkalis to it before combustion (e.g. by spray deposition). When this fuel is combusted, the generation of SO_3 should be considerably offset and the κ_{23} values should be reduced. When in additional combustion experiments with the same alkali doped fuel, the SO_2 level is increased also increasing κ_{23} values should be observed. A similar experiment with increasing SO_2 levels could be done with fuels similar to coals C3 or C4 that are assumed to have ashes that can capture a significant share of the SO_3 formed in the combustion system. Also in these experiments, rising κ_{23} values should be observed with an increase of SO_2. In both cases, κ_{23} should approach a constant value at higher levels of SO_2[89] when the ash is fully deactivated for further SO_3 capture and hence, the SO_3 offset by ash capture becomes small, compared to the measured y_{SO_3} level. Since such experiments were not conducted within the studies leading to this thesis, the proposed SO_3 formation mechanism in which the net SO_3 formation is considerably impacted by capture of SO_3 in the ash could not be validated.

SO_3 capture at a fabric filter: Based on $\bar{y}_{SO_3}$ measured up- and downstream BTS-VR's fabric filter, the SO_3 capture efficiency $\eta_{SO_3,fil}$ was determined. The results are presented in figure 4.39. As introduced on page 150, experiments C1-O2S5H, C1-O0S0H, and C2-CO2 showed unexpectedly high SO_3 concentrations after the fabric filter and hence, their reliability may be compromised. Therefore, results in respect to SO_3 retention on the fabric filter for these experiments and in addition, for experiments with very low SO_3 concentrations (C3-A and C3-CO2)[90] are omitted in the discussions of this section. Nonetheless, the respective results are included in gray color in figure 4.39a.
In air fired conditions, $\eta_{SO_3,fil}$ values of about 70 % (coal A) and 80 % (coal B) were observed. In simulated oxy-fuel operation, $\eta_{SO_3,fil}$ was between 44 and 66 %. In figure 4.39a, $\eta_{SO_3,fil}$ for all experiments is plotted versus $\bar{y}_{SO_3,b.f.}$ at the fabric filter inlet. It can be seen that $\eta_{SO_3,fil}$ is decreasing with increasing $\bar{y}_{SO_3,b.f.}$ (and increasing $\bar{y}_{SO_2}$). Since the fuels have different ash contents and compositions, the experiments for different fuels and combustion conditions may not be fully comparable. However, the effect of decreasing $\eta_{SO_3,fil}$ with increasing $\bar{y}_{SO_3,b.f.}$ can

[89] Assuming that $\kappa_{23,gross}$ is independent of the y_{SO_2} level.
[90] Those are not further discussed due to a high measurement uncertainty at low $\bar{y}_{SO_3}$ and a large impact of small variations of $\bar{y}_{SO_3}$ on $\eta_{SO_3,fil}$.

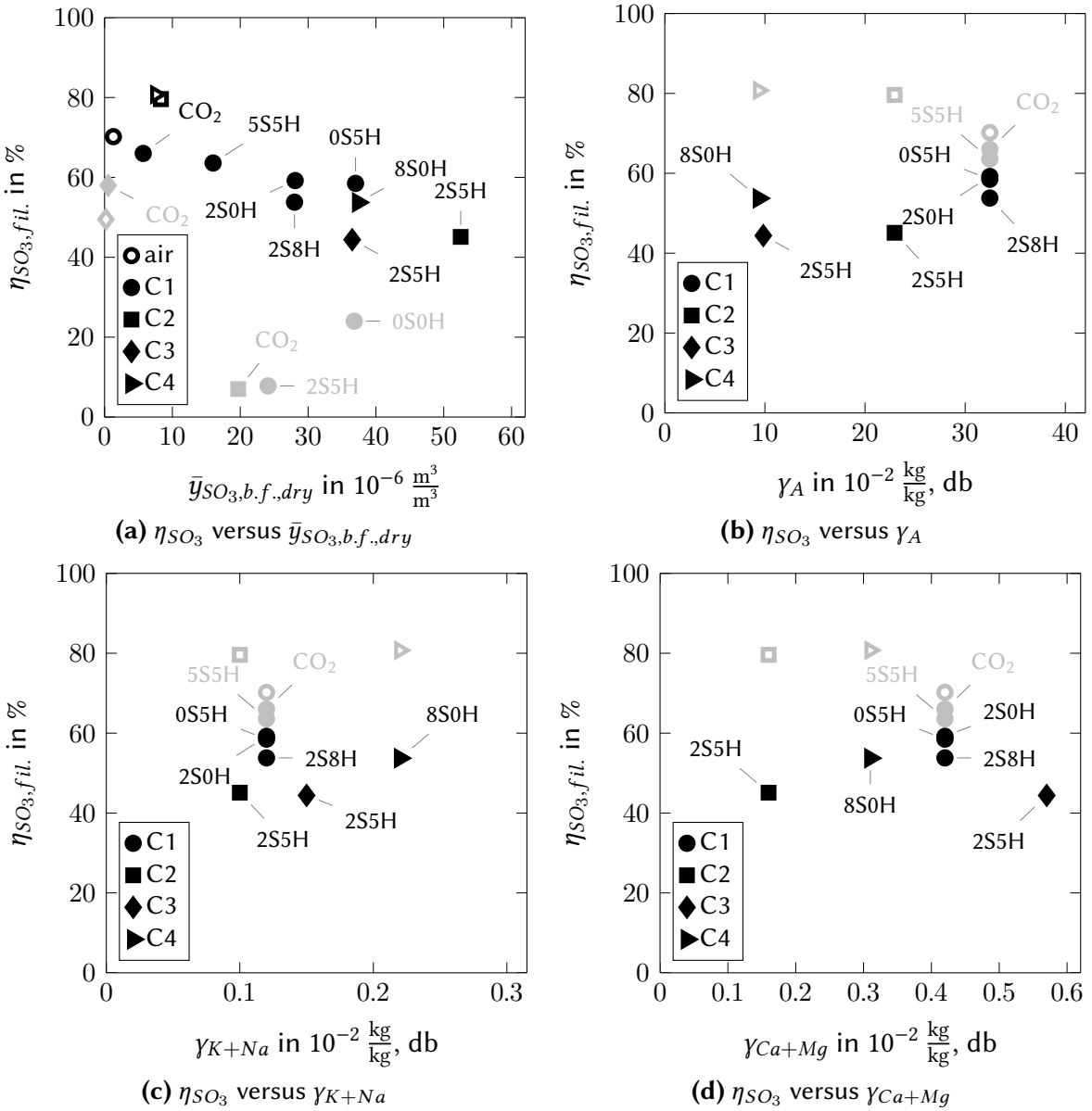

(a) η_{SO_3} versus $\bar{y}_{SO_3,b.f.,dry}$

(b) η_{SO_3} versus γ_A

(c) η_{SO_3} versus γ_{K+Na}

(d) η_{SO_3} versus γ_{Ca+Mg}

Figure 4.39: SO_3 capture efficiencies η_{SO_3} at the BTS-VR's fabric filter (without DSI) measured in air (empty symbols) and simulated oxy-fuel combustion experiments with coals C1, C2, C3, and C4 at BTS-VR versus (a) $\bar{y}_{SO_3,b.f.}$ at filter inlet, (b) ash (γ_A), (c) alkali ($\gamma_{K+Na,db}$), and (d) earth alkali ($\gamma_{Ca+Mg,db}$) contents of coals. In sub-figure (a), gray η_{SO_3} values indicate unexpectedly low results or results calculated on basis of very small $\bar{y}_{SO_3}$ (omitted in other sub-figures), while in sub-figures (b), (c), and (d), gray shaded η_{SO_3} values indicate results outside a range of $\bar{y}_{SO_3,b.f.}$ between 28 and $53 \cdot 10^{-6}$ $\frac{m^3}{m^3}$, dry, that are not considered to be comparable to other results. Empty symbols designate results from air firing.

also be observed for the different oxy-fuel experiments with coal C1 alone that despite the different SO_2 levels were relatively similar and are assumed to be comparable. The described effect may be related to a saturation of the SO_3 capture potential of the ash on the filter or to an insufficient residence time of the flue gas at the fabric filter for capture of higher amounts of

SO_3. This is relevant to the high SO_2 and SO_3 oxy-fuel combustion process since it highlights that SO_3 retention in fabric filter systems is limited especially at higher levels of SO_2 and SO_3. In figure 4.39, also ash (γ_A), alkali (γ_{K+Na}), and earth alkali (γ_{Ca+Mg}) contents of coals C1, C2, C3, and C4 are related to $\eta_{SO_3,fil}$. Since there seems to be a considerable correlation between $\bar{y}_{SO_3,b.f.}$ and $\eta_{SO_3,fil}$, in the following considerations only experiments that had roughly similar SO_3 levels before filter (i.e. $\bar{y}_{SO_3,b.f.} = 28$ to $53 \cdot 10^{-6}$ $\frac{m^3}{m^3}$, dry) are included. As explained above, a separation of the parameters "ash content" and "ash composition" is not possible in a technical scale combustion system, which limits the possibilities for interpretation. Nonetheless, few indications can be made. Coal C1 with the highest ash content shows the highest $\eta_{SO_3,fil}$ values, followed by coals C4, C2, and C3. However, the influence of the ash content on $\eta_{SO_3,fil}$ seems to be week or not present at all for some of the other fuels. γ_{K+Na} and γ_{Ca+Mg} seem not necessarily to be a decisive parameter for the SO_3 capture on the fabric filter, since the trends for $\eta_{SO_3,fil}$ versus γ_{K+Na} and γ_{Ca+Mg} are inconsistent. Possibly, a large fraction of the reactive alkalis and earth alkalis present in the ash have already been sulfated by reactions with SO_x before the ash reaches the filter, and hence, these compounds are not longer active for SO_3 capture.

Calculated sulfuric acid dew point temperatures: SO_3/H_2SO_4 is responsible for low temperature corrosion and fouling in colder parts of a plant. A crucial parameter that influences both issues and can be used to evaluate their risk, is the H_2SO_4 dew point temperature $\vartheta_{H_2SO_4,dew}$. Based on H_2O (y_{H_2O}) and measured SO_3 concentrations before ($\bar{y}_{SO_3,b.f.}$) and after ($\bar{y}_{SO_3,a.f.}$) filter, $\vartheta_{H_2SO_4,dew}$ for the SO_3 experiments at BTS-VR was calculated. The results are summarized in table 4.13. $\vartheta_{H_2SO_4,dew}$ values between 92 °C and 163 °C are found before filter and between 86 °C and 157 °C after filter, with coal C2 having the highest dew point temperatures. The SO_3 capture on the fabric filter was equivalent to a reduction of $\vartheta_{H_2SO_4,dew}$ between 1 °C and 16 °C. $\vartheta_{H_2SO_4,dew}$ after filter under air fired conditions were 12 to 27 °C below those of the combustion tests in pure CO_2/O_2 combustion and 26 to 67 °C below those of the CO_2/O_2 configurations

Table 4.13: $\vartheta_{H_2SO_4,dew}$ before (b.f.) and after (a.f.) filter in air and simulated oxy-fuel experiments at BTS-VR with coals C1, C2, C3, and C4. In addition, the difference of the H_2SO_4 dew point temperatures at filter in- and outlet $\Delta\vartheta_{H_2SO_4,dew}$ is given. Dew points were calculated, according to [123], on basis of y_{H_2O}, $\bar{y}_{SO_3,b.f.}$ and $\bar{y}_{SO_3,a.f.}$.

		coal C1								coal C2			coal C3			C4	
species	unit	C1-A	C1-CO2	C1-5S5H	C1-2S5H	C1-2S0H	C1-2S8H	C1-0S5H	C1-0S0H	C2-A	C2-CO2	C2-2S5H	C3-A	C3-CO2	C3-2S5H	C4-A	C4-8S0H
$\vartheta_{H_2SO_4,dew,b.f.}$		111	129	149	153	155	155	158	158	132	144	163	92	106	158	128	154
$\vartheta_{H_2SO_4,dew,a.f.}$	°C	99	118	140	153	146	147	149	155	116	143	157	86	97	152	111	146
$\Delta\vartheta_{H_2SO_4,dew}$		12	11	10	1	9	7	9	3	16	1	6	7	9	6	17	8

with simulated SO_2 and H_2O recirculation. The higher dew point temperatures in the oxy-fuel experiments with SO_2 and H_2O recirculation cannot only be attributed to the increase of $\bar{y}_{SO_3}$ but also to the increased H_2O levels. Sulfuric acid dew point temperatures have implications on the minimum temperatures at which oxidant preheaters and recycle lines of an oxy-fuel power plant can be operated without risking corrosion or fouling (see section 2.2.2.1). Systems need to be operated reliably above $\vartheta_{H_2SO_4,dew}$ to avoid those problems. The results of this study indicate that in oxy-fuel operation oxidant preheater temperatures in a range of about 30 to 70 °C above the ones used in air firing may be required for an optimal operation.

5 Summary and conclusions

Even though, compared to the years between 2005 and 2015, the activities to implement CO_2 capture technologies in the power and other sectors have slowed down globally and especially in Europe, widely accepted energy system scenarios by IEA [6] predict that accomplishing the goals of the international Paris Agreement[91] [7] will only be possible by a widespread application of CO_2 capture and storage technologies[92]. This will require a rapid industrial implementation of CO_2 capture technologies, such as the oxy-fuel process. This thesis focuses on the behavior of sulfur oxides in PF fired air and oxy-fuel systems. Sulfur oxides are responsible for certain operational problems and gas cleaning requirements. A better understanding of the related issues will help in the technical and economical optimization of the oxy-fuel technology. Within this thesis, a range of experimental investigations on the retention of sulfur oxides and the stability of sulfates in ashes and deposits, on acid gas (SO_2, SO_3, and HCl) control, and on SO_3 formation were conducted. The experimental work is in parts supported by theoretical considerations and thermodynamic equilibrium simulation. In most of the conducted experiments it was possible to comparatively assess air and oxy-fuel fired systems to identify significant alterations between combustion modes. In that way, a broad data basis is provided that will be useful to others that focus on the modeling and design of oxy-fuel fired processes. In practically relevant oxy-fuel configurations, compared to air firing, the exclusion of airborne N_2 from combustion leads to an increase of the SO_2 concentration by a factor of about 3.4 to 4.2, referring to dry and of about 2.9 to 3.5, when referring to wet flue gas conditions. These ranges have been determined for different Eastern German lignites and imported hard coals. The increased SO_2 levels in oxy-fuel combustion lead to an increased stability of sulfates in oxy-fuel power boiler systems. According to a thermodynamic equilibrium study, other effects of the oxy-fuel combustion environment on the behavior of ashes and deposits seem to be minimal, provided the temperatures in the combustion system are not altered. The decomposition temperature of one of the most important sulfatic components, $CaSO_4$, in ashes can be expected to rise by about 50 to 80 °C.

In dedicated experiments, studying the stability of sulfates in deposits under CO_2/O_2 fired furnace conditions, the enhanced stability of sulfates at high temperatures when operating with

[91] i.e. "Holding the increase in the global average temperature to well below 2 °C above pre-industrial levels..." [7].
[92] Capture and storage of 400 $\frac{Mt}{a}$ and 6.8 $\frac{Gt}{a}$ of CO_2 in 2025 and 2060, respectively.

increased SO_2 levels could be clearly demonstrated. In comparative air and oxy-fuel recycle combustion experiments at a 500 kW combustion test facility, a considerable increase of the sulfur retention in the ash has been observed in oxy-fuel combustion. This can be associated to the increased sulfate stability and longer residence times of the flue gases in the furnace. For lignites with a significant sulfur retention potential in their ash, by 10 to 12 percentage points less sulfur was emitted with the flue gases in oxy-fuel firing, leading to significantly reduced energy based SO_2 emissions (i.e. in $\frac{mg}{MJ}$). When firing a hard coal with a lower sulfur retention potential, the effect was much less pronounced and the reduction amounted only to about 5 percentage points, with some uncertainty due to the variability in the sulfur content of this fuel. The enhanced sulfur retention affects the composition of process ashes and deposits, with significantly higher SO_3 contents and greater degrees of sulfation of the respective oxy-fuel samples from lignite combustion and only slight alterations for the hard coal. For the lignites, the increase in sulfur content and ash sulfation degrees was most pronounced in finer ash fractions removed by the ESP system, with the increase in the bottom ash being less prominent. An issue that was observed in one of the oxy-fuel experiments is that combustion instabilities, which caused short term oxygen deficiencies in the furnace, did strongly influence the SO_2 emission behavior of the oxy-fuel fired system, producing significant SO_2 emission peaks and reducing the sulfur retention in the ash. An optimization of the combustion system and the utilization of a sufficient oxygen excess can help to avoid this. Increased sulfate contents of process ashes from oxy-fuel combustion may influence the utilization of coal combustion by-products since the respective SO_3 limits for ashes are low and will likely not be kept with oxy-fuel combustion if fuels have even only a low sulfur retention potential in their ash (i.e. if they contain some calcium, magnesium, sodium, and/or potassium). The compositions of process ashes from oxy-fuel combustion in the 500 kW test facility were similar to the ones from Vattenfall's 30 MW oxy-fuel pilot plant "Schwarze Pumpe" and hence, the smaller scale experimental results from KSVA, in this context, seem to be transferable to larger scale industrial systems.

An analysis of fly ashes and deposits sampled from the furnaces of the 500 kW facility KSVA in air and oxy-fuel operation and from the 30 MW oxy-fuel pilot plant "Schwarze Pumpe" showed that higher SO_3 contents and higher extents of sulfation were present also in the oxy-fuel samples from combustion of lignites. No other significant changes between the samples from air and oxy-fuel combustion and between the samples from the two test facilities were observed. Uncooled oxy-fuel deposit samples from these tests that represent outer heat exchanger deposit layers and were considerably more sulfated at higher temperatures in oxy-fuel operation, indicate that the temperature level at which fouling by sulfatic deposits occurs and may be problematic seems to be shifted to higher temperatures in oxy-fuel combustion. Moreover, sintering of deposits by sulfation may be more pronounced. Cooled deposits from lignite combustion experiments at KSVA had already a high degree of sulfation in air firing and the

differences in respect to sulfation to the cooled oxy-fuel samples were small. Deposits from air and oxy-fuel combustion of a hard coal that had a relatively low earth alkali content did not show a considerable increase in the SO_3 level. This indicates that higher SO_2 concentrations in oxy-fuel combustion do not necessarily affect boiler deposits and the oxy-fuel deposition behavior in this context is highly fuel specific.

Theoretical considerations about the oxy-fuel recycle combustion process indicate that the higher sulfate stability and the recirculation of flue gases enhance the desulfurization performance compared to conventional air firing. One can take advantage of this effect when employing a desulfurization system within the oxy-fuel recycle loop. The simplest method to do so is by injection of dry powdered sorbents. Within this thesis, comprehensive experiments, studying DSI with different sorbents ($CaCO_3$ and $Ca(OH)_2$) and injection locations (co-injection with fuel, injection to the furnace at approx. 1100 °C, and upstream of a fabric filter or ESP) were conducted in air, simulated oxy-fuel, and oxy-fuel recycle combustion. The experiments were conducted with a high sulfur and chlorine hard coal, which allows for assessment of the removal efficiencies of SO_2, SO_3, and HCl. It was shown that in all tested combustion conditions SO_2 capture is most efficient at higher temperatures (i.e. furnace injection at 1100 °C), while the opposite is true for the control of HCl and SO_3. The injection location for the sorbent should thus be selected on basis of the target acid gas species. Nonetheless, one can generally expect to remove SO_2, SO_3, as well as HCl at any of the injection locations, however, with certain differences in the removal efficiencies. An effect that was consistently observed in oxy-fuel recycle combustion experiments at the 500 kW facility KSVA, but not in simulated once-through oxy-fuel combustion at the 20 kW test rig BTS-VR, is a significantly enhanced desulfurization efficiency, compared to air firing. An increase by as much as 29 percentage points has been observed in the respective experiments that seems to be linked to positive effects that the oxy-fuel recycle combustion has on the average residence time of SO_2 molecules in the furnace. The impact of the higher sulfate stability in oxy-fuel combustion seems to be of lower importance. The SO_2 capture by injection of $CaCO_3$ and $Ca(OH)_2$ together with the fuel or to the furnace in oxy-fuel recycle combustion has been proven to be very effective, allowing a capture of 50 % to more than 80 % of the SO_2 at moderate $\alpha_{Ca/S}$ levels between 1.7 and 2.9. Even co-injection of $CaCO_3$ together with the fuel, which is generally considered to be of relatively low efficiency, reached a SO_2 capture efficiency of 73 % (at $\alpha_{Ca/S}$ = 3). DSI upstream an ESP for HCl control reached in a range of 76-78 % HCl reduction (at $\alpha_{Ca/2Cl}$ = 1.1-1.9), with only small differences between combustion modes. Also SO_3 could be reduced considerably by injection of $Ca(OH)_2$ to the furnace and upstream the ESP, even though only a limited number of measurements in this respect are available.

The results in respect to DSI illustrate that this technology may, due to the considerable performance increase, be very interesting for application in oxy-fuel recycle combustion. With minimal investment costs, the technology will allow to capture the bulk of the sulfur within the

oxy-fuel recycle loop, without excessive flue gas cooling, as with other wet and semi-dry flue gas cleaning techniques and with only a moderate excess in sorbent. DSI in oxy-fuel recycle combustion will allow to control gaseous sulfur oxide levels within an oxy-fuel boiler and SO_3 levels in the GPH and recycle lines to tolerable levels (e.g. in respect to fouling and corrosion) and may allow to avoid wet FGD systems completely if the remaining SO_2 can be removed before, during, or after compression in the CPU system.
Experimental investigations on the formation of SO_3 in air and simulated oxy-fuel combustion showed that higher SO_2 levels are the most important parameter responsible for the higher SO_3 concentrations in oxy-fuel operation. Other fuel specific parameters, such as the content of iron oxides and of earth alkalis in the ash that are often considered to play an important role in respect to SO_3 formation, did not show a consistent impact. In the conducted experiments, only the alkali content consistently showed a negative correlation to the observed SO_3 levels. Experiments with fuels having a certain SO_3 self-retention potential indicate that a saturation of their ash by sulfation with the increased SO_2 and SO_3 levels in oxy-fuel combustion may lead to a considerable increase of the net SO_2 to SO_3 conversion efficiency in oxy-fuel compared to air firing.

Recommendations for further work: On basis of the results and observation of this thesis, a number of research topics for further studies can be defined. The most noteworthy ones are listed below:
1. Within this thesis it was shown that high SO_2 levels in oxy-fuel combustion (about 2.9 to 3.5 times higher than in air firing of the same fuel) stabilize sulfates, in particular $CaSO_4$, at higher temperatures. This implies that the sulfate stability in oxy-fuel combustion of a lower sulfur fuel (e.g. $1 \cdot 10^{-2}\ \frac{kg}{kg}$) is comparable to the stability when combusting a high sulfur fuel (e.g. $3 \cdot 10^{-2}\ \frac{kg}{kg}$) in air firing. It can by assumed that sulfate stabilities of such lower sulfur fuels in oxy-fuel combustion can hence be tolerated and boiler cleaning can be handled by standard equipment used in air firing, such as soot blowers. This statement is also in agreement to the opinion of power plant manufacturers [143, 144]. Experimental results from pilot and demonstration plants that were mostly operated with low sulfur fuels support this statement since form such plants no excessive problems by sulfatic fouling was reported. However, it is unclear whether somewhat higher sulfur levels (i.e. up to 1.5 to $2 \cdot 10^{-2}\ \frac{kg}{kg}$) with higher sulfate stabilities would still be tolerable in long term oxy-fuel operation without recycle gas desulfurization. To date no clear maximum tolerable SO_2 level in oxy-fuel boilers can be given. Such information would be useful in the design of oxy-fuel power plants, e.g. to enable a sound decision in respect to the necessity of recycle gas desulfurization and to its extent. Future long term demonstration activities involving oxy-fuel operation of actual power boilers will help to enhance the understanding of the process limitations in respect to SO_2 levels in the boiler. If possible, in such cases, fuels with sulfur contents in the range of 1 to $2 \cdot 10^{-2}\ \frac{kg}{kg}$ should

be tested and the boiler operation should be evaluated in respect to fouling issues and also corrosion to identify limitations. Also higher sulfur fuels could be tested in combination with different extents of recycle gas desulfurization. In addition, oxy-fuel power boiler simulations that include sub-models simulating fouling by sulfates could help to gain a better understanding on this issue.

2. The experiments with injection of dry $CaCO_3$ and $Ca(OH)_2$ showed that in oxy-fuel combustion, DSI can achieve much better desulfurization performances than in air firing. Different to conventional air fired systems it may hence be economically viable that DSI can be applied to remove a large fraction of the acid gases present in oxy-fuel flue gases. The application of DSI may be interesting due to the technology's relatively low investment costs, which may be particularly beneficial for future oxy-fuel power plants running at low capacity factors. To better understand the economics of the application of DSI in oxy-fuel power plants, process configurations with combinations of desulfurization equipment (e.g. DSI, $DeSO_x$ during compression and condensate knock-out and $DeSO_x$ after compression) should be developed and assessed by conducting detailed process simulations and economic analyses of such systems. The assessment could consider different fuel sulfur contents and associated sorbent and by-product disposal costs, different power plant capacity factors and if possible costs linked to increased fouling when DSI is applied to boilers. Also case studies for greenfield, brownfield and retrofit oxy-fuel projects would be sensible. On that basis an economic benchmarking against other $DeSO_x$ configurations (e.g. using CDS, SDA or WFGD systems) could be conducted to identify optimal solutions for desulfurization in oxy-fuel power plants. The experimental data and results of this thesis are an ideal basis for such a study.

3. The experiments conducted in respect to SO_3 formation and control indicate a coal specific increase of the SO_2 to SO_3 conversion ratio with increasing SO_2 levels. This increase was observed for coals with a certain sulfur retention potential in their ash. It may be related to a saturation of the sulfur retention potential if high SO_2 and SO_3 levels are present in the combustion environment as is the case in oxy-fuel operation. The effect could cause unexpectedly high SO_3 levels and associated operational problems in oxy-fuel combustion and is therefore worthwhile to be studied further. This saturation hypothesis could be validated in dedicated experiments: One could test a low alkali and earth-alkali coal that is doped with additional alkalis/earth-alkalis. When this fuel is combusted, the generation of SO_3 should be considerably reduced compared to the undoped fuel and the SO_2 to SO_3 conversion ratios should be reduced. When in additional combustion experiments with the alkali/earth-alkali doped fuel, the SO_2 level is increased by addition of SO_2 to the oxidant, increasing SO_2 to SO_3 conversion ratios should be observed. A similar experiment could involve the combustion of a high alkali and/or earth-alkali coal in atmospheres that are doped with various levels of SO_2. Also in these experiments, rising SO_2 to SO_3 conversion ratios should be observed with an increase of SO_2. In both cases, this conversion ratio might approach a more or less constant

value at higher levels of SO_2 when the ash is fully deactivated for further SO_3 capture and hence, the SO_3 retention in the ash becomes small.

A Apendices

A.1 Complementary phase diagrams for solid compounds without sulfur

The following phase diagrams complement figures 4.3 and 4.4 which are introduced in chapter 4.1.2. For the two considered ash systems (i.e. CaO and Fe_2O_3 and CaO, Fe_2O_3, and SiO_2), these figures present details on thermodynamically stable solid ash compounds in simulated air and oxy-fuel atmospheres that do not contain sulfur.

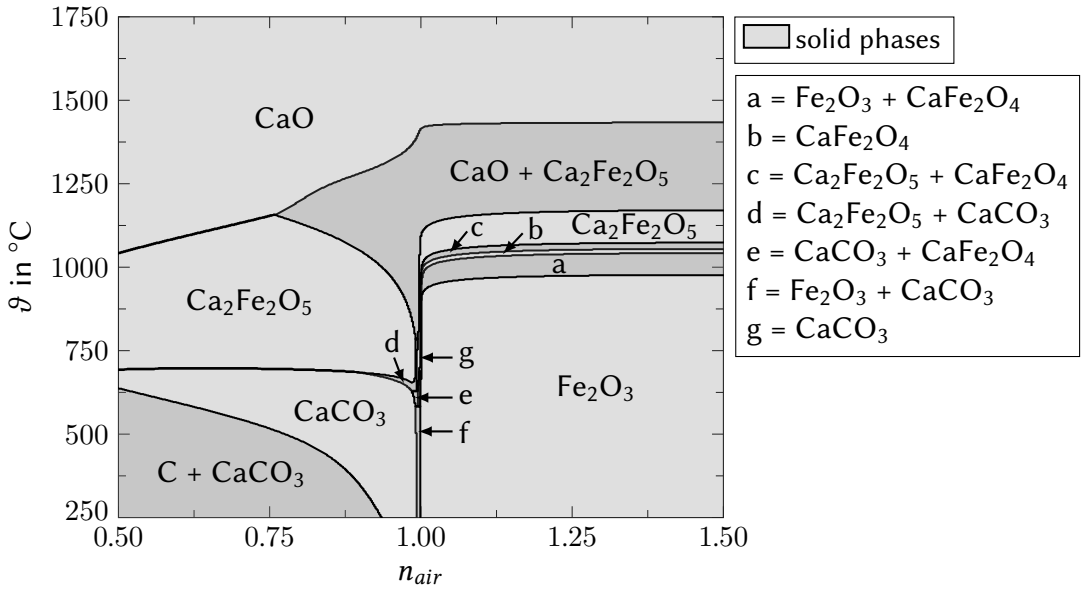

(a) Air

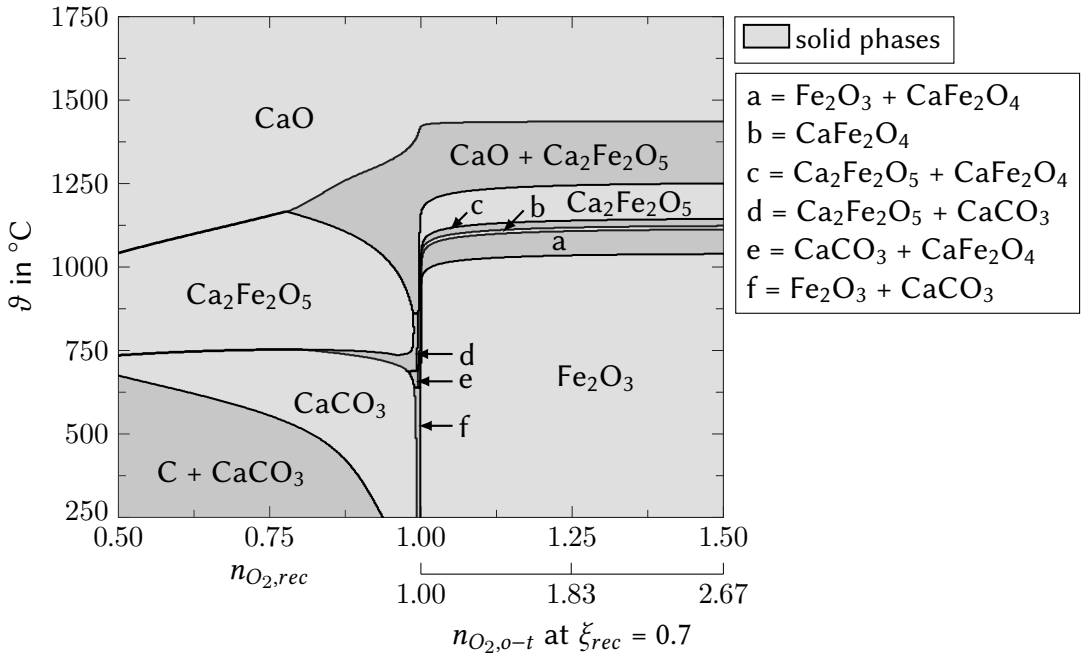

(b) Oxy-fuel

Figure A.1: Thermodynamically stable solid phases without sulfur in a system with **CaO** and **Fe_2O_3** in atmospheres of L3 lignite air and oxy-fuel combustion (solid phases plotted with opacity, i.e. darker gray areas indicate coexisting solid phases; gaseous phases are not shown; this diagram complements figure 4.3 on p. 90).

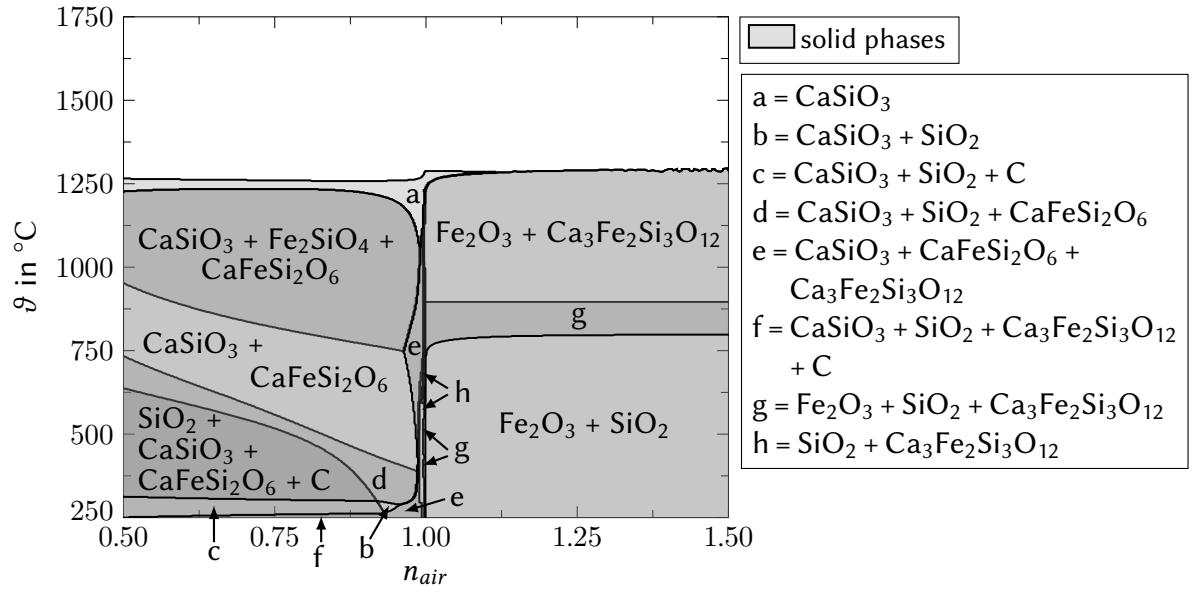

(a) Air

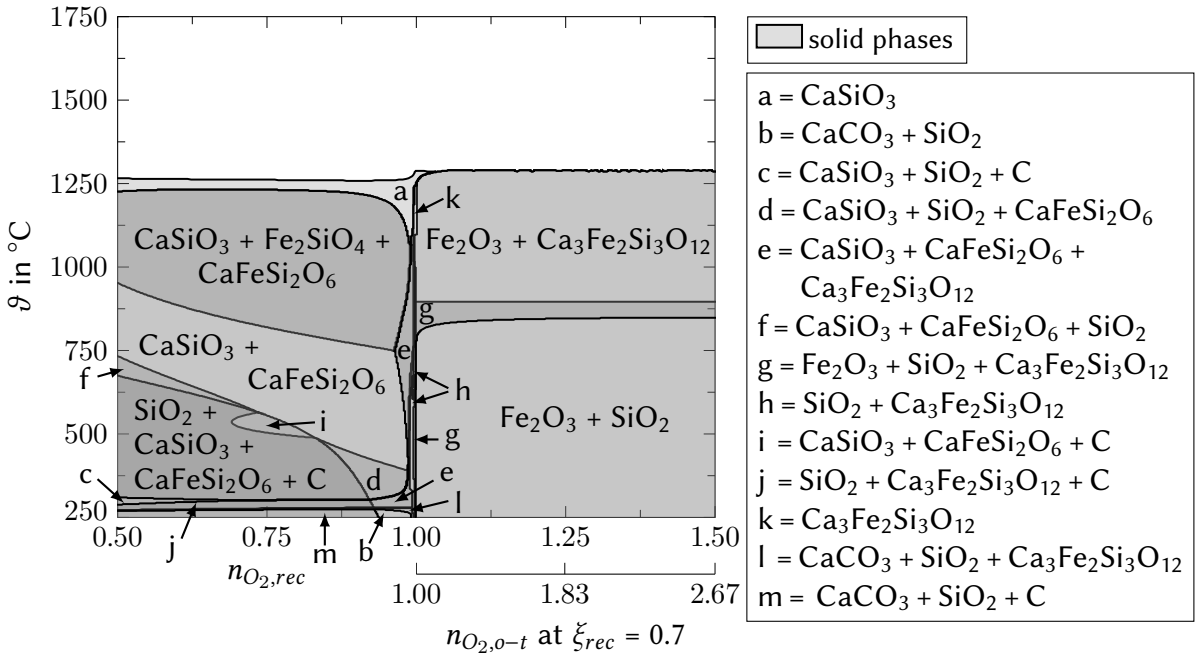

(b) Oxy-fuel

Figure A.2: Thermodynamically stable solid phases without sulfur in a system with **CaO**, **Fe_2O_3**, and **SiO_2** in atmospheres of L3 lignite air and oxy-fuel combustion (solid phases plotted with opacity, i.e. darker gray areas indicate coexisting solid phases; gaseous phases are not shown; this diagram complements figure 4.4 on p. 91).

A.2 Detailed SEM-WDX element maps of deposit samples

On the following pages, additional SEM-WDX element maps that include elements not shown in the main part of this thesis and complement the respective figures 4.10 and 4.17 are shown. The SEM images 4.10, A.3, A.4, A.5 and A.6 were recorded with the magnification and are printed here in a slightly larger scale. The same is the case for figures 4.17, A.7 and A.8.

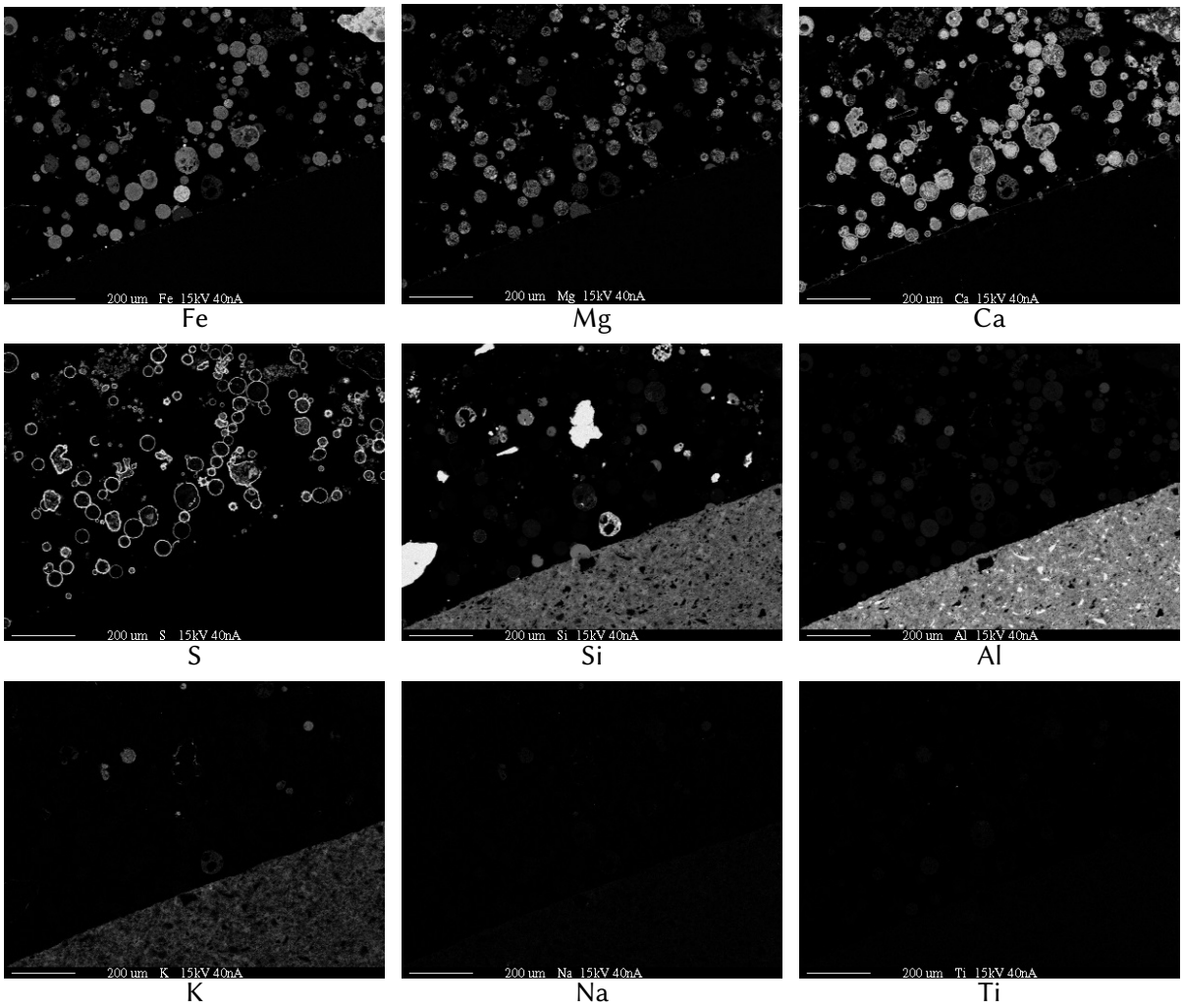

Figure A.3: SEM-WDX element maps of uncooled deposits sampled in sulfate stability tests at BTS-VR (ϑ_{Probe} = 1100 °C, $y_{SO_2,wet}$ = 750 · 10^{-6} $\frac{m^3}{m^3}$; this figure complements figure 4.10a and was recorded at the same magnification but is plotted here in a slightly larger scale).

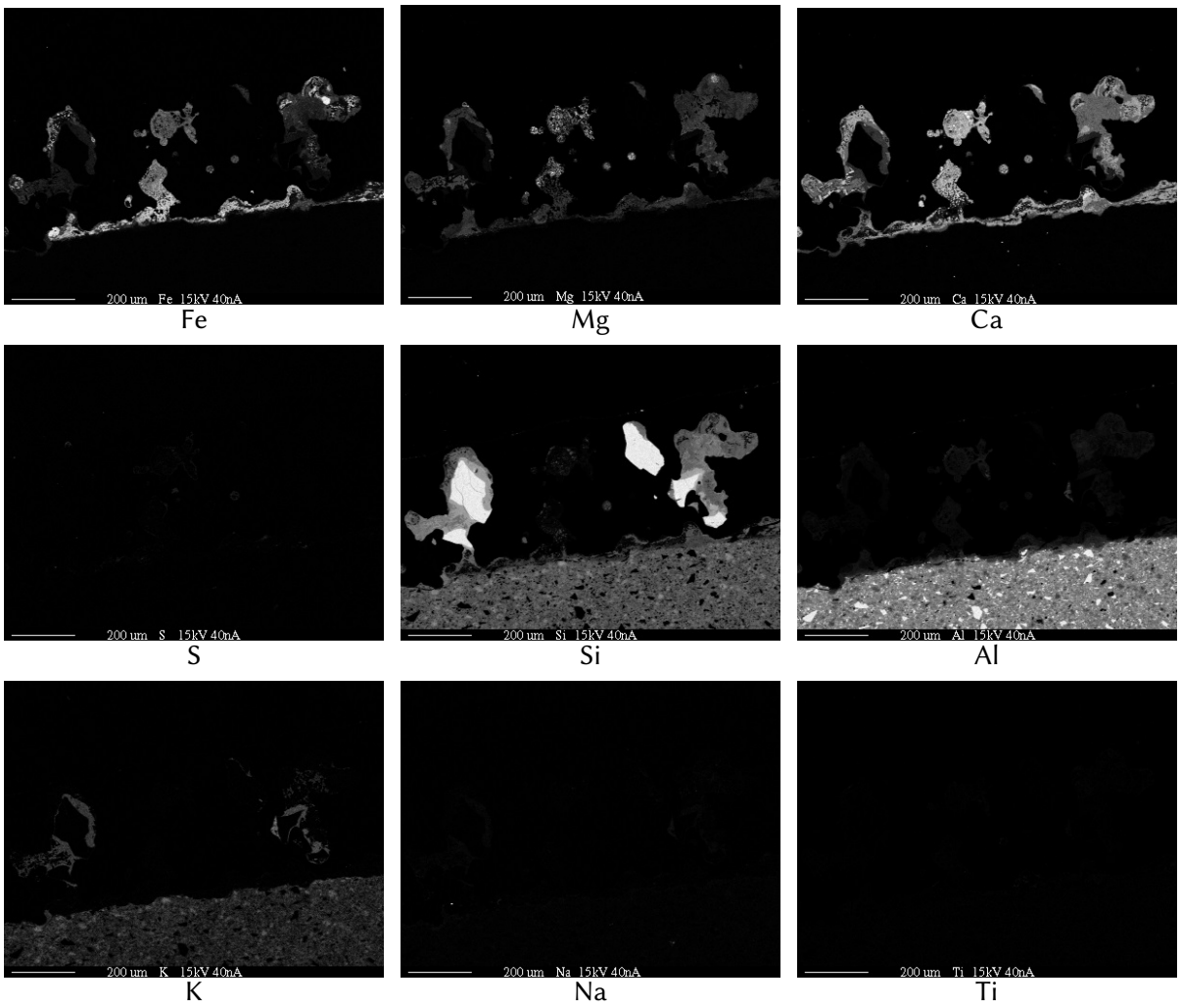

Figure A.4: SEM-WDX element maps of uncooled deposits sampled in sulfate stability tests at BTS-VR (ϑ_{Probe} = 1200 °C, $y_{SO_2,wet}$ = 750 · 10^{-6} $\frac{m^3}{m^3}$; this figure complements figure 4.10b and was recorded at the same magnification but is plotted here in a slightly larger scale).

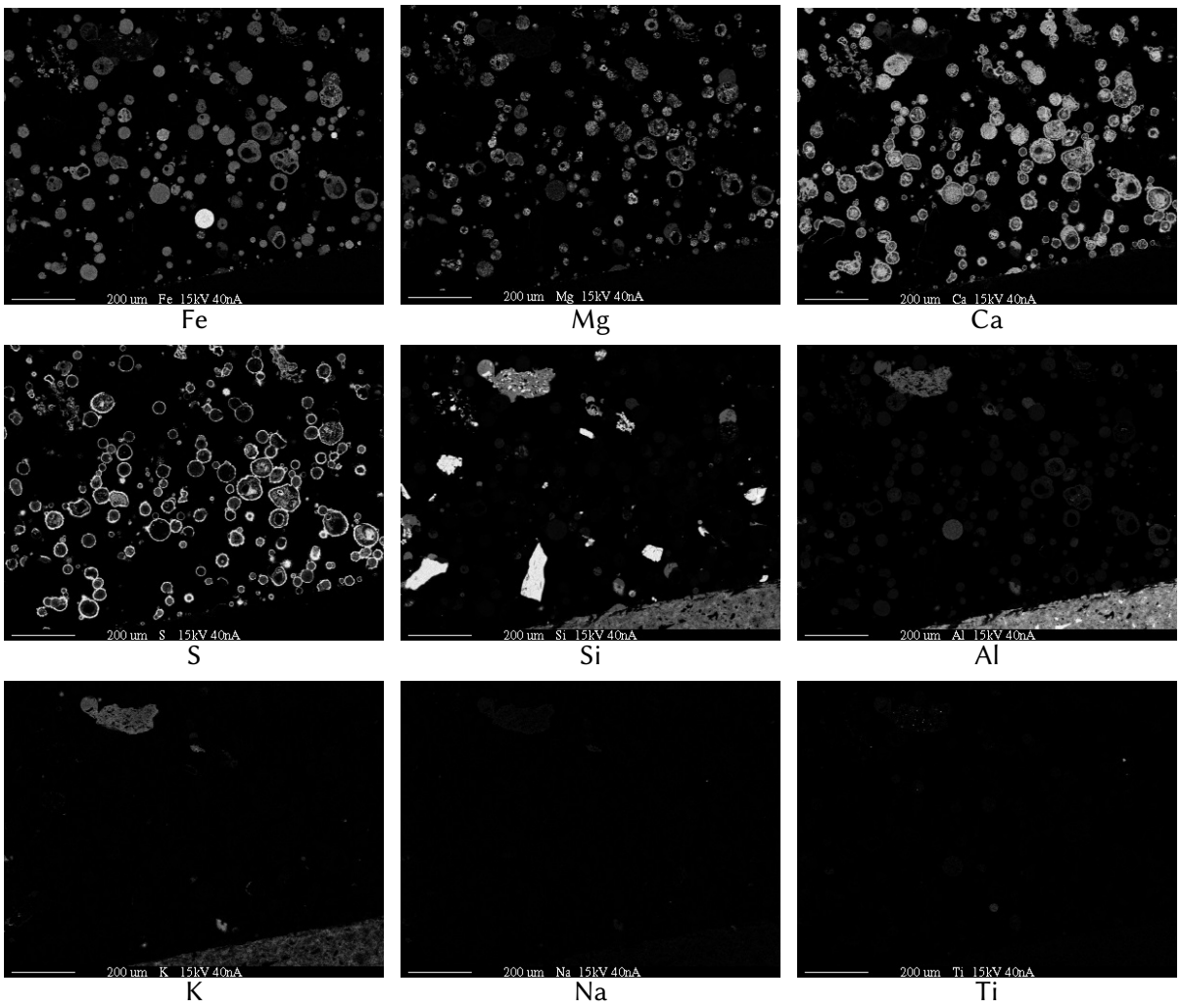

Figure A.5: SEM-WDX element maps of uncooled deposits sampled in sulfate stability tests at BTS-VR (ϑ_{Probe} = 1100 °C, $y_{SO_2,wet}$ = 5530 · 10^{-6} $\frac{m^3}{m^3}$; this figure complements figure 4.10c and was recorded at the same magnification but is plotted here in a slightly larger scale).

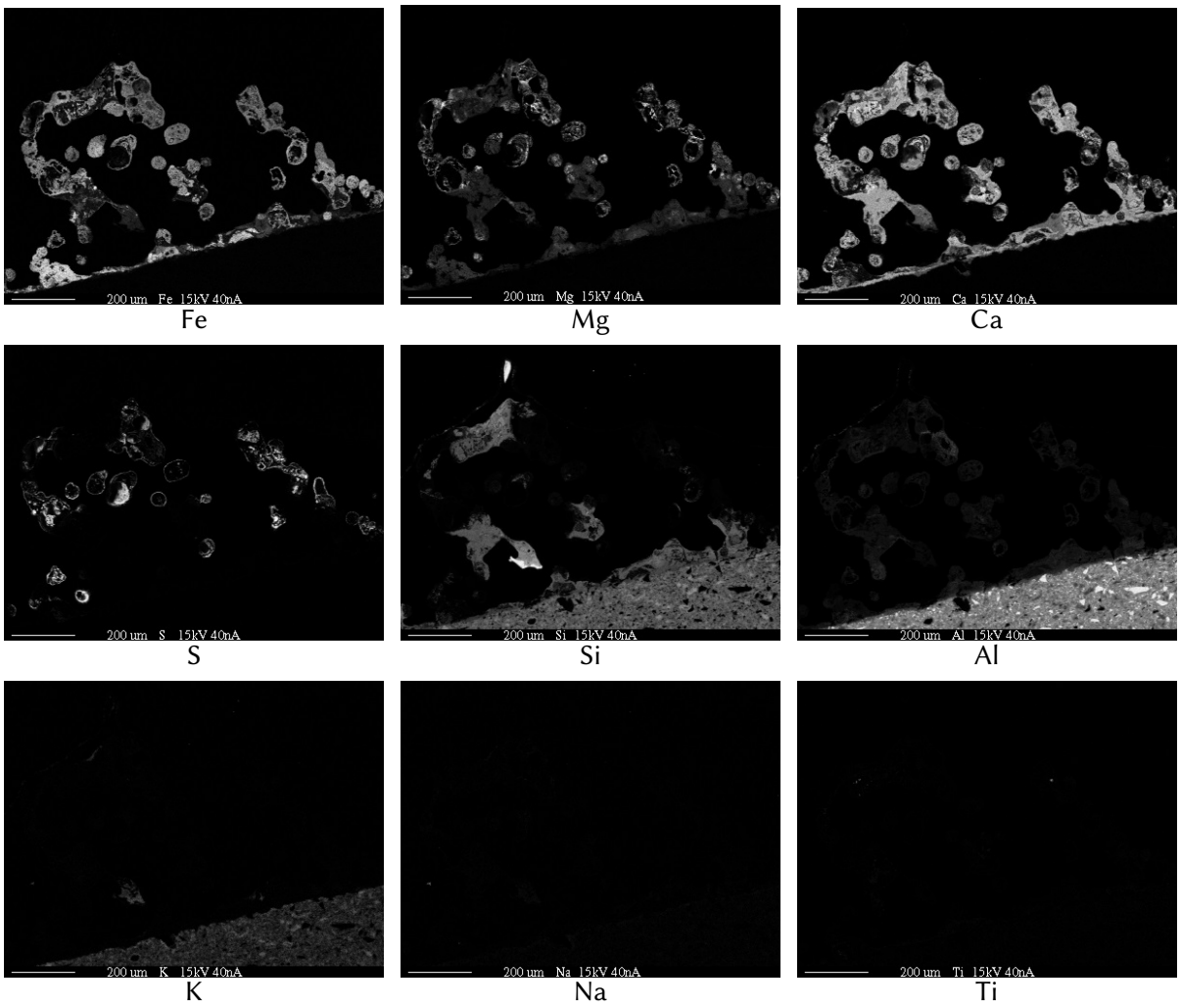

Figure A.6: SEM-WDX element maps of uncooled deposits sampled in sulfate stability tests at BTS-VR (ϑ_{Probe} = 1200 °C, $y_{SO_2,wet}$ = 5530 · 10^{-6} $\frac{m^3}{m^3}$; this figure complements figure 4.10d and was recorded at the same magnification but is plotted here in a slightly larger scale).

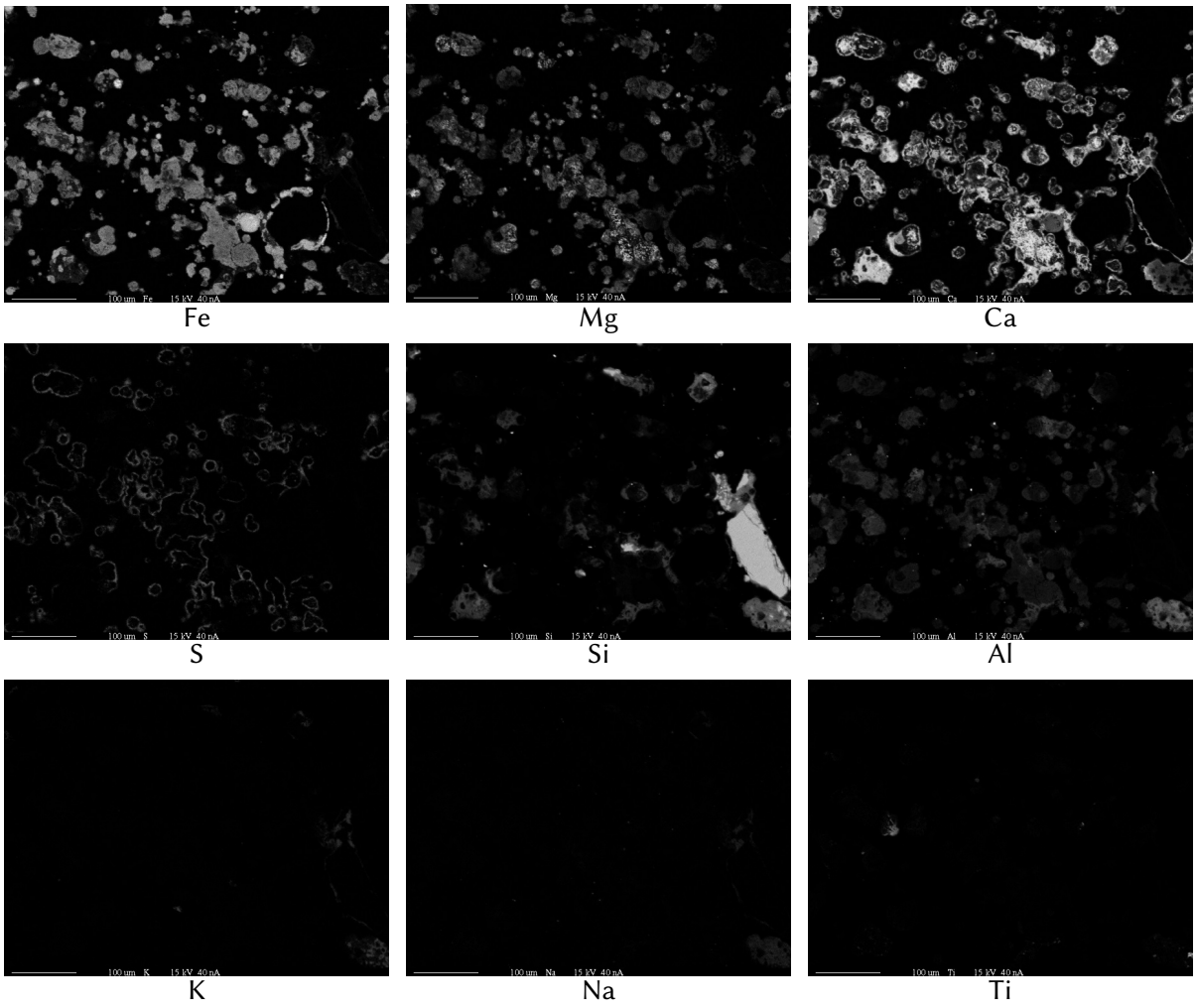

Figure A.7: SEM-WDX element maps of uncooled deposits sampled at a flue gas temperature ϑ_{FG} of 1095 °C (at Lev11) in air firing of lignite L2 at KSVA (this figure complements figure 4.17 and was recorded at the same magnification but is plotted here in a slightly larger scale).

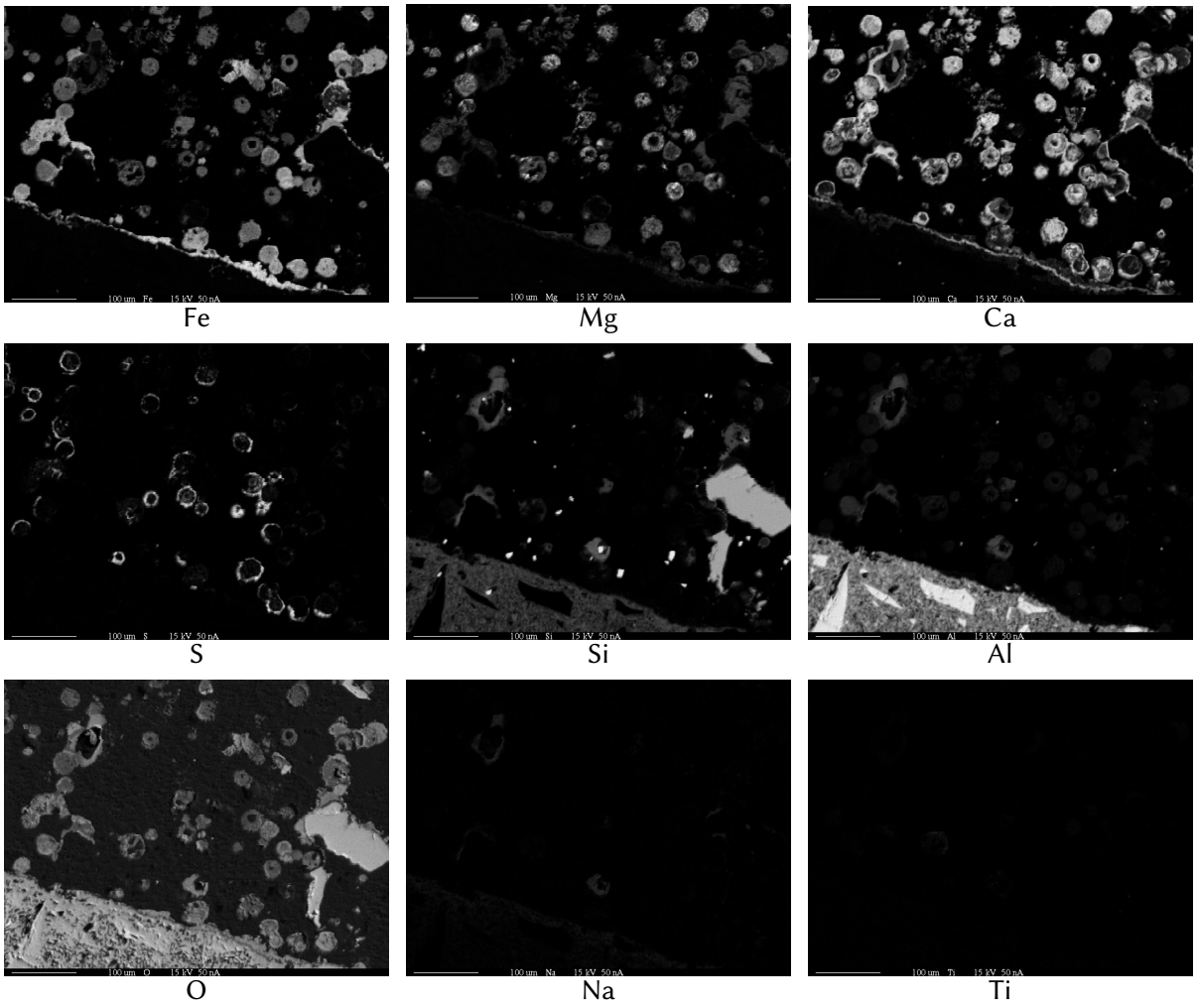

Figure A.8: SEM-WDX element maps of uncooled deposits sampled at a flue gas temperature ϑ_{FG} of 1055 °C (at Lev11) in oxy-fuel firing of lignite L2 at KSVA (this figure complements figure 4.17 and was recorded at the same magnification but is plotted here in a slightly larger scale).

A.3 SEM-EDX particle analyses of samples from Vattenfall's oxy-fuel pilot plant

Figure A.9 shows analyses of characteristic fly ash and deposit particles sampled from the furnace (level 4 and level 8) of Vattenfall's "Schwarze Pumpe" oxy-fuel pilot plant. For these analyses typical particles found in those samples have been selected and were characterized according to their morphology. Sub-figure A.9a shows analyses that were done at different locations of characteristic calcium and iron rich spherical particles with a sulfur rich shell (see figure 4.17 for some examples of such particles). In this sub-figure, spot analyses of the sulfur and calcium rich shell, of a calcium depleted and iron enriched area just below this shell and of the calcium, iron, and sulfur rich core of larger of these particles are included. It is assumed that these particles' core composition is representative to the original bulk composition of such ash particles (see [42] for more details). In sub-figure A.9b, other characteristic particle categories that contained no sulfur and were found in the deposit and ash samples are plotted. Those are, spherical particles and deformed particles that built bridges between other particles, and irregular silicon rich particles that are assumed to origin from sand contained in the fuel. To be able to plot the compositions determined in spot analyses in ternary SiO_2, Fe_2O_3, and CaO diagrams, they had to be normalized to $100 \cdot 10^{-2} \frac{kg}{kg}$ disregarding all other components besides SiO_2, Fe_2O_3, and CaO. In this context, only individual particle spot analyses were used for which the sum of the ash oxides of SiO_2, Fe_2O_3, CaO, and SO_3 was above $75 \cdot 10^{-2} \frac{kg}{kg}$. For comparison, also the fuel's ash analysis is plotted here. All the spot analyses have been conducted by SEM-EDX.

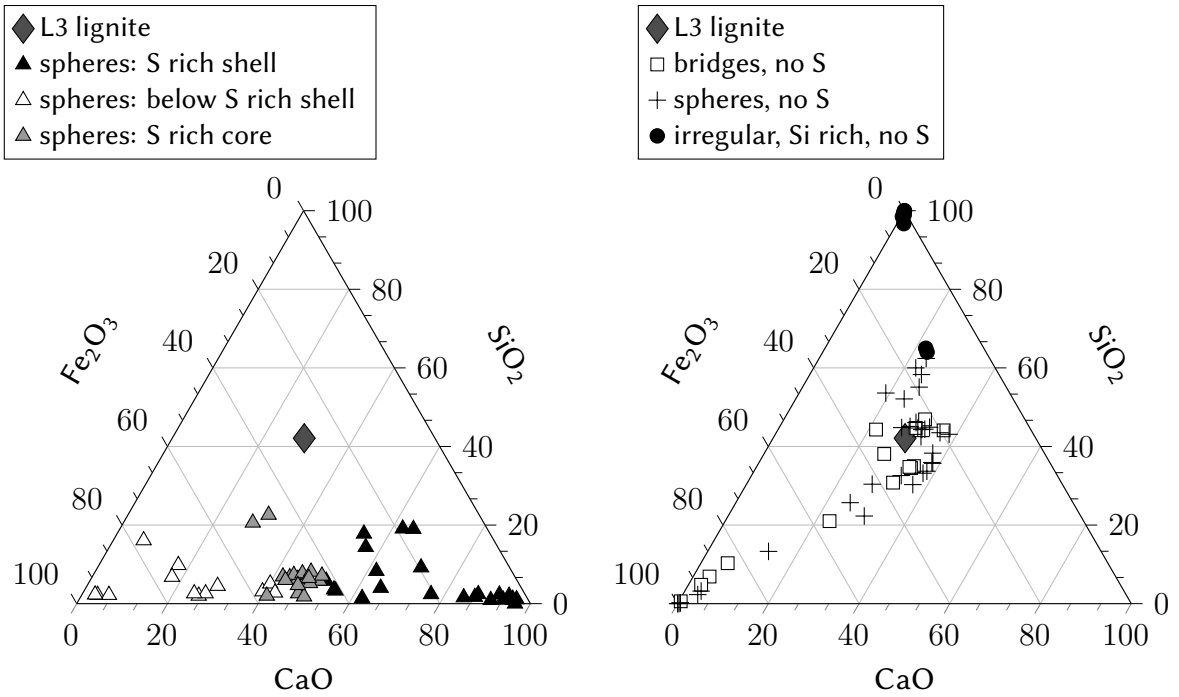

(a) Composition of sulfur rich particles **(b)** Composition of particles without sulfur

Figure A.9: Composition of characteristic particles from deposits and fly ashes sampled from Vattenfall's oxy-fuel pilot plant (a: spot analyses of different locations of characteristic calcium and iron rich spherical particles with sulfur rich shell; b: other characteristic spherical and deformed particles that contained no sulfur). The compositions were determined by SEM-EDX spot analyses. Those have been normalized to $100 \cdot 10^{-2} \frac{\text{kg}}{\text{kg}}$ disregarding all other components besides SiO_2, Fe_2O_3, and CaO. In this context, only particle spot analyses were used, for which the sum of the ash oxides SiO_2, Fe_2O_3, CaO, and SO_3 was above $75 \cdot 10^{-2} \frac{\text{kg}}{\text{kg}}$. For comparison, also the fuel's ash composition is plotted.

A.4 Air and oxy-fuel gas concentration trends

The following plots complement figures 4.19 and 4.20 that are introduced in chapter 4.2.1.4. In figures A.10 and A.13, scatter plots of SO_2 and CO versus O_2 concentrations measured at the end of KSVA's furnace in air and oxy-fuel combustion tests with lignite L1 and measured after ESP in oxy-fuel combustion of lignite L3 at the "Schwarze Pumpe" pilot plant are shown. The concentrations y_{SO_2} and y_{CO} in these plots are not recalculated to a reference O_2 concentration. The measured concentration trends over time that were used to prepare the scatter plots 4.19, A.10, 4.20, and A.13 are presented in figures A.11, A.12, and A.14.

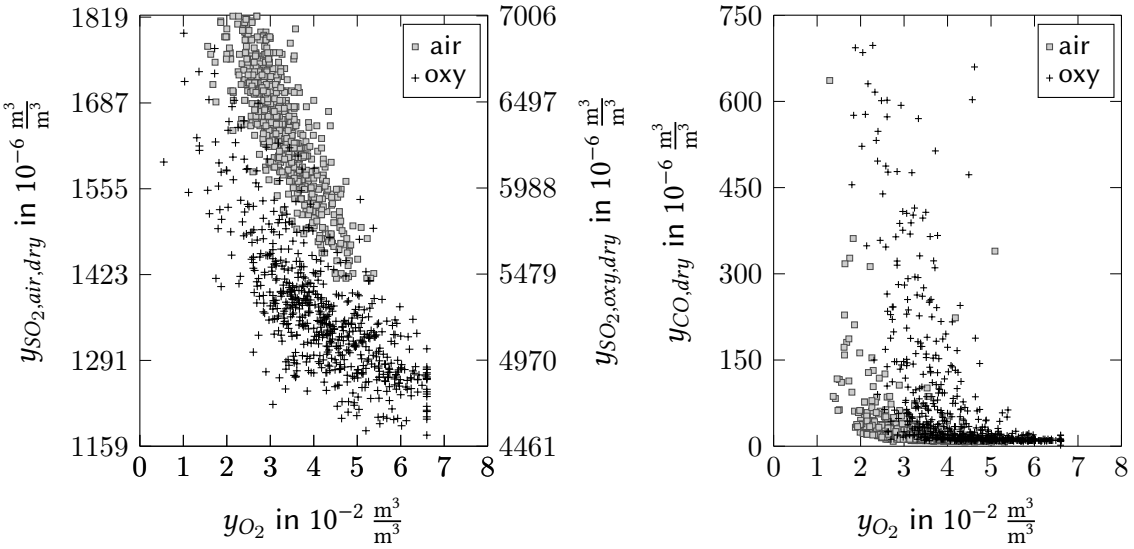

(a) SO_2 vs. O_2 **(b)** CO vs. O_2

Figure A.10: Scatter plots of y_{SO_2} (a) and y_{CO} (b) vs. y_{O_2} measured at KSVA's furnace exit in lignite L1 air and oxy-fuel combustion. Plots show data of 2 h of operation for each combustion setting. The concentrations y_{SO_2} and y_{CO} are **not** recalculated to the same O_2 concentration y_{O_2}. y_{SO_2} axes are scaled to represent between 70 % and 110 % of the theoretical maximum SO_2 concentrations in lignite L1 air and oxy-fuel combustion with an outlet O_2 level of $4 \cdot 10^{-2}\ \frac{m^3}{m^3}$, dry (this plot complements figure 4.19).

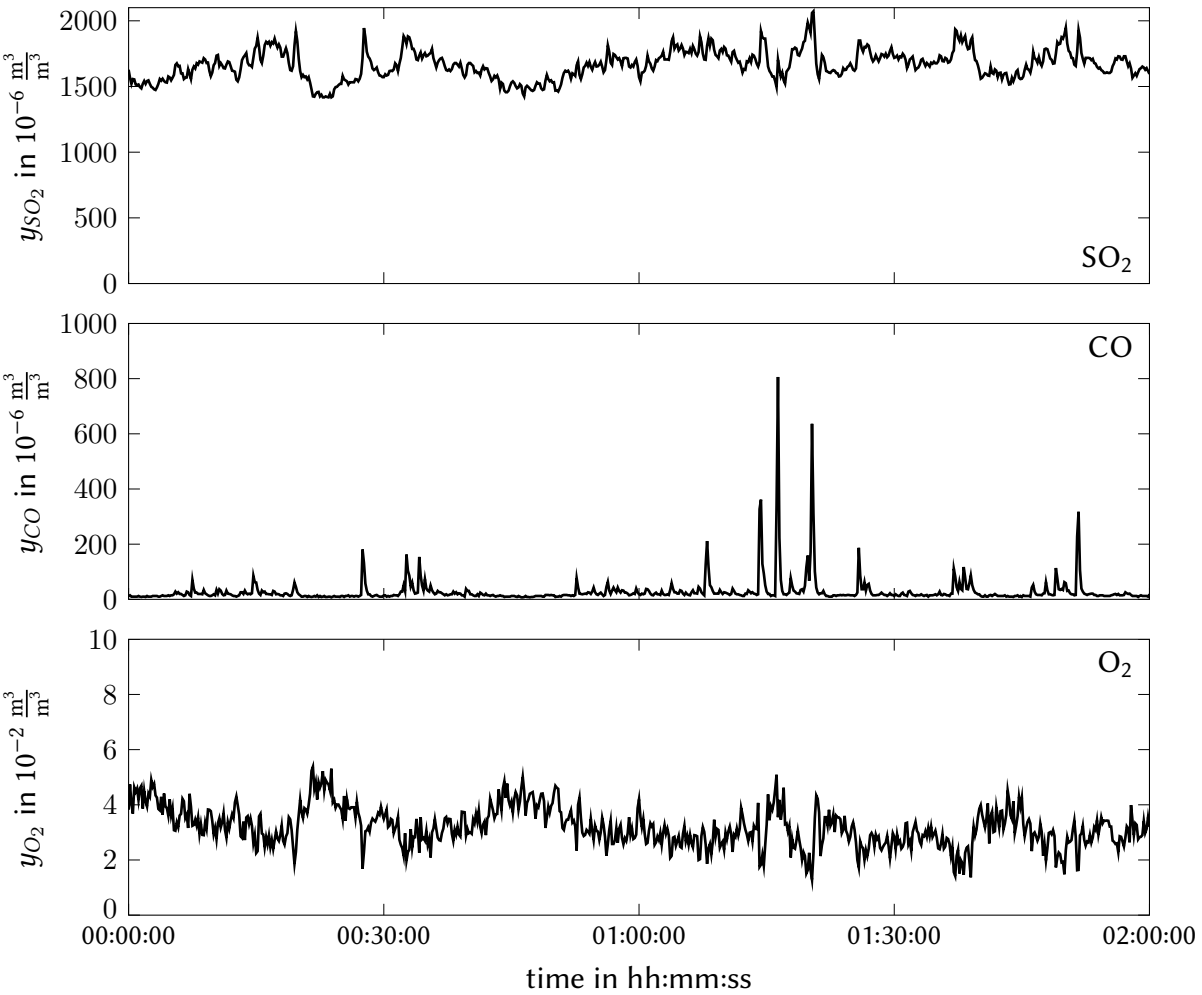

Figure A.11: Concentration trends for SO_2, CO, and O_2 measured during 2 h of air firing of lignite L1 (this plot complements figure 4.19).

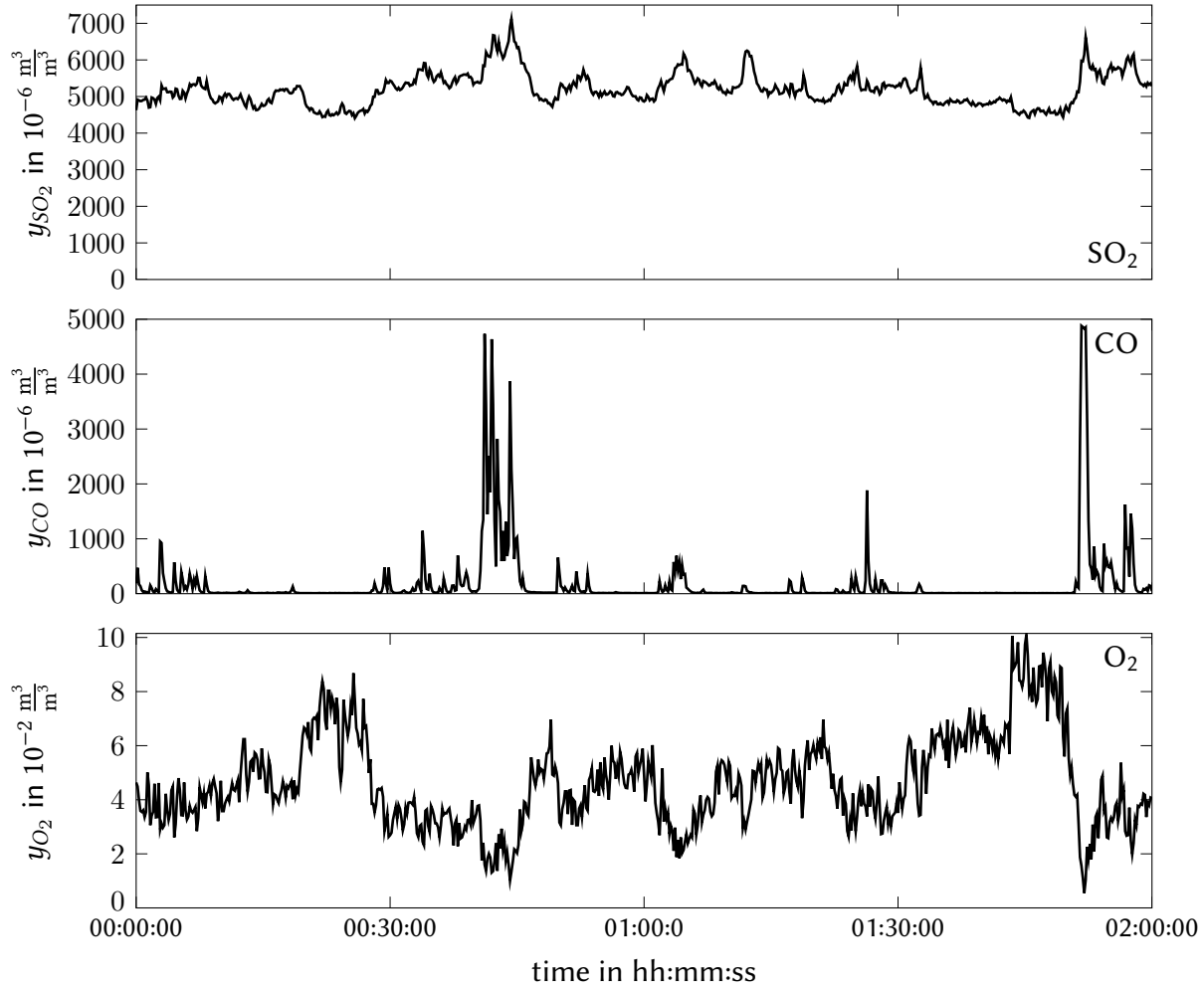

Figure A.12: Concentration trends for SO_2, CO, and O_2 measured during 2 h of oxy-fuel firing of lignite L1 (this plot complements figure 4.19).

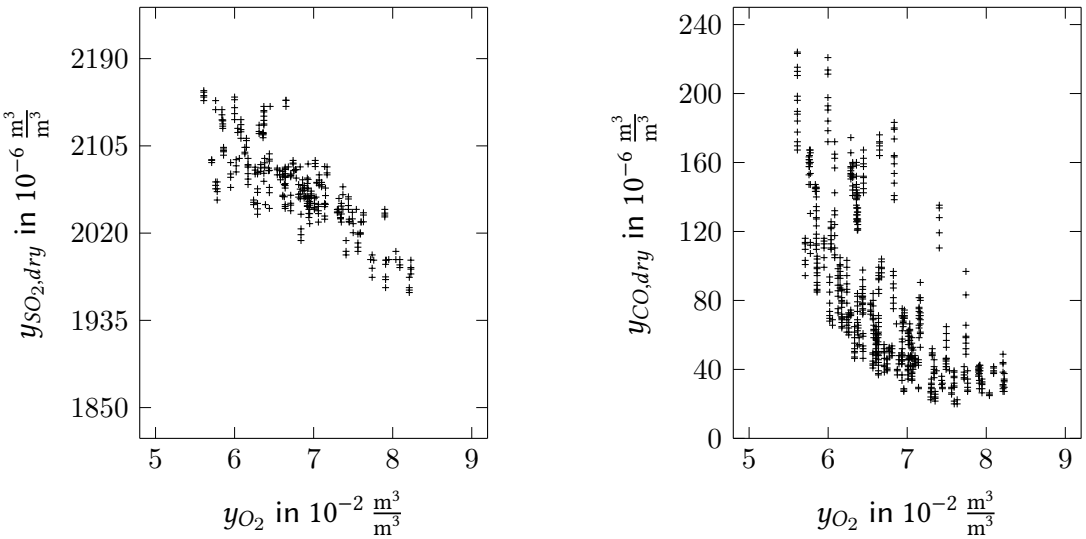

(a) SO_2 vs. O_2 **(b)** CO vs. O_2

Figure A.13: Scatter plots of y_{SO_2} (a) and y_{CO} (b) vs. y_{O_2} measured after ESP during lignite L3 oxy-fuel combustion at the "Schwarze Pumpe" pilot plant. Plots show data of 2 h of operation. The concentrations y_{SO_2} and y_{CO} are **not** recalculated to the same O_2 concentration y_{O_2}. y_{SO_2} axes are scaled to represent between 65 % and 80 % of the theoretical maximum SO_2 concentrations in oxy-fuel combustion of lignite L3 with an outlet O_2 level of $7 \cdot 10^{-2}\ \frac{m^3}{m^3}$, dry (this plot complements figure 4.20).

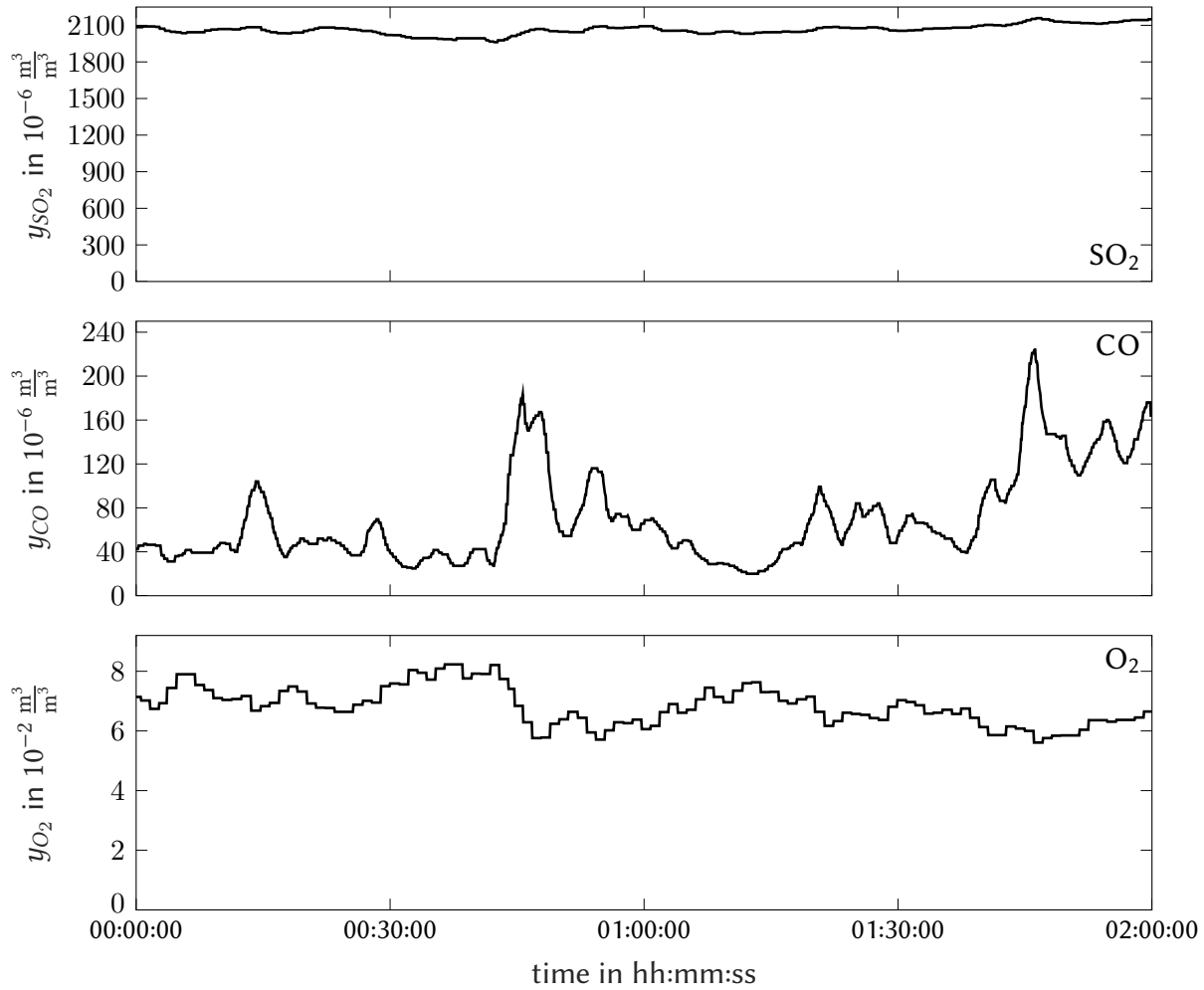

Figure A.14: Concentration trends for SO_2, CO, and O_2 measured during 2 h oxy-fuel firing of lignite L3 at the "Schwarze Pumpe" pilot plant (this plot complements figure 4.20).

A.5 Experiences with $Ca(OH)_2$ injection to oxy-fuel fired processes

In an oxy-fuel process, it is preferable to use CO_2 as a sorbent dispersion and carrier gas to avoid dilution of the CO_2 concentration in the generated flue gas by N_2 contained in the sorbent carrier gas (e.g. air). In this context, N_2 is particularly problematic since it requires a relatively high energetic effort to be separated from the CO_2 rich oxy-fuel flue gas. It is well known that a good dispersion and distribution of sorbents within a boiler or gas duct is the key to enable an efficient reaction of dry sorbents with the impurities contained in the flue gas. As described in section 3.3.3, systems for sorbent injection applied in this thesis use Venturi nozzles to accomplish a good sorbent dispersion. In first preliminary dispersion tests, suitable operational parameters (i.e. optimal gas flows and nozzle pressures) of the used dispersion systems were determined and validated in cold model experiments. These tests revealed that $Ca(OH)_2$ based sorbents cannot be used in combination with CO_2 as carrier and dispersion gas. The reason for this is the very fast reaction between $Ca(OH)_2$ and CO_2 at ambient temperature, according to the following equation:

$$Ca(OH)_2 + CO_2 \longrightarrow CaCO_3 + H_2O \tag{A.1}$$

The $Ca(OH)_2$ sorbent in the feeder and dispersion nozzle reacts rapidly when in contact with gaseous CO_2 becoming sticky (presumably due to the moisture formation) and forming a sintered compound that blocks nozzles and pipes within seconds. In contrast, feeding a $CaCO_3$ based sorbent by CO_2 was unproblematic. As a consequence, all tests using $Ca(OH)_2$ based sorbents conducted for this thesis were carried out with compressed air for sorbent dispersion and injection. Experiments at KSVA with $CaCO_3$ used compressed air for air fired and CO_2 for oxy-fuel fired experiments. An injection of $Ca(OH)_2$ based sorbents without dilution of the flue gas by N_2 may yet be possible applying dedicated technical solutions that can minimize problematic flue gas dilution by N_2. Possible solutions may be, the use of steam as carrier gas that can be easily condensed in downstream unit operations, the use of pure oxygen that can react with the fuel to form H_2O and CO_2, or avoiding carrier gases almost completely (e.g. by using systems based on the concepts of dense phase conveying).

A.6 Sorbent feed rates and measured gas concentrations in DSI experiments

The following tables A.1, A.2, A.3, and A.4 summarize data on sorbent feed rates and O_2, CO_2, CO, SO_2, HCl, and SO_3 concentrations measured during DSI experiments at BTS-VR and KSVA test rigs. The concentration values are not corrected for dilution by air/oxygen but are listed as they have been originally measured. The moisture concentration during the experiments at BTS-VR (measured by FTIR) was approx. $5.5 \cdot 10^{-2}\ \frac{m^3}{m^3}$, wet and approx. $20 \cdot 10^{-2}\ \frac{m^3}{m^3}$, wet in air and oxy-fuel experiments, respectively while at KSVA it was about $7 \cdot 10^{-2}\ \frac{m^3}{m^3}$, wet and $13 \cdot 10^{-2}\ \frac{m^3}{m^3}$, wet.

Table A.1: Sorbent feed and gas concentrations measured after filter in $CaCO_3$ DSI experiments at BTS-VR (concentrations are not O_2 corrected).

Sorb.	Injec.	Mode	$\dot{M}_{Sorb}$	$\alpha_{Ca/S}$	$\alpha_{Ca/2Cl}$	$\bar{y}_{O_2,dry}$	$\bar{y}_{CO_2,dry}$	$\bar{y}_{CO,dry}$	$\bar{y}_{SO_2,dry}$	$\bar{y}_{HCl,dry}$
			$\frac{g}{h}$	$\frac{mol}{mol}$		$10^{-2}\ \frac{m^3}{m^3}$			$10^{-6}\ \frac{m^3}{m^3}$	
$CaCO_3$	co-injection	air	0	0.0	0.0	3.9	14.9	1.5	1600.0	214.4
			44	0.5	2.0	3.9	14.9	1.2	1349.8	210.4
			108	1.3	5.0	3.9	14.9	2.1	1141.7	202.2
			162	2.0	7.5	3.6	15.2	2.0	1061.0	199.8
			200	2.5	9.3	3.8	15.1	2.2	911.1	190.5
			335	4.1	15.5	4.1	14.9	2.0	613.0	152.6
		O_2/CO_2	0	0.0	0.0	3.0	73.0	36.3	4953.6	450.6
			48	0.2	1.2	3.1	75.0	28.5	4495.4	444.5
			106	0.5	2.7	3.3	75.2	30.5	4124.5	438.2
			183	0.9	4.7	3.7	70.4	23.2	3226.1	407.6
			313	1.5	8.0	3.1	73.7	25.7	2942.0	400.0
	furnace	air	0	0.0	0.0	4.3	14.2	13.9	1484.0	191.2
			34	0.4	1.5	4.3	14.4	13.6	1301.2	188.2
			61	0.7	2.7	4.1	13.2	13.8	1129.1	186.4
			128	1.5	5.7	4.6	12.7	10.8	753.2	158.9
			160	1.8	7.0	4.2	13.6	9.0	645.6	156.5
			200	2.3	8.8	4.4	14.4	10.4	507.4	154.6
		O_2/CO_2	0	0.0	0.0	3.0	73.5	54.6	4377.9	366.9
			44	0.2	1.3	3.7	74.4	45.7	3813.5	366.7
			68	0.3	2.0	3.9	74.5	45.8	3552.0	368.2
			108	0.5	3.2	3.7	74.9	47.9	3279.6	361.4
			168	0.8	4.9	3.4	75.3	48.0	2956.2	359.4
			288	1.4	8.5	3.8	74.5	49.1	2245.8	331.7
			358	1.8	10.5	3.4	75.4	49.1	2080.9	331.5
			445	2.2	13.1	3.2	74.2	54.9	1734.1	323.4

Table A.2: Sorbent feed and gas concentrations measured after filter in $Ca(OH)_2$ DSI experiments at BTS-VR (concentrations are not O_2 corrected).

Sorb.	Injec.	Mode	$\dot{M}_{Sorb}$	$\alpha_{Ca/S}$	$\alpha_{Ca/2Cl}$	$\bar{y}_{O_2,dry}$	$\bar{y}_{CO_2,dry}$	$\bar{y}_{CO,dry}$	$\bar{y}_{SO_2,dry}$	$\bar{y}_{HCl,dry}$
			$\frac{g}{h}$	$\frac{mol}{mol}$		$10^{-2}\ \frac{m^3}{m^3}$			$10^{-6}\ \frac{m^3}{m^3}$	
$Ca(OH)_2$	co-injection	air	0	0.0	0.0	4.0	14.5	2.3	1524.2	218.2
			24	0.4	1.6	4.0	14.4	1.9	1440.2	217.9
			66	1.2	4.3	3.8	14.6	2.0	1351.6	215.7
			117	2.0	7.5	4.0	14.4	1.9	1158.3	206.4
			141	2.5	9.1	3.9	14.5	1.9	1071.4	202.9
		O_2/CO_2	0	0.0	0.0	3.1	69.6	21.5	4838.5	391.9
			30	0.2	1.2	3.1	69.1	21.3	4710.7	393.1
			76	0.5	3.0	3.3	68.7	21.3	4460.3	391.5
			126	0.8	4.9	3.6	68.3	21.0	4067.6	383.9
			192	1.2	7.5	3.0	70.2	22.0	3972.6	388.1
	furnace	air	0	0.0	0.0	4.3	14.2	13.1	1575.9	183.4
			22	0.4	1.6	4.2	13.9	9.0	1242.4	174.7
			58	0.8	3.2	4.2	13.8	9.1	972.7	156.3
			84	1.2	5.1	4.4	13.4	9.8	726.8	145.9
			116	1.5	6.4	4.3	13.5	9.2	567.2	138.0
			163	2.3	9.9	4.5	13.4	9.1	257.6	101.8
			165	2.3	10.0	4.3	13.5	9.4	165.4	88.6
			188	2.7	11.4	4.5	13.3	8.8	147.3	81.4
		O_2/CO_2	0	0.0	0.0	3.0	73.4	56.8	4430.9	376.7
			33	0.2	1.3	3.0	73.8	58.4	3662.5	368.2
			42	0.3	1.6	3.0	74.0	55.5	3467.6	364.7
			84	0.5	3.2	3.4	73.6	48.2	3004.5	341.9
			106	0.7	4.1	3.0	74.1	50.3	2768.1	341.3
			134	0.9	5.1	3.1	74.1	52.0	2500.3	336.0
			181	1.2	6.9	3.0	73.9	55.3	2160.7	331.2

Table A.3: Sorbent feed and gas concentrations measured after filter in $Ca(OH)_2$ DSI experiments at BTS-VR (concentrations are not O_2 corrected).

Sorb.	Injec.	Mode	$\dot{M}_{Sorb}$	$\alpha_{Ca/S}$	$\alpha_{Ca/2Cl}$	$\bar{y}_{O_2,dry}$	$\bar{y}_{CO_2,dry}$	$\bar{y}_{CO,dry}$	$\bar{y}_{SO_2,dry}$	$\bar{y}_{HCl,dry}$
			$\frac{g}{h}$	$\frac{mol}{mol}$		$10^{-2}\ \frac{m^3}{m^3}$		$10^{-6}\ \frac{m^3}{m^3}$		
$Ca(OH)_2$	filter	air	0	0.0	0.0	5.7	12.6	9.2	1468.3	183.2
			3	0.1	0.3	5.6	12.6	13.0	1471.8	127.5
			9	0.2	0.7	5.8	12.5	9.4	1441.5	87.5
			12	0.3	1.0	5.6	12.6	9.5	1441.6	73.1
			17	0.4	1.5	5.8	12.5	8.2	1383.2	43.6
			36	0.8	3.0	5.7	12.6	7.1	1287.9	3.0
			70	1.5	5.9	5.8	12.9	7.4	1066.1	0.2
		O_2/CO_2	0	0.0	0.0	2.8	76.8	62.5	4604.9	395.2
			3	0.03	0.2	2.6	79.6	36.3	4455.4	363.3
			7	0.05	0.3	3.0	77.5	37.4	4391.8	277.1

Table A.4: Sorbent feed and gas concentrations measured after ESP in DSI experiments at KSVA (concentrations are not O_2 corrected).

Sorb.	Injec.	Mode	$\dot{M}_{Sorb}$	$\alpha_{Ca/S}$	$\alpha_{Ca/2Cl}$	$\bar{y}_{O_2,dry}$	$\bar{y}_{CO_2,dry}$	$\bar{y}_{CO,dry}$	$\bar{y}_{SO_2,dry}$	$\bar{y}_{HCl,dry}$
			$\frac{g}{h}$	$\frac{mol}{mol}$		$10^{-2}\ \frac{m^3}{m^3}$			$10^{-6}\ \frac{m^3}{m^3}$	
$CaCO_3$	co-injection	air	0.00	0.0	0.0	4.2	14.6	92.5	1502.4	199.1
			2.00	0.8	3.2	4.9	14.1	61.8	1150.3	196.4
			4.50	1.9	7.1	5.1	14.0	42.7	858.0	179.0
			6.50	2.7	10.3	4.3	14.7	60.3	684.9	182.6
		oxy	0.00	0.0	0.0	4.6	78.7	80.9	4709.0	611.8
			2.00	0.9	3.5	3.2	80.0	81.3	3612.2	588.5
			4.50	2.1	7.9	3.3	80.2	86.7	2334.9	524.7
			6.50	3.0	11.5	4.5	85.6	87.6	1269.8	506.4
	furnace	air	0.00	0.0	0.0	4.2	14.4	68.0	1433.7	211.2
			2.00	0.9	3.0	4.3	14.4	58.3	1094.5	202.3
			4.50	2.0	6.7	4.4	13.8	64.5	750.8	180.1
			6.50	2.9	9.7	4.6	13.7	63.8	604.7	171.9
		oxy	0.00	0.0	0.0	4.5	85.3	93.4	4775.9	552.5
			2.00	0.9	3.9	4.7	85.2	94.0	2963.8	519.9
			4.50	2.0	8.8	5.4	85.5	101.6	1510.2	480.4
			6.50	2.9	12.7	5.5	83.1	105.1	845.9	417.1
$Ca(OH)_2$	furnace	air	0.00	0.0	0.0	3.6	14.1	36.5	1458.2	206.3
			0.75	0.4	1.6	3.8	13.8	36.8	1186.3	199.9
			1.70	1.0	3.6	3.8	14.2	44.7	930.3	193.4
			2.70	1.6	5.8	4.1	13.7	44.9	797.6	185.1
		oxy	0.00	0.0	0.0	5.7	77.4	134.8	4537.9	529.3
			0.75	0.5	-	4.8	77.8	134.6	3262.1	-
			1.70	1.1	4.6	5.6	75.4	89.8	1831.3	481.4
			2.70	1.7	7.4	5.2	77.6	91.7	1221.1	459.7
	ESP	air	0.00	0.0	0.0	4.3	14.2	45.9	1469.4	223.9
			0.40	0.2	0.8	4.7	14.0	42.5	1422.9	127.6
			0.60	0.3	1.1	4.9	13.9	43.2	1386.1	73.6
			0.90	0.5	1.7	4.4	14.4	41.8	1387.9	48.4
		oxy	0.00	0.0	0.0	5.1	76.2	86.3	4967.5	518.4
			0.45	0.3	1.3	5.2	76.2	103.1	4954.0	243.2
			0.70	0.4	1.9	5.4	76.4	90.9	4733.6	124.0
			1.00	0.6	2.8	5.3	75.4	97.9	4038.6	76.7

A.7 Calculation of SO_2 specific $Ca(OH)_2$ consumption and by-product generation

The sorbent consumption and by-products generation can also be related to the production of SO_2 in a combustion system. The production of SO_2 can be determined directly from the flue gas production and raw gas SO_2 measurements at a combustor. Equations A.2 and A.3 show how the SO_2 specific values $\xi_{sorb}^{SO_2}$ and $\xi_{byprod,i}^{SO_2}$ were calculated.

$$\xi_{sorb}^{SO_2} = \frac{\dot{M}_{sorb}}{\dot{M}_{SO_2}} \tag{A.2}$$

$$\xi_{byprod,i}^{SO_2} = \frac{\eta_{sorb,i}\dot{M}_{sorb}}{\dot{M}_{SO_2}} \frac{M_{M,byprod,i}}{M_{M,sorb}} \tag{A.3}$$

Analog to the considerations in section 4.2.2.4, $\xi_{sorb}^{SO_2}$ and $\xi_{byprod,i}^{SO_2}$ have been exemplary calculated on basis of the air and oxy-fuel experiments with injection of $Ca(OH)_2$ to the furnace of the 500 kW facility KSVA. In the air and oxy-fuel experiments, $\dot{M}_{SO_2}$ reached 1.33 $\frac{kg}{h}$ and 1.34 $\frac{kg}{h}$, respectively. The results of SO_2 specific sorbent consumption and by-products generation $\xi_{sorb}^{SO_2}$ and $\xi_{byprod,i}^{SO_2}$ are plotted in figures A.15 and A.16, respectively.

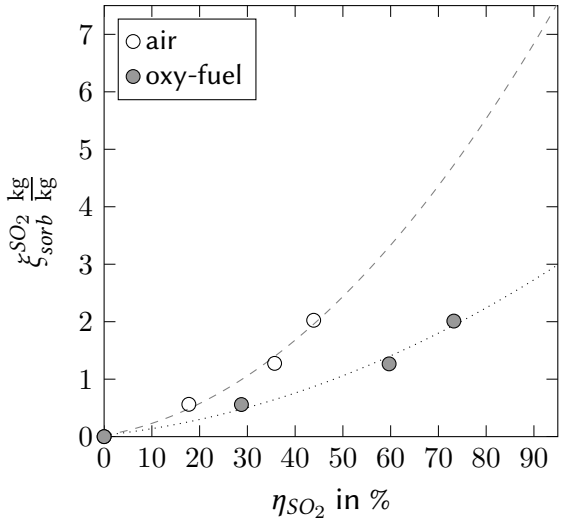

Figure A.15: SO_2 specific sorbent consumption $\xi_{sorb}^{SO_2}$ versus SO_2 capture efficiency η_{SO_2} for injection of $Ca(OH)_2$ to the furnace of the 500 kW facility KSVA for air and oxy-fuel combustion of coal C4. Values of $\xi_{sorb}^{SO_2}$ that have been determined on basis of experimental data are marked by symbols. Dashed (air) and dotted (oxy-fuel) trendlines were approximated by a 2nd order polynomial fit of these results.

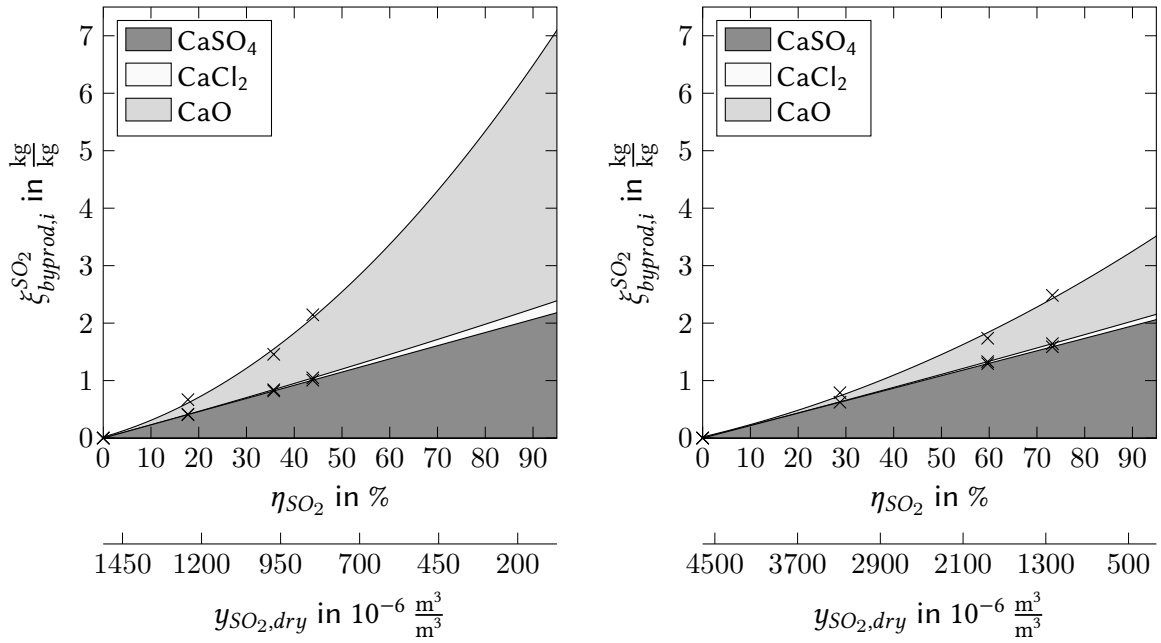

(a) $\xi^{SO_2}_{byprod,i}$ in air firing

(b) $\xi^{SO_2}_{byprod,i}$ in oxy-fuel firing

Figure A.16: SO_2 specific by-product generation $\xi^{SO_2}_{byprod,i}$ versus SO_2 capture efficiency η_{SO_2} and associated outlet SO_2 concentrations $y_{SO_2,dry}$ for injection of $Ca(OH)_2$ to the furnace of the 500 kW facility KSVA for (a) air and (b) oxy-fuel combustion of coal C4. Values of $\xi^{SO_2}_{byprod,i}$ that have been determined on basis of experimental data are marked by "x". In addition, trends were plotted that are approximated by a 2nd order polynomial fit of the experimental results.

References

[1] Scheffknecht, G., Al-Makhadmeh, L., Schnell, U., and Maier, J.: Oxy-fuel coal combustion—A review of the current state-of-the-art, *Int. J. Greenhouse Gas Control*, Vol. 5 (1), pp. 16–35, DOI: 10.1016/j.ijggc.2011.05.020, **2011**.

[2] Stanger, R., Wall, T., Spörl, R., Paneru, M., Grathwohl, S., Weidmann, M., Scheffknecht, G., McDonald, D., Myöhänen, K., Ritvanen, J., Rahiala, S., Hyppänen, T., Mletzko, J., Kather, A., and Santos, S.: Oxyfuel combustion for CO_2 capture in power plants, *Int. J. Greenhouse Gas Control*, Vol. 40, pp. 55–125, DOI: 10.1016/j.ijggc.2015.06.010, **2015**.

[3] Strömberg, L., Lindgren, G., Jacoby, J., Giering, R., Anheden, M., Burchhardt, U., Altmann, H., Kluger, F., and Stamatelopoulos, G.-N.: Update on Vattenfall's 30 MW_{th} oxyfuel pilot plant in Schwarze Pumpe, *Energy Procedia*, Vol. 1 (1), pp. 581–589, DOI: 10.1016/j.egypro.2009.01.077, **2009**.

[4] Spero, C., Yamada, T., Nelson, P., Morrison, T., and Bourhy-Weber, C.: Callide Oxyfuel Project: Combustion and Environmental Performance (Presentation), *3rd IEAGHG Oxy-Fuel Combustion Conference*, 09-13/09/2013, Ponferrada, Spain, **2013**.

[5] Lockwood, T.: Overcoming barriers to carbon capture and storage through international collaboration (IEA-CCC Report: CCC/284), IEA Clean Coal Centre, **2018**.

[6] OECD/IEA: Energy Technology Perspectives 2017: Catalysing Energy Technology Transformations, 06/06/2017, ISBN: 9789264275973, **2017**.

[7] United Nations Framework Convention on Climate Change: Paris Agreement – Decision 1/CP.21 – Report of the Conference of the Parties on its twenty-first session, held in Paris from 30 November to 13 December 2015, Addendum Part two: Action taken by the Conference of the Parties at its twenty-first session., Available: https://unfccc.int/resource/docs/2015/cop21/eng/10a01.pdf, Accessed: 30/07/2018, **2015**.

[8] United Nations Framework Convention on Climate Change: Paris Agreement - Status of Ratification, Available: https://unfccc.int/process/the-paris-agreement/status-of-ratification, Accessed: 17/12/2019, online, **2019**.

[9] Stanger, R. and Wall, T.: Sulphur impacts during pulverised coal combustion in oxy-fuel technology for carbon capture and storage, *Prog. Energy Combust. Sci.*, Vol. 37 (1), pp. 69–88, DOI: 10.1016/j.pecs.2010.04.001, **2011**.

[10] Wall, T., Liu, Y., Spero, C., Elliott, L., Khare, S., Rathnam, R., Zeenathal, F., Moghtaderi, B., Buhre, B., Sheng, C., Gupta, R., Yamada, T., Makino, K., and Yu, J.: An overview on oxyfuel coal combustion—State of the art research and technology development, *Chem. Eng. Res. Des.*, Vol. 87 (8), pp. 1003–1016, DOI: 10.1016/j.cherd.2009.02.005, **2009**.

[11] Liu, H., Katagiri, S., and Okazaki, K.: Drastic SO_x Removal and Influences of Various Factors in O_2/CO_2 Pulverized Coal Combustion System, *Energy Fuels*, Vol. 15 (2), pp. 403–412, DOI: 10.1021/ef000171p, **2001**.

[12] Fleig, D., Andersson, K., Johnsson, F., and Leckner, B.: Conversion of Sulfur during Pulverized Oxy-coal Combustion, *Energy Fuels*, Vol. 25 (2), pp. 647–655, DOI: 10.1021/ef1013242, **2011**.

[13] Croiset, E. and Thambimuthu, K.: NO_x and SO_2 emissions from O_2/CO_2 recycle coal combustion, *Fuel*, Vol. 80, pp. 2117–2121, **2001**.

[14] Mönckert, P., Reber, D., Maier, J., and Scheffknecht, G.: Operation of a retrofited 0.5 MW_{th} PF combustion facility under oxyfuel conditions – an experience report, in: *32nd International Technical Conference on Coal Utilization & Fuel Systems*, 10-15/06/2007, Clearwater, Florida, USA, ed. by Coal Technology Association, **2007**.

[15] Ahn, J., Okerlund, R., Fry, A., Eddings, E. G., Ahn, J., Okerlund, R., Fry, A., and Eddings, E. G.: Sulfur trioxide formation during oxy-coal combustion, *Int. J. Greenhouse Gas Control*, Vol. 5 (1), pp. 127–135, DOI: 10.1016/j.ijggc.2011.05.009, **2011**.

[16] Tan, Y., Croiset, E., Douglas, M. A., and Thambimuthu, K. V.: Combustion characteristics of coal in a mixture of oxygen and recycled flue gas, *Fuel*, Vol. 85 (4), pp. 507–512, DOI: 10.1016/j.fuel.2005.08.010, **2006**.

[17] Dhungel, B.: Experimental investigations on combustion and emission behaviour during oxy-coal combustion (Dissertation), Stuttgart, Germany: Universität Stuttgart - Institut für Feuerungs- und Kraftwerkstechnik, **2010**.

[18] Global CCS Institute: The Global Status of CCS: 2012, Available: http://www.globalccsinstitute.com/publications/global-status-ccs-2012, Accessed: 13/01/2015, Canberra, Australia, **2012**.

[19] Schnurrer, S., Elliott, L., Wall, T., and Liu, Y.: Influence of Oxy-Fuel Environment on Sulfur Species in Ash From Pulverized Coal Combustion, in: *22nd Impacts of Fuel Quality on Power Generation and Environment Conference*, 29/09-03/10/2008, Banff, Canada, **2008**.

[20] Zheng, L. and Furimsky, E.: Assessment of coal combustion in O_2+CO_2 by equilibrium calculations, *Fuel Process. Technol.*, Vol. 81 (1), pp. 23–34, DOI: 10.1016/S0378-3820(02)00250-3, **2003**.

[21] Hjörnhede, A., Montgomery, M., Bjurman, M., Henderson, P., and Alexander, G.: Preliminary experiences with material testing at the oxyfuel pilot plant Schwarze Pumpe, in: *9th Liege conference on Materials for Advanced Power engineering*, ed. by Lecomte-Beckers, J., Contrepois, Q., and Beck, T., Vol. Bd. 94, Schriften des Forschungszentrums Jülich : Reihe Energie & Umwelt, ISBN: 978-3-89336-685-9, Jülich: Forschungszentrum, Zentralbibliothek, **2010**.

[22] Montgomery, M., Hjörnhede, A., Bjurman, M., Henderson, P., and Gerhardt, A.: Preliminary corrosion results from Vattenfall's 30 MW oxyfuel pilot plant, in: *European corrosion congress 2010 (EUROCORR 2010)*, 13-17/09/2010, Moscow, Russia, ISBN: 9781617824029, Red Hook, NY: Curran Assoc, **2010**.

[23] Adams, B., Davis, K., Senior, C., Shim, H. S., van Otten, B., Fry, A., Wendt, J., Eddings, E., Paschedag, A., Shaddix, C., Cox, W., and Tree, D.: Characterization of Oxy-combustion Impacts in Existing Coal-fired Boilers: Final Technical Report, US-DOE Award No.: DE-NT0005288, DOI: 10.2172/1113768, **2013**.

[24] Dhungel, B., Ellul, C., Gibson, J., and Fitzgerald, D.: SO_3 Control in Oxyfuel Applications (Presentation), *IEAGHG workshop, Oxy-fuel combustion: SO_2/SO_3/Hg/Corrosion Issues in Oxyfuel Combustion Boiler and Flue Gas Processing Units*, 26/01/2011, London, UK, **2011**.

[25] Liu, J., Liu, H., Guo, X., Yao, H., and Chen, J.: Nitrogen and Sulfur Behavior During Oxy-fuel Combustion and Its Retention. *In Coll.: Oxy-Fuel Combustion*, pp. 87–127, Elsevier, ISBN: 9780128121450, **2018**.

[26] Fleig, D., Andersson, K., Normann, F., and Johnsson, F.: SO_3 Formation under Oxy-Fuel Combustion Conditions, *Ind. Eng. Chem. Res.*, pp. 8505–8514, DOI: 10.1021/ie2005274, **2011**.

[27] Fleig, D., Andersson, K., and Johnsson, F.: Influence of Operating Conditions on SO 3 Formation during Air and Oxy-Fuel Combustion, *Ind. Eng. Chem. Res.*, Vol. 51 (28), pp. 9483–9491, DOI: 10.1021/ie301303c, **2012**.

[28] Fleig, D., Alzueta, M. U., Normann, F., Abián, M., Andersson, K., and Johnsson, F.: Measurement and modeling of sulfur trioxide formation in a flow reactor under post-flame conditions, *Combust. Flame*, Vol. 160 (6), pp. 1142–1151, DOI: 10.1016/j.combustflame.2013.02.002, **2013**.

[29] Belo, L. P., Elliott, L. K., Stanger, R. J., Spörl, R., Shah, K. V., Maier, J., and Wall, T. F.: High-Temperature Conversion of SO_2 to SO_3: Homogeneous Experiments and Catalytic Effect of Fly Ash from Air and Oxy-fuel Firing, *Energy Fuels*, Vol. 28 (11), pp. 7243–7251, DOI: 10.1021/ef5020346, **2014**.

[30] Qin, S., Spörl, R., and Maier, J.: SO_x Mitigation Technologies for Combustion Systems. *In Coll.: Handbook of Clean Energy Systems*, ed. by Yan, J., Chichester, UK: John Wiley & Sons, Ltd, ISBN: 9781118991978, **2015**.

[31] Spörl, R.: General report on dry sorbent injection, characteristics and selection of sorbents: Deliverable D2.2 of the RFCS research project BiOxySorb (Grant Agreement Number: RFCR-CT-2013-00010), 31/03/2014, IFK, University of Stuttgart, **2014**.

[32] Spörl, R.: Flue Gas Impurities, their Impact and Control under Oxy-Fuel Conditions (Presentation), *5th Oxy-Fuel Capacity Building Course*, 09/09/2013, Ponferrada, Spain, **2013**.

[33] Spörl, R., Grathwohl, S., Maier, J., and Scheffknecht, G.: Impact of oxy-coal combustion on downstream gas cleaning (Presentation), *Oxy-coal Workshop, 18th IFRF Members' Conference*, 2-3/06/2015, Kardinal-Döpfner-Haus, Freising, Germany, **2015**.

[34] Spörl, R. and Maier, J.: Experiences and Results of SO_3 Measurements Performed under Oxy-Coal Fired Conditions (Presentation), *IEAGHG workshop, Oxy-fuel combustion: SO_2/SO_3/Hg/Corrosion Issues in Oxyfuel Combustion Boiler and Flue Gas Processing Units*, 26/01/2011, London, UK, **2011**.

[35] Spörl, R., Maier, J., Belo, L., Shah, K., Stanger, R., Wall, T., and Scheffknecht, G.: Mercury and SO_3 Emissions in Oxy-fuel Combustion, *Energy Procedia*, Vol. 63, pp. 386–402, DOI: 10.1016/j.egypro.2014.11.041, **2014**.

[36] Spörl, R., Maier, J., and Scheffknecht, G.: Sulphur Oxide Emissions from Dust-fired Oxy-fuel Combustion of Coal, *Energy Procedia*, Vol. 37, pp. 1435–1447, DOI: 10.1016/j.egypro.2013.06.019, **2013**.

[37] Spörl, R., Pek, S., Qin, S., Maier, J., and Scheffknecht, G.: Acid Gas Control by Dry Sorbent Injection in Air and Oxy-Fuel Combustion (Presentation), *5th OxyfuelCombustion Research Network Meeting*, 29/10/2015, Wuhan, China, **2015**.

[38] Spörl, R., Walker, J., Belo, L., Shah, K., Stanger, R., Maier, J., Wall, T., and Scheffknecht, G.: SO_3 Emissions and Removal by Ash in Coal-Fired Oxy-Fuel Combustion, *Energy Fuels*, Vol. 28 (8), pp. 5296–5306, DOI: 10.1021/ef500806p, **2014**.

[39] Spörl, R., Youssefi, R., Maier, J., and Scheffknecht, G.: Acid Gas Control by Dry Sorbent Injection in Air and Oxy-Fuel Combustion (Presentation), *33rd Annual International Pittsburgh Coal Conference*, 10/08/2016, Capetown, South Africa, **2016**.

[40] Spörl, R., Hornberger, M., Stade, S., and Scheffknecht, G.: Application of thermodynamic phase mapping in combustion and other high temperature processes, in: *26th Impacts of Fuel Quality on Power Production Conference*, 19-23/09/2016, Prague, Czech Republic, **2016**.

[41] Spörl, R., Paneru, M., Babat, S., Stein-Brzozowska, G., Maier, J., and Scheffknecht, G.: The influence of air and oxy-fuel combustion on fly ash and deposits, *Fuel Process. Technol.*, Vol. 141, pp. 258–265, DOI: 10.1016/j.fuproc.2015.10.005, **2016**.

[42] Spörl, R., Paneru, M., Babat, S., Stein-Brzozowska, G., Ott, S., Maier, J., and Scheffknecht, G.: Fly Ash and Deposit Transformations in Air and Oxy-fuel Combustion, in: *25th Impacts of Fuel Quality on Power Production Conference*, 26-31/09/2014, Snowbird, Utah, USA, **2014**.

[43] Paneru, M., Spörl, R., Stein-Brzozowska, G., Maier, J., and Scheffknecht, G.: Behaviour of Deposit and Fly Ash under Oxyfuel Conditions (Presentation), *3rd IEAGHG Oxy-Fuel Combustion Conference*, 09-13/09/2013, Ponferrada, Spain, **2013**.

[44] Spörl, R., Belo, L., Shah, K., Stanger, R., Giniyatullin, R., Maier, J., Wall, T., and Scheffknecht, G.: Mercury Emissions and Removal by Ash in Coal-Fired Oxy-fuel Combustion, *Energy Fuels*, Vol. 28 (1), pp. 123–135, DOI: 10.1021/ef4014604, **2014**.

[45] Walker, J.: Untersuchungen zur SO_3-Bildung und -Abscheidung an einer 20 kW Kohlenstaubfeuerungsanlage: Thesis No. 3161 (Independent study project), Stuttgart, Germany: University of Stuttgart - IFK, **2013**.

[46] Däuwel, J.: Inbetriebnahme eines FTIR-Gasanalysators und Vergleichsmessungen mit Prüfgasen und Steinkohlefeuerungsabgas: Thesis No. 3315 (Bachelor thesis), Stuttgart, Germany: University of Stuttgart - IFK, **2014**.

[47] Ott, S.: Thermodynamische Gleichgewichtssimulation zur Umwandlung von Braunkohleasche bei Oxy-Fuel- und Luft-Feuerung: Thesis No. 3300 (Bachelor thesis), Stuttgart, Germany: University of Stuttgart - IFK, **2014**.

[48] Pek, S.: Untersuchungen zur SO_x- und HCl-Bildung und Einbindung in die Asche bei der Luft- und Oxy-Fuel-Verbrennung (Investigations on the formation of SO_x and HCl and their capture in the ash in air and oxy-fuel-combustion): Thesis No. 3317 (Master thesis), Stuttgart, Germany: University of Stuttgart - IFK, **2015**.

[49] Gomez, V.: Impact of combustion process alterations on ash utilization routes: Thesis No. 3320 (Master thesis), Stuttgart, Germany: University of Stuttgart - IFK, **2015**.

[50] Ebner, B.: Einfluss von Biomassemitverbrennung und Trockensorbenteindüsung auf die HCl und SO_x Konzentrationen im Luft- und Oxy-Fuel-Betrieb: Thesis No. 3381 (Master thesis), Stuttgart, Germany: University of Stuttgart - IFK, **2015**.

[51] Stade, S.: Thermodynamische Gleichgewichtsuntersuchungen typischer Mineralsysteme aus Kesselbelägen bei Oxy-Fuel- und Luftfeuerung: Thesis No. 3385 (Independent study project), Stuttgart, Germany: University of Stuttgart - IFK, **2016**.

[52] Youssefi, R.: Experimental and theoretic investigations on acid gas removal by dry sorbent injection in air and oxy-fuel combustion: Thesis No. 3415 (Master thesis), Stuttgart, Germany: University of Stuttgart - IFK, **2016**.

[53] Spliethoff, H.: Power Generation from Solid Fuels, Berlin, Germany: Springer-Verlag, ISBN: 9783642028557, **2010**.

[54] Toftegaard, M. B., Brix, J., Jensen, P. A., Glarborg, P., and Jensen, A. D.: Oxy-fuel combustion of solid fuels, *Prog. Energy Combust. Sci.*, Vol. 36 (5), pp. 581–625, DOI: 10.1016/j.pecs.2010.02.001, **2010**.

[55] Bryers, R. W.: Fireside slagging, fouling, and high-temperature corrosion of heat-transfer surface due to impurities in steam-raising fuels: Fireside slagging, fouling, and high-temperature corrosion of heattransfer surface due to impurities in steam-raising fuels, *Prog. Energy Combust. Sci.*, Vol. 22 (1), pp. 29–120, DOI: 10.1016/0360-1285(95)00012-7, **1996**.

[56] Kleinhans, U., Wieland, C., Frandsen, F. J., and Spliethoff, H.: Ash formation and deposition in coal and biomass fired combustion systems: Progress and challenges in the field of ash particle sticking and rebound behavior, *Prog. Energy Combust. Sci.*, Vol. 68, pp. 65–168, DOI: 10.1016/j.pecs.2018.02.001, **2018**.

[57] Muzio, L. J. and Often, G. R.: Assessment of Dry Sorbent Emission Control Technologies: Part I. Fundamental Processes, *J. Air Waste Manag. Assoc.*, Vol. 37 (5), pp. 642–654, DOI: 10.1080/08940630.1987.10466251, **1987**.

[58] Often, G. R., McElroy, M. W., and Muzio, L. J.: Assessment of Dry Sorbenf Emission Control Technologies Part II. Applications, *J. Air Waste Manag. Assoc.*, Vol. 37 (8), pp. 968–980, DOI: 10.1080/08940630.1987.10466288, **1987**.

[59] GE Power: RDK8 (Germany): World's most efficient coal power plant, Available: https://www.ge.com/power/case-studies/rdk8, Accessed: 09/07/2018, **2018**.

[60] EnBW Energie Baden Württemberg AG: Rheinhafen-Dampfkraftwerk Karlsruhe: RDK8, Available: https://www.enbw.com/unternehmen/konzern/energieerzeugung/neubau-und-projekte/rheinhafen-dampfkraftwerk-karlsruhe/, Accessed: 03/01/2019, **2019**.

[61] RWE Generation: Kraftwerk Niederaußem: Wissenswertes kurz zusammengefasst, Available: https://www.rwe.com/web/cms/mediablob/de/2915474/data/60132/2/rwe-power-ag/energietraeger/braunkohle/standorte/kw-niederaussem/Kraftwerk-Niederaussem-Standort-Flyer.pdf, Accessed: 09/07/2018, **2015**.

[62] Osborn, G.: Review of sulphur and chlorine retention in coal-fired boiler deposits, *Fuel*, Vol. 71 (2), pp. 131–142, DOI: 10.1016/0016-2361(92)90001-5, **1992**.

[63] CEN European Committee for Standardization: EN 450 - Fly ash for concrete, **2012**.

[64] DIN Deutsches Institut für Normung e. V.: DIN EN 197-1 - Cement - Part 1: Composition, specifications and conformity criteria for common cements, **2014**.

[65] Ndibe, C., Spörl, R., Maier, J., and Scheffknecht, G.: Experimental study of NO and NO_2 formation in a PF oxy-fuel firing system, *Fuel*, Vol. 107, pp. 749–756, DOI: 10.1016/j.fuel.2013.01.055, **2013**.

[66] Lockwood, T.: Developments in oxyfuel combustion of coal (IEA-CCC Report: CCC/240), London, UK: IEA Clean Coal Centre, ISBN: 9789290295617, **2014**.

[67] Diego, R., López, C., Navarrete, B., Coca, T., and López, L. A.: CIUDEN PC Boiler Technological Development in Power Generation, *2nd IEAGHG Oxyfuel Combustion Conference*, 12-16/09/2011, Yeppoon, QLD, Australia, **2011**.

[68] Zheng, C.: Research and development of oxyfuel combustion in China (Presentation), *3rd IEAGHG Oxy-Fuel Combustion Conference*, 09-13/09/2013, Ponferrada, Spain, **2013**.

[69] Burchhardt, U.: Übersicht zu Tests und Ergebnissen der Oxyfuel-Forschungsanlage Schwarze Pumpe (Presentation), *Public final project meeting of the German research project "ADECOS-Komponenten"*, 07-08/05/2014, Cottbus, Germany, **2014**.

[70] Andersson, K. and Johnsson, F.: Process evaluation of an 865 MW_e lignite fired O_2/CO_2 power plant, *Energy Convers. Manage.*, Vol. 47 (18-19), pp. 3487–3498, DOI: 10.1016/j.enconman.2005.10.017, **2006**.

[71] Buhre, B., Elliott, L. K., Sheng, C. D., Gupta, R. P., and Wall, T. F.: Oxy-fuel combustion technology for coal-fired power generation, *Prog. Energy Combust. Sci.*, Vol. 31 (4), pp. 283–307, DOI: 10.1016/j.pecs.2005.07.001, **2005**.

[72] Davison, J.: Performance and costs of power plants with capture and storage of CO_2, *Energy*, Vol. 32 (7), pp. 1163–1176, DOI: 10.1016/j.energy.2006.07.039, **2007**.

[73] Hellfritsch, S., Gonschorek, S., Wilhelm, R., Löser, J., Klemm, M., Weigl, S., and Gampe, U.: Entwicklungsstand des Oxyfuel-Prozesses für Braunkohlekraftwerke, in: *38. Kraftwerkstechnisches Kolloquium: Kraftwerksbetrieb unter künftigen Rahmenbedingungen*, ISBN: 3000198415, Dresden: Inst. für Energietechnik, **2006**.

[74] Kather, A., Klostermann, M., Hermsdorf, C., Mieske, K., Eggers, R., and Köpke, D.: Konzept für ein 600 MW_{el} Steinkohlekraftwerk mit CO_2-Abtrennung auf Basis des Oxyfuel-Prozesses, in: *38. Kraftwerkstechnisches Kolloquium: Kraftwerksbetrieb unter künftigen Rahmenbedingungen*, ISBN: 3000198415, Dresden: Inst. für Energietechnik, **2006**.

[75] Spero, C., Wall, T. F., Wibberley, L., Kiga, T., and Makino, K.: Japan-Australia oxy-fuel demonstration project – feasibility study, and reference design development, in: *30th International Technical Conference on Coal Utilization and Fuel Systems*, 17-21/04/2005, Clearwater, Florida, USA, ed. by Coal Technology Association, **2005**.

[76] Wall, T. F.: Combustion processes for carbon capture, *Proc. Combust. Inst.*, Vol. 31 (1), pp. 31–47, DOI: 10.1016/j.proci.2006.08.123, **2007**.

[77] Kenison, L., Flanigan, T., Hagerty, G., Gorrie, J., Leclerc, M., Lockwood, F., Falla, L., Macinnis, J., Fedak, M., Yakle, J., Williford, M., and Wood, P.: FutureGen 2.0 Oxy-combustion Large Scale Test: Final Scientific and Technical Report, US-DOE Award No.: DE-FE0005054, DOI: 10.2172/1287331, **2016**.

[78] Kluger, F., Lysk, S., Altmann, H., Krohmer, B., and Stamatelopoulos, G.-N.: 30 MW_{th} Oxyfuel-Pilotanlage – Untersuchungsschwerpunkte und Auslegung des Dampferzeugers, in: *38. Kraftwerkstechnisches Kolloquium: Kraftwerksbetrieb unter künftigen Rahmenbedingungen*, ISBN: 3000198415, Dresden: Inst. für Energietechnik, **2006**.

[79] McDonald, D., Moorman, S., and Humphreys, K.: FutureGen 2.0: Phase II and Beyond, in: *38th International Technical Conference on Clean Coal & Fuel Systems*, 2-6/06/2013, Clearwater, Florida, USA, ed. by Coal Technology Association, Gaithersburg, MD.: Coal Technology Association, **2013**.

[80] McDonald, D.: Oxyfuel Design: The Concepts and Considerations Applied to FutureGen 2.0 (Presentation), *5th Oxy-Fuel Capacity Building Course*, 09/09/2013, Ponferrada, Spain, **2013**.

[81] Spero, C.: Callide Oxyfuel Project (COP) Development status (Presentation), *5th Oxy-Fuel Capacity Building Course*, 09/09/2013, Ponferrada, Spain, **2013**.

[82] Burchhardt, U., Griebe, S., Zimmer, P., Faber, R., Giering, R., and Gerhardt, A.: Erkenntnisse aus dem Testbetrieb und Ausblick zur weiteren Nutzung der Oxyfuel-Forschungsanlage von Vattenfall, in: *44. Kraftwerkstechnisches Kolloquium*, 23-24/10/2012, Dresden, Germany, ed. by Beckmann, M., pp. 169–184, ISBN: 978-3-935317-88-7, Thomé-Kozmiensky Verlag, **2012**.

[83] Zanganeh, K. E. and Shafeen, A.: A novel process integration, optimization and design approach for large-scale implementation of oxy-fired coal power plants with CO_2 capture, *Int. J. Greenhouse Gas Control*, Vol. 1 (1), pp. 47–54, DOI: 10.1016/S1750-5836(07)00035-7, **2007**.

[84] Burchhardt, U., Giering, R., and Weiß, G.: Overview of Burner Tests in Vattenfall's Oxyfuel Pilot Plant (Presentation), *3rd IEAGHG Oxy-Fuel Combustion Conference*, 09-13/09/2013, Ponferrada, Spain, **2013**.

[85] Burchhardt, U., Lysk, S., and Biele, M.: Concept of Vattenfall's Oxyfuel Demo Plant (Presentation), *3rd IEAGHG Oxy-Fuel Combustion Conference*, 09-13/09/2013, Ponferrada, Spain, **2013**.

[86] Álvarez, I.: CIUDEN 30 MW pilot plant (Presentation), *5th Oxy-Fuel Capacity Building Course*, 09/09/2013, Ponferrada, Spain, **2013**.

[87] Dillon, D. J., White, V., Allam, R. J., Wall, R. A., and Gibbins, J.: Oxy Combustion Processes for CO_2 capture from power plant: Report Number 2005/9, IEA Greenhouse Gas Research and Development Programme, **2005**.

[88] Burchhardt, U., Griebe, S., Kass, H., Giering, R., and Preusche, R.: Erfahrungen aus dem Testbetrieb der Oxyfuel-Forschungsanlage von Vattenfall und Ausblick zur Oxyfuel-Technologie, in: *43. Kraftwerkstechnisches Kolloquium*, 18-19/10/2011, Dresden, Germany, ed. by Beckmann, M., pp. 51–72, ISBN: 3935317727, Thomé-Kozmiensky Verlag, **2011**.

[89] Wild, T., Lysk, S., Kluger, F., and Bischoff, H.: Besonderheiten von Feuerungen in Oxyfuel-Dampferzeugern und Auswirkungen auf Auslegung und Betrieb, in: *VGB conference "Brennstofftechnik und Feuerungen 2010"*, 08-09/06/2010, Kassel, Germany, **2010**.

[90] Grathwohl, S., Maier, J., and Scheffknecht, G.: Testing and evaluation of advanced oxyfuel burner and firing concepts (Presentation), *2nd IEAGHG Oxyfuel Combustion Conference*, 12-16/09/2011, Yeppoon, QLD, Australia, **2011**.

[91] Li, H., Yan, J., and Anheden, M.: Impurity impacts on the purification process in oxy-fuel combustion based CO_2 capture and storage system, *Appl. Energy*, Vol. 86 (2), pp. 202–213, DOI: 10.1016/j.apenergy.2008.05.006, **2009**.

[92] Kather, A. and Scheffknecht, G.: Review: The oxycoal process with cryogenic oxygen supply, *Naturwissenschaften*, Vol. 96, pp. 993–1010, **2009**.

[93] Stallman, O., Nilsson, L., and Britz, C.: GPU Pilot Operation and Energy Consumption (Presentation), *3rd IEAGHG Oxy-Fuel Combustion Conference*, 09-13/09/2013, Ponferrada, Spain, **2013**.

[94] White, V., Wright, A., Tappe, S., and Yan, J.: The Air Products - Vattenfall Oxyfuel CO_2 Compression and Purification Pilot Plant Schwarze Pumpe (Presentation), *3rd IEAGHG Oxy-Fuel Combustion Conference*, 09-13/09/2013, Ponferrada, Spain, **2013**.

[95] Preusche, R., Schulz, C., Ecke, H., Faber, R., Jidinger, O., Giering, R., Burchhardt, U., and Gampe, U.: A data-based method for monitoring air in-leakages into the oxyfuel process, *Energy Procedia*, Vol. 4, pp. 876–883, DOI: 10.1016/j.egypro.2011.01.132, **2011**.

[96] Adolphi, P., Störr, M., Mahlberg, P., Murray, H., and Ripley, E.: Sulfur sources and sulfur bonding of some central European attrital brown coals, *Int. J. Coal Geol.*, Vol. 16, pp. 185–188, **1990**.

[97] Chou, C.-L.: Sulfur in coals: A review of geochemistry and origins, *Int. J. Coal Geol.*, Vol. 100, pp. 1–13, DOI: 10.1016/j.coal.2012.05.009, **2012**.

[98] Heinzel, T.: Ascheseitige Probleme bei der Mitverbrennung von Biomasse in Kohlenstaubfeuerungen (Dissertation), Stuttgart, Germany: Universität Stuttgart, **2004**.

[99] Srivastava, R. K., Miller, C. A., Erickson, C., and Jambhekar, R.: Emissions of Sulfur Trioxide from Coal-Fired Power Plants, *J. Air Waste Manag. Assoc.*, Vol. 54 (6), pp. 750–762, DOI: 10.1080/10473289.2004.10470943, **2004**.

[100] Hu, Y., Naito, S., Kobayashi, N., and Hasatani, M.: CO_2, NO_x and SO_2 emissions from the combustion of coal with high oxygen concentration gases, *Fuel* (79), pp. 1925–1932, **2000**.

[101] Chen, J., Yao, H., and Zhang, L.: A study on the calcination and sulphation behaviour of limestone during oxy-fuel combustion, *Fuel*, Vol. 102, pp. 386–395, DOI: 10.1016/j.fuel.2012.05.056, **2012**.

[102] Kirchen, G.: Natürliche SO_2-Einbindung und trockene Entschwefelung durch Zugabe von Additiven in den Feuerraum am Beispiel der Verbrennung Rheinischer Braunkohle (Dissertation), Clausthal, Germany: TU Clausthal, **1989**.

[103] Schopf, N.: Berechnungen und Versuche zur Heissentschwefelung mit Kalkadditiven unter Berücksichtigung der Verbrennungsführung (Dissertation), Clausthal, Germany: TU Clausthal - Institut für Energieverfahrenstechnik, **1990**.

[104] Liu, H., Chao, Y., Dong, S., Yuan, X., Zeng, Z., Ando, T., and Okazaki, K.: Efficient Desulfurization in a New Scheme of Oxyfuel Combined with Partial CO 2 Removal from Recycled Gas and MILD Combustion, *Energy Fuels*, Vol. 27 (3), pp. 1513–1521, DOI: 10.1021/ef3019063, **2013**.

[105] Liu, H., Yao, H., Yuan, X., Dong, S., Ando, T., and Okazaki, K.: Scheme of O 2 /CO 2 Combustion with Partial CO 2 Removal from Recycled Gas. Part 2: High Efficiency of In-Furnace Desulfurization, *Energy Fuels*, Vol. 26 (2), pp. 835–841, DOI: 10.1021/ef201464z, **2012**.

[106] Sarofim, A. F.: Oxy-fuel combustion: Progress and remaining issues, *2nd meeting of the IEAGHG oxy-fuel network*, 25-26/01/2007, Windsor, CT, USA, **2007**.

[107] Chen, C. and Zhao, C.: Mechanism of Highly Efficient In-Furnace Desulfurization by Limestone under O_2/CO_2 Coal Combustion Atmosphere, *Ind. Eng. Chem. Res.*, Vol. 45 (14), pp. 5078–5085, DOI: 10.1021/ie060196x, **2006**.

[108] Chen, C., Zhao, C., Liang, C., and Pang, K.: Calcination and sintering characteristics of limestone under O_2/CO_2 combustion atmosphere, *Fuel Process. Technol.*, Vol. 88 (2), pp. 171–178, DOI: 10.1016/j.fuproc.2006.03.003, **2007**.

[109] Fleig, D., Normann, F., Andersson, K., Johnsson, F., and Leckner, B.: The fate of sulphur during oxy-fuel combustion of lignite, *Energy Procedia*, Vol. 1 (1), pp. 383–390, DOI: 10.1016/j.egypro.2009.01.052, **2009**.

[110] Davidson, R. M. and Santos, S. O.: Oxyfuel combustion of pulverised coal (IEA-CCC Report: CCC/168), July 2010, London, UK: IEA Clean Coal Centre, ISBN: 9290294884, **2010**.

[111] Walsh, P. M., McCain, J. D., and Cushing, K. M.: Evaluation and Mitigration of Visible Acidic Aerosol Plumes from Coal Fired Power Boilers: Final Report, Available: http://www.epa.gov/nrmrl/pubs/600r06156/600r06156.pdf, Accessed: 15/06/2011, U.S. Environmental Protection Agency, **2006**.

[112] Hochbruck, W.: Entwicklung eines Verfahrens zur Bestimmung von SO_3 im Rauchgas (Dissertation), Aachen, Germany: RWTH Aachen, **1989**.

[113] Belo, L. P.: Reactions, transformations and impacts of sulfur oxides during oxy-fuel combustion (Dissertation), DOI: 10.13140/RG.2.1.2311.6644, Newcastle, Australia: University of Newcastle, **2015**.

[114] Choudhury, N. N. and Padak, B.: A comprehensive experimental and modeling study of sulfur trioxide formation in oxy-fuel combustion, *Int. J. Greenhouse Gas Control*, Vol. 51, pp. 165–175, DOI: 10.1016/j.ijggc.2016.05.016, **2016**.

[115] Marier, P. and Dibbs, H.: The catalytic conversion of SO_2 to SO_3 by fly ash and the capture of SO_2 and SO_3 by CaO and MgO, *Thermochim. Acta*, Vol. 8, pp. 155–165, **1974**.

[116] Ellison, W. and Weiler, H.: Experience with Twelve-Months-a-Year European Operation of SCR as Applied to System Design in U.S., High-Sulfur, Coal Service (Presentation), *Pittsburgh Coal Conference*, 12-15/09/2005, Pittsburgh and USA, **2005**.

[117] Cao, Y., Zhou, H., Jiang, W., Chen, C.-W., and Pan, W.-P.: Studies of the Fate of Sulfur Trioxide in Coal-Fired Utility Boilers Based on Modified Selected Condensation Methods, *Environ. Sci. Technol.*, Vol. 44 (9), pp. 3429–3434, DOI: 10.1021/es903661b, **2010**.

[118] Kenney, J., Clrak, M., Levasseur, A., and Kang, S.: SO_3 Emissions From a Tangentially Fired Pilot Scale Boiler Operating Under Oxy-Combustion Conditions (Presentation), *IEAGHG workshop, Oxy-fuel combustion: SO_2/SO_3/Hg/Corrosion Issues in Oxyfuel Combustion Boiler and Flue Gas Processing Units*, 26/01/2011, London, UK, **2011**.

[119] Hardman, R., Stacy, R., and Dismukes, E.: Estimating Sulfuric Acid Aerosol Emissions from Coal-Fired Power Plants, in: *FETC Conference on Formation, Distribution, Impact, and Fate of Sulfur Trioxide in Utility Flue Gas Streams*, March 1998, Pittsburgh, PA, USA, ed. by U. S. Department of Energy, **1998**.

[120] Perujo, M. P.: Condensation of Water Vapor and Acid Mixtures from Exhaust Gases (Dissertation), Berlin, Germany: Technische Universität Berlin - Institut für Energietechnik, **2004**.

[121] Verhoff, F. and Banchero, J.: Predicting dewpoints of flue gases, *Chem. Eng. Prog.*, Vol. 70, pp. 71–72, **1974**.

[122] Okkes, A. G.: Get acid dewpoint of flue gas, *Hydrocarbon Process.*, Vol. 7, pp. 53–55, **1987**.

[123] ZareNezhad, B.: New correlation predicts flue gas sulfuric acid dewpoints, *Oil Gas J.*, Vol. 107, pp. 60–63, **2009**.

[124] Wigley, F., Fitzgerald, D., Kensington, S., and Babcock, D.: Coal mineral transformations under oxy-fuel combustion conditions: Final report for BCURA Project B81, **2009**.

[125] Sheng, C. and Li, Y.: Experimental study of ash formation during pulverized coal combustion in O_2/CO_2 mixtures, *Fuel*, Vol. 87 (7), pp. 1297–1305, DOI: 10.1016/j.fuel.2007.07.023, **2008**.

[126] Kull, R., Maier, J., Mönckert, P., Scheffknecht, G., Hjornhede, A., and Anheden, M.: Summary report on fly ash, deposit, slagging and corrosion under oxyfuel conditions in a 500kW test rig: Public summary report of the ENCAP Project, IFK, University of Stuttgart, **2008**.

[127] Fryda, L., Sobrino, C., Glazer, M., Bertrand, C., and Cieplik, M.: Study of ash deposition during coal combustion under oxyfuel conditions, *Fuel*, Vol. 92 (1), pp. 308–317, DOI: 10.1016/j.fuel.2011.08.013, **2012**.

[128] Li, G., Li, S., Dong, M., Yao, Q., Guo, C. Y., and Axelbaum, R. L.: Comparison of particulate formation and ash deposition under oxy-fuel and conventional pulverized coal combustions, *Fuel*, Vol. 106, pp. 544–551, DOI: 10.1016/j.fuel.2012.10.035, **2013**.

[129] Yu, D., Morris, W. J., Erickson, R., Wendt, J. O., Fry, A., and Senior, C. L.: Ash and deposit formation from oxy-coal combustion in a 100kW test furnace, *Int. J. Greenhouse Gas Control*, Vol. 5, pp. 159–167, DOI: 10.1016/j.ijggc.2011.04.003, **2011**.

[130] Anheden, M., Burchhardt, U., Ecke, H., Faber, R., Jidinger, O., Giering, R., Kass, H., Lysk, S., Ramström, E., and Yan, J.: Overview of operational experience and results from test activities in Vattenfall's 30 MWth oxyfuel pilot plant in Schwarze Pumpe, *Energy Procedia*, Vol. 4, pp. 941–950, DOI: 10.1016/j.egypro.2011.01.140, **2011**.

[131] Stein-Brzozowska, G., Norling, R., Viklund, P., Maier, J., and Scheffknecht, G.: Fireside Corrosion during Oxyfuel Combustion Considering Various SO_2 Contents, *Energy Procedia*, Vol. 51, pp. 234–246, DOI: 10.1016/j.egypro.2014.07.027, **2014**.

[132] Huczkowski, P., Schiek, M., Gerhardt, A., and Burchhardt, U.: Oxidation behaviour of possible construction materials for heat exchanging components in oxy-fuel plants in the temperature range 550-650°C (Presentation), *3rd IEAGHG Oxy-Fuel Combustion Conference*, 09-13/09/2013, Ponferrada, Spain, **2013**.

[133] Gagliano, M., Seltzer, A., Agarwal, H., Robertson, A., and Wang, L.: Oxy-Combustion Boiler Material Development: Final Technical Report, US-DOE Award No.: DE-NT0005262, DOI: 10.2172/1084024, **2012**.

[134] Fry, A., Adams, B., Davis, K., Swenson, D., and Munson, S.: Fire-Side Corrosion of Heat Transfer Surface Materials for Air- and Oxy-coal Combustion, in: *36th International Technical Conference on Clean Coal & Fuel Systems*, 05-09/06/2011, Clearwater, Florida, USA, ed. by Coal Technology Association, ISBN: 9780932066364, **2011**.

[135] Holcomb, G. R., Tylczak, J., Meier, G. H., Jung, K. Y., Mu, N., Yanar, N., and Pettit, F.: Fireside Corrosion in Oxy-Fuel Combustion of Coal, in: *220th ECS Meeting and Electrochemical Energy Summit*, 09-14/10/2011, Boston, MA, ECS Transactions, pp. 73–84, DOI: 10.1149/1.4718001, ECS, **2012**.

[136] Oakey, J., Hussain, T., Sued, A., Simms, N., Jurado, N., and Darabkhanai, H. G.: Fireside Corrosion: implication and solutions for oxy-fuel boilers (Presentation), *3rd IEAGHG Oxy-Fuel Combustion Conference*, 09-13/09/2013, Ponferrada, Spain, **2013**.

[137] European Parliament and Council of the European Union: Directive 2010/75/EU of the European Parliament and of the Council of 24 November 2010 on industrial emissions on industrial emissions (integrated pollution prevention and control): IED directive, **2010**.

[138] Bundesministerium für Verkehr, Bau und Stadtentwicklung: 13. Verordnung zur Durchführung des Bundes- Immissionsschutzgesetzes (Verordnung über Großfeuerungs-, Gasturbinen- und Verbrennungsmotoranlagen): 13. BImSchV, **2017**.

[139] NSW Environment Protection Authority: Review of Coal Fired Power Stations Air Emissions and Monitoring: EPA 2018P0700, Available: https://www.epa.nsw.gov.au/-/media/epa/corporate-site/resources/air/18p0700-review-of-coal-fired-power-stations.pdf, Accessed: 19/07/2018, **2018**.

[140] Nalbandian, H.: Expert systems and coal quality in power generation (IEA-CCC Report: CCC/186), IEA Clean Coal Centre, **2011**.

[141] IEAGHG: Effects of Impurities on Geological Storage of CO_2: Report: 2011/04, IEAGHG, **2011**.

[142] Ritter, R.: CO_2-Abscheidung in der Oxyfuel-Pilotanlage (Presentation), *Public final project meeting of the German research project "ADECOS-Komponenten"*, 07-08/05/2014, Cottbus, Germany, **2014**.

[143] Mancuso, L., Ferrari, N., White, V., and Davision, J.: Integration of carbon capture unit with power generation: technology advances in oxy-combustion plants (Presentation), *3rd IEAGHG Oxy-Fuel Combustion Conference*, 09-13/09/2013, Ponferrada, Spain, **2013**.

[144] McDonald, D.: Personal discussion on tolerable SO_x levels in PF oxy-fuel boilers with the representative of the PF power plant manufacturer Babcock and Wilcox, 09/09/2013, Ponferrada, Spain, **2013**.

[145] Takeshita, M. and Soud, H.: FGD Performance and Experience on Coal-Fired Plants: IEA Coal Research (Report No: IEACW58), London, UK: IEA, **1993**.

[146] Srivastava, R. K. and Jozewicz, W.: Flue Gas Desulfurization: The State of the Art, *J. Air Waste Manag. Assoc.*, Vol. 51 (12), pp. 1676–1688, DOI: 10.1080/10473289.2001.10464387, **2001**.

[147] Electric Utility Engineer's FGD Manual, Volume 1: FGD Process Design (Final Report), DOI: 10.2172/629398, Morgantown, WV: US DoE-FETC, **1996**.

[148] Kiil, S.: Experimental and theoretical investigations of wet flue gas desulphurisation (Dissertation), Copenhagen, Denmark: Technical University of Denmark, **1998**.

[149] Pandey, R. A., Biswas, R., Chakrabarti, T., and Devotta, S.: Flue Gas Desulfurization: Physicochemical and Biotechnological Approaches, *Crit. Rev. Env. Sci. Technol.*, Vol. 35 (6), pp. 571–622, DOI: 10.1080/10643380500326374, **2005**.

[150] Sargent and Lundy LLC: Flue gas desulfurization technology evaluation: Dry lime vs. wet limestone FGD: Prepared for the National lime association; Project number 1131-001, **2007**.

[151] Béasse, G., Bourhy-Weber, C., Daeden, S., Granados, L., Lockwood, F., Moreschini, P., and Rivière, M.: Callide Oxyfuel Project - Results from CPU (Presentation), *3rd IEAGHG Oxy-Fuel Combustion Conference*, 09-13/09/2013, Ponferrada, Spain, **2013**.

[152] Spero, C.: Callide Oxyfuel Project - Lessons Learned, Available: http://www.globalccsinstitute.com/publications/callide-oxyfuel-project-lessons-learned, Accessed: 13/01/2015, Global CCS Institute/Oxyfuel Technologies Pty Ltd, **2014**.

[153] White, V., Torrente-Murciano, L., Sturgeon, D., and Chadwick, D.: Purification of oxyfuel-derived CO_2, *Int. J. Greenhouse Gas Control*, Vol. 4 (2), pp. 137–142, DOI: 10.1016/j.ijggc.2009.07.004, **2010**.

[154] Burchhardt, U., Griebe, S., Lösche, C., Kaß, H., and Zimmer, P.: Übersicht zu Tests und Ergebnissen aus der Forschungsanlage von Vattenfall, in: *46. Kraftwerkstechnisches Kolloquium*, 14-15/10/2014, Dresden, Germany, ed. by Beckmann, M., pp. 216–233, ISBN: 978-3-934409-64-4, Saxonia Verlag, **2014**.

[155] Faber, R., Yan, J., Stark, F., and Priesnitz, S.: Flue gas desulphurization for hot recycle Oxyfuel combustion: Experiences from the 30 MW_{th} Oxyfuel pilot plant in Schwarze Pumpe, *Int. J. Greenhouse Gas Control*, Vol. 5 (1), pp. 210–223, DOI: 10.1016/j.ijggc.2011.05.027, **2011**.

[156] Yan, J., Giering, R., Faber, R., Burchhardt, U., Zennegg, M., and Schmidt, T.: Performance and System Optimisation of Flue Gas Desulfurisation for Oxy-coal Combustion (Presentation), *3rd IEAGHG Oxy-Fuel Combustion Conference*, 09-13/09/2013, Ponferrada, Spain, **2013**.

[157] Toole-O'Neil, B.: Dry scrubbing technologies for flue gas desulfurization, Boston: Kluwer Academic Publishers, ISBN: 9780792383468, **1999**.

[158] Tavoulareas, E. S. and Jozewicz, W.: Multipollutant emission control technology options for coal-fired power plants (Report No. EPA-600/R-05/034), Washington, DC: U.S. Environmental Protection Agency, **2005**.

[159] Hunt, G., Heiszwolf, J. J., and Sewell, M.: Enhanced hydrated lime — A simple solution for acid gas compliance, in: *Proceedings of the 2017 IEEE-IAS/PCA Cement Industry Technical Conference*, 21-25/05/2017, Calgary, AB, Canada, pp. 1–16, DOI: 10.1109/CITCON.2017.7951849, **2017**.

[160] Institute of Clean Air Companies: Dry Sorbent Injection for Acid Gas Control: Process Chemistry, Waste Disposal and Plant Operational Impacts, Available: https://c.ymcdn.com/sites/icac.site-ym.com/resource/resmgr/white_papers/ICAC_Industrial_DSI_Ancillar.pdf, Accessed: 25/07/2018, Institute of Clean Air Companies, **2016**.

[161] Sakadjian, B., Silva, A., and Campobenedetto, E.: Multi-Pollutant Control Demonstration In a Pilot Plant with Dry Sorbent Injection (Presentation), *Air Quality VIII - An International Conference on Carbon Management, Mercury, Trace Substances, SO_x, NO_x, and Particulate Matter*, 26/10/2011, Arlington, Virginia, USA, **2011**.

[162] Laird, C. P., Smith, K. J., and Looney, B.: Results of Dry Sorbent Injection Testing to Reduce HCl, in: *Power Plant Air Pollutant Control "MEGA" Symposium 2012*, 20-23/08/2012, Baltimore, Maryland, USA, ed. by Air and Waste Management Association, ISBN: 978-1-62276-816-5, **2012**.

[163] Walter, D.: Personal discussion during BiOxySorb project meeting with the representative of the sorbent producer Rheinkalk/Lhoist, 19/07/2013, IFK - University of Stuttgart, **2013**.

[164] Fitzgerald, H.: Hydrated Lime DSI - Solution for Acid Gas Control (SO_3, HCl, and HF) (Presentation), *MARAMA (Mid-Atlantic Regional Air Management Association Inc.) / ICAC SO_2 & HCl Control Technologies Webinar*, online webinar, Available: https://cdn.ymaws.com/www.icac.com/resource/resmgr/icac_regulatory_resources/lhoist_presentation_marama_w.pdf, Accessed: 19/07/2012, **2012**.

[165] Burnett, T. A. and Anderson, K. D.: Technical review of dry FGD systems and economic evaluation of spray dryer FGD systems: EPA report no.: EPA/600/7-81/014, Available: https://www.arlis.org/docs/vol2/hydropower/APA_DOC_no._2640.pdf, Accessed: 21/07/2019, U.S. Environmental Protection Agency, **1981**.

[166] Balekdjian, O.: Abscheidung von Chlorwasserstoff und Schwefeldioxid an calciumhaltigen Absorbentien (Dissertation), Karlsruhe, Germany: Universität Fridericana Karlsruhe, **1987**.

[167] Pflughoeft-Hassett, D., Ladwig, K., Hassett, D., Dockter, B., Heebink, L., Eylands, K., and Hoffarth, J.: Characteristics and Performance of Fly Ash from Sodium Sorbent Scrubbing of SO_3 Emissions from Coal-Based Power Plants (Presentation), *World of Coal Ash Conference*, 04-07/05/2009, Lexington, KY, USA, **2009**.

[168] Schantz, M. D. and Sewell, M. R.: The Growth of Dry Sorbent Injection (DSI) and The Impacts on Coal Combustion Residue, *World of Coal Ash Conference*, 22-25/04/2013, Lexington, KY, USA, **2013**.

[169] Cheng, J., Zhou, J., Liu, J., Zhou, Z., Huang, Z., Cao, X., Zhao, X., and Cen, K.: Sulfur removal at high temperature during coal combustion in furnaces: a review, *Prog. Energy Combust. Sci.*, Vol. 29, pp. 381–405, **2003**.

[170] Lin, G.-M. and Chyang, C.-S.: Removal of HCl in Flue Gases by Calcined Limestone at High Temperatures, *Energy Fuels*, Vol. 31 (11), pp. 12417–12424, DOI: 10.1021/acs.energyfuels.7b01830, **2017**.

[171] Blythe, G. and Paradis, J.: Impact of Air Emissions Controls on Coal Combustion Products: Report (1015544), Electric Power Research Institute (EPRI), Palo Alto, CA, USA: Electric Power Research Institute (EPRI) and Ameren Corporation, **2008**.

[172] Dahlin, R. S., Snyder, T. R., and Bush, P. V.: Effects of Sorbent Injection on Particulate Properties: Part II. High-Temperature Sorbent Injection, *Air Waste*, Vol. 43 (1), pp. 91–96, DOI: 10.1080/1073161X.1993.10467119, **1993**.

[173] Kong, Y. and Davidson, H.: Dry Sorbent Injection of Sodium Sorbents for SO_2, HCl and Mercury Mitigation, in: *18^{th} Annual North American Waste-to-Energy Conference*, 11-13/05/2010, Orlando, Florida, USA, pp. 317–320, DOI: 10.1115/NAWTEC18-3560, **2010**.

[174] Kong, Y.: A Better Alternative to SO_3 for conditioning Electrostatic Precipitators (ESP): McIlvaine Company Hot Topic Hour on "Improving ESP Performance", Available: http://www.solvair.us/SiteCollectionDocuments/presentations/EUEC_2010.pdf, Accessed: 20/03/2014, **2011**.

[175] Jozewicz, W. and Gullett, B. K.: Reaction Mechanisms of Dry Ca-Based Sorbents with Gaseous HCl, *Ind. Eng. Chem. Res.*, Vol. 34 (2), pp. 607–612, DOI: 10.1021/ie00041a022, **1995**.

[176] Chin, T., Yan, R., and Liang, D. T.: Study of the Reaction of Lime with HCl under Simulated Flue Gas Conditions Using X-ray Diffraction Characterization and Thermodynamic Prediction, *Ind. Eng. Chem. Res.*, Vol. 44 (23), pp. 8730–8738, DOI: 10.1021/ie058021v, **2005**.

[177] Partanen, J., Backman, P., Backman, R., and Hupa, M.: Absorption of HCl by limestone in hot flue gases. Part II: Importance of calcium hydroxychloride, *Fuel*, pp. 1674–1684, DOI: 10.1016/j.fuel.2005.02.012, **2005**.

[178] Partanen, J.: Chemistry of HCl and Limestone in Fluidised Bed Combustion (Dissertation), Turku, Finland: Åbo akademi University, **2004**.

[179] Dal Pozzo, A., Moricone, R., Antonioni, G., Tugnoli, A., and Cozzani, V.: Hydrogen Chloride Removal from Flue Gas by Low-Temperature Reaction with Calcium Hydroxide, *Energy Fuels*, Vol. 32 (1), pp. 747–756, DOI: 10.1021/acs.energyfuels.7b03292, **2018**.

[180] Partanen, J., Backman, P., Backman, R., and Hupa, M.: Absorption of HCl by limestone in hot flue gases. Part III: Simultaneous absorption with SO_2, *Fuel*, pp. 1685–1694, DOI: 10.1016/j.fuel.2005.02.013, **2005**.

[181] Lin, G.-M. and Chyang, C.-S.: Simultaneous HCl/SO 2 Capture by Calcined Limestone from Hot Gases, *Energy Fuels*, Vol. 30 (12), pp. 10696–10704, DOI: 10.1021/acs.energyfuels.6b02565, **2016**.

[182] Silva, A. A., Krout, A., and Biehn, C.: HCl Control Using Hydrated Lime Dry Sorbent Injection, in: *Power Plant Air Pollutant Control "MEGA" Symposium 2012*, 20-23/08/2012, Baltimore, Maryland, USA, ed. by Air and Waste Management Association, ISBN: 978-1-62276-816-5, **2012**.

[183] Gambin, A., Françoisse, O., and Laudet, A.: Traitement des gaz acides par voie sèche. Performances d'un hydroxyde de calcium à haute porosité (Presentation), *8ème Congrès Francophone de Génie des Procédés*, 17-19/10/2001, Nancy, France, **2001**.

[184] Foutrel, G., Le Clerc, F., Coquelet, P., Gambin, A., and Françoisse, O.: Traitement des gaz d'Incinération par voie sèche : Comparison de deux absorbants à haute réactivité, *Déch. Sci. Tech.*, Vol. 15 (3), pp. 3–7, **1999**.

[185] Toole-O'Neil, B.: Furnace Sorbent Injection, *J. Air Waste Manag. Assoc.*, Vol. 40 (12), pp. 1716–1718, DOI: 10.1080/10473289.1990.10466817, **1990**.

[186] Dahlin, R. S., Snyder, T. R., and Bush, P. V.: Effects of Sorbent Injection on Participate Properties: Part I. Low-Temperature Sorbent Injection, *J. Air Waste Manag. Assoc.*, Vol. 42 (12), pp. 1592–1602, DOI: 10.1080/10473289.1992.10467103, **1992**.

[187] Mastropietro, R.: Fly Ash Resistivity with Injected Reagents and Predicted Impacts on Electrostatic Precipitators, Available: http://www.kccottrell.us/pdfs/LCI_inj_reagents_fly_ash_resistivity_ESP_perf.pdf, Accessed: 20/03/2014, **2000**.

[188] American Society for Testing and Materials (ASTM) International: ASTM C1567 - Standard Test Method for Determining the Potential Alkali-Silica Reactivity of Combinations of Cementitious Materials and Aggregate, **2011**.

[189] American Society for Testing and Materials (ASTM) International: ASTM C618 - Standard Specification for Coal Fly Ash and Raw or Calcined Natural Pozzolan for Use in Concrete, **2012**.

[190] Liu, H., Katagiri, S., Kaneko, U., and Okazaki, K.: Sulfation behavior of limestone under high CO_2 concentration in O_2/CO_2 coal combustion, *Fuel*, Vol. 79 (8), pp. 945–953, DOI: 10.1016/S0016-2361(99)00212-4, **2000**.

[191] Liu, H., Yao, H., Yuan, X., Xu, X., Fan, Y., Ando, T., and Okazaki, K.: Efficient Desulfurization in O_2/CO_2 Combustion: Dependence on Combustion Conditions and Sorbent Properties, *Chem. Eng. Commun.*, Vol. 199 (8), pp. 991–1011, DOI: 10.1080/00986445.2011.633288, **2012**.

[192] Liu, H. and Okazaki, K.: Simultaneous easy CO_2 recovery and drastic reduction of SO_x and NO_x in O_2/CO_2 coal combustion with heat recirculation, *Fuel*, Vol. 82 (11), pp. 1427–1436, DOI: 10.1016/S0016-2361(03)00067-X, **2003**.

[193] Sturgeon, D. W., Rogerson, J. W., and Hesselmann, G. J.: Doosan Power Systems OxyCoal™ Burner Technology Development, *Energy Procedia*, Vol. 37, pp. 6481–6488, DOI: 10.1016/j.egypro.2013.06.578, **2013**.

[194] Kluger, F., Prodhomme, B., Mönckert, P., Levasseur, A., and Leandri, J.-F.: CO_2 capture system–Confirmation of oxy-combustion promises through pilot operation, *Energy Procedia*, Vol. 4, pp. 917–924, DOI: 10.1016/j.egypro.2011.01.137, **2011**.

[195] DIN Deutsches Institut für Normung e. V.: DIN 51900-1 - Prüfung fester und flüssiger Brennstoffe-Bestimmung des Brennwertes mit dem Bomben-Kalorimeter und Berechnung des Heizwertes, **2000**.

[196] DIN Deutsches Institut für Normung e. V.: DIN 51734 - Prüfung fester Brennstoffe – Immediatanalyse und Berechnung des Fixen Kohlenstoffs, **2008**.

[197] DIN Deutsches Institut für Normung e. V.: DIN 51718 - Prüfung fester Brennstoffe Bestimmung des Wassergehaltes und der Analysenfeuchtigkeit, **2002**.

[198] DIN Deutsches Institut für Normung e. V.: DIN 51719 - Prüfung fester Brennstoffe-Bestimmung des Aschegehaltes, **1997**.

[199] DIN Deutsches Institut für Normung e. V.: DIN 51720 - Prüfung fester Brennstoffe Bestimmung des Gehaltes an Flüchtigen Bestandteilen, **2001**.

[200] DIN Deutsches Institut für Normung e. V.: DIN 51732 - Testing of solid mineral fuels – Determination of total carbon, hydrogen and nitrogen – Instrumental methods, **2007**.

[201] DIN Deutsches Institut für Normung e. V.: DIN 51727 - Prüfung fester Brennstoffe – Bestimmung des Chlorgehaltes, **2011**.

[202] DIN Deutsches Institut für Normung e. V.: DIN 51724-1 - Prüfung fester Brennstoffe – Bestimmung des Schwefelgehaltes – Teil 1: Gesamtschwefel, **2011**.

[203] DIN Deutsches Institut für Normung e. V.: DIN 51733 - Prüfung fester Brennstoffe – Bestimmung der Elementarzusammensetzung und Berechnung des Sauerstoffgehaltes, **2008**.

[204] DIN Deutsches Institut für Normung e. V.: DIN 51729-11 - Bestimmung der chemischen Zusammensetzung von Brennstoffasche Teil 11 - Atomemissionsspektrometrische Bestimmung mit induktiv gekoppeltem Plasma (ICP-OES), **1998**.

[205] VGB - Technische Vereinigung der Großkraftwerksbetreiber: VGB Richtlinie zur Prüfung von DeNO$_x$-Katalysatoren: VGB-S-302-00-2013-04-DE, **2013**.

[206] Babat, S., Spörl, R., Maier, J., and Scheffknecht, G.: Investigation of deposit formation and its characterization for a pulverized bituminous coal power plant, *Fuel Process. Technol.*, Vol. 141, pp. 225–234, DOI: 10.1016/j.fuproc.2015.10.001, **2016**.

[207] DIN Deutsches Institut für Normung e. V.: DIN 19539 - Untersuchung von Feststoffen – Temperaturabhängige Differenzierung des Gesamtkohlenstoffs (TOC$_{400}$, ROC, TIC$_{900}$), **2016**.

[208] DIN Deutsches Institut für Normung e. V.: DIN 38414-4 - Deutsche Einheitsverfahren zur Wasser-, Abwasser- und Schlammuntersuchung; Schlamm und Sedimente (Gruppe S); Bestimmung der Eluierbarkeit mit Wasser (S 4), **1984**.

[209] DIN Deutsches Institut für Normung e. V.: DIN EN ISO 10304-1 - Water quality - Determination of dissolved anions by liquid chromatography of ions - Part 1: Determination of bromide, chloride, fluoride, nitrate, nitrite, phosphate and sulfate (ISO 10304-1:2007); German version EN ISO 10304-1:2009, **2009**.

[210] DIN Deutsches Institut für Normung e. V.: DIN 51729-11 - Prüfung fester Brennstoffe-Bestimmung der chemischen Zusammensetzung von Brennstoffasche, **1998**.

[211] DIN Deutsches Institut für Normung e. V.: DIN EN 1911 - Stationary source emissions - Determination of mass concentration of gaseous chlorides expressed as HCl - Standard reference method; German version EN 1911:2010, **2010**.

[212] VDI e.V.: VDI 2462, Blatt 2 - VDI-Richtlinie: Messen gasförmiger Emissionen - Bestimmung von Schwefeltrioxid in wasserdampfhaltigen Abgasen - Kondensationsverfahren (VDI Guideline: Measurement of gaseous emissions - Determination of sulphur trioxide in water vapour containing exhaust gas - Condensation method), **2011**.

[213] DIN Deutsches Institut für Normung e. V.: DIN 1343 - Reference conditions, normal conditions, normal volume; concepts and values, **1990**.

[214] Lindberg, D., Backman, R., Chartrand, P., and Hupa, M.: Towards a comprehensive thermodynamic database for ash-forming elements in biomass and waste combustion — Current situation and future developments, *Fuel Process. Technol.*, Vol. 105, pp. 129–141, DOI: 10.1016/j.fuproc.2011.08.008, **2013**.

[215] Koukkari, P., Penttilä, K., Hack, K., and Petersen, S.: CHEMSHEET - An Efficient Worksheet Tool for Thermodynamic Process Simulation. *In Coll.: Microstructures, Mechanical Properties and Processes - Computer Simulation and Modelling*, ed. by Bréchet, Y., pp. 323–330, Weinheim, FRG: Wiley-VCH Verlag GmbH & Co. KGaA, ISBN: 9783527606153, **2000**.

[216] Zevenhoven-Onderwater, M., Backman, R., Skrifvars, B.-J., and Hupa, M.: The ash chemistry in fluidised bed gasification of biomass fuels. Part I: Predicting the chemistry of melting ashes and ash–bed material interaction, *Fuel*, Vol. 80 (10), pp. 1489–1502, DOI: 10.1016/S0016-2361(01)00026-6, **2001**.

[217] Zevenhoven-Onderwater, M., Backman, R., Skrifvars, B.-J., Hupa, M., Liliendahl, T., Rosén, C., Sjöström, K., Engvall, K., and Hallgren, A.: The ash chemistry in fluidised bed gasification of biomass fuels. Part II: Ash behaviour prediction versus bench scale agglomeration tests, *Fuel*, Vol. 80 (10), pp. 1503–1512, DOI: 10.1016/S0016-2361(01)00004-7, **2001**.

[218] Zevenhoven-Onderwater, M., Blomquist, J.-P., Skrifvars, B.-J., Backman, R., and Hupa, M.: The prediction of behaviour of ashes from five different solid fuels in fluidised bed combustion, *Fuel*, Vol. 79 (11), pp. 1353–1361, DOI: 10.1016/S0016-2361(99)00280-X, **2000**.

[219] Paneru, M., Babat, S., Maier, J., and Scheffknecht, G.: Role of potassium in deposit formation during wood pellets combustion, *Fuel Process. Technol.*, Vol. 141, pp. 266–275, DOI: 10.1016/j.fuproc.2015.10.008, **2016**.

[220] Skoglund, N., Bäfver, L., Fahlström, J., Holmén, E., and Renström, C.: Fuel design in co-combustion of demolition wood chips and municipal sewage sludge, *Fuel Process. Technol.*, Vol. 141, pp. 196–201, DOI: 10.1016/j.fuproc.2015.08.037, **2016**.

[221] Johansen, J. M., Jakobsen, J. G., Frandsen, F. J., and Glarborg, P.: Release of K, Cl, and S during Pyrolysis and Combustion of High-Chlorine Biomass, *Energy Fuels*, Vol. 25 (11), pp. 4961–4971, DOI: 10.1021/ef201098n, **2011**.

[222] Kaknics, J., Michel, R., and Poirier, J.: Miscanthus ash transformation and interaction with bed materials at high temperature, *Fuel Process. Technol.*, Vol. 141, pp. 178–184, DOI: 10.1016/j.fuproc.2015.08.041, **2016**.

[223] Ma, C., Backman, R., and Öhman, M.: Thermochemical Equilibrium Study of Slag Formation during Pressurized Entrained-Flow Gasification of Woody Biomass, *Energy Fuels*, Vol. 29 (7), pp. 4399–4406, DOI: 10.1021/acs.energyfuels.5b00889, **2015**.

[224] Tantau, T. and Feuersänger, C.: PGF and TikZ - Graphic systems for TeX: (program and documentation), Available: http://sourceforge.net/projects/pgf/, Accessed: 05/07/2018, **2005**.

[225] Kull, R., Stein-Brzozowska, G., Theye, T., Maier, J., and Scheffknecht, G.: Corrosion of super-heater materials under oxy-fuel conditions (Presentation), *1st IEAGHG Oxyfuel Combustion Conference*, 08-11/09/2009, Cottbus, Germany, **2009**.

[226] Toftegaard, M. B.: Oxy-fuel combustion of coal and biomass (Dissertation), Lyngby, Denmark: Technical University of Denmark, **2011**.

[227] Wild, T., Kluger, F., Lysk, S., and Bischoff, H.: Feuerungen in Oxyfuel-Dampferzeugern: Besonderheiten und Auswirkungen auf Auslegung und Betrieb, *VGB PowerTech*, Vol. 90 (11), **2010**.

[228] Donato, G. and Belongie, S.: Approximation methods for thin plate spline mappings and principal warps, Available: http://cseweb.ucsd.edu/~sjb/pami_tps.pdf, Accessed: 22/04/2017, San Diego, USA: Department of Computer Science and Engineering, University of California, **2002**.

[229] Kluger, F., Mönckert, P., Wild, T., and Levasseur, A. A.: Untersuchung zur Verbrennung unterschiedlicher Brennstoffqualitäten an den Oxyfuel Pilotanlagen, in: *44. Kraftwerktechnisches Kolloquium*, 23-24/10/2012, Dresden, Germany, ed. by Beckmann, M., pp. 351–366, ISBN: 978-3-935317-88-7, Thomé-Kozmiensky Verlag, **2012**.

[230] Tan, Y.: Pollutant formation and emissions from oxy-coal power plants. *In Coll.: Oxy-fuel combustion for power generation and carbon dioxide (CO_2) capture*, ed. by Zheng, L., pp. 145–165, Cambridge, UK: Woodhead Publishing, ISBN: 978-1-84569-671-9, **2011**.